


1-1-2016

Dendrimer Nanoconjugates And Their Oral Inhalation Formulations For Lung Cancer Therapy

Qian Zhong
Wayne State University,

Follow this and additional works at: https://digitalcommons.wayne.edu/oa_dissertations

 Part of the [Biomedical Engineering and Bioengineering Commons](#), and the [Materials Science and Engineering Commons](#)

Recommended Citation

Zhong, Qian, "Dendrimer Nanoconjugates And Their Oral Inhalation Formulations For Lung Cancer Therapy" (2016). *Wayne State University Dissertations*. 1501.
https://digitalcommons.wayne.edu/oa_dissertations/1501

This Open Access Dissertation is brought to you for free and open access by DigitalCommons@WayneState. It has been accepted for inclusion in Wayne State University Dissertations by an authorized administrator of DigitalCommons@WayneState.

**DENDRIMER NANOCONJUGATES AND THEIR ORAL INHALATION
FORMULATIONS FOR LUNG CANCER THERAPY**

by

QIAN ZHONG

DISSERTATION

Submitted to the Graduate School

of Wayne State University,

Detroit, Michigan

in partial fulfillment of the requirements

for the degree of

DOCTOR OF PHILOSOPHY

2016

MAJOR: MATERIALS SCIENCE

Approved By:

Advisor

Date

©COPYRIGHT BY

QIAN ZHONG

2016

All Rights Reserved

ACKNOWLEDGEMENTS

How time flies! I still clearly remembered the moment I arrived at Detroit 5 years ago. The 5 years' study and life at Wayne State University is one of the most memorable periods in my life. In retrospect on the past 5 years, I would like to thank my relatives, professors and friends who have given me invaluable help and support. First of all, I want to express my warmest gratitude to my wife for her love, care, comprehension, patience, and motivation, which have lead me to pursue my goals each day. Without my wife, I would never have reached this final destination. I would also like to thank my parents and relatives in China who supported me in my decision to pursue my Ph.D. degree.

I would like extend my thanks to my Ph.D. advisor, Dr. Sandro da Rocha, for supervising me over my entire doctoral period. During this time, not only did he do the role of a mentor for academic research, but has been a friend giving me suggestions to help overcome every obstacle that I have encountered as a graduate student.

Special thanks are also extended to all professors at Wayne State University I have worked with during my doctoral research: Dr. Joshua Reineke and Dr. Olivia Merkel at Pharmaceutical Sciences, Dr. Haipeng Liu at Chemical Engineering, Dr. Lisa Polin and Dr. Arun Rishi at Oncology, Dr. Judith Whittum-Hudson and Dr.

Bonfil from School of Medicine, whose supervision, expertise and suggestions greatly aided the completion of my research in the past 5 years.

My research would never have been completed without the friendship and help of my former labmates — Balaji Bhwartwaj, Denise Conti, Lin Yang, Ingrid Ganda, Rodrigo Heyder, Bruno Humia, Radovan Dimovski, Leonan Rodrigue, Alisha Punjabi, Ashura Molla, Hamad Mirza — and current labmates — Dr. Wagner Priamo, Dr. K.S.V. Krishna Rao, Elizabeth Bielski, Naira Carniel, Matthew Brown.

In my research period, many other senior scientists from instrumentation center also provide me generous help, including Dr. Zhi Mei "Mike", Dr. Bashar Ksebati, Dr. Yuriy Danylyuk, and Dr. Olena Palyvoda from Lumigen Instrumentation Center (LIC) at Department of Chemistry; Dr. Jessica Back, Mr. Eric Van Buren, Ms. Mary Olive, Ms Linda Mayernik, and Mr. Daniel de Santis from Microscopy, Imaging & Cytometry Resource (MICR).

Last, I would also like to thank the Department of Chemical Engineering and The Graduate School at Wayne State University for their financial support during my tenure as a graduate student.

TABLE OF CONTENTS

ACKNOWLEDGEMENTS	ii
LIST OF FIGURES	x
LIST OF TABLES	xvi
LIST OF ABBREVIATIONS	xviii
CHAPTER 1 — Introduction	1
1.1 Overviews and Objectives	1
1.2 Literature review	10
1.2.1 Inadequate biodistribution of chemotherapeutics upon i.v. administration	10
1.2.2 Pulmonary extracellular barriers to delivery of therapeutics to/through the lungs..	11
1.2.3 Pressurized metered-dose inhalers (pMDIs) as oral inhalation for pulmonary delivery	14
1.2.4 Doxorubicin as leading anticancer therapeutics in lung cancer treatment.....	15
1.2.5 Polymeric nanocarriers (PNCs) for targeted intracellular DOX delivery.....	16
1.2.6 PEGylation of PNCs help overcome pulmonary extracellular barriers and improve biodistribution	18
1.2.7 Development of in vivo lung cancer murine model.....	19
1.3 Relevance and Innovation.....	20
CHAPTER 2 — The Effect of the Route of Administration and PEGylation of Poly(amidoamine) Dendrimers on their Systemic and Lung Cellular Biodistribution	21
2.1 Introduction.....	21
2.2 Materials.	24
2.3 Methods.....	25
2.3.1 Cy3 labeling of PAMAM dendrimer (G3NH ₂ -Cy3).....	25
2.3.2 Synthesis of PEGylated PAMAM dendrimers (G3NH ₂ -PEG1000-Cy3)	25

2.3.3	Size and Surface Charge of the Conjugates.....	26
2.3.4	Pulmonary administration of the dendrimer conjugates	26
2.3.5	Pharmacokinetics (PK) of the administered dendrimer conjugates	26
2.3.6	Systemic biodistribution of the administered dendrimer conjugates.....	27
2.3.7	Ex-vivo imaging of excised tissues.....	27
2.3.8	Quantification of dendrimer conjugates in tissues.....	27
2.3.9	Single cell staining for pulmonary cellular biodistribution of the nanocarriers	28
2.3.10	Statistical analysis	28
2.4	Results and discussion	29
2.4.1	Synthesis of PEGylated dendrimer conjugates	29
2.4.2	Plasma concentration profiles of dendrimer conjugates administered via pulmonary and I.V. routes.....	32
2.4.3	Systemic biodistribution of the dendrimer conjugates delivered via the pulmonary and intra-venous (I.V.) routes.....	34
2.4.4	Lung cellular biodistribution of the dendrimer conjugates administered via pulmonary route.....	39
2.5	Conclusions.....	41
2.6	Acknowledgements.....	42
2.7	Supplemental information.....	43
CHAPTER 3 — Poly(amidoamine) Dendrimer-Doxorubicin Conjugates: In vitro characteristics and Pseudo-Solution Formulation in Pressurized Metered-Dose Inhalers.....		
3.1	Introduction.....	44
3.2	Materials	46
3.3	Methods.....	47
3.3.1	Synthesis and characterization of acid-labile, PEGylated PAMAM-DOX conjugates (G3NH ₂ -mPEG-nDOX).....	47

3.3.2	Synthesis and characterization of non-labile, PEGylated PAMAM-DOX conjugates (G3NH ₂ -mPEG-nDOXNL).....	48
3.3.3	Culture of A549 Cells.....	48
3.3.4	<i>In vitro</i> release of acid-labile G3NH ₂ -mPEG-nDOX and acid-non-labile G3NH ₂ -mPEG-nDOXNL conjugates.	48
3.3.5	Cell kill of acid-labile G3NH ₂ -mPEG-nDOX and acid-non-labile G3NH ₂ -mPEG-nDOXNL conjugates.	49
3.3.6	Cellular internalization of acid-labile G3NH ₂ -mPEG-nDOX conjugates by A549 cells.....	50
3.3.7	Intracellular release and nuclear colocalization of DOX from acid-labile G3NH ₂ -mPEG-nDOX conjugates.....	50
3.3.8	Preparation and characterization of the pMDI formulations	51
3.4	Results and Discussion	53
3.4.1	Synthesis and characterization of acid-labile G3NH ₂ -mPEG-nDOX and non-labile G3NH ₂ -mPEG-nDOXNL conjugates.....	53
3.4.2	<i>In vitro</i> release of DOX from acid-labile G3NH ₂ -mPEG-nDOX and non-labile G3NH ₂ -mPEG-nDOXNL conjugates at extracellular physiological and lysosomal pH.....	60
3.4.3	Kill of lung adenocarcinoma cells with acid-labile G3NH ₂ -mPEG-nDOX and non-labile G3NH ₂ -mPEG-nDOXNL conjugates.....	62
3.4.4	Cellular internalization of acid-labile G3NH ₂ -mPEG-nDOX conjugates	64
3.4.5	Intracellular release and colocalization of DOX from acid-labile G3NH ₂ -mPEG-nDOX conjugates.....	67
3.4.6	Physical stability of the acid-labile G3NH ₂ -mPEG-nDOX conjugates in HFA Propellant.....	70
3.4.7	Aerosol characteristics of pMDI formulations of acid-labile G3NH ₂ -mPEG-nDOX conjugates.....	73
3.5	Conclusion	76
3.6	Acknowledgements.....	77
3.7	Supplemental information.....	78

CHAPTER 4 — Design of Dendrimer-Doxorubicin Conjugates for Transport Modulation across <i>in vitro</i> Pulmonary Epithelium and their Solution Formulation in pMDIs	79
4.1 Introduction.....	79
4.2 Materials	82
4.3 Methods.....	83
4.3.1 Synthesis of acid-labile PEGylated PAMAM-DOX conjugates (G3NH ₂ -mPEG-nDOX, m=0, 9, 21, and n=3, 7).	83
4.3.2 Cell kill ability of acid-labile G3NH ₂ -mPEG-nDOX conjugates against Calu-3 cells.	83
4.3.3 <i>In vitro</i> transport of G3NH ₂ -mPEG1000-nDOX conjugates across polarized Calu-3 monolayers.....	84
4.3.4 Transport of G3NH ₂ -mPEG1000-nDOX conjugates across mucus	86
4.3.5 Preparation and Characterization of the pMDI Formulations.....	86
4.4 Results and discussion	88
4.4.1 Physicochemical properties of acid-labile G3NH ₂ -mPEG-nDOX conjugates	88
4.4.2 Cytotoxicity of acid-labile G3NH ₂ -mPEG-nDOX conjugates	90
4.4.3 <i>In vitro</i> transport of acid-labile G3NH ₂ -mPEG-nDOX conjugates across polarized pulmonary epithelial monolayer	91
4.4.4 Pseudo solution pMDI formulations of acid-labile G3NH ₂ -mPEG-nDOX conjugates	98
4.4.5 Impact of heating process on aerosol performance of pseudo solution pMDI formulation.....	99
4.4.6 Deposition-tunable pMDI formulation of G3NH ₂ -mPEG-nDOX conjugates by the addition of triblock copolymer LA _n -EO _m -LA _n	101
4.5 Conclusion	104
4.6 Acknowledgements.....	105
CHAPTER 5 — Conjugation to Poly(amidoamine) Dendrimers and Pulmonary Delivery Enhances the Antitumor Activity of Doxorubicin in Lung Metastasis ...	106

5.1	Introduction.....	106
5.2	Materials	108
5.3	Methods.....	109
5.3.1	Cell culture.....	109
5.3.2	Animals for <i>in vivo</i> experiments	109
5.3.3	Synthesis and characterization of dendrimer-DOX conjugates with an acid-labile bond (G4COOH-nDOX).....	110
5.3.4	<i>In vitro</i> release of DOX from the G4COOH-nDOX conjugate	112
5.3.5	Cell kill (<i>in vitro</i>) of the G4COOH-nDOX conjugate	113
5.3.6	Cellular internalization of the G4COOH-nDOX conjugate by B16F10 cells	113
5.3.7	Efficacy of free and dendrimer-conjugated DOX in treating lung metastasis.....	114
5.3.8	Systemic distribution of the G4COOH-nDOX conjugate	115
5.3.9	Statistical analysis	115
5.4	Results and discussion	116
5.4.1	Synthesis and characterization of the dendrimer-DOX conjugates (G4COOH-nDOX).....	116
5.4.2	Sustained <i>in vitro</i> release of acid-labile G4COOH-12DOX conjugate	119
5.4.3	Cell kill of B16F10 melanoma cells lines by the G4COOH-12DOX conjugates..	120
5.4.4	Enhanced cellular internalization of DOX by its conjugation to dendrimer conjugate	122
5.4.5	Effect of the G4COOH-12DOX conjugates in treating lung metastasis	124
5.4.6	Impact of administration route and DOX conjugation on systemic biodistribution	128
5.5	Conclusion	134
5.6	Acknowledgements.....	134
5.7	Supplemental information.....	135
CHAPTER 6 — CONCLUSIONS AND FUTURE DIRECTIONS		136

6.1 Conclusions and future directions.....	136
APPENDIX A SUPPORTING INFORMATION OF CHAPTER 2	142
APPENDIX B SUPPORTING INFORMATION OF CHAPTER 3	155
APPENDIX C SUPPORTING INFORMATION OF CHAPTER 5	163
APPENDIX D PUBLICATION 1	164
APPENDIX E PUBLICATION 2.....	165
REFERENCES	166
ABSTRACT	201
AUTOBIOGRAPHICAL STATEMENT.....	203

LIST OF FIGURES

- Figure 1.1** Diagram of the human lungs and particle deposition based on size..... 13
- Figure 1.2** Schematic representation of intracellular release of Polymer-DOX conjugates (e.g. polyamidoamine-PAMAM). The conjugates are internalized by endocytosis into endosomes and then end up in lysosomes. DOX is released from polymer-DOX conjugates with pH-sensitive linkers broken as pH drops to 5.0-4.5 in lysosomes. Released DOX subsequently moves out of lysosome towards nucleus..... 17
- Figure 2.1** Schematic diagram of the synthesis of the Cy3-labeled, PEGylated dendrimer conjugates. The Cy3 terminology is dropped in the results and discussion part. For simplicity, the conjugates are referred to G3NH₂ and G3NH₂-*m*PEG1000, where *m* is the number of PEG 1000Da graft moieties – the number of Cy3 is the same for all conjugates. r.t. = room temperature 29
- Figure 2.2** Plasma concentration (C_p) as a function of time after administration of G3NH₂ and G3NH₂-24PEG1000 via (a) pharyngeal aspiration (P.A.) and (b) intravenous injection (I.V.) (n=3 per group). The statistical analysis was performed between G3NH₂ and G3NH₂-24PEG1000 with Student's t-test (*p < 0.05, **p < 0.01, and ***p < 0.001)..... 31
- Figure 2.3** Ex vivo biodistribution of G3NH₂ and G3NH₂-24PEG1000 delivered via pharyngeal aspiration (P.A.) or I.V., determined 6.5 h after administration (n=3 per group). ALN: axillary lymph nodes; BLN: bronchial lymph nodes; CLN: cervical lymph nodes; MLN: mesenteric lymph nodes. The tissues that are enlarged for better visualization in the figure are ALN, BLN, CLN and MLN. Liver is shrunk instead for better visualization. The inset is the scale bar of fluorescence intensity.. 35
- Figure 2.4** *In vivo* biodistribution of G3NH₂ and G3NH₂-24PEG1000 delivered via (a) pharyngeal aspiration (P.A.) and (b) I.V., 6.5 hours after administration (n=3 per group). The insets highlight the biodistribution of the conjugates in the different lymph nodes; when they are all combined, they are represented in the main figure as LN. ALN: axillary lymph nodes; BLN: bronchial lymph nodes; CLN: cervical lymph nodes; MLN: mesenteric lymph nodes. The statistical analysis was performed between G3NH₂ and G3NH₂-24PEG1000 with Student's t-test (*p<0.05, **p<0.01, and ***p<0.001). 36
- Figure 2.5** Lung cellular distribution studies upon lung delivery of the dendrimer conjugates. Break down in terms of cell type (out of those cells that had internalized dendrimer conjugates) and dendrimer conjugate PEGylation. *Inset*: % of lung cells, out of all the cells in the tissue single cell suspensions, which had internalized dendrimer conjugates (n=3 per group). Statistical analysis was performed with Student's t-test (*p<0.05). n.s.d = not significantly different..... 39

- Figure 3.1** Synthesis of the PEGylated, generation 3, amine-terminated PAMAM dendrimer (G3NH₂) conjugated with DOX. DOX conjugated via an acid-labile linker: G3NH₂-mPEG-nDOX; DOX conjugated via a non-labile linker: G3NH₂-mPEG-nDOXNL..... 55
- Figure 3.2** Example of (a) ¹H NMR spectra of PEGylated G3NH₂ dendrimer with acid-labile DOX conjugates (G3NH₂-3DOX and G3NH₂-21PEG-7DOX). *Inset*: chemical structure of G3NH₂-mPEG-nDOX. Spectral shifts for all compounds are provided in *Supplemental Information S2 in Appendix 2*, and (b) MALDI spectra of a PEGylated G3NH₂ dendrimer with acid-labile DOX conjugates (G3NH₂-21PEG-7DOX) and the intermediates synthesized via two-step PEGylation strategy..... 57
- Figure 3.3** *In vitro* release profiles of DOX from the acid-labile (G3NH₂-mPEG-nDOX) and non-labile (G3NH₂-mPEG-nDOXNL) conjugates at (i) lysosomal pH = 4.5: (a) and (b); (ii) physiological pH = 7.4: (c) and (d), all at 37 °C. 60
- Figure 3.4** Cell kill of (a) G3NH₂ and PEGylated dendrimers (G3NH₂-mPEG), (b) acid-non-labile conjugates (G3NH₂-mPEG-nDOXNL), and (c) acid-labile conjugates (G3NH₂-mPEG-nDOX), as determined by the MTT assay after 72 h incubation with A549 cells. (d) Cell kill of acid-labile conjugates (G3NH₂-mPEG-nDOX) determined by the MTT assay after 144 h incubation with A549 cells. Free DOX is used as control. Results denote mean ± s.d. (n=8)..... 62
- Figure 3.5** Synthesis of the PEGylated, generation 3, amine-terminated PAMAM dendrimer (G3NH₂) conjugated with DOX. DOX conjugated via an acid-labile linker: G3NH₂-mPEG-nDOX; DOX conjugated via a non-labile linker: G3NH₂-mPEG-nDOXNL..... 64
- Figure 3.6** (a) Selected confocal images of A549 cells contacted with free DOX, acid-labile G3NH₂-3DOX and acid-non-labile G3NH₂-3DOXNL conjugates. (b) Cross section of 3D rendered confocal image of acid-labile G3NH₂-3DOX and acid-non-labile G3NH₂-3DOXNL conjugates. Image (a) and (b) were obtained 48 h after A549 cells were incubated with the samples. Blue color represents nuclei, red color for DOX, and pink color for DOX co-localized with nuclei. 67
- Figure 3.7** Pearson's Correlation Coefficient (PCC) of DOX free and from acid-labile G3NH₂-mPEG-nDOX conjugates as a function of incubation time. PCC was determined by confocal microscopy, and calculated based on the colocalization of blue-stained nuclei and red DOX. 68
- Figure 3.8** Dispersion of acid-labile G3NH₂-mPEG-nDOX in HFA227 propellant as a function of time after sonication. Conditions were: 0.2 mg/mL DOX equivalent; 0.37% anhydrous ethanol (v/v relative to the propellant), at 25°C. 71
- Figure 3.9** (a) Structure diagram of an Andersen Cascade Impactor (ACI) and correlation of stages in ACI to anatomical regions of the lungs. (b) Aerosol characteristics of the pMDI formulations containing acid-labile conjugates (G3NH₂-mPEG-nDOX) in

HFA227 propellant at 0.2 mg/mL DOX equivalent and 0.37% anhydrous ethanol v/v relative to propellant, as determined using ACI at 25 °C. AC, IP, 0-7 and F denote actuator, induction port, Stage 0-7 and filter, respectively. 73

- Figure 3.10** Schematic diagram of the proposed mechanism for the formation of the micron size aerosol particles from the nanometer size conjugates. (a) Acid-labile G3NH₂-mPEG-nDOX are solvated as individual particles or nanoaggregates of a few molecules in liquid HFA227 in pMDI at its saturated pressure. (b) As the aerosol forms, the conjugates are (i) initially fully solvated; (ii) as the propellant evaporates, the dendrimer solution phase separates, forming dendrimer nuclei that continue to increase in size to form particles until; (iii) the propellant completely evaporates. (c) Phase separation as the concentration of dendrimer conjugates increases upon evaporation of propellant at ambient pressure. 76
- Figure 4.1** Viability of Calu-3 cells 72 h post incubation with varying concentrations of bare dendrimer, free DOX or acid-labile conjugates (G3NH₂-mPEG1000-nDOX, with $m = 0, 9, \text{ or } 21$ and $n = 3 \text{ or } 7$), as determined by the MTT assay. Results denoted as mean \pm s.d. (n=6). The inset of IC₅₀ values of the free DOX (DOX) various conjugates at 72 h incubation. The IC₅₀ values were obtained with non-linear regression Log(inhibitor) vs. Response (variable slope) 90
- Figure 4.2** Apical to basolateral (A→B) transport of free DOX and DOX from acid-labile G3NH₂-mPEG1000-nDOX conjugates across polarized Calu-3 cell monolayers as a function of time (n=6). Statistical significance was calculated with respect to free DOX by one-way ANOVA Dunnett's test (* $p < 0.05$). 91
- Figure 4.3** Apparent permeability (P_{app}) of G3NH₂-mPEG1000-nDOX conjugates across Calu-3 cell monolayer (n=6). P_{app} was determined at 5 h post incubation of the cell monolayer with the conjugates, with the transport being from the apical to basolateral (A→B) side. Statistical significance was calculated with respect to free DOX by one-way ANOVA Dunnett's test (* $p < 0.05$). 92
- Figure 4.4** Variation in transepithelial electrical resistance (TEER) across polarized Calu-3 monolayer grown on Transwell® inserts during the 5 h *in vitro* transport experiments (n=6), and up to 36h after the completion of transport experiment (n=3) – after washing of the apical side of the monolayer where the conjugates had been pulsed..... 94
- Figure 4.5** Transport of the acid-labile G3NH₂-mPEG1000-nDOX conjugates across the synthetic mucus layer as a function of time. Statistical significance was calculated with respect to free DOX by one-way ANOVA Dunnett's test (* $p < 0.05$)..... 95
- Figure 4.6** Mass balance of DOX conjugates during the *in vitro* transport experiments. The mass transported from apical to basolateral side (A→B), the mass internalized into Calu-3 cells, and the mass retained on apical side were determined for the mass balance. 97

- Figure 4.7** (a) Aerosol characteristics of the pMDI formulations containing the acid-labile G3NH₂-21PEG1000-3DOX conjugates. Method A = formulation prepared by heating the conjugate or conjugate and polymer mixture before addition of propellant; Method B = anhydrous ethanol (EtOH) at 0.37% v/v relative to HFA227 propellant was added to the formulation as co-solvent. (b) Differential scanning calorimetry (DSC) thermograms of PEG1000 and acid-labile G3NH₂-21PEG1000-3DOX conjugates..... 99
- Figure 4.8** ¹H NMR and MALDI spectra of LA₄₆-EO₂₃-LA₄₆ triblock copolymer.. 102
- Figure 4.9** Effect of the concentration of LA₄₆-EO₂₃-LA₄₆ triblock copolymer on the aerosol characteristics of the pMDI formulations of G3NH₂-21PEG1000-3DOX in HFA227 (0.2 mg DOX equivalent per mL propellant). The formulation was prepared by Method A. 103
- Figure 5.1** Synthesis of the generation 4, carboxyl-terminated PAMAM dendrimer (G4COOH) conjugated with acid-labile DOX (G4COOH-nDOX). NMM = N-methylmorpholine; IBCF = isobutyl chloroformate; TFA = trifluoroacetic acid; DCM = dichloromethane..... 110
- Figure 5.2** (a) ¹H NMR spectra of acid-labile G4COOH-12DOX conjugate. *Inset*: chemical structure of G4COOH-12DOX. Spectral shifts for all compounds are provided in Section 2.4 and (b) MALDI spectra of G4COOH-12DOX conjugate and intermediates. 117
- Figure 5.3** *In vitro* release profiles of DOX from acid-labile G4COOH-12DOX at (i) lysosomal pH = 4.5 and physiological pH = 7.4, both at 37 °C. Results represent mean ± s.d. (n=3 per group). s.d. = standard deviation. The diffusion of free DOX out of dialysis membrane (MWCO=3000Da) is used as control..... 119
- Figure 5.4** Cell kill of acid-labile G4COOH-12DOX as determined by MTT assay after 48 h incubation with B16-F10 melanoma cells. Free DOX is used as control. Results represent mean ± s.d. (n=8 per group). s.d. = standard deviation. IC₅₀ was calculated based on non-linear regression Log(inhibitor) vs. Response (variable slope) with G4COOH-12DOX being 6.0 μM and free DOX being 2.6 μM. 121
- Figure 5.5** Cellular internalization of the acid-labile G4COOH-12DOX in B16-F10 melanoma cells as a function of time, as determined by flow cytometry. Results denote mean ± s.d. (n=3 per group). Statistical significance is calculated with respect to free DOX by *Student's t test* (**p*<0.05, ***p*<0.01, and ****p*<0.001). The rates of internalization of G4COOH-12DOX (conjugated DOX) and free DOX are 268.7 a.u.h⁻¹ (R² = 0.963) and 35.7 a.u.h⁻¹ (R² = 0.981), respectively. The rate is calculated by linear fitting of 3 initial time points. 122
- Figure 5.6** Images of lungs collected from C57BL/6 mice bearing lung metastases (n=6 per group). PBS, free DOX or G4COOH-12DOX is administered through i.v. or p.a. route. i.v.: intravenous injection; p.a.: pharyngeal aspiration (pulmonary route).

The lungs excised from normal mice are used as negative control (top row). “+” in tumor column denotes mice bearing lung tumors from metastatic melanoma and “-” represents the lungs excised from negative control group..... 125

- Figure 5.7** Weight of lungs excised from healthy C57BL/6 mice (negative control group; n=3 per group) and tumor-metastases bearing mice treated with different therapies (n=6 per group) at 17 days post implantation (DPI17). Results represent mean \pm s.d. Statistical analysis is performed with *one-way ANOVA Tukey's test*. * p <0.05, ** p <0.01, and *** p <0.001. p.a. = pharyngeal aspiration; i.v. = intravenous injection; s.d. = standard deviation..... 126
- Figure 5.8** Survival rate of mice bearing lung metastases over 17 days, as plotted on a Kaplan-Meier survival curve. The survival rate of each group is analyzed using *Log-rank (Mantel-Cox) test* (* p <0.05) with respect to the positive control of same administration route (PBS). n.s. = not significant. 127
- Figure 5.9** Systemic distribution of DOX and G4COOH-12DOX delivered via (a) p.a. and (b) i.v.. Mice bearing lung metastases were euthanized at 17 days post implantation (DPI17) or terminal point prior to DPI17. Results represent mean \pm s.d. (n=6 per group). The groups of same administration (p.a. or i.v.) are analyzed using *one-way analysis of variance (ANOVA) with Tukey's post hoc test*. * p <0.05, ** p <0.01 and *** p <0.001. % of TD = % of total dosage. p.a. = pharyngeal aspiration; i.v. = intravenous injection; s.d. = standard deviation. 128
- Figure 5.10** (a) Accumulation of DOX (free/conjugated form) in the lungs at terminal point (DPI17). Therapeutics were given through i.v. or p.a. route. Statistical analysis is performed with *one-way analysis of variance (ANOVA) with Tukey's post hoc test*. (b) Temporal effect on accumulation of DOX in the lungs. Therapeutics were given through p.a.. The mice were euthanized at DPI13 (n=3 per group) and DPI17 (n=6 per group). Statistical analysis is performed in 2 different ways: (i) all groups at DPI13 or DPI17 are analyzed with *one-way analysis of variance (ANOVA) with Tukey's post hoc test*; (ii) same therapy groups (e.g. DOX p.a.) at DPI13 and DPI17 are analyzed with *Student's t test*. * p <0.05, ** p <0.01 and *** p <0.001. Results represent mean \pm s.d.. % of TD = % of total dosage. i.v. = intravenous injection; p.a. = pharyngeal aspiration; DPI = days post implantation; s.d. = standard deviation..... 130
- Figure 5.11** (a) Accumulation of DOX (free/conjugated form) in the heart at terminal point (DPI17). Therapeutics were given through i.v. or p.a.. Statistical analysis is performed with *one-way analysis of variance (ANOVA) with Tukey's post hoc test*. (b) Temporal effect on accumulation of DOX in the lungs. Therapeutics were given through p.a.. The mice were euthanized at DPI13 (n=3 per group) and DPI17 (n=6 per group). Statistical analysis is performed in 2 different ways: (i) all groups at DPI13 or DPI17 are analyzed with *one-way ANOVA Tukey's test*; (ii) same therapy groups (e.g. DOX p.a.) at DPI13 and DPI17 are analyzed with *Student's t test*. * p <0.05, ** p <0.01 and *** p <0.001. Results represent mean \pm

s.d.. % of TD = % of total dosage. i.v. = intravenous injection; p.a. = pharyngeal aspiration; DPI = days post implantation; s.d. = standard deviation..... 132

LIST OF TABLES

Table 2.1	Characterization of the Cy3-labeled, PEGylated dendrimer conjugates (G3NH ₂ and G3NH ₂ -24PEG1000). Molecular weight (MW), number of PEG grafts (<i>m</i>), size (hydrodynamic diameter, HD), and zeta potential (ζ) as determined by MALDI, ¹ H NMR, UV spectrometry and light scattering (LS).	29
Table 3.1	Molecular weight (MW), number of PEG1000 grafts (<i>m</i>), number of doxorubicin (DOX) conjugates (<i>n</i>), hydrodynamic diameter (HD), and zeta potential (ζ) of the PEGylated, generation 3, amine-terminated PAMAM dendrimer (G3NH ₂) conjugates. DOX conjugated via an acid-labile linker: G3NH ₂ -mPEG-nDOX; DOX conjugated via a non-labile linker: G3NH ₂ -mPEG-nDOXNL. Results obtained by ¹ H NMR, MALDI, and light scattering (LS) at 25°C. s.d. = standard deviation.	58
Table 3.2	Solvated diameter (SD) of the PEGylated (<i>m</i>), generation 3, amine-terminated PAMAM dendrimer (G3NH ₂) conjugates with DOX measured in the model propellant HFPF. DOX conjugated via an acid-labile linker (G3NH ₂ -mPEG-nDOX). Results determined by light scattering (LS) at 25°C and 0.2 mg/mL DOX equivalent. n.p. = not present; % in parenthesis = volume fraction within that diameter range.	72
Table 3.3	Median mass aerodynamic diameter (MMAD), geometric standard deviation (GSD), respirable fraction (RF), fine particle fraction (FPF) and recovery (%) of the pMDI formulation containing the PEGylated (<i>m</i>), generation 3, amine-terminated PAMAM dendrimer (G3NH ₂) dendrimers conjugated with DOX via an acid-labile linker (G3NH ₂ -mPEG-nDOX). Aerosol results determined using the Andersen Cascade Impactor (ACI), at 25°C. Formulation containing 0.2 mg of DOX equivalent per mL of propellant and anhydrous ethanol at 0.37% v/v relative to the propellant. Propellant is HFA227.	75
Table 4.1	Median mass aerodynamic diameter (MMAD), geometric standard deviation (GSD), respirable fraction (RF) and fine particle fraction (FPF) of the pMDI formulations containing acid-labile G3NH ₂ -21PEG1000-3DOX conjugate and LA ₄₆ -EO ₂₃ -LA ₄₆ triblock copolymer surfactants, as determined by Andersen Cascade Impactor (ACI). The formulations were prepared with Method A (no ethanol) and contained 0.2 mg DOX equivalent per mL HFA227 propellant and varying concentrations of LA ₄₆ -EO ₂₃ -LA ₄₆ copolymer (0, 0.12 and 0.53 mM). Statistical significance was performed with respect to the pMDI formulation with 0 mM LA ₄₆ -EO ₂₃ -LA ₄₆ prepared by Method A using one-way ANOVA Dunnett's test with * <i>p</i> <0.05, ** <i>p</i> <0.01, and *** <i>p</i> <0.001. † denotes the formulation was prepared by the Method B, formulations containing anhydrous ethanol at 0.37% v/v relative to HFA227 propellant.	100
Table 5.1	Molecular weight (MW), number of conjugated doxorubicin (DOX) (<i>n</i>), hydrodynamic diameter (HD), and zeta potential (ζ) of generation 4, carboxyl-	

terminated PAMAM dendrimer (G4COOH) conjugate. DOX was conjugated through an acid-labile hydrazone linker. Results obtained by ^1H NMR, MALDI, and light scattering (LS) at 25°C. s.d. = standard deviation.117

LIST OF ABBREVIATIONS

- AC** Actuator
- ACI** Anderson Cascade Impactor
- AIC** Air-interface Culture
- ALN** Axillary Lymph Node
- ATCC** American Type Culture Collection
- AUC** Area under the Curve
- BLN** Bronchial Lymph Node
- CLN** Cervical Lymph Node
- COPD** Chronic Obstructive Pulmonary Disorder
- CS** Chitosan
- Cy3** Cyanine 3
- DAPI** 4',6-diamidino-2-phenylindole, dilactate
- DCC** N,N'-dicyclohexylcarbodiimide
- DCM** Dichloromethane
- DCU** Dicyclohexylisourea
- DOX** Doxorubicin
- DI** Deionized Water
- DLS** Dynamic Light Scattering
- DMF** Dimethylformamide
- DMEM** Dulbecco's Modified Eagle Medium
- DMSO** Dimethyl sulfoxide
- DNCs** Dendrimer Nanocarriers

DPIs Dry Powder Inhalers

EDC 1-ethyl-3-(3-dimethylaminopropyl) carbodiimide

EDTA Ethylenediamine tetraacetic acid

EO Ethylene Oxide

FACS Fluorescence activated cell sorting

FBS Fetal Bovine Serum

FITC Fluorescein isothiocyanate

FPF Fine Particle Fraction

G3NH₂ Generation 3, amine-terminated polyamidoamine dendrimer

G4COOH Generation 3, carboxyl-terminated polyamidoamine dendrimer

GSD Geometric Standard Deviation

HBSS Hank's Balanced Salt Solution

HD Hydrodynamic Diameter

HEPES 4-(2-hydroxyethyl)-1-piperazineethanesulfonic acid

HFA Hydrofluoroalkanes

HPFP 2H,3H-perfluoropentane

HPLC High Performance Liquid Chromatography

IBCF isobutyl chloroformate

IC₅₀ (minimum inhibitory concentration required to kill 50% of viable cells)

IP Induction Port

I.T. Intratrachea

I.V. Intravenous

LA Lactide

LN Lymph Node

MALDI-TOF Mass Assisted Laser Desorption/Ionization – Time of Flight

MFI Mean Fluorescence Intensity

MLN Mesenteric Lymph Node

MMAD Mass Median Aerosol Diameter

MPS Mononuclear Phagocytic System

MTT 3-(4,5-Dimethylthiazol-2-yl)-2,5-diphenyltetrazoliumbromide

MW Molecular Weight

MWCO Molecular Weight Cutoff

NCs Nanocarriers

NHS N-hydroxysuccinimide

NMM N-methylmorpholine

NMR Nuclear Magnetic Resonance

NPs Nanoparticles

OI Oral Inhalation

P.A. Pharyngeal Aspiration

Papp Apparent Permeability Co-efficient

PAMAM Polyamidoamine

PBS Phosphate Buffered Saline

PCC Pearson Correlation Coefficient

PEG Poly(ethylene glycol)

PK Pharmacokinetic

PLGA Poly(d,l-lactide-co-glycolide)

pMDIs Pressurized Metered-Dose Inhalers

PNCs Polymeric Nanocarriers

PNPs Polymeric Nanoparticles

Pro-SPC Pro-Surfactant Protein C

p-TSA para-toluenesulfonic acid monohydrate

PVA Poly-vinyl alcohol

RES Reticulo-Endothelial System

RF Respirable Fraction

SD Solvation Diameter

Sn(oct)₂ Stannous Octoate

TBC Tert-butyl carbamate

TD Total Dose

TEER Transepithelial Epithelial Resistance

UV-Vis Ultraviolet-Visible Light

CHAPTER 1 — INTRODUCTION

1.1 Overviews and Objectives

Cancer is one of the most deadly disease in both men and women throughout the US.[1, 2] An estimated 1.7 million new cases will be diagnosed in 2014, and 600 thousand patients are expected to die of cancer.[1, 2] Among many malignant tumors, lung cancer is of great relevance as it is the leading cause of cancer death. Lung cancers cause more death cases than three most common cancers combined (prostate, breast and colon) (cases of death: 160,340 in 2012, 159,480 in 2013).[1, 2] Lung cancer is mainly divided into two groups: non-small cell lung cancer (NSCLC, 85-90%) and small cell lung cancer (SCLC, 10-15%) [3]. The largest type in NSCLC is adenocarcinoma (50-60%) which is pulmonary neoplasia of epithelial tissues that contains glandular origin and glandular characteristics.[4] Common treatments of lung cancer include surgery, chemotherapy, radiotherapy and all combined. Because of the challenges in early detection of lung cancer, it is usually diagnosed at later stages of the disease, and thus only a small number of patients are eligible for surgery. Even in those cases where surgery is possible, the rate of recurrence is high. Due to most of lung cancers are metastatic, surgical treatment in patients with metastatic lung cancer is also not usually recommended due to the generally poor respiratory and overall clinical profile of the patients. Therefore, chemotherapy is widely used against primary and secondary lung cancers. However, chemotherapeutic strategies have done limited roles to improve therapeutic outcomes for patients with lung cancer, who have a 5 year survival rate after initial prognosis of only 16.6%.[5] One major challenge is the low concentration (2-4% of initial dose) of chemotherapeutics found in the lung cancer spots upon i.v. administration.[6-8] Dose limiting toxicity for chemotherapeutics also limits lung cancer treatment.[9] This problem is complicated as high i.v. dosages are usually required due the poor distribution profile of anti-

cancer therapeutics to the lung tumor.[8] Drug delivery systems of combined chemotherapeutics are promising means to overcome most of issues above such as targeted delivery of chemotherapy agents, dose level increase in neoplastic lesion, sustained drug release and protection of attached cargo from metabolism.[10-18]

Chemotherapy agent, such as doxorubicin (DOX), plays a vital role in cancer treatment. It is also used in conjunction with other treatments such as surgery, radiation therapy and hyperthermia therapy.[19] However, hydrophobic nature of most of chemotherapy agents result in limited aqueous solubility and rapid elimination from blood circulation. Common administration route of chemotherapeutics is intravenous injection which non-specifically distributes DOX to whole body. Systemic distribution, however, does not just significantly reduce local concentration level at lesion, but damage healthy tissues.[20, 21] The accumulation of DOX in the heart results in increased oxidative stress, down-regulated protein function, decreased cardiac gene expression, and up-regulated apoptosis of cardiomyocytes, which eventually leads to lethal cardiomyopathy.[22] Synthetic polymeric nanocarriers (PNCs) have been widely used and validated in anticancer therapeutics delivery, since PNCs are able to protect its cargos from enzymatic degradation, improve pharmacokinetics/pharmacodynamics of therapeutics, promote sustainable drug release and reduce cytotoxicity to healthy tissues.[23-26] Among these PNCs, dendrimer nanocarriers (DNCs) as drug vehicles or scaffolds is one of the most promising frontiers in designing anticancer therapeutics delivery system.[27] In addition to those general strengths of PNCs, hyperbranched polyamidoamine (PAMAM) dendrimer has its own featured advantages as anticancer therapeutics carrier:[28, 29] (i) good water solubility that enhances water solubility of hydrophobic anticancer drugs and peptides; (ii) monodispersity and predictable molecular weight that ensures consistent pharmacokinetics and pharmacodynamics; (iii) high density of reactive

surface groups on dendrimer that empowers dendrimer to enhance therapeutics payload and carry diverse chemical moieties for different purposes at one time;[30-32] (iv) high membrane-penetrating potential that enhances the paracellular transport and intracellular uptake of anticancer therapeutics.[33, 34]

Lungs have a few advantages over invasive and other non-invasive administration routes: (i) large surface area. It is estimated that there are 300 million of alveolar cells in human lungs, which thus leads to 80-90 m² surface area for gas exchange in lungs.[35] Alveolar sacs consist of only one epithelial monolayer, thus facilitating the rapid translocation of molecules from lungs to systemic circulation; (ii) reduced enzymatic degradation. Some drugs (e.g. imipramine,[36] propranolol,[37] and midazolam[38]) can be inactivated by first-pass metabolism which occurs in digestive system and liver. Drug delivery to lungs is one of alternative routes of medication administration that avoids first-pass effect; (iii) high local concentration. Drug delivery to the lungs is especially promising in treating pulmonary disorders such as lung cancer, chronic obstructive pulmonary disease (COPD), and cystic fibrosis (CF), since high local drug concentration, rapid therapeutics action and minimization of systemic adsorption allowing for decreased side effects. Therefore, oral inhalation (OI), an attractive non-invasive route of delivering small molecules and macromolecular therapeutics, has drawn more and more attention as it can reach different pulmonary regions and even systemic tissues.[39, 40] Nebulizers, pressurized metered-dose inhalers (pMDIs), and dry powder inhalers (DPIs) are three major categories.[41, 42] pMDIs are a well-developed aerosol technology and widely accepted by patients due to its portability, straightforwardness in use and enhanced lung deposition of inhaled therapeutics. pMDIs consist of 60% aerosol products in market. However, most of drugs are not soluble in propellant-based pMDIs. The surfactants and/or co-solvents are required to disperse

small drugs. The difficulty in the development of the surfactants restricts the application of pMDIs. Additionally, environmentally unfriendly propellant also limits the use of pMDIs to some extent.[43]

Based on the challenges and opportunities discussed earlier, we propose strategies for treating lung cancers to (i) design polymer-bound DOX conjugates to promote spatial and temporal release—thus decreasing the plasma concentration of free DOX; (ii) modulate the transport of DOX across pulmonary epithelium with nanocarrier surface chemistry manipulation; (iii) enhance the local concentration of DOX in lung tumors upon pulmonary administration, potentially improving therapeutic efficacy and decreasing systemic exposure of DOX; (iv) develop oral inhalation (OI) formulations (pMDIs) for the local delivery to the lung tissue. Such strategies are expected to improve the survival rate and quality of life of the ca. 225,000 people diagnosed with lung cancer per year.[2]

Within the context, the **objectives** of this dissertation are:

Objective #1. Investigate effect of PEGylation and route of administration on systemic and lung regional biodistribution of dendrimer nanocarriers. Chemotherapy is widely used in the fight against primary lung cancers and lung metastasis.[6, 44-46] However, there are several limitations in using chemotherapeutics to treat lung cancers. One major challenge is the low chemotherapeutic concentration found in the lung tumor upon intravenous (i.v.) administration.[6, 7] It is estimated that only a few percent (ca. 2-4%) of the total dose administered i.v. reaches the lung tumor.[8] Dose limiting toxicity is another major issue in the chemotherapeutic treatment of lung cancers.[9] This problem is compounded as high i.v. dosages are usually required due to the poor distribution profile of chemotherapeutics.[8] Nanocarriers have the potential to improve the biodistribution and pharmacokinetic profiles of various therapeutics including anti-cancer

drugs.[47-50] Dendrimers are particularly relevant nanocarrier systems as they have a large number of surface groups amenable to the conjugation of therapeutic molecules and other ligands that allow for different purposes. Direct delivery of drug to the lungs has attracted much attention due to enhanced local drug concentration, fast drug action, and low enzymatic degradation in the lungs. However, a few extracellular barriers that potentially decrease the efficiency of pulmonary delivery includes bifurcating airways, mucociliary escalator, and alveolar macrophage phagocytosis. A few studies have focused on the systemic biodistribution of nanocarriers upon pulmonary administration,[39] including gold nanoparticles,[51] PEGylated polylysine dendrimers,[52] PEGylated poly(ethylene imine),[53] diethylaminopropylamine-poly (vinyl alcohol)-poly (lactide-co-glycolide) copolymer [54] and polystyrene nanoparticles.[55] Meanwhile, PEGylation of PAMAM dendrimer on surface has shown to significantly prolong the residence of nanocarriers in blood circulation and potentially accumulate nanocarriers in solid tumors upon i.v. administration. However, the systemic and local biodistribution of PAMAM dendrimer nanocarriers administered via pulmonary route is still unclear. Therefore, the elucidation of systemic and lung regional biodistribution of PEGylated PAMAM dendrimers is the prerequisite of assessing pulmonary delivery as route of administration for lung cancers. Bare PAMAM dendrimers and fully PEGylated dendrimers were synthesized and characterized. The dendrimer nanocarriers were then delivered to the lungs via pulmonary route. The pharmacokinetics and systemic biodistribution of both dendrimers were characterized by *ex-vivo* imaging and quantified by extracting PAMAM dendrimers from tissues. Lung regional distribution in different cell populations were investigated by specific cell-tagged flow cytometry. As compared, the same dendrimers were injected intravenously to mice and the same experiments

are performed. Detailed studies regarding the systemic and local biodistribution will be further described in the following chapters.

Objective #2 Design PAMAM dendrimer conjugates with temporal and spatial release of doxorubicin for lung cancer treatment. Doxorubicin (DOX) is one of the most effective anti-cancer therapeutics available in the clinic today for treating a variety of cancers including lung tumors.[56, 57] The applicability of DOX is limited, however, partly due to its cardiac toxicity and myelosuppression.[21] The free DOX in bloodstream that gradually accumulates in the heart results in increased oxidative stress, down-regulated protein function, decreased cardiac gene expression, and up-regulated apoptosis of cardiomyocytes, which eventually leads to lethal cardiomyopathy.[22] To address this issue, we designed a nanocarrier-based strategy to promote the maximization of intracellular delivery of DOX to lung tumor cells, and at the same time minimization of systemic exposure of DOX. PAMAM dendrimers are particularly interesting nanocarrier drug delivery systems as they are highly monodispersed (predictable pharmacokinetics/biodistribution) and can be easily functionalized with therapeutic agents through linkages that allow for temporal and spatial control of drug release. Therefore, DOX was conjugated to PAMAM dendrimers with a pH-responsive linker. The linker is only cleavable at mild acidic environment (e.g. lysosomal pH), but stable at extracellular/physiological pH condition. The DOX released in acidic subcellular compartments are then migrated to nuclei to inhibit nuclear DNA synthesis. PEG was also attached to PAMAM-DOX conjugates to prolong the residence of the conjugate in blood circulation and improve biodistribution. The potency of acid-labile PAMAM-DOX conjugates against lung tumors were tested on *in vitro* and *in vivo* models, respectively. The details regarding the design of acid-labile PAMAM-DOX conjugates,

and studies of *in vitro* and *in vivo* potency of these conjugates against lung cancers were described in the following chapters.

Objective #3: Develop pMDI formulations for non-invasive pulmonary delivery of acid-labile PAMAM-DOX conjugates. Since OI has demonstrated its advantages over systemic administration in treating pulmonary disorders. However, the use of pMDI formulations containing polymeric nanocarriers is still relatively unexploited mainly due to strong aggregation of PNCs in propellant. To address the issue, co-solvents and/or surfactants are added to improve dispersibility of PNCs. However, the less volatile/nonvolatile co-solvents and surfactants may reduce aerosol performance, although drug solubility can be improved. We attached PEG chains to dendrimer-DOX on surface for improving the dispersibility of dendrimer conjugates in propellant-based pMDI formulation. Ether bond of PEG has been shown to strongly interact with HFA propellant, aiding the solvation of drug particles in propellant.[58] The effect of PEG density and DOX payload was on the stability formulation and aerosol performance were tested. The addition of biodegradable and biocompatible surfactant were further added to modulate lung deposition of the pMDI formulation for the delivery to various lung regions.

In Chapter 1, we presented the literature review about polymeric nanocarriers for chemotherapeutics delivery, extra and intracellular barriers to pulmonary delivery of chemotherapeutics, and pMDIs for drug delivery via OI administration.

In Chapter 2, we studied the effect of surface PEGylation and routes of administration on systemic and local biodistribution of PAMAM dendrimers. Generation 3, amine-terminated PAMAM dendrimer was labeled with Cy3 probes. The surface of the dendrimers was modified with high grafting density of polyethylene glycol 1000Da (PEG1000). The PEGylation can significantly change the surface chemistry and surface charge, which modulates the interaction of

dendrimers with extracellular and intracellular barriers *in vivo*. The Cy3-labeled dendrimer and PEGylated dendrimer were delivered to the lungs via pharyngeal aspiration (PA) and also through tail intravenous injection (IV). The plasma concentration of dendrimer as a function of time was studied. Major tissues were excised and then imaged for Cy3 fluorescence. To quantify the biodistribution, dendrimers were extracted from tissue homogenates. Furthermore, cellular uptake of dendrimer and PEGylated dendrimers were evaluated based on four major lung cellular populations — myeloid, epithelial, endothelial and ciliated cells. The selected cell populations were tagged with corresponding primary/secondary antibodies and then analyzed with flow cytometry. The chapter is based on the manuscript Zhong Q., Merkel O, Reineke J, da Rocha S.R.P. The Effect of the Route of Administration and PEGylation of Poly(amidoamine) Dendrimers on their Systemic and Lung Cellular Biodistribution. *To be submitted to Molecular Pharmaceutics, 2015.*

In Chapter 3, we discussed the development of PEGylated, acid-labile PAMAM-DOX conjugates and their propellant-based aerosol formulations. A series of PEGylated poly(amidoamine) dendrimer nanocarriers with acid-labile DOX conjugates were synthesized, and characterized with ^1H NMR for chemical composition, MALDI-TOF for molecular weight, light scattering for hydrodynamic diameters and surface charge. We employed a two-step PEGylation strategy to increase the payload of the hydrophobic DOX, while reaching high PEGylation degree which is expected to improve *in vivo* pharmacokinetics and biodistribution. We investigated the impact of pH (neutral and acidic pH), PEGylation density (low, medium and high) and number of DOX conjugates (low and medium) on the release of DOX from the dendrimer nanocarrier, the kinetics of carrier uptake, intracellular release kinetics of DOX from the nanocarrier, and toxicity in an alveolar adenocarcinoma cell line (A549). These dendrimer-DOX conjugates were then

formulated into HFA-based inhalers, forming a pseudo solution formulations which are confirmed by light scattering. The effect of PEG density and DOX payload on the stability were assessed by visualizing the dispersity as a function of time. The aerosol performance of these formulations were assessed by an *in vitro* lung model — Andersen Cascade Impactor (ACI). The chapter is based on the manuscript: **Zhong Q.**, da Rocha S.R.P. Poly(amidoamine) Dendrimer-Doxorubicin Conjugates: In vitro characteristics and Pseudo-Solution Formulation in Pressurized Metered-Dose Inhalers. *Submitted to Molecular Pharmaceutics, 2015*

The modification of amine-terminated PAMAM dendrimers with PEG provides several advantages to the dendrimers. Some of them include, lower cytotoxic potential, enhancement of mucosal transport and increased circulation time. Chapter 4 studied the effect of PEGylation degree and DOX payload on their ability to modulate transport of PAMAM-DOX conjugates across polarized pulmonary Calu-3 monolayers. The role of paracellular pathways in transepithelial transport of dendrimer-DOX conjugates was also investigated. The PEGylated PAMAM-DOX conjugates have been readily formulated in HFA-based formulation with the aid of a trace of ethanol in Chapter 3. We developed another facile co-solvent free method to prepare pMDI formulation containing PEGylated dendrimer-DOX conjugates. The lung deposition position of the aerosol formulations can be modulated by the addition of biodegradable and biocompatible triblock copolymer. The aerosol performance of these formulations containing dendrimer conjugates and triblock copolymers were assessed by an *in vitro* lung model — Andersen Cascade Impactor (ACI). The chapter is based on the manuscript: **Zhong Q.**, Humia B., Punjabi A., da Rocha S.R.P. Design of Dendrimer-Doxorubicin Conjugates for Transport Modulation across in vitro Pulmonary Epithelium and Their Solution Formulation in Pressurized-Metered Dose Inhalers. *To be submitted to Molecular Pharmaceutics, 2015*

In Chapter 5, we assessed the potency of acid-labile dendrimer-DOX conjugates upon pulmonary delivery with a mouse lung tumor model. Poly(amidoamine) dendrimer (PAMAM) with doxorubicin (DOX) conjugated via a pH-labile spacer was synthesized for controlled intracellular release. We investigated pH impact (pH 4.5 = lysosomal pH and pH 7.4 = physiological/extracellular pH) on the DOX release from the dendrimer, and cellular uptake kinetics and cell kill with B16F10 melanoma cells. The *in vivo* lung tumor model was developed by injecting B16F10 melanoma intravenously through tail vein of mouse. 3 doses of therapeutics with 20 µg per dose and one dose every other day were given to tumor-bearing mice through pharyngeal aspiration (pulmonary administration), as well as intravenous injection (i.v.) as compared. The lung tumor burdens at terminal point were evaluated by counting the number of black nodules per lung. The *in vivo* systemic distribution of the PAMAM-DOX conjugate was also quantified by extracting DOX from tissue homogenates. The focus were especially placed on the retention of PAMAM-DOX conjugates in the lungs and accumulation of DOX in heart tissues as a function of time. The chapter is based on the manuscript: Zhong Q., Reineke J., da Rocha S.R.P. Conjugation to Poly(amidoamine) Dendrimers and Pulmonary Delivery Enhances the Antitumor Activity of Doxorubicin in Lung Metastasis. *To be submitted to Journal of Controlled Release, 2015.*

In Chapter 6, we discussed the conclusions drawn from this work and future research suggestions.

1.2 Literature review

1.2.1 Inadequate biodistribution of chemotherapeutics upon i.v. administration

As high enough (therapeutic) doses at the lung tumor site usually cannot be reached without inducing substantial systemic toxicity.[6] For example, the maximum concentration of CIS

administered i.v is limited by strong renal toxicity, which may lead to acute renal failure,[59] while i.v. DOX presents high cardiotoxicity, which may lead to congestive heart failure and death. [60] The concentration of DOX reaching the lung tumor upon i.v. administration has been determined to be as low as 2% of the total dose. [8] This low concentration of chemotherapeutic at the tumor site also contributes to the development of MDR, as cells cancer cells that survive due to low dosages, may become resistant.[61] Local delivery of chemotherapeutics to the lung tissue is a promising alternative to i.v. administration in the treatment in lung cancer.

Direct lung administration of therapeutic agents to the lungs via OI therapy offers several potential advantages, including the delivery of lower dosages compared to i.v., which will lead to reduced systemic side effects, as well as enhancing tumor exposure by improving the retention of the therapeutic agents.[62] Clinical trials show that anti-cancer therapeutics delivered to lung cancer patients as aerosol before surgery appear only in trace concentrations in plasma, and that the drug concentration can be as high as 15x in tumor compared to normal lung tissue.[63] Pre-clinical studies show that the relative concentration of chemotherapeutics in the lungs after pulmonary administration can be 26 fold higher than that after i.v. administration.[64] Inhaled DOX formulated in lipid vesicles and delivered as aerosol from nebulizers show no dose limiting toxicity.[65] The toxicity profile of inhaled DOX in patients with metastatic lung cancer shows pulmonary dose limiting toxicity, but no systemic toxicity.[65] Ongoing clinical trials on inhalation chemotherapy for the treatment of primary or metastatic lung cancer with both DOX also demonstrate the potential of local lung delivery.[66]

1.2.2 Pulmonary extracellular barriers to delivery of therapeutics to/through the lungs

Respiratory airway consists of nose, pharynx, larynx, trachea, bronchi, bronchioles, and alveoli sacs. Since 17th generation of bronchioles, alveoli appear in the wall of respiratory airways

and by 20th generation the entire walls were composed of alveoli — alveoli ducts. The bronchi and bronchioles narrow as the generation increases. Finally, alveoli ducts ends in blind sacs at 23rd generation.[67] As the surface area of alveoli is estimated 80-90 m², lungs are a potentially excellent place to deliver biopharmaceuticals for treating both local and systemic disorders. However, some extracellular barriers restrict efficient pulmonary delivery and deposition in deep lungs, including hyperbranched lung architecture, clearance processes (mucociliary defense) and macrophage-mediated immune response. The deposition of inhaled particle in lungs is assessed by aerodynamic diameter. It is defined as $d_a = d_g \sqrt{\frac{\rho}{\rho_a}}$, where ρ is mass density of the particle, ρ_a is unit density (1 g/cm³) and d_g is geometric diameter.[68] The particle with d_a bigger than 10 μm is deposited on bronchial region away from bronchioles and alveolar area, while the particle less than 1 μm is highly exhalable. Therefore, 1-5 μm is found optimal size for particle to reach respiratory airways and peripheral lungs.[69] However, most of PNCs used for drug delivery is

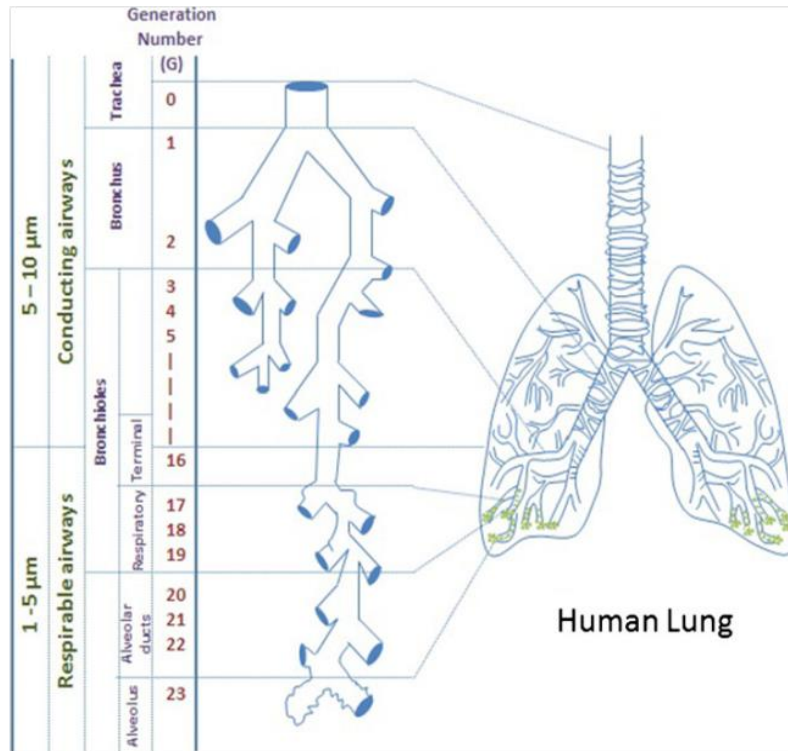


Figure 1.1 Diagram of the human lungs and particle deposition based on size.[57]

smaller than $1 \mu\text{m}$, hence PNCs formulated into micron-sized particle is necessary for efficient deposition on respiratory airways and entry into lungs.

The respiratory airways from nose to terminal bronchioles are covered by mucus layer which is composed of mucin glycoproteins, cells, bacteria, lipids, salts, proteins and cell debris.[70, 71] The miscellaneous components act together to form a nanoscopically heterogeneous environment to prevent the transport of foreign particulate across respiratory airways.[72] The PNCs to cross mucus layer are hindered by (i) size-dependent diffusion. It is reported that average pore size for particle penetration was to be 100 nm :[73-75] (ii) strong electrostatic interaction with positively and negatively charged components. Therefore, the PNCs must be shielded by hydrophilic and neutral macromolecules; (iii) rapid mucociliary clearance. The luminal mucus

layer of respiratory tract is renewed every 10 to 20 min, leading to efficient clearance of invading particles.[76]

1.2.3 Pressurized metered-dose inhalers (pMDIs) as oral inhalation for pulmonary delivery

In lung cancer treatment, current route to administer DOX is i.v. injection which results in non-specific systemic distribution. The non-specific whole body distribution lowers dose level at pulmonary cancerous lesion, but increases side effect to normal tissues. In contrast, oral inhalation is a promising non-invasive approach to efficiently deliver anticancer therapeutics to the lungs, since it may retain high drug dose in pulmonary area and thus lowers side effect.[77] OI technique can be broken into three major categories: nebulizer, pressurized metered-dose inhalers (pMDI), and dry powder inhalers (DPI).[41, 42] Generally, nebulizers can produce small particles (2-5 μm) that penetrate airways, deposit on deep lungs easily, and deliver large doses of aerosol with little requirement of patient skills. Inconvenience in handling and considerable sedimentation of particles on oral cavity, larynx, and trachea result in large waste of delivered drugs.[43] pMDIs are a well-developed aerosol technology and widely accepted by patients due to its portability, straightforwardness in use and enhanced lung deposition of inhaled therapeutics. pMDIs formulations can be divided into two types: solution formulation and suspension formulation. The drugs completely dissolved in the propellant can be formulated into a solution formulation,[78, 79] while the drugs practically insoluble is dispersed in the propellant to make a suspension formulation and create a heterogeneous system.[80-82] Compared to suspension formulation, the solution formulation of pMDIs can give rise to a homogenous formulation without shaking prior to use, a larger fine particle dosage [83] and finer residual aerosol.[84] However, many drugs and PNCs are not readily soluble in propellants, limiting the amount of drugs that can be used in pMDIs formulations. Cosolvents and surfactants, such as PEG, Span 20, Tween 80 and Pluronic block

polymer, are widely added to help increase the solubility of the insoluble drugs.[78, 85] However, aerosol characteristics may be attenuated by the addition of surfactants and/or cosolvents as they evaporate more slowly in atomized droplets. Therefore, the dispersion of drug crystals in propellant and difficulties in screening of surfactants and co-solvents significantly limit the use of pMDIs. Additionally, the transition from ozone-depleting propellant such as chlorofluorocarbon (CFC) to more environment-friendly substitutes such as hydrofluoroalkanes (HFA) can cause complicated issues due to the strong effect of thermodynamic properties of propellants on solubility of drug crystal and PNCs [86].

1.2.4 Doxorubicin as leading anticancer therapeutics in lung cancer treatment

Doxorubicin (DOX) is an anticancer chemotherapeutics that was first isolated from *Streptomyces peucetius* in 1967.[87] Today DOX is a leading therapeutic in clinical oncology, having a broad range of activity against both solid and “liquid” tumors.[88] DOX is used in the treatment of several cancers, including breast, ovarian, lung, sarcoma, acute lymphoblastic and myeloid leukemia.[89] DOX is also used in pediatric oncology.[90, 91] Since the discovery of DOX, thousands of other anthracyclines have been screened for their anticancer properties, but only few have emerged as clinically relevant.[92] The lasting relevance of DOX in the fight against malignant tumors is also demonstrated by the fact that DOX shows up in over 1,500 clinical trials currently listed in the US NIH registry.[93] There are two proposed mechanisms in which DOX works: (i) inhibition of topoisomerase-II-mediated DNA repair by intercalating DNA; (ii) generation of free radicals that rupture cellular and subcellular membrane structure.[94, 95] It was reported that the transport of DOX across cellular membrane was through simple diffusion due to electrostatic binding to anionic phospholipid on membrane and direct insertion of hydrophobic chromophore into lipid layer.[95-97] While nuclear DNA is the most studied DOX, DOX has also

shown to have mitochondrial activity and this action has been shown to promote apoptosis, even in MDR cells.[98-100] However, the entire mechanism of how DOX interacts with various processes in the mitochondria is not yet known.[101, 102] Short term incubation of DOX with cancerous cells brought about rapid changes in mitochondrial function including changes in mitochondrial redox potentials towards an increased oxidative state, depolarization of the inner mitochondrial membrane, increased matrix calcium levels, and increased mitochondrial ROS production.[103] Long-term effects include an inhibition of respiration, ATP depletion, and increased production of proteins association with cell cycle arrest and cell death.[103] DOX's ability to intercalate with DNA may affect the integrity of mitochondrial DNA, which could also contribute to a decrease in electron transport chain complexes.

1.2.5 Polymeric nanocarriers (PNCs) for targeted intracellular DOX delivery

DOX is an anticancer therapeutics widely used in cancer chemotherapy. DOX is administered intravenously in the form of its hydrochloride salt. Since DOX administered via i.v route is distributed non-specifically in the body, affecting both tumor tissues and healthy tissues. Such non-specific distribution leads to insufficient dose in tumor and severe toxicity to normal tissues. More importantly, the damage of DOX to heart tissue can cause life-threatening cardiac toxicity. To improve therapeutic efficacy of DOX, several drug delivery systems based upon polymer nanoparticles,[104-109] liposomes,[71, 109, 110] monoclonal antibodies,[111] polymer conjugates, [34, 112-116] and polymer micelles[117] have been extensively employed. DOX is either physically encapsulated in or covalently bound to polymeric matrices. Polymer-based DOX delivery systems, by using both passive and active targeting strategies, can enhance extracellular or intracellular concentration of DOX in tumor cells whereas avoiding toxicity to normal tissues. The encapsulation of DOX into liposomes, polymer micelles and polymeric nanoparticles is an

effective strategy to increase DOX payload, enhance cellular uptake, and improve pharmacokinetics. The biodistribution of liposomal DOX and DOX-entrapped PNCs have shown

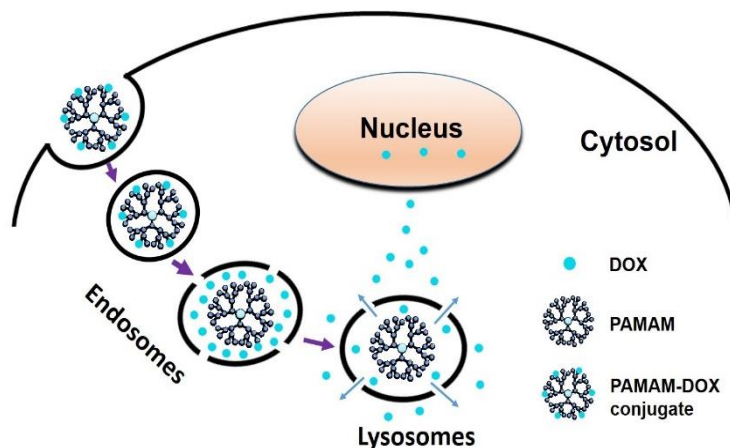


Figure 1.2 Schematic representation of intracellular release of Polymer-DOX conjugates (e.g. polyamidoamine-PAMAM). The conjugates are internalized by endocytosis into endosomes and then end up in lysosomes. DOX is released from polymer-DOX conjugates with pH-sensitive linkers broken as pH drops to 5.0-4.5 in lysosomes. Released DOX subsequently moves out of lysosome towards nucleus.

higher dose level in tumor and inhibition of tumor growth due to EPR effect [118] and specific targeting.[119] However, they are still flawed on inconsistent drug payload, weak particle stability and limited controllability of drug release. Therefore, an alternative strategy where DOX is conjugated to polymer via a labile linkage has been developed. The protruding advantage of the conjugate is to achieve reliable sustained drug release. In analogous to DOX-entrapped PNCs, EPR effect and active targeting strategy facilitate polymer-DOX conjugates to accumulate in tumor vasculature and are internalized to tumor cells by endocytosis (receptor-mediated, adsorptive, and fluid phase endocytosis). Subsequently, the polymer-DOX conjugates end up in acidic endosome (pH 6.0-5.0)/lysosome (pH 5.0-4.5) [120, 121] where DOX is released from polymer by non-specific pH-controlled hydrolysis [23, 113, 122] or specific enzymolysis [123, 124] shown in Figure 1. Of the labile bonds, cis-aconitic spacer,[115, 125] hydrazone,[115, 126]

and Gly-Phe-Lys-Gly peptide sequence [127, 128] have been mostly used for preparation of polymer-DOX conjugates.[129] These linkers are sensitive to lysosomal pH or enzymes while are maintained stable at extracellular environment. Furthermore, the polymer-DOX conjugate also showed higher cytotoxicity against cancer cells than bare DOX *in vivo* experiment.[130, 131] Therefore, the selective intracellular release of DOX can be accomplished by polymer-DOX conjugates with pH-sensitive or enzyme-degradable linkers.

1.2.6 PEGylation of PNCs help overcome pulmonary extracellular barriers and improve biodistribution

Apart from controlled intracellular release and effective tumor selectivity, other challenges of PNCs-based drug delivery systems include limited hydrophilicity, short blood circulation residence, and strong serum protein binding and particle aggregation. The modification of PNCs with biocompatible and hydrophilic polymer is an effective strategy to solve those challenges. One of the most widely accepted polymers for this modification is polyethylene glycol (PEG) which has been approved by Food and Drug Administration (FDA).[132] It bears an array of attributes: neutral molecule, very low toxicity, excellent solubility in aqueous solution, non-immunogenicity, and no detrimental influence on protein conformation or enzymes activities.[133] PEGylation of PNCs-DOX has been widely studied at both *in vitro* and *in vivo* level. The overall charges on PNCs surface can be significantly masked after PEGylation such as PLA-PEG,[134] PAMAM-PEG,[34] and polylysine-PEG nanoparticles,[52] leading to weak serum protein binding and decreased cytotoxicity and immunogenicity. Furthermore, PEGylated PNCs showed prolonged blood circulation residence, thus resulting in improved pharmacokinetics and less drug administration frequency. [113, 135, 136] However, PEGylated nanocarriers are also known to be less efficiently taken up by the cells.[137] Therefore, a balance between overall charges of PNCs,

size of PEG chains, and PEG density must be modulated in order to maximize the potency of anticancer therapeutics.

1.2.7 Development of in vivo lung cancer murine model

The in vivo preclinical evaluation of new chemotherapeutics for cancer therapy requires relevant and appropriate animal models mainly including subcutaneous and orthotopic xenograft tumor models. Each model has its advantages and disadvantages. Subcutaneous xenografts are very convenient way to implant tumor cells, and the consequent tumors are palpable and easy to quantify the tumor growth. However, orthotopic xenograft models provide an accurate representation of tumor microenvironment as cells are implanted directly into the organ in which the disease originates. This allows for a reliable prediction of toxicity and understanding of microenvironment-dependent responses to selected therapies, thereby leading to more reliable translation to clinical cases.[138] The most practical orthotopic lung tumor models involves the endobronchial inoculation of A549 and H460 cell lines into athymic NCr nu/nu mice.[139] Despite the benefits of orthotopic models, the development of these models are quite time-consuming and challenging as cells typically conducted endobronchially, requiring precision and practice. Additionally, once tumors start proliferation, it is more difficult to handle and quantify their growth than in traditional xenograft models. Besides primary lung cancers, pulmonary metastasis model is the other widely used model for evaluating therapy in many tumors. Essentially, all tumors upon intravenous injection can be found in the lungs and the resulting pulmonary metastatic nodules are technically viewed as an independent primary tumor rather than a metastasis.[140] B16 melanoma is transplantable tumor that originated from C57BL/6 mice. The strain F10 of B16 melanoma (B16-F10) characterized by its robust ability to colonize in the

lungs has been widely used to develop pulmonary metastasis upon intravenous injection of melanoma cells.[141-143]

1.3 Relevance and Innovation

This work is greatly relevant and innovative in a few aspects. Since DOX is one of the most important chemotherapy for various lung cancers, the design of advanced DOX delivery system and its efficient delivery to lungs via OI are very attractive. This is the first time for (i) the elucidation of systemic and local biodistribution of PAMAM dendrimers via pulmonary delivery and effect of PEGylation on these aspects; (ii) development of a novel strategy for lung cancer treatment, which combines pulmonary delivery with PEGylated PAMAM dendrimer with DOX conjugated via an acid-labile linker. The developed strategy can significantly increase local dose of DOX in the lungs, while reduce the accumulation of DOX in heart tissues; (iii) polymer nanocarrier drug delivery system is formulated into propellant-based inhalers, forming a pseudo solution aerosol formulation. This research will contribute to designing novel dendrimer therapeutics delivery system that may be employed in the treatment of lung cancer, as well as provide a potential platform for other pulmonary disease treatment such as tuberculosis, and asthma. Finally, the research is also valuable on subsequent formulation in inexpensive inhalation devices.

CHAPTER 2 — The Effect of the Route of Administration and PEGylation of Poly(amidoamine) Dendrimers on their Systemic and Lung Cellular Biodistribution

2.1 Introduction

Pulmonary administration is an attractive and effective route for the non-invasive delivery of small molecule drugs and biomacromolecules for the treatment of lung disorders such as asthma, chronic obstructive pulmonary disease (COPD) and cystic fibrosis.[144-149] Oral inhalation (O.I.) also has several notable advantages when compared to intravenous (I.V.) and other non-invasive administration routes (e.g. nasal and oral) with respect to the systemic delivery of therapeutics *through* the lungs that arise due to the large total surface area for drug absorption, the avoidance of first-pass metabolism and the potentially rapid therapeutic onset.[35, 150]

In spite of the many potential advantages in the local or systemic delivery of drugs to and through the lungs, there is a notably small number of commercial O.I. products, and only very few classes of drugs are formulated as O.I.. Those include adrenocorticoid steroids (e.g. beclomethasone), bronchodilators (e.g. isoproterenol, metaproterenol, albuterol), antiallergics (e.g. cromoglicinic acid), and inhalable insulin for diabetes (Afrezza®).[151]

There are, therefore, many opportunities for further development in the pulmonary drug delivery market. Advances in the formulation of portable aerosol systems and the ability to develop innovative nanotechnologies capable of modulating the interaction between the therapeutic agents and the local physiological environment [39, 51, 52, 55, 152-154] are both expected to support and accelerate the development of O.I. formulations. New formulations have a broad application range such as the many therapeutics that are under clinical trials for local and systemic delivery to/through the lungs.[57, 155-159]

Dendrimers represent a promising class of nanocarrier systems for the delivery of small molecule therapeutics and biomacromolecules.[113, 160-163] Dendrimers are hyperbranched polymers that are highly monodisperse and possess a high density of functionalizable surface groups.[31, 164, 165] A particular class of dendrimers, those with a polyamidoamine (PAMAM) architecture, has received a lot of attention in the literature, particularly those with amine-terminated (NH₂) surface groups. These dendrimers can be obtained and functionalized with therapeutics and other ligands and have the ability to efficiently gain access to the intracellular milieu.[166] Toxicity [167] and rapid clearance [168, 169] of unmodified NH₂ PAMAM dendrimers have somewhat reduced the excitement towards these carriers. However, surface modification of such dendrimers with polyethylene glycol (PEG), also called PEGylation, has been shown to be one effective strategy in the development of dendrimer nanocarriers with reduced toxicity,[167] improved pharmacokinetic (PK) profiles,[168, 169] and improved aqueous solubility. The latter becomes a major issue upon conjugation of hydrophobic therapeutics such as doxorubicin to such nanocarriers.[170, 171]

The tissue distribution and PK of PEGylated PAMAM dendrimers have been extensively studied *in vivo* upon I.V. administration, and the results suggest significantly decreased toxicity,[172] prolonged systemic circulation,[172, 173] and effective accumulation in target tissues through passive [34] and active targeting strategies.[174] Meanwhile, a few studies have focused on the systemic biodistribution of nanocarriers upon pulmonary administration,[39] including gold nanoparticles,[51] PEGylated polylysine dendrimers,[52] PEGylated poly(ethylene imine),[53] diethylaminopropylamine-poly (vinyl alcohol)-poly (lactide-co-glycolide) copolymer [54] and polystyrene nanoparticles.[55] However, few attempts have been made on the systemic distribution of PAMAM dendrimers and their PEGylated counterparts upon pulmonary

administration. Additionally, the distribution of PAMAM dendrimers amongst different cell types of the lung upon pulmonary administration has not been reported yet. Such results are of great relevance for the ability to passively target various tissues by simply tuning the chemistry of the nanocarriers. This knowledge will help guide the design of such nanocarriers for targeting different diseases both in terms of systemic distribution and lung cellular distribution. For example, knowledge on the distribution to lymph nodes may help us design improved vaccine delivery systems,[175] while alveolar macrophage targeting may provide us a way to develop new strategies for the treatment of pulmonary tuberculosis.[176, 177]

The goal of this work is to investigate the systemic and local biodistribution of amine-terminated PAMAM dendrimers upon lung delivery, and the effect of PEGylation on their distribution profile. We have selected generation 3, amine-terminated PAMAM (G3NH₂) and 1000Da PEG (G3NH₂-PEG1000) for this study. The pharmacokinetic parameters of the bare dendrimer and highly PEGylated dendrimer were investigated *in vivo*, upon lung delivery and benchmarked against the profiles obtained upon I.V. administration. The systemic biodistribution was qualitatively determined by *ex vivo* imaging, and quantitative characterization was achieved by tissue extraction of the dendrimer conjugates. The local distribution of dendrimer conjugates in different pulmonary cell populations was quantified using cell tagging and flow cytometry. The results help us understand how the chemistry of such carrier systems may be used to target different tissues and cell populations, and thus serve as a guide for the design of new dendrimer-based carriers for the spatially and temporally controlled delivery of a variety of therapeutics for the treatment of lung and systemic disorders upon O.I. administration.

2.2 Materials.

Generation 3, amine-terminated, poly(amido amine) (PAMAM) dendrimers (G3NH₂), with 32 -NH₂ surface groups and theoretical molecular weight of 6909 was purchased from Dendritech, Inc (Midland, MI). Cyanine 3 (Cy3) NHS ester was purchased from Lumiprobe Corporation (Hallandale Beach, FL). Polyethylene glycol 1000Da (PEG1000) succinimidyl ester (PEG1000-SC) was purchased from NANOCS Inc (New York, NY). Paraformaldehyde solution 4% in PBS, saponin, dispase, and 10 kU heparin sodium salt from porcine intestinal mucosa were purchased from Sigma-Aldrich (St Louis, MO). Sodium phosphate (dibasic, anhydrous) and sodium phosphate (monobasic, monohydrate) were purchased from EMD Chemicals, Inc (Gibbstown, NJ). Deuterium oxide (D₂O, D: 99.9%) was purchased from Cambridge Isotope Laboratories (Andover, MA). Rat anti-mouse CD16/CD32 monoclonal antibody (Fc blocker) was provided by Thermo Fisher (Waltham, MA). PerCP-Cy5.5 labeled anti-CD45 (30-F11) and PE-labeled anti-CD31 were purchased from EBioscience (San Diego, CA). A primary anti-prosurfactant protein C antibody (pro-SPC) (1:100) and a primary anti-tubulin antibody (1:100) were obtained from abcam (Cambridge, United Kingdom). Alexa Fluor®647 F(ab')₂ goat anti-mouse IgG secondary antibody (1:100) and pacific blue F(ab')₂ goat anti-mouse IgG secondary antibody (1:100) were purchased from Life Technologies (Grand Island, NY). Falcon cell strainers with mesh size 100 µm were obtained from Thermo Fisher Scientific (Waltham, MA). Ultrapure deionized water (DI H₂O) was obtained with the Barnstead NANOpure DIamond System (D11911) from Thermo Fisher Scientific (Waltham, MA). Amicon® Ultra 15 centrifugal filters (MWCO=3kDa) were purchased from EMD Millipore (Billerica, MA). Thin layer chromatography (TLC) Silica gel 60 F₂₅₄ plastic sheet was purchased from Merck KGaA (Darmstadt, Germany). All reagents were used as received unless otherwise specified.

2.3 Methods

2.3.1 Cy3 labeling of PAMAM dendrimer (G3NH₂-Cy3)

G3NH₂ (27.2 mg, 3.94 μmol) was dissolved in 3.0 ml phosphate buffer solution (0.2 M, pH 8.4). A 0.5 ml dimethylsulfoxide (DMSO) of Cy3 NHS ester (7.29 mg, 12.35 μmol) was added dropwise to the above aqueous buffer. The reaction mixture was stirred for 2h at 4°C and another 4h at room temperature. The unreacted Cy3 was removed using centrifugal filter device (MWCO=3kDa) until TLC showed no free Cy3 in the product. The product was lyophilized and then stored at 4°C for further use. The resulting structure of the G3NH₂-Cy3 (number of Cy3 conjugated to the dendrimer) was determined using proton nuclear magnetic resonance (¹H NMR) and mass-assisted laser desorption/ionization-time of flight (MALDI-TOF). ¹H NMR (DMSO-d₆, ppm) spectra and peak assignment and MALDI spectra are provided in the Figure S1 of *Supplemental Information in Appendix 1*. The ratio of Cy3 to dendrimer was also determined using UV spectrometry. The UV spectra of Cy3-labeled dendrimer were recorded using Varian Cary® 50 UV-Vis spectrometer (Santa Clara, CA). The concentration of Cy3 was calculated using Beer-Lambert law $A = \epsilon bc$ to quantify the ratio, where molar absorptivity ϵ at 555 nm is 150,000 L·mol⁻¹·cm⁻¹, path length of quartz cuvette b is 1 cm, and c is concentration of sample with mol·L⁻¹ as unit. The result was compared with the data from ¹H NMR and MALDI.

2.3.2 Synthesis of PEGylated PAMAM dendrimers (G3NH₂-PEG1000-Cy3)

The resulting Cy3-labeled G3NH₂ (15.2 mg, 1.84 μmol) was dissolved in 3.0 ml phosphate buffer (0.2 M pH 8.0). A 1 ml anhydrous p-dioxane of PEG1000-SC (56.2 mg, 55.2 μmol) was added to the above aqueous buffer. The reaction was stirred for 2h at 0°C, and another 4h at room temperature. The unreacted PEG1000 was removed using a centrifugal filter device (MWCO = 3kDa). The resulting PEGylated dendrimer (G3NH₂-PEG1000-Cy3) was lyophilized and then

stored at 4°C for further use. ¹H NMR (DMSO-d₆, ppm) spectra and peak assignment, and MALDI spectra are provided in the *Supplemental Information in Appendix 1*.

2.3.3 Size and Surface Charge of the Conjugates.

The hydrodynamic diameter (HD) and zeta potential (ζ) of bare and PEGylated dendrimer conjugates were measured using a Malvern NanoCS Zetasizer (Malvern Instruments; Worcestershire, UK). The sample (1.0 mg/ml) was dissolved in DI H₂O. The aqueous suspension was equilibrated for 120 s before measurement, and the Mitoschi model was used as scattering model. The average values and standard errors of HD ($n \geq 14$) and ζ ($n \geq 50$) were statistically calculated using the built-in software.

2.3.4 Pulmonary administration of the dendrimer conjugates

Pulmonary delivery of the bare and PEGylated Cy3-labeled dendrimers was performed using the pharyngeal aspiration (P.A.) technique.[55] Briefly, male balb/c mice (25 g, 10-12 weeks old) were deeply anesthetized with 2.5% v/v isoflurane/oxygen and then placed on a tilted board in a supine position. The tongue was held gently in extension while a 50 μ l saline solution of G3NH₂-PEG1000-Cy3 (4.09 mg/ml) or G3NH₂-Cy3 (1.03 mg/ml) conjugate – same total G3NH₂ concentration - was gradually dripped in the pharynx region with a micro syringe. The tongue was continuously held until after a few breaths. As the whole solution was administered, the mice were left under anesthesia for 5 min and returned to the cage for monitoring of rapid recovery. The P.A. technique has comparable effectiveness to intratracheal instillation, while less invasive, and also allows for the delivery of high dosages.[178]

2.3.5 Pharmacokinetics (PK) of the administered dendrimer conjugates

After the administration of dendrimer conjugates, blood samples were collected at predetermined time points (0.25, 0.5, 1, 3.25 and 6.5 h). A volume of 80 μ l of blood collected

from tail vein was mixed with 20 μ l of heparin saline (10 U/ml). The mixture was centrifuged at 5000 rpm for 45 s, and the plasma obtained was pulsed into a flat bottom 96-well plate for Cy3 fluorescence determination using BioTek Synergy HT multi-code microplate reader (Winooski, VA, US).

2.3.6 Systemic biodistribution of the administered dendrimer conjugates

The mice were sacrificed 6.5 h after the administration of the conjugates. This time point is based on our previous experience where we measured the PK profile for G3NH2 in the same model by using the same route.[168] The various tissues were excised and washed with saline, including axillary lymph nodes (ALN), bronchial lymph nodes (BLN), cervical lymph nodes (CLN), mesenteric lymph nodes (MLN), thymus, brain, heart, liver, lungs, kidneys, stomach and spleen. The residual saline was wiped off using a filter paper, and the excised tissues were immediately used for analysis. We bench-marked our studies by delivering the same dose of dendrimer conjugates I.V. through the tail vein. These mice were sacrificed, harvested and samples analyzed in the same manner as the pulmonary study groups.

2.3.7 Ex-vivo imaging of excised tissues

The excised tissues were visualized using a Carestream In Vivo Xtreme (Rochester, NY, US) imaging system (Excitation/Emission: 555/571 nm). The exposure time was set to 30 s. Visible light and Cy3 fluorescence images were taken and overlaid using the manufacturer's software.

2.3.8 Quantification of dendrimer conjugates in tissues

The excised tissues were fully homogenized using a Cole-Parmer LabGEN 7 Series Homogenizer (Vernon Hills, IL) in a 3 ml aqueous solution of 3 N sodium hydroxide (NaOH) and the dendrimer conjugates were then extracted for 72 h at room temperature in darkness. The

extracted dendrimer conjugates were collected by centrifugation (14,000 g, 10 min) at 4°C. The amount of dendrimer conjugates in each tissue was quantified according to established calibration curves in the corresponding tissue. Briefly, the tissue was spiked with a known amount of G3NH₂-Cy3 or G3NH₂-24PEG1000-Cy3 and the extracted as described above. The fluorescence intensity was plotted as a function of the amount of G3NH₂-Cy3 or G3NH₂-24PEG1000-Cy3.[179]

2.3.9 Single cell staining for pulmonary cellular biodistribution of the nanocarriers

Pulmonary myeloid cells, alveolar epithelial cells, endothelial cells and ciliated airway epithelial cells were stained by probe-labeled antibodies and then analyzed with flow cytometry following a reported method with modifications (See *Supplemental Information in Appendix I*).[180] Briefly, the excised lungs were ground gently and incubated with dispase and DNase to break extracellular matrix. The resulting homogenate was filtered with 100 µm nylon cell strainers. The obtained cells were fixed with 4% paraformaldehyde solution and then incubated with 0.15% saponin buffer for permeabilization at 4°C. Subsequently, the cells were incubated with Fc-blocker for 20 min and then stained with the probe-labeled antibodies against CD45, CD31, pro-SPC and β-tubulin for another 25 min at 4°C in darkness. The stained cells were analyzed with a BD Bioscience BD LSR II Analyzer (San Jose, CA, US). Data analysis was performed with TREESTAR FlowJo software (Ashland, OR, US). Cells were sorted in two ways: those that contained and those that did not contain internalized dendrimer conjugates. Secondly, from those that contained dendrimer conjugates, the fraction of myeloid (CD45), (alveolar) epithelial (pro-SPC), endothelial (CD31) and ciliated (β-tubulin) cells was determined. Studies were performed for both G3NH₂-Cy3 and G3NH₂-PEG1000-Cy3 conjugates, so that the effect of chemistry could also be assessed.

2.3.10 Statistical analysis

Graphpad Prism 5 was used to perform the statistical analysis. Data were compared using Student's t test. Means were considered statistically significantly different with a **p* value <0.05.

2.4 Results and discussion

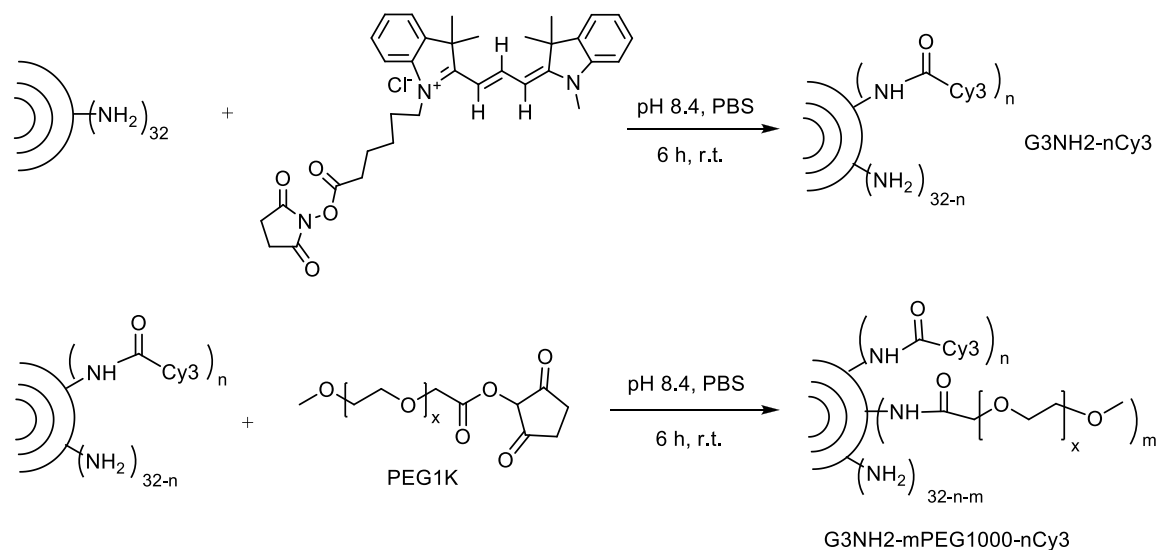


Figure 2.1 Schematic diagram of the synthesis of the Cy3-labeled, PEGylated dendrimer conjugates. The Cy3 terminology is dropped in the results and discussion part. For simplicity, the conjugates are referred to G3NH2 and G3NH2-*m*PEG1000, where *m* is the number of PEG 1000Da graft moieties – the number of Cy3 is the same for all conjugates. r.t. = room temperature

2.4.1 Synthesis of PEGylated dendrimer conjugates

Table 2.1 Characterization of the Cy3-labeled, PEGylated dendrimer conjugates (G3NH2 and G3NH2-24PEG1000). Molecular weight (MW), number of PEG grafts (*m*), size (hydrodynamic diameter, HD), and zeta potential (ζ) as determined by MALDI, ^1H NMR, UV spectrometry and light scattering (LS).

Compound	MW (Da)	<i>m</i>		<i>n</i>			HD \pm s.d (nm)	ζ \pm s.d (mV)
		MALDI	NMR	MALDI	NMR	UV		
G3NH2 (as received)	6900	0	0	0	0	0	+3.8 \pm 1.3	+18.8 \pm 5.0
G3NH2	8285	0	0	3.1	3.3	2.8	+5.1 \pm 1.4	+24.5 \pm 6.9
G3NH2-24PEG1000	33312	24.5	23.9	3.1	3.3	2.8	+9.9 \pm 3.6	-3.7 \pm 5.0

Both Cy3 labeling and PEGylation were performed using a primary amine/NHS ester chemistry, resulting in the formation of an alkyl amide bond in each case, which is a bond known to be stable under both *in vitro* and *in vivo* conditions.[181] The synthetic route is shown in Figure 2.1. The first step in the preparation of the conjugates was to label G3NH₂ with Cy3 before PEGylation to guarantee the same number of Cy3 molecules on both the non-PEGylated and PEGylated dendrimers. The ¹H NMR with peak assignments and the MALDI spectra are shown in the *Supporting Information in Appendix 1*. The NMR peaks at 7.614-7.163 ppm, 6.476 ppm, 1.509 ppm, and 1.353 ppm indicate successful conjugation of Cy3 to G3NH₂. Similarly, the molecular weight shift in MALDI from 6900 Da to 8285 Da after Cy3 tagging, also confirm the successful conjugation of Cy3. The UV spectrometry is also used to quantify the ratio of conjugated Cy3 to dendrimer due to the Cy3 absorption at 555 nm. As shown in Table 2.1, an average of ca. 3 Cy3 molecules was conjugated per dendrimer as determined (in close agreement) by ¹H NMR (3.3), MALDI (3.1) and UV spectrometry (2.8).

Subsequently, dendrimers with a high PEG density were prepared by reacting G3NH₂-Cy3 with PEG1000 succinimidyl ester. The ¹H NMR peak at 4.02 ppm revealed the successful conjugation of PEG1000 to dendrimer-Cy3 with an amide bond. ¹H NMR and MALDI were also used for quantification of PEG1000 density, revealing an average of 23.9 and 24.6 PEG1000/dendrimer, respectively.

The size and surface charge of bare dendrimer and PEGylated dendrimer conjugates were determined by light scattering (LS). Compared to the bare dendrimer, the size of G3NH₂-Cy3 increased only slightly to 5.1 nm, while at high PEG density the HD of the dendrimer increased dramatically, to nearly 10 nm. This increase may be attributed to the stretching of the densely packed layer of PEG1000.[182] The surface charge of G3NH₂-3Cy3 was seen to be even more

cationic than the bare dendrimer due to the introduction of tertiary amines of Cy3, which have a stronger electron donating capacity. Even though a primary amine from the dendrimer was used up in the conjugation of each Cy3 molecule, two tertiary amines were brought into the conjugate per Cy3. In contrast, the surface charge of the dendrimer was reversed upon PEGylation, resulting in a slightly negative charge. The change in ζ upon PEGylation was in good agreement with a previous report.[168] These two carriers are thus different in two very important ways: their surface charge (one is positive and the other negative/neutral) and their size (PEGylated dendrimer is twice as big as non-PEGylated). The PEGylation of the nanocarriers is expected to prolong their residence in systemic circulation and reduce nanocarrier toxicity.[168, 169, 183] The surface charge of the conjugates and their size is also expected to impact their transport across the extracellular/apical barriers of the lung tissue,[39, 41, 168, 184] whose gap junctions are in the order of 3 nm.[185, 186]

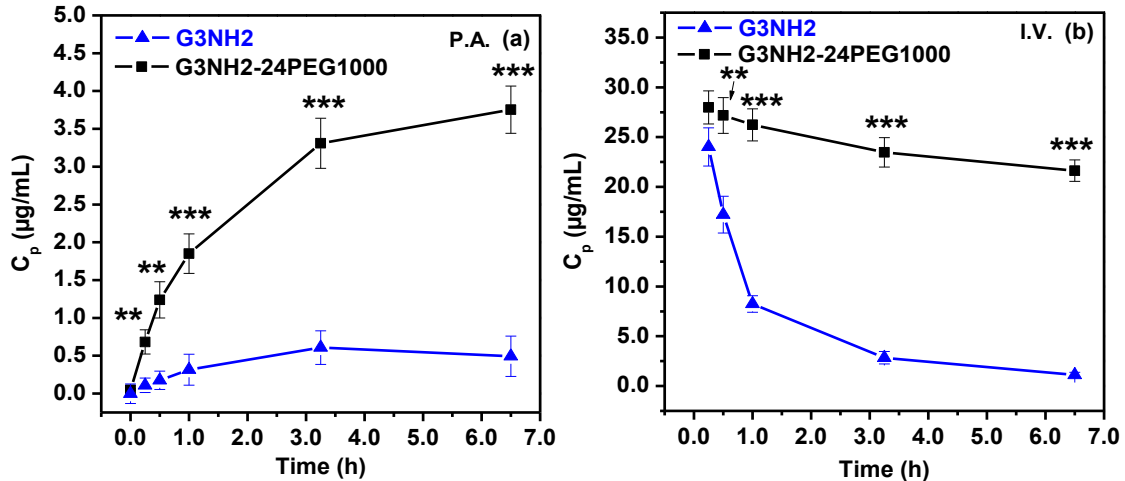


Figure 2.2 Plasma concentration (C_p) as a function of time after administration of G3NH2 and G3NH2-24PEG1000 via (a) pharyngeal aspiration (P.A.) and (b) intravenous injection (I.V.) (n=3 per group). The statistical analysis was performed between G3NH2 and G3NH2-24PEG1000 with Student's t-test (*p < 0.05, **p < 0.01, and ***p < 0.001).

For simplicity, in the following discussion “Cy3” will no longer be mentioned when describing the conjugate structures – the conjugates will be referred to simply as G3NH₂ or G3NH₂-PEG1000.

2.4.2 Plasma concentration profiles of dendrimer conjugates administered via pulmonary and I.V. routes.

The plasma concentration-time profiles of the bare dendrimer (G3NH₂) and highly PEGylated dendrimer (G3NH₂-PEG1000) following pulmonary (P.A.) and intra-venous (I.V.) administration are summarized in Figure 2.2.

The plasma concentration of dendrimer conjugates delivered via the pulmonary route (Figure 2.2a) is seen to increase soon after administration. For G3NH₂-24PEG1000, it levels off at 3.25 h post administration (plasma concentration not statistically different at 3.25 h and 6.5 h), while for G3NH₂, a peak is reached at 3.25 h (plasma concentration at 6.5h significantly lower than at 3.25 h). The plasma concentration of the PEGylated dendrimer was 6-fold higher than that of the bare dendrimer (peak concentration: $0.6 \pm 0.2 \mu\text{g/ml}$ vs $3.8 \pm 0.4 \mu\text{g/ml}$ or $2.1 \pm 0.6\%$ vs $13.2 \pm 1.7\%$ of overall dose). The plasma concentration of the G3NH₂ conjugates administered I.V. decreased quickly, reaching $1.1 \pm 0.3 \mu\text{g/ml}$ (3.8% of overall dose) at 6.5 h post administration as can be seen in Figure 2.2b. However, the plasma concentration of the highly PEGylated dendrimer G3NH₂-24PEG1000 decreased only slightly within the same time remaining at 76% of the delivered dose. At 6.5 h the plasma concentration of the PEGylated dendrimer is 19.5-fold higher than that of bare dendrimer ($21.6 \pm 1.5 \mu\text{g/ml}$ vs $1.1 \pm 0.3 \mu\text{g/ml}$). A similar plasma concentration-time profile was also found for PEGylated polylysine dendrimers of 11kDa, 22kDa and 78kDa, upon delivered to the lungs via intratracheal instillation.[52]

The effect of PEGylation on plasma concentration is in line with previous results for PAMAM dendrimers and other polymeric nanoparticles.[34, 173, 187] The plasma concentration and *in vivo* biodistribution of the dendrimer conjugates is mainly affected by its absorption, distribution, metabolism and elimination.[169] Surface charge, size and surface functionality of the dendrimer conjugates determine their interaction with serum proteins and blood cells, uptake into target and non-target organs, and potential routes of elimination. It has been demonstrated that PEGylation can neutralize surface charge of cationic polymers [125, 174] and reduce the binding affinity of proteins to nanocarriers,[188-191] which attenuates plasma protein adsorption, opsonization, phagocytosis and stimulation of immune cells.[30, 172, 191, 192] Therefore, the blood circulatory residence of PEGylated dendrimers was significantly prolonged.

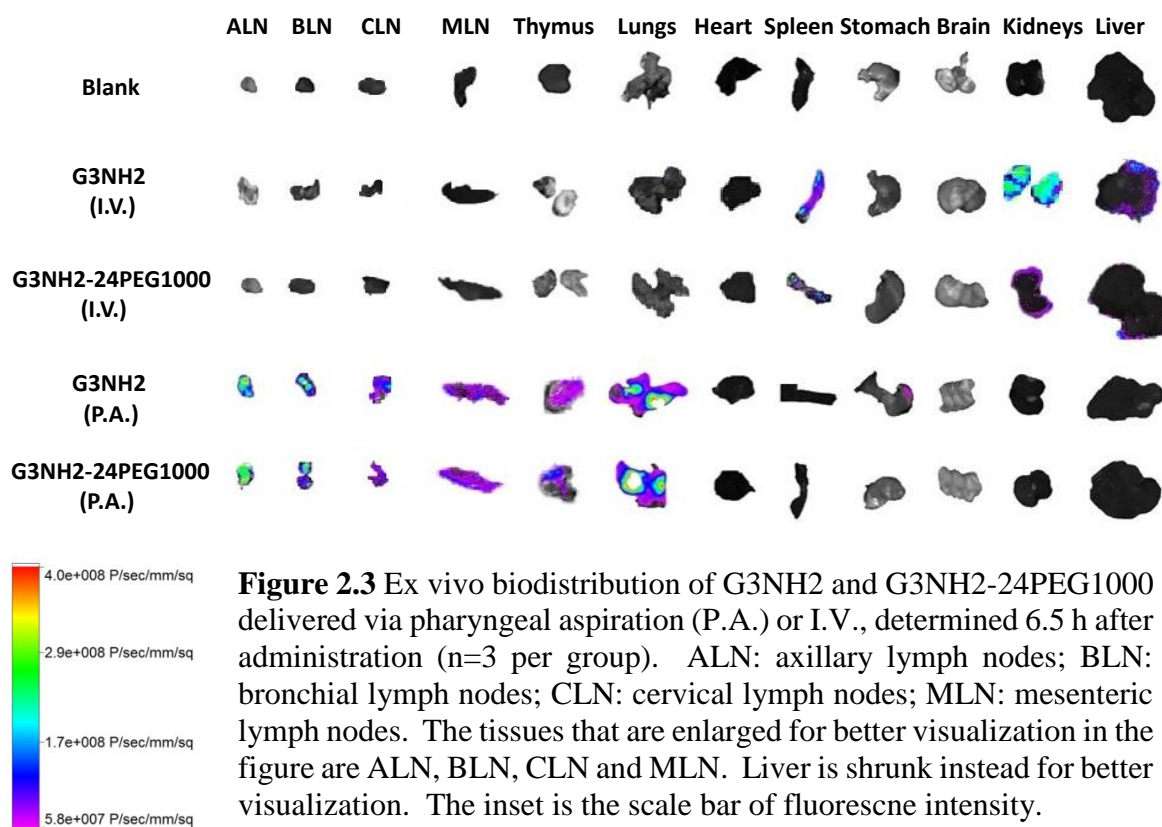
In contrast to I.V. administration, dendrimer conjugates administered via pulmonary route need to cross several extracellular barriers to enter the local/systemic blood circulation. These extracellular barriers include the fast-renewing mucus gel layer and ciliated epithelial cells on the airways, resident alveolar macrophages, lung surfactant and the alveolar epithelial cells in the deep lungs. The significantly different plasma concentration profiles for G3NH₂ and G3NH₂-24PEG1000 suggest that their charge and/or size have a significant impact on how they interact with the extracellular barriers before they reach systemic circulation. We have previously observed that even though dendrimers are much smaller than the mucus mesh size (ca. 100 nm),[72] they may be retained in the mucus layer depending on their charge. Cationic dendrimers interact with the mucus environment much more strongly, and thus take longer to traverse the mucus layer compared to neutral/negatively charged PEGylated dendrimers.[72, 168] The increase in size of the PEGylated conjugates may in principle also have an effect as the tight junctions of the epithelial barriers strongly modulate the transport of molecules as a function of time – for example,

macromolecular therapeutics with sizes $< 40\text{-}50\text{kDa}$ (HD: 5-6 nm) are known to be peak in systemic circulation in a matter of minutes,[179] while those larger molecules peak in systemic circulation upon lung delivery over periods of hours, days, or weeks.[67] However, *in vitro* results show that even highly PEGylated dendrimers can interact with the tight junctions of the pulmonary epithelium, and thus modulate their way across, reducing the impact of their size,[168] at least within the size range being investigated and discussed here.

The impact of the dendrimer size can perhaps more strongly affect the route of elimination upon reaching systemic circulation. The HD of the non-PEGylated dendrimer (5.1 ± 1.4 nm) is smaller than the size limit (ca. 6 nm) in which nanoparticles are quickly eliminated from blood circulation, and it can thus be eliminated by the kidneys (glomerular filtration),[193] while those nanocarriers larger than 6 nm, as for example G3NH₂-24PEG1000 (HD = 10.9 ± 3.6 nm), cannot be eliminated by kidneys, but accumulate in liver and spleen through the mononuclear phagocyte system (MPS), which is a relatively slow process.[49, 194] However, the hydrophilicity imparted by the PEGylation reduces or delays MPS processing [190, 195] and prolongs systemic circulation.[168] Thus, once the dendrimers are absorbed systemically, the PEGylation prevents glomerular filtration (due to their size) and also reduces MPS processing (due to their hydrophilicity).

2.4.3 Systemic biodistribution of the dendrimer conjugates delivered via the pulmonary and intra-venous (I.V.) routes.

The effect of the administration route and PEGylation on the systemic distribution of dendrimer conjugates was investigated in this work. Mice were sacrificed 6.5 h after P.A. or I.V. administration, and the major organs were excised, including lymph nodes, thymus, heart, lungs, stomach, spleen, liver and kidneys. *Ex vivo* imaging was used to qualitatively assess the



biodistribution of the dendrimer conjugates in these tissues. The results, using representative tissues, are summarized in Figure 2.3.

Quantitative assessment of the concentration of the conjugates was performed by fluorescence spectroscopy by recovering the tagged dendrimers from the various tissues as discussed in *Materials and Methods*. The results, in terms of % of (total) Dose, as a function of route of administration and conjugate chemistry are summarized Figure 2.4. The results are also

summarized in terms of the *mass dendrimer / mass tissue* – they are shown in Figure S4 - *Supplemental Information in Appendix 1*.

The results demonstrate that administration route (compare Figure 2.4a and 2.4b) and chemistry of the conjugates (comparing G3NH₂ and G3NH₂-24PEG1000 in Figure 2.4a and

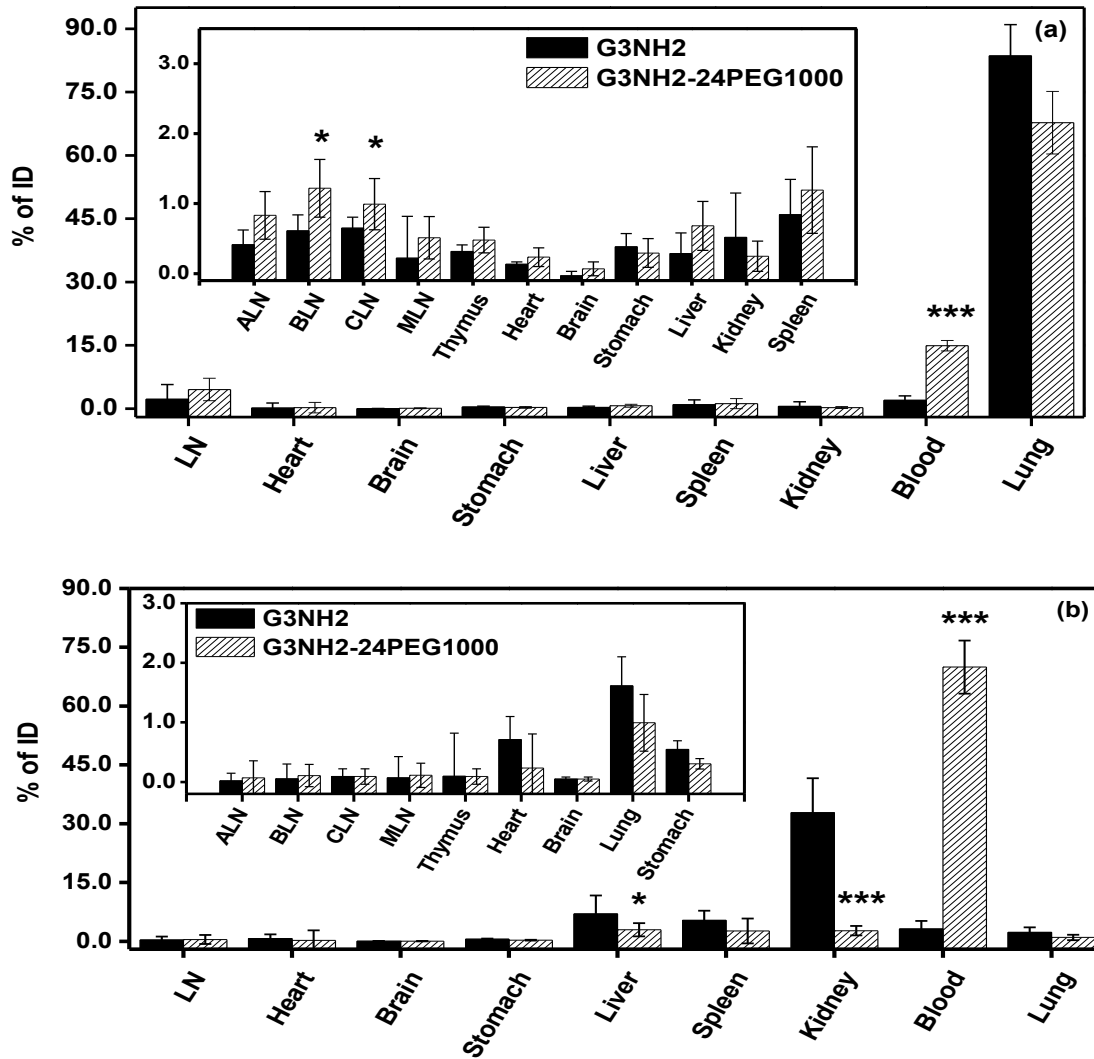


Figure 2.4 *In vivo* biodistribution of G3NH₂ and G3NH₂-24PEG1000 delivered via (a) pharyngeal aspiration (P.A.) and (b) I.V., 6.5 hours after administration (n=3 per group). The insets highlight the biodistribution of the conjugates in the different lymph nodes; when they are all combined, they are represented in the main figure as LN. ALN: axillary lymph nodes; BLN: bronchial lymph nodes; CLN: cervical lymph nodes; MLN: mesenteric lymph nodes. The statistical analysis was performed between G3NH₂ and G3NH₂-24PEG1000 with Student's t-test (*p<0.05, **p<0.01, and ***p<0.001).

Figure 2.4(b) have a significant impact on the dendrimer biodistribution. The impact of the

conjugate chemistry, however, is observed to be much less pronounced following I.V. delivery when compared to P.A. administration. It can also be observed that the amount of conjugate found in the lungs is much higher when they are administered via P.A. than compared to I.V. delivery, as expected. While $83.4 \pm 7.3\%$ of the injected dose for G3NH₂ and $67.7 \pm 7.4\%$ of injected dose for G3NH₂-24PEG1000 are present in the lungs 6.5 h hours post P.A. administration, only $1.6 \pm 0.5\%$ G3NH₂ and $0.9 \pm 0.4\%$ G3NH₂-24PEG1000 can be found in the lungs at the same time when administered I.V. The lung retention upon P.A. delivery is also impacted by the chemistry of the nanocarriers. The positively charged G3NH₂ is retained longer in the lungs, while the PEGylated dendrimer translocates to systemic circulation and leaves the lungs to a higher extent. These results suggest the potential of the dendrimer nanocarriers for the targeting of lung diseases when combined with oral inhalation formulations as the chemistry of the conjugates can be used to modulate the transport of therapeutics across the pulmonary epithelium. The potential in using such nanocarrier systems is supported by our recent results where we demonstrate that dendrimer nanocarriers can be formulated in portable oral inhalation devices,[184] and those can be used for the delivery of small molecules [146, 184] or biomacromolecules such as nucleic acids.[144, 163]

We also observed that the dendrimers administered via P.A. show up in significant quantities in the lymph nodes (LN), while no accumulation is observed upon I.V. administration. In fact, on a mass/tissue basis (Figure S4), the mass of conjugates found in the LN upon P.A. is second only to the lungs. It can also be observed that the chemistry of the conjugates plays a major role in terms of their biodistribution to the LNs upon P.A. delivery. The PEGylated dendrimer appears in significantly greater concentrations in the bronchial lymph nodes (BLN) and cervical lymph nodes (CLN), and in the thymus as well compared to the non-PEGylated conjugates.

Charge effects on biodistribution have been reported for solid nanoparticles.[39, 194] Neutral (polystyrene-polyacrylate) and hydrophilic (PEG20kDa) organic nanoparticles smaller than 38 nm and with PEG ligands were rapidly translocated to mediastinal lymph nodes, while anionic and cationic charged nanoparticles readily adsorbed on endogeneous protein in the lungs. When polystyrene nanoparticles ranging from 50 to 900 nm are administered to the lungs, the highest nanoparticle deposition (35 – 50% of extrapulmonary distribution) was also detected in the lymph nodes 3 h after pulmonary administration.[55]

These results point to a strategy for passively targeting the lymph nodes with dendrimers upon delivery via P.A., which may prove relevant for the development of various dendrimer-based therapies, including pulmonary vaccination (e.g. influenza,[196] tuberculosis,[145] HPV infection[197]) and diseases of the lymphatic system such as metastasis (e.g. breast cancers [198]).

No obvious fluorescence was found in the major organs responsible for elimination of the dendrimers such as liver, spleen and kidneys at 6.5 h post administration when the conjugates were delivered via P.A.. In contrast, significant quantities of the conjugates are detected in liver, spleen and kidneys when the conjugates were administered intravenously. In that case, greater concentrations of the non-PEGylated dendrimers are cleared/found in the kidneys ($32.8 \pm 8.8\%$), spleen ($5.3 \pm 2.5\%$) and liver ($7.0 \pm 3.7\%$) when compared to the than PEGylated conjugates ($2.7 \pm 1.2\%$ in kidneys, $2.9 \pm 1.7\%$ in liver, and $2.7 \pm 1.6\%$ in spleen). These results are in excellent agreement with the PK results discussed above. In fact, the accumulation of bare dendrimer in the kidneys may be underestimated to some extent since previous studies showed PAMAM dendrimers can be detected in urine 2 h after I.V. injection.[199] The distribution of dendrimer in both kidneys and liver/spleen revealed renal excretion and MPS are able to play roles in dendrimer elimination. Noticeably, the kidneys showed the greatest fluorescence in the case of bare dendrimer,

demonstrating that the bare dendrimer was mainly eliminated renally due to its small size (5.1 nm).[49] However, the PEGylated conjugates show no preferable accumulation site at 6.5 h.

2.4.4 Lung cellular biodistribution of the dendrimer conjugates administered via pulmonary route.

The internalization of the dendrimer conjugates in selected lung cell types upon P.A. was also assessed. Four typical pulmonary cell populations were selected to be tagged during the flow cytometry experiments, namely myeloid, endothelial, alveolar epithelial and airway ciliated epithelial cells. The characteristic receptors of these cells are CD45 on myeloid cells, CD31 on endothelial cells, lung pro-surfactant protein C (pro-SPC) on alveolar epithelial type II cells, and cilia layer on apical side of airway epithelial cells. Cilium is a microtubule-based cytoskeleton that is constructed by β -tubulin in combination with α -tubulin. Therefore, ciliated airway epithelium has much higher levels of β -tubulin than other cells do. The flow cytometry results are summarized in Figure 2.5 – representative dot plots are shown in the *Supplemental Information in Appendix I*– Figure S3.

The flow cytometry results (inset in Figure 2.5) indicate that G3NH2 is found internalized in $32.8 \pm 3.6\%$ of the pulmonary cells upon P.A. delivery, while the % of the cells that had

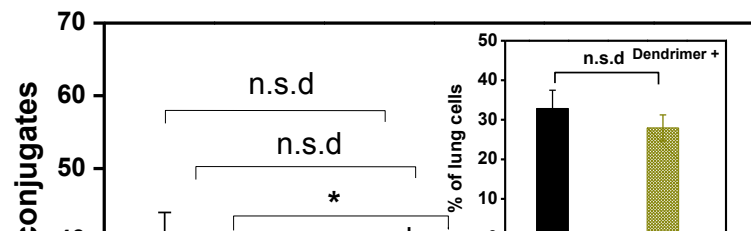


Figure 2.5 Lung cellular distribution studies upon lung delivery of the dendrimer conjugates. Break down in terms of cell type (out of those cells that had internalized dendrimer conjugates) and dendrimer conjugate PEGylation. *Inset:* % of lung cells, out of all the cells in the tissue single cell suspensions, which had internalized dendrimer conjugates (n=3 per group). Statistical analysis was performed with Student's t-test (*p<0.05). n.s.d = not significantly different.

internalized G3NH2-24PEG1000 was $27.9 \pm 2.7\%$. While no statistically significant difference was found when comparing the average for both groups, a lower percentage of internalization of the PEGylated dendrimer would be in agreement with the fact that PEGylation has been shown to decrease the rate and extent of internalization within this time frame - as shown *in vitro*, [168, 183]. This observed trend also confirms that the PEGylated dendrimers seem to be transported into systemic circulation faster (PK results) and are found at a lower concentration in the lungs (biodistribution results).

Myeloid cells, including monocytes, granulocytes, dendritic cells and macrophages, were observed to internalize the largest fraction of dendrimers when compared to all other cells. While the specific cell subpopulation was not determined, these results suggest that such dendrimer conjugates would be able to target cells that are relevant in the treatment of medically important diseases such as tuberculosis, [145] and in vaccine delivery applications. [196] It is also observed that the cell populations interact differently with the different chemistries. For example, while 37.2% of the cells that internalized G3NH2 were myeloid type, the preference of myeloid cells was lower towards G3NH2-24PEG1000. As a matter of fact, the percentage of all cells (based on cell type) that had internalized G3NH2-24PEG1000 was lower than the percentage of cells that internalized G3NH2. This was not true for endothelial cells, where 20.4% contained G3NH2-24PEG1000, compared to only 6.0% for G3NH2. These results support the view that the PEGylated dendrimers can more efficiently transport across the epithelial barrier of the pulmonary epithelium, and gain access to the endothelial layer, where they are internalized, while at the same being able to evade internalization by myeloid cells.

In addition, the dendrimer nanocarriers can be also significantly internalized by alveolar epithelial cells (G3NH2 vs. G3NH2-24PEG1000 = $22.9 \pm 3.7\%$ vs. $16.1 \pm 4.5\%$ of those cells

internalizing dendrimer nanocarriers) and ciliated airway epithelium (G3NH₂ vs. G3NH₂-24PEG1000 = 12.4±4.2% vs. 8.3±1.8% of those that internalized dendrimer). These results show that highly positively charged bare dendrimers are entrapped by or interacts with the epithelial layer to a larger extent than their PEGylated counterparts. The internalization of dendrimer nanocarriers by alveolar/airways epithelial cells implies its potential for drug delivery to the diseases that cause acute/chronic dysfunctional respiratory tract and lungs such as pneumonia (usually in alveolar sacs), and asthma (airways and lungs).

Combined, the biodistribution, PK and lung cellular distribution results shown here provide us with clues that can help formulate a reasonable hypothesis as to why the dendrimer conjugates are so effectively drained into the lymph nodes upon P.A. While big particles (> 500 nm) require the activation of antigen-presenting cells (e.g. dendritic cells, B cells) to be trafficked to lymph nodes,[55] dendrimer nanocarriers with hydrodynamic diameters < 10 nm tend to rapidly translocate across pulmonary epithelium from airway/alveolar luminal surface to septal interstitium, followed by rapid accumulation to lymph nodes. This step doesn't need to activate antigen-presenting cells (APCs). It is believed that the passive pathway may play a major role in targeting dendrimer nanocarriers to lymph nodes.[200] Although APCs would rather phagocytize large particles than small ones, the abundance of APCs in the respiratory tract and lungs can also effectively take up smaller carriers such as dendrimers. The macrophages and dendritic cells activated by the phagocytosis of dendrimer nanocarriers migrate via lymph flow to tracheobronchial and bronchiolar lymph nodes including bronchial-associated lymphatic tissue (BALT), and are eventually carried into draining lymph nodes.[152, 201, 202] In addition, the routing of dendrimer nanocarriers to lymph nodes is dictated by their surface chemistry.

2.5 Conclusions

In this work we investigated the effect of the surface chemistry (PEGylated vs. non-PEGylated) and the route of administration (pulmonary delivery vs. intravenous injection) on the systemic tissue biodistribution and local (lung) cellular distribution of G3NH₂ dendrimers. The results show that both have a strong impact on how the dendrimers interact with the physiological environment. Biodistribution results show much greater accumulation of dendrimer nanocarriers in lungs and a variety of lymph nodes upon pulmonary delivery, for both PEGylated and non-PEGylated dendrimers when compared to I.V. administration. PEGylation is seen to further promote the passive targeting of dendrimers to lymph nodes upon pulmonary administration. Upon systemic delivery, PEGylation was seen to increase circulation times, as expected, with very little lung or lymph node accumulation. PEGylation also helps modulated the uptake of dendrimers by different lung cell populations. The results shown here suggest that both the pulmonary route of administration and dendrimer chemistry combined can be used to passively target tissues of great interest, and can thus be used as guiding principles in the development of dendrimer-based drug delivery strategies for medically relevant diseases including lung ailments, pulmonary vaccination, and malignant metastases among others.

2.6 Acknowledgements

This work was supported in part by a National Science Foundation grant (NSF-CBET grant no. 0933144 and NSF-DMR grant no. 1508363), the Nano@WSU incubator awarded to SRP da Rocha, and the WSU start-up grant and ERC-2014-StG-637830 awarded to Olivia Merkel. The authors also would like to thank Dr. Jessica Back and Mr. Van Buren (Microscopy, Imaging and Cytometry Resources Core at Wayne State University) for help with flow cytometry data analysis and valuable discussions. The MICR Core is supported, in part, by NIH CenterGrant

P30CA022453 to The Karmanos Cancer Institute, and the Perinatology Research Branch of the National Institutes of Child Health and Development, both at WSU.

2.7 Supplemental information

Description of characterization of dendrimer and PEGylated counterpart including ^1H NMR and MALDI-TOF are provided. The preparation of single cell suspension and examples of flow cytometry histograms of selected cell populations are also included. These information can be found *Appendix A*.

CHAPTER 3 — Poly(amidoamine) Dendrimer-Doxorubicin Conjugates: In vitro characteristics and Pseudo-Solution Formulation in Pressurized Metered-Dose Inhalers

3.1 Introduction

Cancer is the second most common cause of death in the United States.[2, 203] An estimated 1.7 million new cases are diagnosed yearly, with ca. 600 thousand cancer deaths.[204] Among the many types of malignant tumors, lung cancers are of great relevance as they are the leading cause of cancer death among both men and women.[1, 205] More people die of lung cancer than colorectal, breast, pancreatic, and prostate cancers combined.[2]

Chemotherapy is widely used in the fight against primary lung cancers and lung metastasis.[6, 44-46] However, there are several limitations in using chemotherapeutics to treat lung cancers. One major challenge is the low chemotherapeutic concentration found in the lung tumor upon intravenous (i.v.) administration.[6, 7] It is estimated that only a few percent (ca. 2-4%) of the total dose administered i.v. reaches the lung tumor.[8] Dose limiting toxicity is another major issue in the chemotherapeutic treatment of lung cancers.[9] This problem is compounded as high i.v. dosages are usually required due to the poor distribution profile of chemotherapeutics.[8]

Doxorubicin (DOX) is a leading therapeutic in clinical oncology, having a broad range of activity against both “liquid” and solid tumors,[88] including lung cancers.[6, 57, 206] Since the discovery of DOX, thousands of other anthracyclines have been screened for their anticancer properties, but only few have emerged as clinically relevant.[92] In spite of its immense acceptability, however, DOX causes a series of side effects, of particularly relevance being its toxicity to the cardiac tissue.[207-209] While DOX-induced cardiomyopathy is clinically manageable, it is associated with 50% mortality in those patients that develop congestive heart

failure during treatment,[210, 211] thus limiting the range of applicability of this powerful therapeutic. The ability to efficiently deliver DOX locally to the lungs, and to improve DOX's biodistribution by minimizing its concentration in the cardiac tissue may, therefore, represent an important step forward in the use of such a relevant anti-cancer therapeutic in the treatment of lung cancers.

Nanocarriers have the potential to improve the biodistribution and pharmacokinetic profiles of various therapeutics including anti-cancer drugs.[47-50] Dendrimers are particularly relevant nanocarrier systems as they are highly monodisperse,[31] have a large number of surface groups amenable to the conjugation of therapeutic molecules and also other agents and ligands that allow for the enhancement of the properties of the nanocarriers such as increased aqueous solubility upon conjugation of hydrophobic therapeutics[30] (as is the case for DOX), and enhanced pharmacokinetic and biodistribution profiles,[169] as well as the tagging of imaging agents for theranostics,[199, 212] among others. Particularly relevant to this work is the fact that we have also recently shown that the chemistry of generation 3, amine-terminated PAMAM dendrimers (G_3NH_2) can be used to modulate their interaction with the pulmonary epithelium both *in vitro* and *in vivo*,[168] and can thus be potentially used to improve therapeutic outcomes of DOX.

Based on the challenges and opportunities discussed above, the goal of this work was to evaluate the interaction of PAMAM dendrimer-DOX conjugates with an *in vitro* lung cancer model, and to develop portable oral inhalation (OI) formulations for the local delivery of the DOX conjugates to the lungs. More specifically, we propose to synthesize and characterize G_3NH_2 -DOX conjugates with an intracellular degradable linker and varying densities of PEG 1000Da, and to evaluate the kinetics of cellular internalization, intracellular DOX release and organelle

colocalization, and cell kill on A549 cells – a model of the alveolar epithelial human adenocarcinoma. Moreover, we also propose to develop HFA-based pMDI formulations of the G3NH₂-DOX conjugates with aerosol characteristics conducive to deep lung deposition of DOX.

3.2 Materials

Generation 3, amine-terminated, poly(amido amine) (PAMAM) dendrimer (G3NH₂, 32 - NH₂ surface groups, theoretical molecular weight = 6909) was purchased from Dendritech, Inc (Miland, MI, USA). PEG1000Da succinimidyl ester (PEG1K-SE) was purchased from NANOCS Inc (New York, NY, USA). Doxorubicin hydrochloride salt (DOX) was purchased from LC Laboratories (Woburn, MA, USA). Cis-aconityl anhydride, succinic anhydride, triethylamine (TEA), 2, 5-dihydroxybenzoic acid (2, 5-DHB), ethyl-3-(3-dimethylaminopropyl) carbodiimide (EDC) and N-hydroxysuccinimide (NHS) were purchased from Sigma-Aldrich (St Louis, MO, USA). 3-(4, 5-dimethylthiazol-2-yl)-2, 5-diphenyltetrazolium bromide (MTT) was purchased from Life Technologies (Grand Island, NY, USA). Deuterated dimethylsulfoxide (DMSO-d₆) was purchased from Cambridge Isotope Laboratories (Andover, MA, USA). Ultrapure deionized water (DI H₂O, Ω=18.0-18.2) was sourced from a Barnstead NANOpure DIamond System (D11911), equipment purchased from Thermo Fisher Scientific (Waltham, MA, USA). 1,1,1,2,3,3,3-heptafluoropropane (HFA227) with trade name Dupont™ FM-200® and 2H, 3H perfluoropentane (HPFP) with trade name Vertrel™ XF were purchased from Dupont (Wilmington, DE, USA). A549 human lung cancer cell line was purchased from American Type Culture Collection (Manassas, VA, USA). Spectra®Por dialysis membrane (MWCO = 3000Da) was purchased from Spectrum Laboratories, Inc (Rancho Dominguez, CA, USA). Amicon® Ultra 15 centrifugal filter device (MWCO = 3000Da) was purchased from EMD Millipore (Billerica, MA, USA). Thin layer chromatography (TLC) Silica gel 60 F₂₅₄ plastic sheet was purchased from

Merck KGaA (Darmstadt, Germany). All reagents were used as received unless specified elsewhere.

3.3 Methods

3.3.1 Synthesis and characterization of acid-labile, PEGylated PAMAM-DOX conjugates (G3NH₂-mPEG-nDOX).

As shown in Figure 1, DOX was reacted with cis-aconityl anhydride in basic aqueous solution to obtain cis-aconityl DOX. Acid-labile, PEGylated conjugates were synthesized via two different routes: *Direct PEGylation* or *Two-step PEGylation*. In the *Direct PEGylation* approach, cis-aconityl DOX was first conjugated to G3NH₂ using EDC/NHS chemistry. PEG was subsequently conjugated to G3NH₂-nDOX to obtain the final product G3NH₂-mPEG-nDOX. Various PEG densities ($m = 0, 9$ and 21) were achieved by reacting different ratios of PEG-SE to G3NH₂-nDOX. The *Two-step PEGylation* strategy was required in order to achieve higher payloads of DOX (in this particular case for $n = 7$), as G3NH₂-nDOX becomes too hydrophobic and crashes out of solution for $n > 3$. In the *Two-step PEGylation* strategy, G3NH₂ is first pre-PEGylated at a low/medium PEG density. Cis-aconityl DOX is subsequently conjugated (to a high/desired payload) to the pre-PEGylated dendrimer using EDC/NHS chemistry. Finally, additional PEG is conjugated onto the pre-PEGylated dendrimer-DOX conjugates, so as to achieve the desired/final PEG density. Proton nuclear magnetic resonance (¹H NMR) was recorded using Mercury 400 spectrometer (Agilent Technologies, Inc. Santa Clara, CA, USA). The molecular weight (MW) of the various intermediates and final products was determined by electrospray ionization (ESI) mass spectrometry using a ZQ-Waters TERS/Micromass spectrometer (Waters Corporation, Milford, MA, USA) and matrix-assisted laser desorption ionization-time of flight (MALDI-TOF) using a Bruker Daltonics UltrafleXtreme mass spectrometer (Bruker Corporation.

Billerica, MA, USA). Hydrodynamic diameter (HD) and zeta potential (ζ) were determined using Zetasizer Nano ZS (Malvern Instruments Ltd. Malvern, Worcestershire, UK). Solvated diameter (SD) was also determined using the Zetasizer Nano ZS, but in that case in HPFP (non-aqueous solvent). Detailed procedures for these measurements are described in *Supplemental Information S1*, and all synthetic details of the conjugates are also described in *Supplemental Information S2 in Appendix 2*.

3.3.2 Synthesis and characterization of non-labile, PEGylated PAMAM-DOX conjugates (G3NH₂-mPEG-nDOXNL).

The non-labile G3NH₂-mPEG-nDOXNL conjugates were synthesized via the same strategy—direct PEGylation and two-step PEGylation—as described in *Section 3.1*. The only one difference is that DOX was first reacted with succinic anhydride in non-aqueous solution.

3.3.3 Culture of A549 Cells.

Human lung alveolar adenocarcinoma epithelia cells (A549), passages 10 to 15, were plated in 75 cm² cell culture flask at a density of 10⁴ cells/mL, and cultured with Dulbecco's Modified Eagle's Medium (DMEM, Life Technologies) supplemented with 10% Fetal Bovine Serum (FBS, Atlanta Biologicals) and penicillin (100 U/ml)-streptomycin (100 µg/ml) (Pen-Strep. Life Technologies). The cells were grown in Thermo Scientific™ CO₂ incubator (Thermo Fisher Scientific) at 37 °C and 5% CO₂. The medium was exchanged every two days and the cells were split when they reached ca. 80% confluence.

3.3.4 *In vitro* release of acid-labile G3NH₂-mPEG-nDOX and acid-non-labile G3NH₂-mPEG-nDOXNL conjugates.

In vitro release was determined at both pH 7.4 and 4.5, representing the extracellular physiological pH and the lysosomal pH, respectively. A 2 mL of phosphate buffer saline (PBS, 1X, pH 7.4) or

citrate buffer (0.01 M, pH 4.5) containing free DOX or the conjugates (all with 0.38 μmol DOX or equiv.) was added to a dialysis membrane (MWCO = 3000Da), and the system immersed in 30 mL PBS or citrate buffer. The *in vitro* release studies were performed in MaxQ thermostatic water bath shaker (Thermo Fisher Scientific), preset to 37.0 ± 0.2 °C. A 0.1 mL solution from outside the dialysis bag was sampled at predetermined time points, and the concentration of DOX determined using a Biotek Synergy 2 Multi-Mode Microplate Reader (Biotek Instruments, Inc. Winnooski, VT, USA), at 490 nm. The samples were returned after each time point. These experiments were run in triplicate. The cumulative release of DOX from G3NH₂-mPEG-nDOX and G3NH₂-mPEG-nDOXNL was plotted as a function of time.

3.3.5 Cell kill of acid-labile G3NH₂-mPEG-nDOX and acid-non-labile G3NH₂-mPEG-nDOXNL conjugates.

The ability of DOX, G3NH₂-mPEG, G3NH₂-mPEG-nDOX, and G3NH₂-mPEG-nDOXNL conjugates to kill A549 lung cancer cells was assessed using the MTT assay. A series of concentrations were sterilized by filtering sample-laden DMEM (no phenol red) through 0.22 μm sterile syringe filter (VWR International, Radnor, PA, USA). 1×10^4 cells/well (n=8 per concentration) were seeded in tissue culture treated 96-well plate (VWR International) with DMEM (no phenol red). The medium was removed after 24 h, and 100 μL of the sample-laden DMEM (no phenol red) was added to each well. The samples were incubated with cells for 72 h or 144 h. The sample-laden medium was then removed from each well. The cells were washed with PBS (1X, pH 7.4) twice. 100 μL of fresh DMEM (no phenol red) and 10 μL of MTT PBS solution (5 mg/ml) were added to each well. After 4 h (37 °C, 5% CO₂), 75 μL of medium was removed, and 60 μL DMSO was added into each well to dissolve formazan crystal. The cells were allowed to sit in the incubator (37 °C, 5% CO₂) for another 2 h. Finally, the absorbance of each

well was recorded at 540 nm using Biotek Synergy 2 Multi-Mode Microplate Reader (Biotek Instruments, Inc).

3.3.6 Cellular internalization of acid-labile G3NH₂-mPEG-nDOX conjugates by A549 cells.

3×10^5 A549 cells/well were seeded in 24-well plates 24 h before the experiment. A 0.5 mL sterile Hanks Balanced Salt Solution (HBSS, 1X, pH 7.4) of free DOX or G3NH₂-mPEG-nDOX conjugates (0.1 μ M DOX equivalent) was added to each well and then incubated with cells for different lengths of time (0.5, 1, 1.5, 2, 3, 4 and 5 h. n=3 per time point). The cellular internalization was ceased at each time point by replacing sample-laden HBSS with cold blank HBSS. The cells were detached with 0.2 mL 0.25% trypsin-0.53 mM EDTA solution (Life Technologies). The detached cells were pelletized by centrifugation at 350 g. The cell pellet was resuspended in 0.5 mL blank HBSS (4 °C) and immediately analyzed for DOX fluorescence using flow cytometry (BD LSR II Analyzer, BD Bioscience. San Jose, CA, USA). At least 10,000 events were counted for statistical significance. Median fluorescence intensity (MFI) was plotted as a function of time to evaluate the effect of dendrimer chemistry (PEG density and DOX payload) on cellular internalization.

3.3.7 Intracellular release and nuclear colocalization of DOX from acid-labile G3NH₂-mPEG-nDOX conjugates.

2×10^5 cells were seeded on a cover slide, which was placed in a 24-well plate. After 24 h, a 0.5 mL DMEM (no phenol red) solution of the acid-labile G3NH₂-mPEG-nDOX conjugates (4 μ M DOX equivalent) was incubated with the cells for 48 h. The sample-containing medium was then thoroughly removed by washing the cells with PBS (1X, pH 7.4) three times. Nuclei were then stained with Hoechst 33342 (Life Technologies) for 10 min and excess dye was thoroughly washed away with PBS three times. The cells were fixed with 4% paraformaldehyde PBS solution (Sigma-

Aldrich) at 4 °C for 20 min and then mounted for imaging. The fixed cells were imaged with Zeiss LSM 780 Confocal Laser Scanning Microscope (Carl Zeiss Microscopy. Oberkrochen, Germany). To evaluate the intracellular release of DOX from acid-labile G3NH₂-mPEG-nDOX conjugates as a function of time (and the free DOX control), the DOX or conjugate-laden medium was incubated with cells for different lengths of time (24, 48, 96 and 144 h, with n=3 per time point). The Pearson's correlation coefficient (PCC) was calculated as a function of time using the Leica LAS AF Lite software (Leica Microsystems. Buffalo Grove, IL, USA). The results were compared with free DOX. Colocalization of the non-labile conjugates was also qualitatively assessed by rendering the 3D confocal images of A549 cell incubated with the G3NH₂-mPEG-nDOXNL conjugates, and stained with nuclear stain.

3.3.8 Preparation and characterization of the pMDI formulations

3.3.8.1 *Physical stability of acid-labile G3NH₂-mPEG-nDOX conjugate formulation in HFA227 propellant.*

A predetermined amount of G3NH₂-mPEG-nDOX conjugates and anhydrous ethanol were weighed into pressure proof glass vial (West Pharmaceutical Services. Exton, PA, USA). Subsequently, the glass vial was crimped manually using 63 µL metering valves (Bespak. Norfolk, UK). HFA227 propellant (4 mL) was added to the sealed glass vial with the help of a manual syringe pump (HiP 50-6-15) and a home-made high pressure filler. The resulting formulation was placed in VWR P250D low energy sonication bath (VWR Internationals) for 30 min, which was set to 180 W and 0-5 °C. The physical stability of the formulations was evaluated by visually monitoring the dispersion as a function of time after sonication.

3.3.8.2 *Particle size measurement.*

The solvated diameters (SD) of G3NH₂-mPEG-nDOX conjugates were determined using light scattering (LS). Briefly, the aqueous solution of G3NH₂-mPEG-nDOX conjugate was filtered with 0.22 µm syringe filter (VWR Internationals) and then lyophilized. HPFP was also filtered with 0.22 µm syringe filter (VWR Internationals) to remove any impurities in solvent. The purified G3NH₂-mPEG-nDOX conjugate (0.2 mg DOX equivalent) was added to 1 mL HPFP with the help of anhydrous ethanol (0.37 % v/v). The HPFP was added and then sonicated at 0-5 °C for 30 min. The SD of the conjugate in HPFP was determined using Zetasizer Nano ZS (Malvern Instruments). The average SD and standard deviation (s.d.) were calculated based on at least three measurements.

3.3.8.3 *Aerosol performance of the pMDI formulations.*

The *in vitro* aerosol characteristics of G3NH₂-mPEG-nDOX pMDI formulations were determined with Andersen Cascade Impactor (CroPharm, Inc. Milford, CT, USA) fitted with a USP induction port. All measurement was operated at a flow rate of 28.3 L/min, 25 °C and 75% relative humidity.[163] The pMDI formulations were prepared as described above and several shots were fired to waste. Subsequently, 10 shots were released into an Anderson Cascade Impactor (ACI) with 10 s interval between shots. The run was promptly stopped 10 s after the last shot. The ACI was disassembled carefully. Actuator, induction port, eight plates and filter membrane were thoroughly rinsed with 10 mL DI H₂O each. The concentration of the G3NH₂-mPEG-nDOX conjugates collected in the aqueous solutions was measured at 490 nm using Cary 50 UV-Vis spectrometer (Agilent Technologies. Santa Clara, CA, USA). The mass of the conjugates deposited on the actuator, induction port, and each plate were calculated relative to an established calibration curve. The following aerosol parameters were calculated: respirable

fraction (RF), fine particle fraction (FPF), mass median aerodynamic diameter (MMAD), geometric standard deviation (GSD) and recovery. The RF is defined as the ratio of mass of particles collected on Stage 0 to filter to the mass of particles released into the ACI. The FPF is defined as the ratio of mass of particles on Stage 3 to filter, to the mass of particles on Induction port to Filter. The MMAD represents the median of the distribution of airborne particle mass with respect to aerodynamic diameter. MMAD is usually reported along with the GSD, which characterizes the variability of the particle size distribution. GSD is defined as the square root of the ratio of 84.13% over 15.87% particle size distribution. Further details on the calculation of MMAD and GSD has been previously reported.[80] The recovery is calculated by dividing collected dose (mass of particles in actuator, induction port, stage 0-7 and filter) by theoretical dose (concentration \times volume per puff \times puff number).

3.4 Results and Discussion

3.4.1 Synthesis and characterization of acid-labile G3NH₂-mPEG-nDOX and non-labile G3NH₂-mPEG-nDOXNL conjugates.

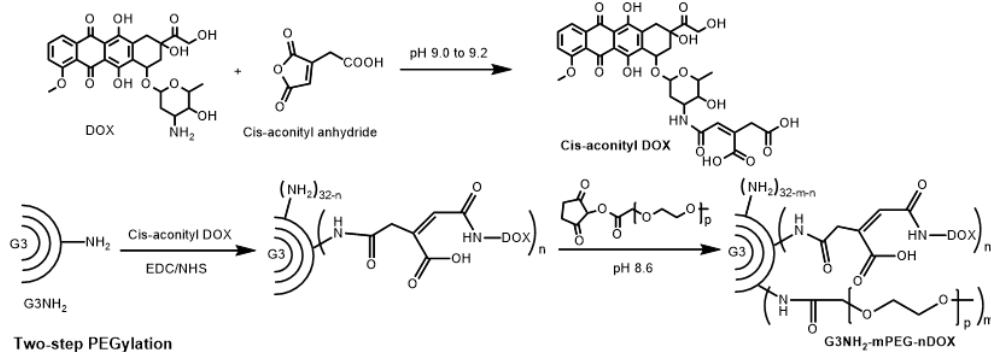
DOX was conjugated to generation 3, amine-terminated PAMAM dendrimers (G3NH₂) through an acid-labile cis-aconityl spacer. After forming two amide bonds with DOX and G3NH₂, cis-aconityl anhydride has one free carboxyl group (-COOH) left, which can readily catalyze the cleavage of its neighboring intra-molecular amide bond at acidic conditions (i.e. pH < 5), and thus release conjugated DOX – not the pro-drug but DOX itself.[213]

Two synthetic strategies were developed for synthesis of PEGylated PAMAM dendrimers containing different DOX payloads: direct PEGylation for low DOX payloads, and two-step PEGylation for high DOX payloads, as shown in Figure 3.1.

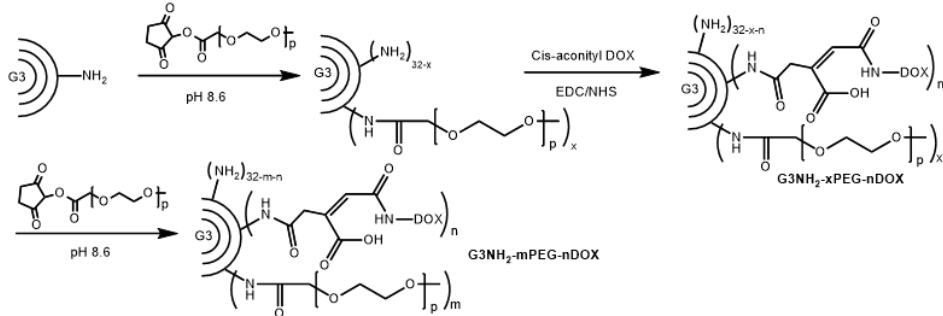
In the direct PEGylation strategy, cis-aconityl DOX was first conjugated to G3NH₂, followed by PEGylation. However, the maximum payload that can be obtained before the conjugate becomes water insoluble is ca. 3.3 DOX. Therefore, an alternative strategy is required in order to prepare G3NH₂-DOX conjugates with higher DOX payloads. The way we approached the problem was to first prepare G3NH₂ with an initial loading of PEG1000, and only then conjugate the hydrophobic DOX. For a pre-PEGylated G3NH₂ with 7PEG1000, we observed that up to 8.8 DOX molecules can be conjugated before the nanoconstruct becomes water insoluble.

Acid-labile conjugate

Direct PEGylation

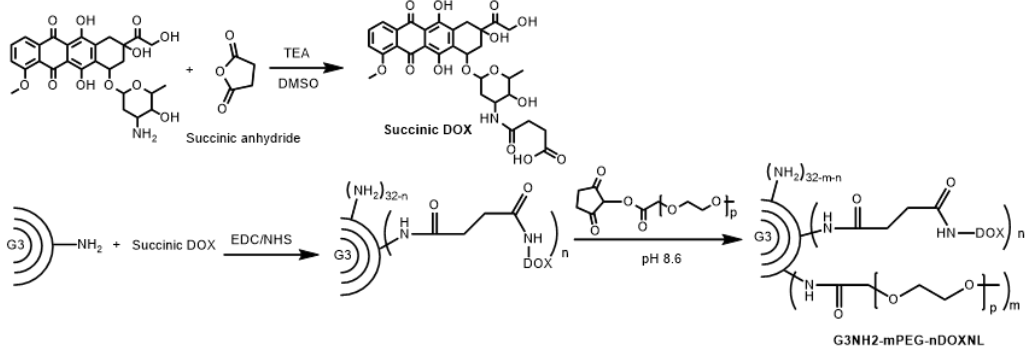


Two-step PEGylation



Acid-nonlabile conjugate

Direct PEGylation



Two-step PEGylation

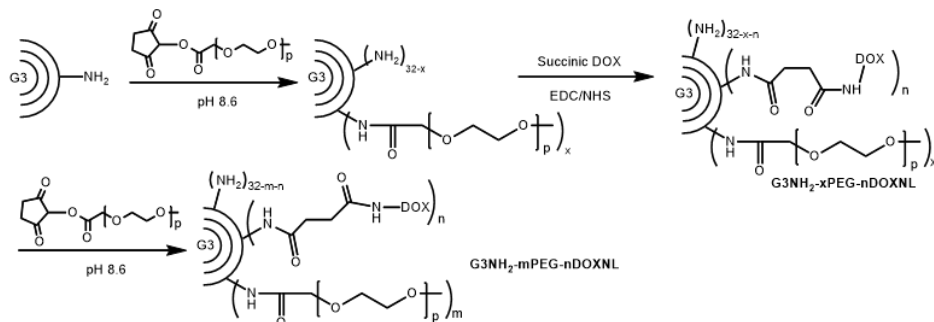


Figure 3.1 Synthesis of the PEGylated, generation 3, amine-terminated PAMAM dendrimer (G3NH₂) conjugated with DOX. DOX conjugated via an acid-labile linker: G3NH₂-mPEG-nDOX; DOX conjugated via a non-labile linker: G3NH₂-mPEG-nDOXNL.

Based on these observations, it seems that a further increase in DOX payload can be achieved by initially conjugating higher number density of PEG1000. Using this approach, in order to achieve the final / desired PEG density (if greater than 7PEG100), a second round of PEGylation is needed. This two-step PEGylation strategy is a viable approach to achieve both high degree of PEGylation and high DOX payload.

We also attempted another strategy in which high PEGylation preceded DOX conjugation, so as to avoid a two PEGylation strategy. However, only 4.4 DOX can be conjugated to G3NH₂-22PEG1000, leading to the failure to achieve high DOX payload. A similar strategy in which PEGylation precedes DOX conjugation has been also reported in an earlier work. High density of peripheral PEG, however, was not attempted (20 PEG out of 64 surface groups) in these reports.[34, 125] However, we will show later that in our work high PEGylation densities are required for the formulation of these nanoconstructs in pMDIs.

In summary, the synthesis of PEGylated PAMAM with low DOX payload (i.e. 3-4 DOX/G3NH₂) can be performed independently of the sequence of DOX and PEG conjugation, while the conjugates with high DOX payload (> 7-9 DOXs/G3NH₂) need to follow the conjugation sequence: 1st PEGylation → DOX conjugation → 2nd PEGylation.

As described for the acid-labile counterparts, the acid-non-labile conjugates with low and high payloads were synthesized via direct PEGylation or two-step PEGylation, with cis-aconityl spacer replaced by succinic linker. The disappearance of free carboxyl group in succinic spacer renders the conjugates stable under both acidic and neutral conditions (G3NH₂-mPEG-nDOXNL).

The acid-labile G3NH₂-mPEG-nDOX and non-labile G3NH₂-mPEG-nDOXNL conjugates were characterized by ¹H NMR, MALDI, and ESI. The ESI (m/z) peaks at 700.2016 ([cis-aconityl DOX+H]⁺), 722.1509 ([cis-aconityl DOX+Na]⁺), and 738.1769 ([cis-aconityl

DOX+K⁺) confirm the successful reaction between DOX and cis-aconityl anhydride, while 666.1815 ([succinic DOX+Na]⁺) and 682.1591 ([succinic DOX+K]⁺) were assigned to succinic

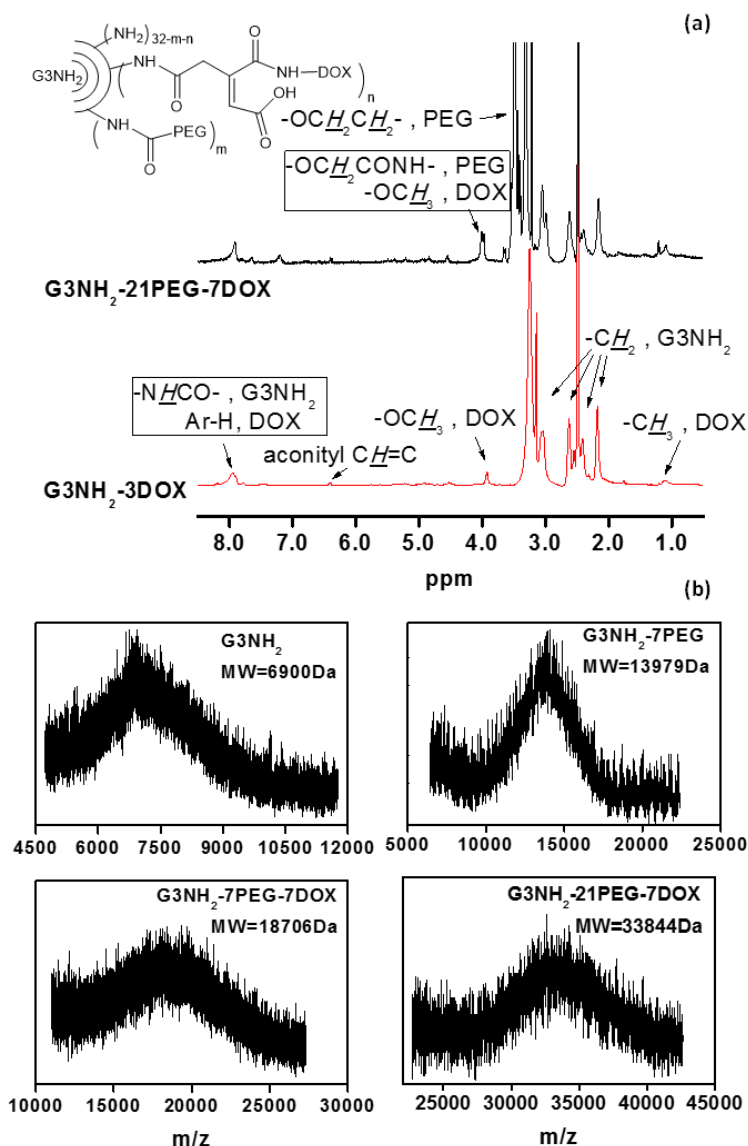


Figure 3.2 Example of (a) ¹H NMR spectra of PEGylated G3NH₂ dendrimer with acid-labile DOX conjugates (G3NH₂-3DOX and G3NH₂-21PEG-7DOX). *Inset*: chemical structure of G3NH₂-mPEG-nDOX. Spectral shifts for all compounds are provided in *Supplemental Information S2 in Appendix 2*, and (b) MALDI spectra of a PEGylated G3NH₂ dendrimer with acid-labile DOX conjugates (G3NH₂-21PEG-7DOX) and the intermediates synthesized via two-step PEGylation strategy.

DOX (*Supplemental Information in Appendix 2*). The ¹H NMR peaks at 6.397 ppm (-CH=C- of

aconityl spacer), 4.025 to 3.936 ppm ($-\underline{C}H_2-$ in PEG) and characteristic peaks of DOX (see *Supplemental Information in Appendix 2*) indicate that DOX was successfully conjugated to dendrimer to form G3NH₂-mPEG-nDOX – Figure 3.2a. In Figure 3.2b we show an example of MW change of the conjugates prepared in the two-step approach (G3NH₂-21PEG-7DOX), as monitored by MALDI-TOF. Results for the all other materials are provided in *Supplemental Information in Appendix 2*.

Table 3.1 Molecular weight (MW), number of PEG1000 grafts (m), number of doxorubicin (DOX) conjugates (n), hydrodynamic diameter (HD), and zeta potential (ζ) of the PEGylated, generation 3, amine-terminated PAMAM dendrimer (G3NH₂) conjugates. DOX conjugated via an acid-labile linker: G3NH₂-mPEG-nDOX; DOX conjugated via a non-labile linker: G3NH₂-mPEG-nDOXNL. Results obtained by ¹H NMR, MALDI, and light scattering (LS) at 25°C. s.d. = standard deviation.

Conjugate	MW	m _{PEG}		n _{DOX}		HD ± s.d. (nm)	ζ ± s.d. (mV)
		¹ H NMR	MALDI	¹ H NMR	MALDI		
G3NH ₂	6900	-	-	-	-	3.8 ± 1.3	+18.8 ± 5.0
G3NH ₂ -10PEG	16436	9.8	9.0	-	-	4.6 ± 1.4	+3.0 ± 4.1
G3NH ₂ -24PEG	32419	24.5	24.1	-	-	8.8 ± 3.7	-2.1 ± 5.4
G3NH ₂ -3DOXNL	8915	-	-	3.4	3.1	4.3 ± 1.5	+14.2 ± 3.3
G3NH ₂ -9PEG-3DOXNL	18975	9.4	9.5	2.6	3.1	7.7 ± 3.5	+2.0 ± 3.6
G3NH ₂ -21PEG-3DOXNL	31077	20.7	21.0	3.1	3.1	8.9 ± 4.2	-3.7 ± 4.9
G3NH ₂ -3DOX	9133	-	-	3.5	3.3	4.0 ± 2.3	+6.3 ± 3.5
G3NH ₂ -9PEG-3DOX	19130	8.8	7.5	2.9	3.3	6.9 ± 3.2	-2.1 ± 4.3
G3NH ₂ -21PEG-3DOX	31220	21.4	20.9	3.1	3.3	9.6 ± 4.9	-6.6 ± 2.7
G3NH ₂ -21PEG-7DOX	33844	21.1	20.5	7.4	6.9	11.3 ± 4.3	-10.5 ± 6.1

The PEG density, DOX payload, and MW of acid-labile G3NH₂-mPEG-nDOX and acid-non-labile G3NH₂-mPEG-nDOXNL conjugates were quantified and are summarized in Table 3.1 along with their hydrodynamic diameter (HD) and zeta potential (ζ).

A series of dendrimers linked with 3 DOX through a pH labile bond or stable bond (control) and varying PEG1000 density were prepared. Another system with 7 DOX was also prepared to compare the effect of DOX loading. The HD is seen to increase upon PEGylation and DOX conjugation, with sizes ranging from 4.0 to 11.3 nm. At low DOX density, the HD is dominated by the PEG density, as all dendrimers with the same PEG density have similar HD, except for G3NH₂-10PEG. G3NH₂-10PEG's small HD may be related to the fact that PEG can more easily form strong bonds with the protonated terminal amine groups of G3NH₂, and thus assume a more collapsed configuration.[182, 214] The addition of 7DOX to the dendrimer with high PEG density seems to have an impact on the overall size, albeit not statistically significant.

We can also observe that the ζ of the nanocarriers decreases from a large positive value for the conjugates with no PEG, to negatively charged at high PEG density – note here that this is the case in spite of the fact that not all surface groups have been modified with PEG, and thus protonated amines are still expected to be present. This effect may be related to the fact that ether oxygen from PEG can strongly interact with the protonated surface amines, thus shielding the surface charge of the nanocarriers.[182, 215] The presence of the extra carboxyl group of the acid-labile DOX linker also helps decrease the overall charge of the dendrimer, as can be observed by comparing for example G3NH₂ (ζ = +18.8 mV) and G3NH₂-3DOX (ζ = +6.3 mV). PEGylation also strongly impacts the ζ , with the dendrimers experiencing charge reversal (to negative ζ) at high PEG densities.[168]

Sizes and charges are some of the most relevant parameters in the design of nanocarriers for drug delivery applications, as these properties dictate how the dendrimer nanocarriers interact with the physiological environment, and thus their fate, including bioavailability, pharmacokinetics and pharmacodynamics.[30, 169] The next step in our work was to evaluate the

success of the acid-labile DOX conjugation strategy, by determining the release at relevant physiological pHs.

3.4.2 *In vitro* release of DOX from acid-labile G3NH₂-mPEG-nDOX and non-labile G3NH₂-mPEG-nDOXNL conjugates at extracellular physiological and lysosomal pH

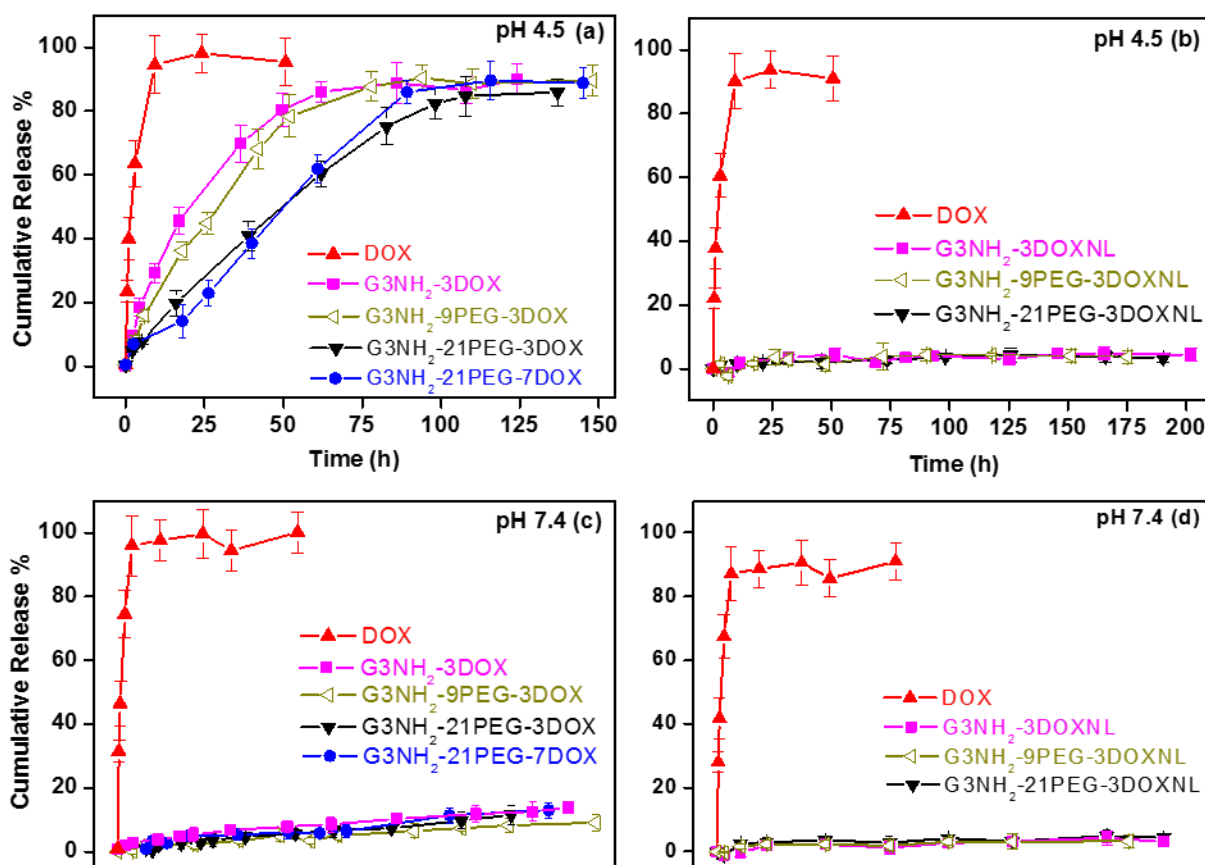


Figure 3.3 *In vitro* release profiles of DOX from the acid-labile (G3NH₂-mPEG-nDOX) and non-labile (G3NH₂-mPEG-nDOXNL) conjugates at (i) lysosomal pH = 4.5: (a) and (b); (ii) physiological pH = 7.4: (c) and (d), all at 37 °C.

The DOX released from the acid-labile G3NH₂-mPEG-nDOX conjugates and the effect of PEG density on the release of DOX were investigated at pH 7.4 (extracellular physiological pH) and 4.5 (lysosomal pH). The release profiles were compared to that of the acid-non-labile G3NH₂-mPEG-nDOXNL conjugates and free DOX, the controls. The results are summarized in Figure 3.3.

As shown in Figure 3.3 (b and d), only very small amounts of conjugated DOX are released from the acid-non-labile G3NH₂-mPEG-nDOXNL conjugates at either physiological or acidic pH conditions (<4%). In contrast, the release of DOX from G3NH₂-mPEG-nDOX is shown to be a strong function of pH. While small (<9%) amounts of DOX are released from G3NH₂-mPEG-nDOX at pH 7.4, when G3NH₂-mPEG-nDOX is in contact with an acidic medium, > 80-85% DOX is released from the acid-labile conjugates. Based on the released profile of free DOX, we expect the losses of up to ca. 7% of DOX (lack of recovery) due to interactions of DOX with the dialysis bag and to a lesser extent due to photobleaching.

The rate and total amount of DOX released from the acid-labile conjugates is also seen to be a function of the PEGylation density of G3NH₂-mPEG-nDOX. An increase in PEG density is seen to retard the release of DOX. At 50 h, for example, the % release of DOX for G3NH₂-21PEG-3DOX is only 47.6%, while that for G3NH₂-3DOX is 80.3%. The effect of PEGylation can be explained by the increased steric hindrance for proton access to initiate the degradation of the acid-labile linker and also by providing a prolonged diffusion of released hydrophobic DOX out of hydrophilic PEG coating layer.[214]

In summary, the acid-labile PEGylated PAMAM-DOX conjugates showed the potential of being stable at extracellular physiological pH, while a sustained DOX release in conditions mimicking intracellular acidic compartments is achieved. It was also shown that the release of DOX can be further modulated by tailoring the peripheral PEG density. The crucial advantage from acid-labile linker is the potential to decrease the concentration of free DOX in plasma by

promoting drug release intracellularly, thus diminishing DOX potential toxicity in general and cardiotoxicity in particular, which may lead to congestive heart failure and death.

3.4.3 Kill of lung adenocarcinoma cells with acid-labile G3NH₂-mPEG-nDOX and non-labile G3NH₂-mPEG-nDOXNL conjugates.

The cytotoxicity of the various DOX conjugates and controls, including free DOX, free

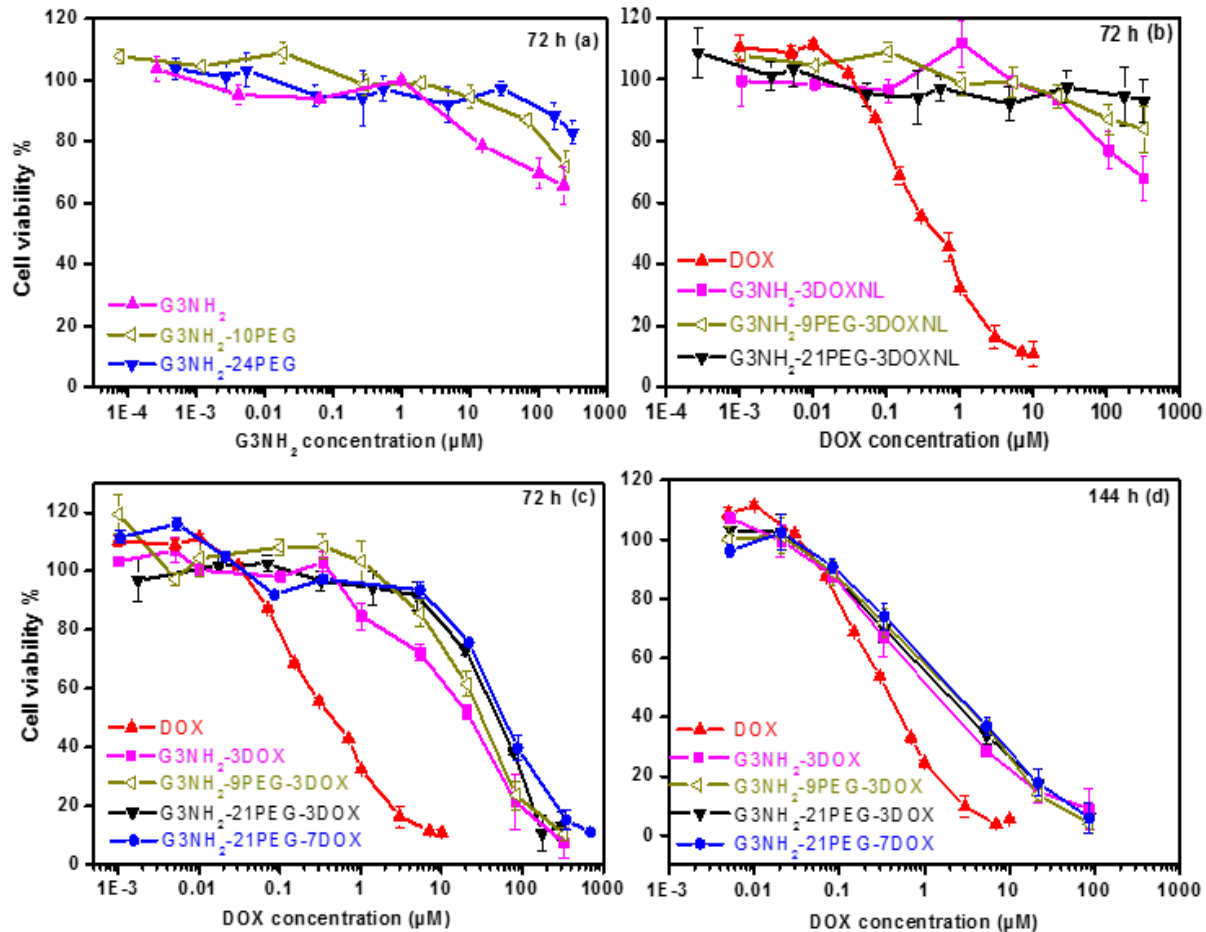


Figure 3.4 Cell kill of (a) G3NH₂ and PEGylated dendrimers (G3NH₂-mPEG), (b) acid-non-labile conjugates (G3NH₂-mPEG-nDOXNL), and (c) acid-labile conjugates (G3NH₂-mPEG-nDOX), as determined by the MTT assay after 72 h incubation with A549 cells. (d) Cell kill of acid-labile conjugates (G3NH₂-mPEG-nDOX) determined by the MTT assay after 144 h incubation with A549 cells. Free DOX is used as control. Results denote mean ± s.d. (n=8).

dendrimer, and free dendrimer-PEG conjugates was assessed by MTT assay on A549 cells. The

results are summarized in Figure 3.4. Corresponding IC_{50} values are listed in *Supplemental Information Table S1 in Appendix 2*.

Neither PAMAM (PEGylated or non-PEGylated) nor acid-non-labile G3NH₂-mPEG-nDOXNL showed strong toxicity against A549 cells within the concentration range and incubation time investigated – Figure 4a. Their IC_{50} values could not be detected in the measured range. The toxicity of bare G3NH₂ was similar to that of G3NH₂-3DOXNL (Figure 3.4b), demonstrating that the toxicity of the conjugates containing non-labile DOX was mainly induced by the peripheral NH₂ groups of the dendrimers.

In contrast, free DOX and acid-labile conjugates induced significant cell kill on alveolar cancer cells. In Figure 3.4c it can be observed that the profiles for free DOX and acid-labile DOX are similar, but free DOX is seen to have higher activity at lower concentration. This is to a large extent related to the fact that free DOX can quickly diffuse through the cell bilayer[104, 216] and reach the nucleus, while DOX from the nanocarriers only starts to be released after internalization and traffic to the lysosomes, where the liable bonds will be broken – allowing DOX to finally reach the nucleus.[217, 218] After cleavage, the diffusion of DOX out of lysosome is also a time-consuming process as the base form of weak bases (e.g. DOX) can readily diffuse across internal membrane of lysosome, while their cationic forms (major form of weak bases in lysosomes) diffuse very slowly across the membrane.[219] This effect can be seen to be dominant, as the cell kill profiles for free DOX and conjugated DOX are seen to be much closer to each other at 144 h post exposure to the dendrimer-DOX conjugates. Another possible reason for the reduced toxicity of conjugated DOX is related to the isomerization during the conjugation of cis-aconityl DOX to dendrimer (cis-aconityl to trans-aconityl DOX),[220] which may result in the failure of original

DOX release from the dendrimer conjugates – a pro-drug is released instead. The reduced toxicity of polymer-bound DOX conjugates is consistent with previously published results.[34, 221]

In summary, the conjugation of DOX to dendrimer nanocarriers promotes the control of its release, both temporally and also spatially (intracellular/low pH), and further control can be achieved upon PEGylation. The cell kill curves reflect this temporal controlled release, with DOX toxicity of the conjugates progressively becoming more similar to free DOX profile, as the DOX-dendrimer bonds are slowly broken down upon cellular internalization and transport of the carriers to acidic compartments, and finally diffusion of DOX to reach the nucleus. The impact of PEGylation density on cell kill is small, and becomes negligible at long incubation times, a very

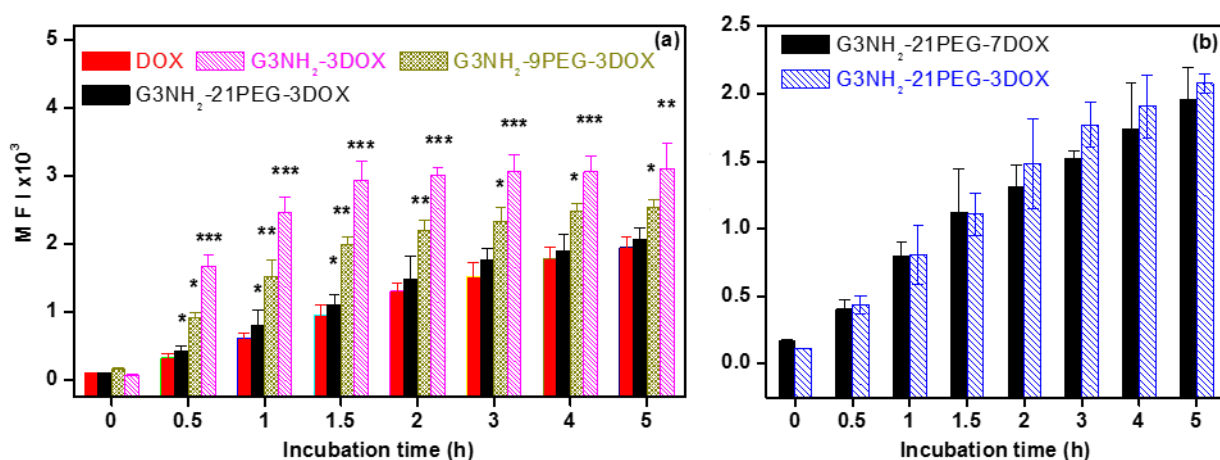


Figure 3.5 Synthesis of the PEGylated, generation 3, amine-terminated PAMAM dendrimer (G3NH₂) conjugated with DOX. DOX conjugated via an acid-labile linker: G3NH₂-mPEG-nDOX; DOX conjugated via a non-labile linker: G3NH₂-mPEG-nDOXNL.

favorable result as the interaction of the carriers *in vivo* can be controlled by changing the PEGylation density/surface characteristics of the nanocarriers, [222, 223] and so can its behavior in HFA-propellants used in pMDI formulation, as will be shown later.

3.4.4 Cellular internalization of acid-labile G3NH₂-mPEG-nDOX conjugates

The kinetics of cellular internalization of the acid-labile G3NH₂-mPEG-nDOX conjugates in A549 cells was evaluated by flow cytometry, by measuring the median fluorescence intensity

(MFI) of DOX internalized within the cells as a function of time, for a period of 5 h. The results are summarized in Figure 3.5.

It can be observed from Figure 3.5a that the rate and extent of internalization of DOX within 5h is enhanced upon conjugation to G3NH₂. The rate of internalization of DOX in G3NH₂-3DOX is 4.7 times greater than free DOX, and the total internalization is statistically different and about 1.6 times as high as free DOX at the end of 5 h. The difference in extent of internalization of free DOX and conjugated DOX is seen to decrease as a function of time. PEGylation is seen to decrease the rate and extent in cellular internalization of conjugated DOX – Figure 3.5a. It is interesting to note, however, that at the highest PEG density (G3NH₂-21PEG-3DOX), the rate and extent of internalization of conjugated DOX is not much different than free DOX, and the means (MFI and rate) are not statistically different at later time points when compared to the same conjugates.

It has been reported that hydrophobic DOX is taken up through passive diffusion and that the diffusion rate is determined by the concentration gradient and interaction with the lipid bilayer.[216, 224] Dendrimer nanocarriers are internalized through different endocytic pathways such as receptor-mediated endocytosis,[217, 225, 226] macropinocytosis,[226] and non-specific, adsorptive endocytosis.[225, 227, 228] The difference in internalization rate of PAMAM-DOX conjugates can be attributed to changes in surface charge. G3NH₂-3DOX with a ζ of +6.3 mV is readily adsorbed and quickly saturates the negative plasma membrane.[227] As a consequence, rapid internalization and uptake plateau (1.5 h after incubation) are observed. The uptake plateau may also reveal the equilibrium of internalization and exocytosis of those conjugates. The non-specific, adsorptive endocytosis is faster and less energy-dependent than other endocytic pathways due to its electrostatic interaction.[217] For the PEGylated nanocarriers on the other hand, the ζ

becomes less positive as the PEG density increases (Table 1), reaching negative ζ at the highest density of PEG. The interaction between the negatively charged G3NH₂-mPEG-nDOX and the plasma membrane is thus attenuated, leading to a slowdown in internalization. However, it is important to note that the long-term cytotoxicity studies suggest that high DOX internalization is achieved for all carrier systems, as similar IC₅₀ concentrations are observed independent of the PEGylation density.

We also investigated the impact of the DOX loading of the conjugates on the rate and extent of internalization of DOX. The results from Figure 3.5b show that the rate and extent of internalization of the dendrimer with the higher payload (G3NH₂-21PEG-7DOX) is not statistically different from that for the dendrimer with lower payload (G3NH₂-21PEG-3DOX), indicating that PEGylation dominates the rate and extent of internalization at short times, which is reasonable considering that there are 21PEG and only 7/3DOX per dendrimer, and both impart negative charged characteristics to the dendrimer.

In summary, conjugating DOX to dendrimer nanocarriers enhances their rate and extent of cellular uptake, at least at early times. Cellular internalization of dendrimer-DOX conjugates can be further modulated by PEG density, while the DOX payload on the periphery of the conjugates does not affect uptake when at high PEG densities.

3.4.5 Intracellular release and colocalization of DOX from acid-labile G3NH₂-mPEG-nDOX conjugates

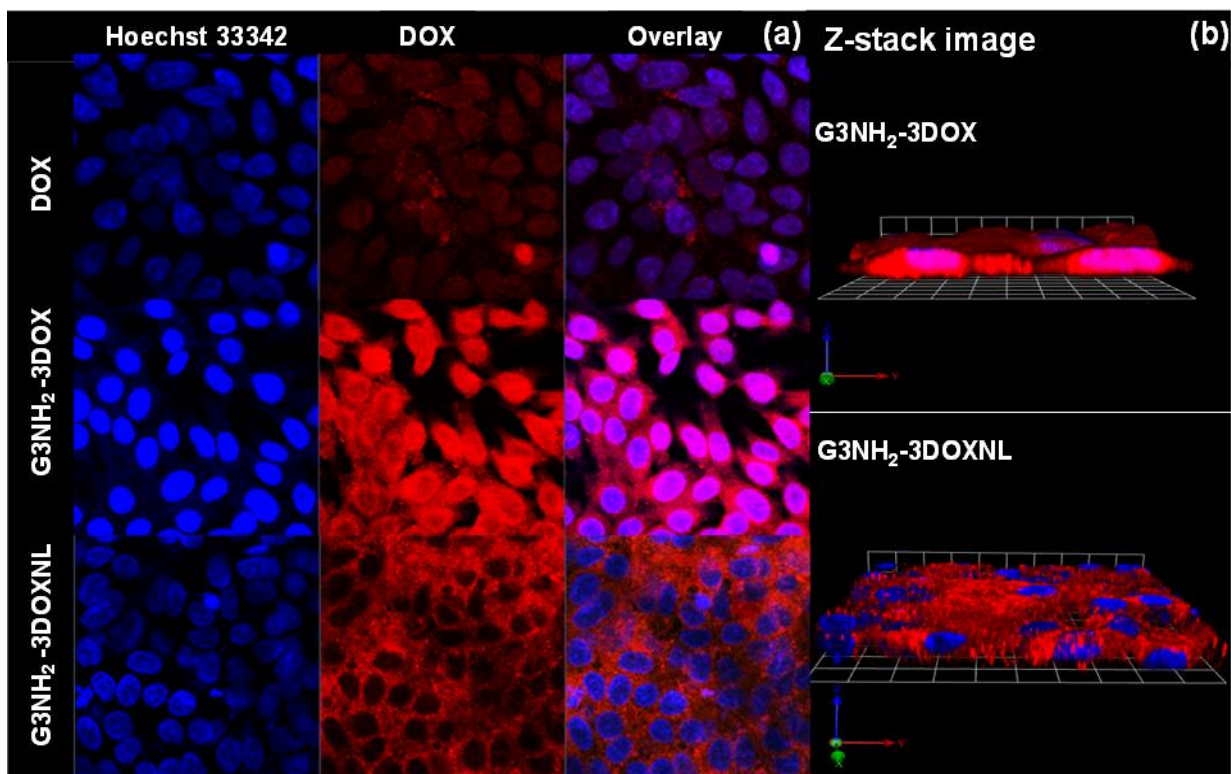


Figure 3.6 (a) Selected confocal images of A549 cells contacted with free DOX, acid-labile G3NH₂-3DOX and acid-non-labile G3NH₂-3DOXNL conjugates. (b) Cross section of 3D rendered confocal image of acid-labile G3NH₂-3DOX and acid-non-labile G3NH₂-3DOXNL conjugates. Image (a) and (b) were obtained 48 h after A549 cells were incubated with the samples. Blue color represents nuclei, red color for DOX, and pink color for DOX co-localized with nuclei.

The intracellular colocalization of free DOX, and DOX from the acid-labile G3NH₂-3DOX and acid-non-labile G3NH₂-3DOXNL conjugates in A549 cells was determined by confocal microscopy. As shown in Figure 3.6a (“*Overlay*” column), the red fluorescence of DOX in the case of free DOX (first row) and of the DOX from the G3NH₂-DOX conjugate (second row) was highly superposed with the blue staining of the nucleus (Hoechst 33342), revealing significant colocalization of DOX with the nuclei of A549 cells, the target organelle. Perinuclear colocalization of DOX from G3NH₂-DOX indicates that not all DOX had been released at that

time. No red fluorescence from DOX was observed in the nuclei for acid-non-labile G3NH₂-3DOXNL (third row).

The 3D rendering of the confocal layers for G3NH₂-3DOX and G3NH₂-3DOXNL shown in Figure 3.6b further confirms the ability of the conjugates to gain intracellular access, to be trafficked through an acidic pathway, thus releasing the DOX conjugated through the acid labile bond to G3NH₂, and finally to co-localize with the nucleus. These results support the cell kill experiments shown in Figure 3.5. We can also observe that DOX in G3NH₂-3DOXNL does not gain access to the nucleus as is not released due to the presence of a pH stable bond between DOX and the dendrimer, and the fact that the dendrimer-DOX conjugate seems to be too large to passively cross the nuclear pores.

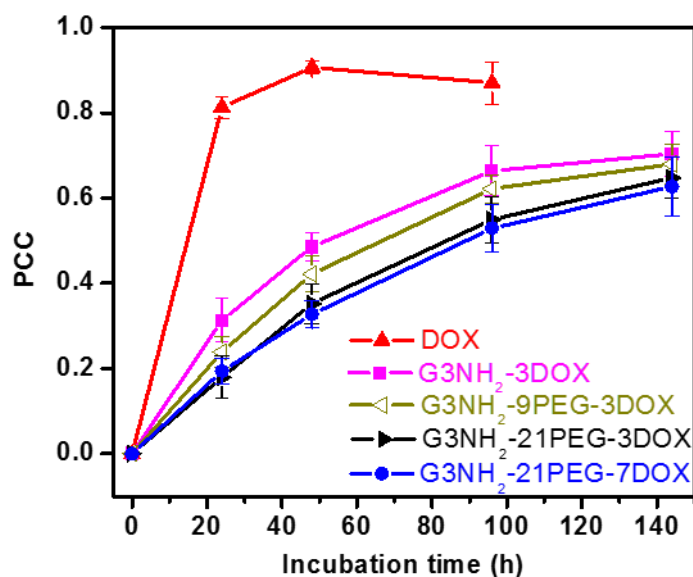


Figure 3.7 Pearson's Correlation Coefficient (PCC) of DOX free and from acid-labile G3NH₂-mPEG-nDOX conjugates as a function of incubation time. PCC was determined by confocal microscopy, and calculated based on the colocalization of blue-stained nuclei and red DOX.

These qualitative observations are complemented by quantitative results of the colocalization of DOX (red fluorescent pixels from the confocal slices) with the nucleus (blue fluorescent pixels) as a function of incubation time, upon determination of the Pearson's

Correlation Coefficient (PCC) for those fluorescent signals. A PCC = 1 represents complete correlation, while a PCC = 0 represents no correlation.[229] The PCC values for DOX:nucleus for G3NH₂-mPEG-nDOX conjugates, and for free DOX (control) are summarized in Figure 3.7.

The PCC of free DOX is seen to reach 0.87, which represents very high correlation, and this happens at early times - 24 h due to fast colocalization of free DOX within the nucleus. The PCC is seen to level off after ca. 48 h. The PCC for DOX:nucleus in the experiments with the acid-labile G3NH₂-mPEG-nDOX conjugates is also seen to be very high at 0.7, indicating strong nuclear colocalization, with a maximum PCC happening at 144 h. However, the maximum PCC for the conjugated DOX is smaller than that seen for free DOX. This lower maximum PCC may be attributed to the isomerization of the conjugates and the fact that there are many potential endocytic pathways for internalization of the conjugates. As cis-aconityl DOX is conjugated to PAMAM dendrimer, cis-aconityl spacer may isomerize to trans-aconityl form.[220] The PAMAM-DOX conjugates with cis-aconityl spacer releases free DOX, whereas the counterparts with trans-aconityl spacer gives rise to aconityl DOX due to the cleavage of amide bond between G3NH₂ and linker. The aconityl DOX is not able to get into nucleus due to the loss of the NH₂ group, which is the driving force of DOX to reach the negatively charged DNA.[96] In addition, the conjugates that are internalized by certain endocytic pathways that do not lead to the acidic lysosomes (i.e. caveolae-mediated endocytosis) will have a retarded rate of release for DOX.[230]

The PCC curves are also impacted by PEGylation. They are supported by the cellular internalization (Figure 3.5) and controlled release (Figure 3.3) results that show a slowdown in uptake and release as the PEG density increases. The DOX loading is shown not to affect the PCC curves – see curves for G3NH₂-21PEG-3DOX and G3NH₂-21PEG-7DOX. Finally, it is worth pointing out that the rate of increase in PCC with time is also slower in the case of the conjugates

– compared to free DOX, but it is not clear whether a plateau has been reached at the terminal point of the experiment, which may suggest that higher PCCs for DOX from the conjugates may be achieved.

3.4.6 Physical stability of the acid-labile G3NH₂-mPEG-nDOX conjugates in HFA Propellant.

Once the efficacy of the DOX conjugation strategy was assessed *in vitro*, we developed a strategy to formulate dendrimer-DOX conjugates in pMDI formulations for local lung delivery. We are particularly interested in pMDIs due to the many advantages of such portable inhalers, including ease of use and the fact that they are the least expensive OI devices in the market today.[231-233]

We started by investigating the impact of PEGylation and DOX loading on the dispersibility / pseudo-solubilization of the G3NH₂-mPEG-nDOX conjugates in HFA277, one of the propellants approved by the FDA for formulation in pMDIs.[234] The stability of the formulations was assessed by visually monitoring the dispersion of G3NH₂-mPEG-nDOX conjugates in HFA227 as a function of time after sonication.[58] In order to improve the solubilization/dispersion of the conjugates, a small amount of ethanol (EtOH) cosolvent was added. EtOH is an excipient commonly used in commercial pMDI products, usually at much higher concentrations - up to ca. 15% v/v in commercial formulations [235] However, because the presence of large amounts of EtOH is known to negatively impact aerosol quality in pMDIs,[78, 233, 236] we kept the EtOH concentration to a minimum. The physical stability results of the formulations are summarized in Figure 3.8.

We can observe that the dispersibility / pseudo-solubilization of the G3NH₂-mPEG-nDOX conjugates is dramatically impacted by the presence of PEG1000. As the PEG1000 density increases, so does the dispersibility of the conjugate, with the conjugate having 21PEG1000

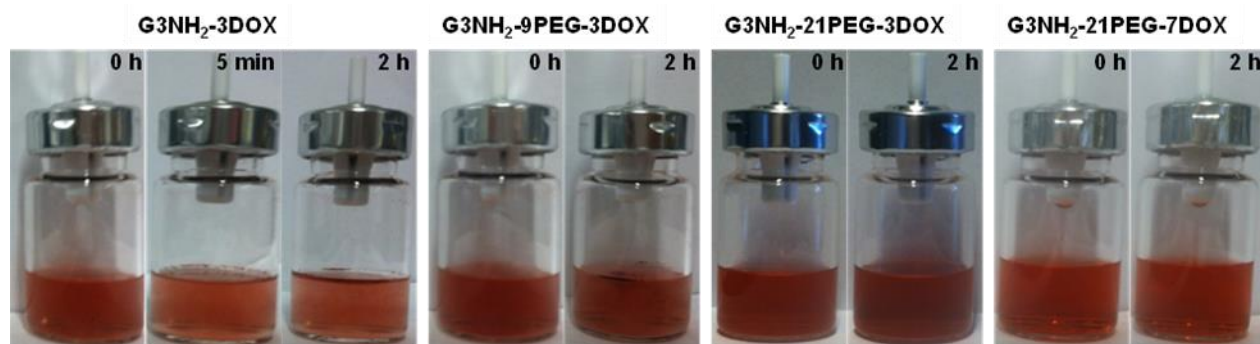


Figure 3.8 Dispersion of acid-labile G3NH₂-mPEG-nDOX in HFA227 propellant as a function of time after sonication. Conditions were: 0.2 mg/mL DOX equivalent; 0.37% anhydrous ethanol (v/v relative to the propellant), at 25°C.

showing excellent dispersibility in HFA227. Our previous ab initio calculations and chemical force microscopy results have revealed that ether-containing functionalities (e.g. -CH₂CH₂O-) can be well solvated in HFA propellants as the ether oxygen atom can strongly interact with the dipole of the propellant.[237] The precise conformation of the PEG layer around the dendrimer when the system is dispersed in HFA propellant is still unclear. However, we speculate that some of the segments of the PEG chain may protrude into the propellant, thus acting as a stabilizer as they strongly interact with HFA molecules (HFA-ether complexes),[237] whereas the rest of domains cover the dendrimer surface to form a compact architecture, so as to reduce attractive forces among the dendrimer nanocarriers.[182] Therefore, it is likely that the conjugates in propellant HFA227 take on a core-shell conformation in which PAMAM and DOX consist of the core and PEG chains are situated in the outer shell layer. We also see that at high PEG1000 density the increased payload of HFA-phobic DOX does not affect the dispersibility of the conjugate in the propellant.

It is believed that 7 peripheral DOX molecules can be still thoroughly coated by an abundance of grafted PEG chains.

In order to further clarify the nature of the pseudo-solutions/dispersions of the conjugates in HFA, we determined their solvated diameters (SD). We use an HFA that is liquid at ambient conditions and a model liquid propellant — 2H,3H perfluoropentane (HPFP).[81, 238] The results are summarized in Table 3.2.

Table 3.2 Solvated diameter (SD) of the PEGylated (*m*), generation 3, amine-terminated PAMAM dendrimer (G3NH₂) conjugates with DOX measured in the model propellant HPFP. DOX conjugated via an acid-labile linker (G3NH₂-mPEG-nDOX). Results determined by light scattering (LS) at 25°C and 0.2 mg/mL DOX equivalent. n.p. = not present; % in parenthesis = volume fraction within that diameter range.

Conjugate	SD ± s.d.	
	Peak A	Peak B
G3NH ₂ -3DOX	0.5 ± 0.1 μm (13.3%)	6.1 ± 2.8 μm
G3NH ₂ -9PEG-3DOX	0.7 ± 0.1 μm (15.1%)	4.2 ± 1.2 μm
G3NH ₂ -21PEG-3DOX	26.1 ± 7.8 nm (100%)	n.p.
G3NH ₂ -21PEG-7DOX	38.3 ± 11.6 nm (100%)	n.p.

At low/no PEG1000 density, the G3NH₂-mPEG-nDOX conjugates formed large, micron-sized aggregates, which indicates the lack of dispersibility in HFAs. However, upon increasing density of PEG1000 to 21, no micron-sized aggregates can be found. The SDs of the highly PEGylated conjugates were around 30-40 nm. These sizes may represent aggregates of a few conjugates only, or even a single dendrimer conjugate whose SD in HPFP (26 nm for G3NH₂-21PEG-3DOX) turns out to be a few times larger than their HD (SD in water – 10 nm G3NH₂-21PEG-3DOX) - which are reported in Table 3.1.

3.4.7 Aerosol characteristics of pMDI formulations of acid-labile G3NH₂-mPEG-nDOX conjugates.

While good dispersibility was found for the PEGylated conjugates, the results discussed

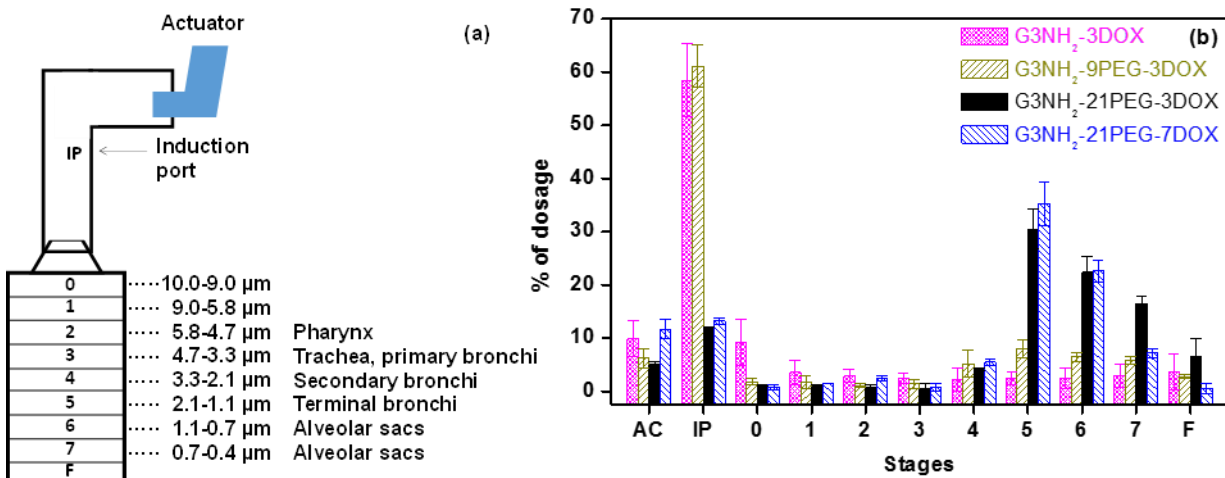


Figure 3.9 (a) Structure diagram of an Andersen Cascade Impactor (ACI) and correlation of stages in ACI to anatomical regions of the lungs. (b) Aerosol characteristics of the pMDI formulations containing acid-labile conjugates (G3NH₂-mPEG-nDOX) in HFA227 propellant at 0.2 mg/mL DOX equivalent and 0.37% anhydrous ethanol v/v relative to propellant, as determined using ACI at 25 °C. AC, IP, 0-7 and F denote actuator, induction port, Stage 0-7 and filter, respectively.

before do not address the aerosol quality of the resulting formulations. Andersen Cascade Impactor (ACI) is widely used as an *in vitro* lung model to determine drug deposition in the lungs. The correlation of stages to anatomical pulmonary regions are summarized in Figure 3.9a. Stage 3 and higher represent the lower respiratory tract and deep lung deposition. The effect of PEG density on the aerosol performance of pMDI formulations of G3NH₂-mPEG-nDOX conjugates was evaluated and are summarized in Figure 3.9b and Table 3.3.

Formulations were prepared at the same conditions as in the physical stability studies discussed earlier - HFA227 propellant at 0.2 mg/mL DOX equivalent and 0.37% v/v EtOH. It can be observed from Figure 9b that the fraction of DOX (in the conjugate) deposited on stages 3-F increase dramatically at the high PEG density (21PEG1000) compared to no PEG and 9PEG1000.

The mass deposition on each stage is summarized in *Supplementary Information Table S2 of*

Appendix B. The mean mass aerodynamic diameter (MMAD), and the geometric standard deviation (GSD) of the formulations were determined from the ACI results and are summarized in Table 3.3, along with the respirable fraction (RF) and fine particle fraction (FPF), which represent respirable dose of the formulation and the dose deposited on low respiratory and deep lung area, respectively.

While the MMAD for all conjugates fall within the optimum range (5.0-0.5 μ m), the GSD is much smaller for the highly PEGylated conjugates. More importantly, the RF and FPF for the conjugates with 21PEG1000 (both low and high DOX payload) are much higher than those for G3NH₂-3DOX and G3NH₂-9PEG-3DOX, the conjugates that showed low dispersibility of the propellant. The RF and FPF for G3NH₂-21PEG-3DOX was found to be 82.0% and 78.1%, respectively. For comparison, most of marketed formulations have RF<45% [239-241] of emitted dose and FPF<55%. [163] The RF of the formulation is even higher than HFA-based solution formulations of small molecules (RF: ca. 60-80%) containing soluble excipients. [239, 242] The recovery for the formulations containing G3NH₂-21PEG-3DOX and G3NH₂-21PEG-7DOX is much higher than that of the poorly dispersed counterparts. We believe that the loss of the delivered dose of the formulation containing highly PEGylated conjugates is mainly from small particles with exhalable size range (aerodynamic diameter < 0.5 μ m), whereas the strong aggregation of non-PEGylated/low PEGylated conjugates in propellant (big aggregates may not be puffed out) causes the relatively low recovery rate for those nanocarrier systems.

One interesting aspect of this study is the fact that pMDI formulations containing dendrimer conjugates with such small SD – thousand fold smaller than the optimum aerosol diameter - between 0.5 to 5 μm , [243] are capable of generating corresponding aerosols with such exceptional quality.

Table 3.3 Median mass aerodynamic diameter (MMAD), geometric standard deviation (GSD), respirable fraction (RF), fine particle fraction (FPF) and recovery (%) of the pMDI formulation containing the PEGylated (*m*), generation 3, amine-terminated PAMAM dendrimer (G3NH₂) dendrimers conjugated with DOX via an acid-labile linker (G3NH₂-mPEG-nDOX). Aerosol results determined using the Andersen Cascade Impactor (ACI), at 25°C. Formulation containing 0.2 mg of DOX equivalent per mL of propellant and anhydrous ethanol at 0.37% v/v relative to the propellant. Propellant is HFA227.

Conjugates	MMAD (μm)	GSD (μm)	RF (%)	FPF (%)	Recovery (%)
G3NH ₂ -3DOX	4.5 \pm 1.9	6.6 \pm 2.4	31.8 \pm 3.9	16.1 \pm 1.8	65.7 \pm 6.4
G3NH ₂ -9PEG-3DOX	3.3 \pm 0.8	3.9 \pm 1.4	33.1 \pm 5.9	29.7 \pm 3.7	69.2 \pm 7.1
G3NH ₂ -21PEG-3DOX	1.2 \pm 0.1	1.9 \pm 0.1	82.0 \pm 4.8	78.1 \pm 4.3	86.9 \pm 4.7
G3NH ₂ -21PEG-7DOX	1.2 \pm 0.1	1.6 \pm 0.1	75.4 \pm 3.0	70.8 \pm 5.4	84.6 \pm 5.5

We propose here a mechanism to explain the results, a schematic diagram of which is shown in Figure 3.10. In Figure 3.10a, the pseudo-solution of the G3NH₂-mPEG-nDOX conjugates in HFA propellant is shown – this picture is supported by the SD and physical stability results discussed above. Upon depressing the actuator, droplets containing G3NH₂-mPEG-nDOX and propellant are formed. As the HFA227 propellant evaporates – Figure 3.10b, the polymer concentration within the droplets increases and it eventually crosses the phase boundary illustrated in Figure 10c – from a single phase to a phase-separated system. Micron-sized particles made of phase-separated G3NH₂-mPEG-nDOX are formed with the appropriate aerosol diameter for deep lung deposition - Figure 3.10b (iii).

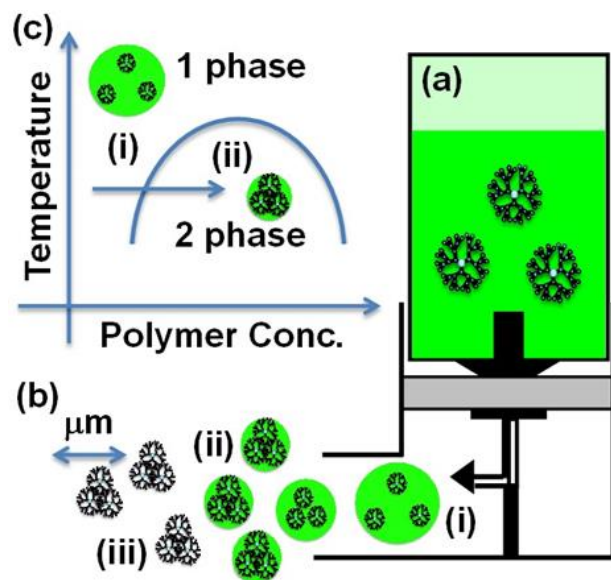


Figure 3.10 Schematic diagram of the proposed mechanism for the formation of the micron size aerosol particles from the nanometer size conjugates. (a) Acid-labile G3NH₂-mPEG-nDOX are solvated as individual particles or nanoaggregates of a few molecules in liquid HFA227 in pMDI at its saturated pressure. (b) As the aerosol forms, the conjugates are (i) initially fully solvated; (ii) as the propellant evaporates, the dendrimer solution phase separates, forming dendrimer nuclei that continue to increase in size to form particles until; (iii) the propellant completely evaporates. (c) Phase separation as the concentration of dendrimer conjugates increases upon evaporation of propellant at ambient pressure.

3.5 Conclusion

In this work we demonstrated the ability of G3NH₂-DOX conjugates to effectively kill A549 cells, an *in vitro* model of alveolar adenocarcinoma. We also developed a novel strategy for the formulation of the conjugates in pMDIs, consisting in forming a pseudo-solution of the nanocarrier/polymer-drug conjugates in the propellant, which can be achieved upon surface modification of the nanocarrier with a moiety that has high affinity to HFA. DOX was conjugated to G3NH₂ through a pH sensitive bond, which was shown to be a suitable strategy to provide a

sustained intracellular release, while being very stable at extracellular physiological conditions. We showed that the release profile of DOX at low pH can be further modulated by the number density of PEG conjugated onto the G3NH₂ surface. PEGylation is used to enhance the aqueous solubility of the conjugate at high DOX payloads, and also to promote the formation of the pseudo-solution in the propellant HFA of pMDIs. The impact of PEG is also observed on the rate and extent of internalization of the dendrimer-DOX conjugates in A549 cells at short times (up to 5h). Nuclear colocalization studies indicate that the dendrimer-DOX conjugates are not only taken up by A549 cells, but the DOX released colocalizes with its target organelle, the nucleus, very efficiently. Interestingly, PEGylation does not affect the ability of the conjugates to kill the adenocarcinoma cells, as all conjugates show similar IC₅₀'s at the same DOX equivalent loading at long incubation times. Highly stable pseudo-solution of the G3NH₂-nDOX conjugates were formed at high PEG densities, as the dipole of HFA can interact very strongly with the ether oxygen of the PEG layer covering the drug-dendrimer conjugate, and thus promote its pseudo-solubilization. The aerosol characteristics of the resulting pMDI formulations were shown to be exceptional, with respirable fractions as high as 82%. The relevance of the aerosol study goes beyond the formulation of DOX, as other small molecule therapeutics have similar potential to be formulated in pMDIs as dendrimer-drug pseudo solutions using the strategy discussed here.

3.6 Acknowledgements

We would like to acknowledge financial support from National Science Foundation (NSF-CBET grant no.0933144 and NSF-DMR grant no. 1508363) and the NanoIncubator at WSU. We would also like to thank Dr. Jessica Back and Mr. Eric Van Buren (Microscopy, Imaging and Cytometry Resources Core) for useful discussions regarding flow cytometry analysis. The MICR Core is supported, in part, by NIH CenterGrant P30CA022453 to the Karmanos Cancer Institute

and the Perinatology Research Branch of the National Institutes of Child Health and Development, both at WSU.

3.7 Supplemental information

Description of synthesis and characterization of the acid-labile and acid-non-labile PEGylated dendrimer-DOX conjugates/structures including ^1H NMR, ESI, MALDI-TOF and LS. The IC_{50} of free DOX and various PEGylated dendrimer-DOX conjugates and aerosol mass deposition in ACI of pMDI formulation containing dendrimer-DOX conjugates are also provided. This material is available in *Appendix B*.

CHAPTER 4 — Design of Dendrimer-Doxorubicin Conjugates for Transport Modulation across *in vitro* Pulmonary Epithelium and their Solution Formulation in pMDIs

4.1 Introduction

Of all malignant tumors, lung cancers hold great relevance as it is the leading cause of cancer death for both men and women throughout the world.[2] The mortality of lung cancer is higher than that of colorectal, breast and prostate cancers combined. 5-year survival rate of lung cancers after initial prognosis is only 16.6% since most of patients are diagnosed at late phase, thus limiting surgical treatment in the alleviation of lung cancers.[244] Therefore, chemotherapy is widely used as a tool to treat lung cancers. However, limited progress has been made by chemotherapy in the fight against lung cancers. One of major challenges is low therapeutic concentration found in lung tumors upon systemic administration (e.g. intravenous and intraperitoneal injection).[8] Therefore high dosage of drug with strong systemic adverse effects is required due to poor distribution to lung tumors.

The lungs as a portal of entry for regional [245, 246] and even systemic [247, 248] drug delivery is often characterized by enhanced bioavailability, which is to some extent associated with long drug retention, large respiratory surface area (ca. 100 m²),[249] low enzymatic degradation of drugs in lung tissues, fast action of drug, reduced systemic adverse effect, and thin cellular barriers for entry of drugs to blood circulation.[250] Several anatomical barriers that entrap drugs administered through pulmonary route include bifurcated bronchi, epithelial layers with viscous mucus, fast-renewed mucociliary clearance, and alveolar macrophage.[251] One major challenge in pulmonary drug delivery is limited transport across respiratory epithelial barriers, which attenuates drug distribution in lung tissues and even its entry to systemic circulation. For example,

tight junction with small pore size (ca. 0.5-2 nm),[185] junctional protein complex that regulates paracellular transport,[185] and transmembrane drug transporters in charge of transcytosis.[186]

Oral inhalation (OI) has showed its great promise not only for regional administration of therapeutics to the lungs, but also as a promising noninvasive route to systemic circulation through the lungs.[245, 252] Pressurized-metered dose inhalers (pMDIs) have been seen the most promising OI technique due to its portability, ease of use and reliable dosage delivery. However, the biggest challenge for pMDIs formulation is that few drugs are soluble, even with the aid of co-solvents or surfactants, in propellants used for pMDIs.[78] The addition of co-solvents and surfactants help solubilize and disperse drugs to in propellants, making a drug suspension that is a heterogeneous system. In contrast, solution formulation gives rise to a homogenous system characterized by a larger fine particle dosage [83] and finer residual aerosol,[84] which leads to efficient delivery of drug to low respiratory tract and deep lung areas. Additionally, the fraction of nonvolatile components added to both solution and suspension formulation can modulate aerosol performance of pMDI formulations.

Doxorubicin (DOX), as a leading chemotherapeutics, has been widely used for treating many cancers including lung cancers. Fast clearance and severe cardiac toxicity, however, limit its application in some patient populations. Dendrimer nanocarriers (DNCs) have been successfully explored for targeted and controlled delivery of DOX in cancer treatment.[33, 125, 253] Polyamidoamine (PAMAM) is a hyperbranched synthetic dendrimer with monodispersity, highly controlled size, and multivalent surface groups.[30, 31] By attaching different ligands, the multifunctional surface groups of PAMAM dendrimer could be potentially used to (i) target tumor cells,[170] (ii) modulate cellular uptake,[254] (iii) facilitate transepithelial transport,[41, 42, 192] and (iv) deliver therapeutics to subcellular organelles.[170] However, amine-terminated PAMAM

dendrimer showed generation-dependent toxicity and hemolysis.[255] PEGylation has been an effective strategy to help DNCs improve pharmacokinetics,[173, 256] reduce toxicity,[170, 257] and escape mucus entrapping.[72] Recent study showed an additional significant attribute of PEG as ligand for pulmonary administration: the modulation of *in vitro* transepithelial transport of DNCs across airway epithelium and *in vivo* entry of DNCs to systemic circulation.[256]

Based on those challenges and opportunities of pulmonary route for lung cancer treatment, the work was to design DNCs for controlled intracellular delivery of DOX that can modulate the transport across pulmonary epithelium, as well as to develop facile DNC-laden pMDI formulation with superior aerosol performance. To achieve this goal, DOX was conjugated to generation 3 amine-terminated PAMAM dendrimer with varying peripheral PEG density via an acid-labile cis-aconityl spacer. The effects of PEGylation degree and DOX payload on *in vitro* release, cytotoxicity, and transepithelial transport were investigated on airway epithelial cancer cell model (Calu-3). The PEGylated PAMAM-DOX conjugates were directly formulated in portable pMDI with HFA227 propellant. The effect of PEGylation degree on physical stability, particle size and aerosol characteristics was also evaluated with scanning electronic microscopy, dynamic light scattering and Andersen Cascade Impactor (ACI). The deposition of the conjugates in different pulmonary regions was modulated by adjusting conjugate concentration in pMDI formulation. Broadly, this work is of great relevance because to our best knowledge it is for the first time that polymeric nanocarrier-based drug delivery system has been formulated into propellant-based solution pMDI formulation which holds aerosol performance superior to current marketable pMDI products and formulations in literatures.

4.2 Materials

Generation 3 amine-terminated poly(amido amine) (PAMAM) dendrimer (G3NH₂, 32 - NH₂ surface groups, theoretical molecular weight = 6909) was purchased from Dendritech, Inc (Miland, MI, USA). Doxorubicin hydrochloride salt (DOX) was purchased from LC Laboratories (Woburn, MA, USA). Polyethylene glycol succinimidyl ester, 1000Da (PEG1000-SE) was purchased from NANOCS, Inc (New York, NY, USA). Polyethylene glycol 1000Da (PEG1000), cis-aconityl anhydride, sodium hydroxide (NaOH), stannous octoate (95%), 4% para-formaldehyde phosphate buffer saline and mucin from porcine stomach (type III, bound sialic acid 0.5-1.5 %) were purchased from Sigma-Aldrich (St Louis, MO, USA). D, L-lactide was a gift from Purac Biomaterials (Amsterdam, Netherland). Pierce[®] BCA Protein Assay Kit was purchased from Thermo Fisher Scientific (Waltham, MA, USA). Dulbecco's Modified Eagle's Medium (DMEM) and penicillin (10,000 U/mL)-streptomycin (10,000 µg/mL) were purchased from Life Technologies (Grand Island, NY, USA). Fetal bovine serum (FBS) was purchased from Atlanta Biologicals, Inc (Flowery Branch, GA, USA). Deuterated dimethylsulfoxide (DMSO-d₆) was purchased from Cambridge Isotope Laboratories (Andover, MA, USA). Ultrapure deionized water (DI H₂O) was obtained from a Barnstead NANOpure DIamond System (D11911) from Thermo Fisher Scientific (Waltham, MA, USA). Calu-3 human lung adenocarcinoma epithelial cell lines were purchased from American Cell Collection (Manassas, VA, USA). Amicon[®] Ultra 15 centrifugal filter device (MWCO = 3000Da) was purchased from EMD Millipore (Billerica, MA, USA). Costar Transwell[®] Permeable Support (pore size: 0.4 µm; surface area = 0.33 cm²) was purchased from Corning Incorporated (Corning, NY, USA). Thin layer chromatography (TLC) Silica gel 60 F₂₅₄ plastic sheet was purchased from Merck KGaA (Darmstadt, Germany). All reagents were used as received unless otherwise stated.

4.3 Methods

4.3.1 Synthesis of acid-labile PEGylated PAMAM-DOX conjugates (G3NH₂-mPEG-nDOX, m=0, 9, 21, and n=3, 7).

The synthesis of the acid-labile (cis-aconityl), PEGylated DOX-dendrimer conjugates used in this work has been discussed in detail in **Chapter 2**. All the products were characterized with proton nuclear magnetic resonance (¹H NMR), matrix-assisted laser desorption/ionization-time of flight (MALDI-TOF), and light scattering (LS). The characteristics of the various conjugates are summarized in Table 1.

4.3.2 Cell kill ability of acid-labile G3NH₂-mPEG-nDOX conjugates against Calu-3 cells.

The ability of free DOX and G3NH₂-mPEG-nDOX conjugates in killing the human lung adenocarcinoma Calu-3 cell was assessed using the MTT assay. Approximately 1×10⁴ cells/well (n=8 per concentration) were seeded in tissue culture treated 96-well plates (VWR Internationals, Radnor, PA, USA) with DMEM (no phenol red). The medium was removed after 24h and 100 μl of the free or conjugated DOX solution in DMEM (no phenol red) was pulsed to each well. The samples were incubated with the cells for 72h. The sample-laden medium was then removed from each well. The cells were washed with PBS (1X, pH 7.4) twice. 100 μl of fresh DMEM (no phenol red) and 10 μl of MTT PBS solution (5 mg/mL) were added to each well and incubated for 4h (37 °C, 5% CO₂). Subsequently, 75 μl medium was removed from each well and 60 μl DMSO was added back into the wells to dissolve the formazan crystal. The cells were incubated (37 °C, 5% CO₂) for another 2h. Finally, the absorbance of formazan at 540 nm was recorded using a Biotek Synergy 2 Multi-Mode Microplate Reader (Biotek Instruments, Inc. Winooski, VT, USA).

4.3.3 *In vitro* transport of G3NH₂-mPEG1000-nDOX conjugates across polarized Calu-3 monolayers

4.3.3.1 *Cell growth on Transwell® inserts.*

Approximately 5×10^4 Calu-3 cells (passage 10-20) were seeded on the apical compartment of each insert, which was placed onto 24-well plates with 0.2 mL DMEM (20% FBS, 100 U/mL penicillin and 100 μ g/mL streptomycin). The basolateral compartment of each insert was filled with 0.6 mL DMEM (20% FBS, 100 U/mL penicillin and 100 μ g/mL streptomycin). The cells were grown for 48h (37 °C, 5% CO₂) and the medium was removed from the apical side at that time. The cells were allowed to grow at the air-liquid interface (AIC). The medium in the basolateral compartment was changed every 2 days. The transepithelial electrical resistance (TEER) of the cell were monitored every day, to assess the formation of confluent and polarized monolayers.[256] TEER measurements were performed with a chopstick electrodes (STX-2) and EVOM voltmeter (World Precision Instruments. Sarasota, FL, USA) as reported previously.[256] The actual monolayer TEER was obtained by subtracting the EVOM reading of a blank insert from that of cell-laden insert, and normalizing for the surface area of the insert (0.33 cm²).

4.3.3.2 *In vitro transepithelial transport.*

In vitro transport was conducted as the TEER of cell monolayer started leveling off at ca. 450 Ω (ca. 11 days). The TEER was measured prior to the addition of free DOX or G3NH₂-mPEG1000-nDOX conjugates. HBSS (1X, pH 7.4) was added to apical (0.2 mL) and basolateral (0.6 mL) compartments of the insert and the TEER was again measured as described above. The obtained TEER was used as that at t = 0h. Subsequently, the inserts were moved to the next well and the blank HBSS in apical compartment was replaced with 0.2 mL HBSS with 50 nM (DOX equivalent) of free DOX or G3NH₂-mPEG1000-nDOX conjugates (n=6 per sample). The TEER

was measured after 1 h (the conjugate-laden HBSS in the apical compartment was used rather than blank HBSS) and the insert was then moved to a new well. TEER measurement and insert movement were repeated. The process was terminated at 5h post pulsing free DOX or the DOX conjugates. A 0.1 mL HBSS solution was taken from each of the basolateral compartment to determine the DOX concentration (fluorescence, with Biotek Synergy 2 Multi-Mode Microplate Reader). The transport from apical to basolateral side ($A \rightarrow B$) was represented by apparent permeability ($P_{app} A \rightarrow B$), calculated as $P_{app} = \frac{F}{A \times C_0}$, where F is the flux or rate of change of cumulative mass transported from apical to basolateral direction, A is the area of the insert and C_0 is the initial concentration of free DOX or DOX in the conjugates. Subsequently, the HBSS at the apical side of the monolayer was recovered to determine the remaining amount of DOX in the apical side of the chamber. After that, 3 inserts from each sample ($n=6$) were used to monitor TEER recovery of the cell monolayer over time when free DOX or conjugated DOX was removed, while the other 3 inserts were used for determining the extent of internalization as described next. The cell monolayer was washed with fresh HBSS twice and 0.2 mL DMEM was added to apical side. The TEER was measured at 24, 48 and 72 h after the terminal transport point.

4.3.3.3 Internalization during in vitro transport.

The cell monolayers on the other 3 wells were washed with 4 °C blank HBSS thrice. The cell monolayer on each insert was detached by 0.2 mL 0.25% trypsin-EDTA solution and was then lysed overnight using 0.5 mL Triton-X100 aqueous solution (0.5% by weight). The supernatant collected by centrifuging the lysate was measured for DOX fluorescence analysis. The uptake of free DOX or conjugates was normalized to cellular protein content using BCA protein assay. To perform a mass balance, the mass of the samples that were (i) internalized, (ii) transported in $A \rightarrow B$ direction, or (iii) retained at apical side was summed up and compared to the total initial mass.

4.3.4 Transport of G3NH₂-mPEG1000-nDOX conjugates across mucus

The transport of the conjugates across an artificial mucus layer was also studied to deconvolute the impact of the mucus and that of the polarized cell layer on the transport of the nanocarriers. The synthetic mucus gel was composed of mucin (23 mg/mL) and buffer (85 mM NaCl, 20 mM HEPES, pH 7.3).[256] The mucus was shaken at 4 °C overnight. A 30 µL mixture of free DOX or conjugates (50 nM DOX equivalent, n=3 per sample) and mucus gel (ca. 900 µm thick) was pulsed onto the apical side of each insert which were placed onto a 24-well plate. The basolateral compartment was filled with 0.6 mL HBSS-HEPES (1X, pH 7.4, HEPES 0.1 mM). The insert was moved every hour to a new well and the transport assay was terminated at 5h. The solution from the basolateral side (0.1 mL) was analyzed for DOX fluorescence to quantify the extent to which the free DOX or DOX from conjugates transport across the mucus layer.

4.3.5 Preparation and Characterization of the pMDI Formulations

4.3.5.1 Synthesis of the polylactide-PEG-polylactide (LA_n - EO_m - LA_n) tri-block copolymer.

The LA_n - EO_m - LA_n tri-block copolymer was prepared as reported previously, with small modifications.[258] Briefly, PEG1000Da (1 g, 1 mmol) was reacted with D, L-lactide (10 g, 0.183 mol) with 0.1% wt/wt stannous octoate as catalyst. The reaction was stirred under N₂ atmosphere at 145°C for 1h. The resulting copolymer was dissolved in 3 mL dichloromethane and then precipitated with 100 mL cold methanol. The product was isolated by centrifugation and dried completely under reduced pressure. The resulting LA_n - EO_m - LA_n tri-block copolymer, where n and m are the number of repeat units, was characterized with ¹H NMR and MALDI-TOF.

4.3.5.2 Preparation of pseudo-solution formulation containing G3NH₂-21PEG1000-3DOX conjugate.

G3NH₂-21PEG1000-3DOX (0.2 mg DOX equivalent per mL HFA227) with varying concentrations of copolymer stabilizer LA_n-EO_m-LA_n (0, 0.12 and 0.53 mM) were added into pressure proof glass vials (West Pharmaceutical Services. Exton, PA, USA). The glass vials were placed onto a hot plate (60 °C) for a few seconds (Method A) or trace amounts of anhydrous ethanol (0.37% v/v relative to HFA227 propellant) was added to the conjugate and copolymer mixture (Method B). The glass vial was immediately crimped manually using 63 µl metering valve (Bespak. King's Lynn, Norfolk, UK). HFA227 propellant (4 mL) was filled to the sealed glass vial using a manual syringe pump (HiP 50-6-15) and a home-made high pressure filler. The formulation was sonicated for 30 min at 0-5 °C in a sonicating bath (P250D, VWR International), set to 180 W.

4.3.5.3 Solvated diameter (SD) of pseudo-solutions in HFAs.

The SD of G3NH₂-21PEG1000-3DOX conjugate was determined in 2H, 3H perfluoropentane (HPFP), a model for propellant HFA that is liquid at ambient conditions, using Nano ZS Zetasizer (Malvern Instrumetns Ltd. Malvern, Worcestershire, UK). Briefly, the aqueous solution of the conjugate was filtered with 0.22 µm syringe filter (VWR Internationals) and then lyophilized carefully. G3NH₂-21PEG1000-3DOX conjugate (0.2 mg DOX equivalent per mL HPFP) was dissolved in HPFP with the aid of anhydrous ethanol (0.30 % v/v relative to HPFP). The HPFP was sonicated at 0-5 °C for 30 min. Average size and standard deviation (s.d.) of over 14 repeats are reported here.

4.3.5.4 *Aerosol performance of the pseudo-solution formulations.*

The aerosol characteristics of the formulations were determined with an Andersen Cascade Impactor (ACI, CroPharm, Inc. Milford, CT, USA) fitted with a USP induction port at a flow rate of 28.3 L/min, 25°C and 75% relative humidity.[82] The pMDI formulations were prepared as described above. Several shots were fired to waste. Subsequently, 20 shots were released into the ACI with 10s interval between each shot. Air flow was maintained 10s after the last shot. The actuator, induction port, plate on each stage and nylon filter membrane were thoroughly rinsed with 10 mL acetone each. 3 mL sample-containing acetone solution was used for measuring UV absorption of DOX at 494 nm using Cary 50 UV-Vis spectrometer (Agilent Technologies. Santa Clara, CA, USA). The mass of the conjugate was determined according to an established calibration curve. The measurements were performed in triplicate (n=3). The respirable fraction, representing respirable dose of the formulation, was calculated following Equation 1. Fine particle fraction, denoting the dose deposited on low respiratory and deep lung, was calculated following Equation 2. Mass median aerodynamic diameter (median of the distribution of airborne particle mass with respect to aerodynamic diameter) and geometric standard deviation (variability of particle size distribution) were calculated as reported previously.[80]

$$RF = \frac{\text{Stage 0 to Filter}}{\text{Actuator} + \text{Induction port} + \text{Stage 0 to Filter}} \quad \text{Eq. 1}$$

$$FPF = \frac{\text{Stage 3 to Filter}}{\text{Induction port to Filter}} \quad \text{Eq. 2}$$

4.4 Results and discussion

4.4.1 Physicochemical properties of acid-labile G3NH₂-mPEG-nDOX conjugates

The synthesis and characterization of the acid-labile G3NH₂-mPEG-nDOX conjugates have been discussed in detail in **Chapter 2**. Briefly, we synthesized acid-labile G3NH₂-mPEG-

nDOX conjugates with varying PEG density (low = 0, medium = 9 and high = 21) and DOX payload (low = 3 and medium = 7). Two PEGylation strategies were developed for dendrimers containing different DOX payloads: direct PEGylation for low DOX payloads, and two-step PEGylation for high DOX payloads. In direct PEGylation, DOX was conjugated to generation 3 amine-terminated PAMAM dendrimer via an acid-cleavable cis-aconityl spacer. The PAMAM-DOX conjugates were then covalently attached with varying density of PEG1000Da. For the dendrimer conjugates carrying high DOX payload, DOX was conjugated to the dendrimers that have been PEGylated beforehand (PAMAM-xPEG1000; x = average 7 PEG1000 per dendrimer), and followed by second PEGylation step to achieve high density of PEGylation.

Both ^1H NMR and MALDI-TOF demonstrated the successful conjugation of DOX and PEGylation. The hydrodynamic diameters (HD) and zeta potentials of G3NH₂-mPEG-nDOX conjugates measured with light scattering (LS). That is, 4.0 ± 2.3 nm and $+6.3 \pm 3.5$ mV for G3NH₂-3DOX, 6.9 ± 3.2 nm and -2.1 ± 4.3 mV for G3NH₂-9PEG-3DOX, 9.6 ± 4.9 nm and -6.6 ± 2.7 mV for G3NH₂-21PEG1000-3DOX, and 11.3 ± 4.3 nm and -10.5 ± 6.1 mV for G3NH₂-9PEG-7DOX. The in vitro release of DOX from the conjugates determined at pH 7.4 and pH 4.5 showed DOX (80-85%) is released from dendrimer conjugates only at acidic pH (lysosomal pH), while is stable at extracellular/physiological conditions (<8 % DOX is released). Additionally, the rate at which DOX is released decreases as PEGylation degree increases. Therefore, the intracellular release of DOX in response to pH drop potentially decrease the concentration of free DOX in plasma, thus reducing systemic adverse effects.

4.4.2 Cytotoxicity of acid-labile G3NH₂-mPEG-nDOX conjugates

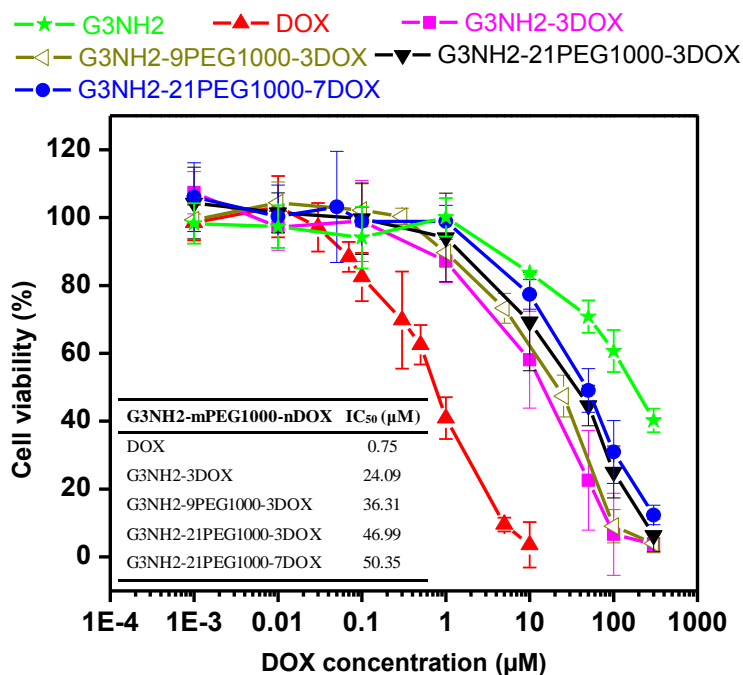


Figure 4.1 Viability of Calu-3 cells 72 h post incubation with varying concentrations of bare dendrimer, free DOX or acid-labile conjugates (G3NH₂-mPEG1000-nDOX, with $m = 0, 9, \text{ or } 21$ and $n = 3 \text{ or } 7$), as determined by the MTT assay. Results denoted as mean \pm s.d. ($n=6$). The inset of IC₅₀ values of the free DOX (DOX) various conjugates at 72 h incubation. The IC₅₀ values were obtained with non-linear regression Log(inhibitor) vs. Response (variable slope).

The cytotoxicity of the various dendrimer-DOX conjugates and controls (free DOX) was assessed by MTT assay on Calu-3 cells. As shown in Figure 4.1, free DOX and acid-labile conjugates induce significant cell kill on airway epithelial cells. The cell kill profiles for free DOX and acid-labile dendrimer-DOX conjugates follow similar trend, but free DOX have greater potency at 72 h incubation (see both profiles and IC₅₀ values). As discussed in **Chapter 2**, we believe the cytotoxicity of the acid-labile conjugates could be comparable to that of free DOX as incubation time was prolonged and the impact of PEGylation was negligible at long incubation times. The stronger time-dependent cell kill is mainly related to the sustained release of DOX

from dendrimer conjugates and different cellular uptake pathways for free DOX and acid-labile DOX.

4.4.3 *In vitro* transport of acid-labile G3NH₂-mPEG-nDOX conjugates across polarized pulmonary epithelial monolayer

Our recent work has shown surface chemistry of generation 3, amine-terminated PAMAM

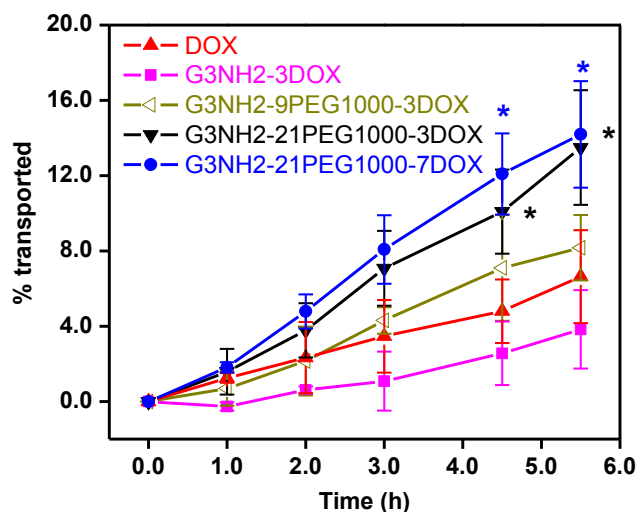


Figure 4.2 Apical to basolateral (A→B) transport of free DOX and DOX from acid-labile G3NH₂-mPEG1000-nDOX conjugates across polarized Calu-3 cell monolayers as a function of time (n=6). Statistical significance was calculated with respect to free DOX by one-way ANOVA Dunnett's test (* $p < 0.05$).

dendrimers (G3NH₂) can be used to modulate their interaction with the pulmonary epithelium both *in vitro* and *in vivo*, [168] and thus be potentially used to improve permeability of DOX across pulmonary epithelial barriers. In this work, we studied the effect of PEGylation degree and DOX payload on the transport of acid-labile G3NH₂-mPEG-nDOX conjugates across epithelial monolayer with an *in vitro* Calu-3 cell monolayer model — upper airway cancer cell line. [184] The G3NH₂-mPEG-nDOX conjugates are pulsed to apical side of cell monolayer and the amount of the conjugate collected at basolateral side are measured. The results are plotted in Figure 4.2. It is observed that the dendrimers with medium (9 PEG) and high (21 PEG; * $p < 0.05$ at 4.5 and 5.5

h with respect to free DOX) PEGylation degree transport more DOX from apical to basolateral side ($A \rightarrow B$) of cell monolayer than free DOX, while non-PEGylated dendrimer transports less DOX in $A \rightarrow B$ direction. Additionally, the amount of DOX collected at basolateral side increases as PEGylation degree increases. The cumulative mass of DOX transported in $A \rightarrow B$ direction slightly increases as DOX payload increases, but no statistical significance is observed.

We also calculate overall apparent $A \rightarrow B$ permeability ($P_{app} A \rightarrow B$) of free DOX and

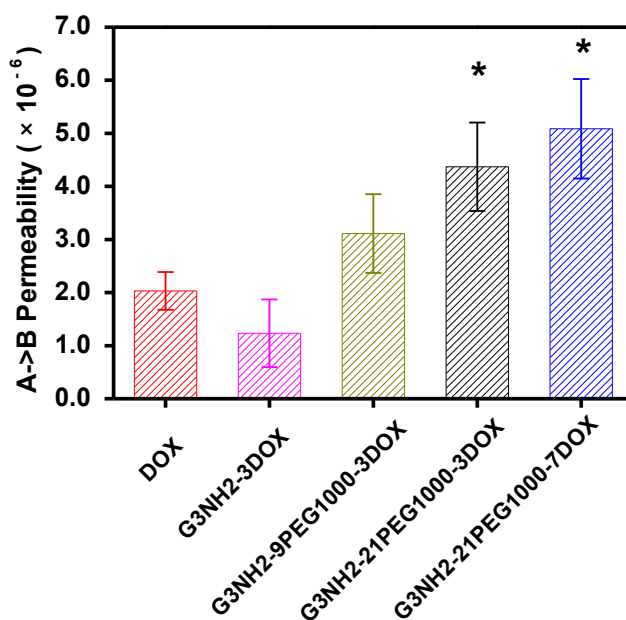


Figure 4.3 Apparent permeability (P_{app}) of G3NH2-mPEG1000-nDOX conjugates across Calu-3 cell monolayer ($n=6$). P_{app} was determined at 5 h post incubation of the cell monolayer with the conjugates, with the transport being from the apical to basolateral ($A \rightarrow B$) side. Statistical significance was calculated with respect to free DOX by one-way ANOVA Dunnett's test ($*p < 0.05$).

G3NH₂-mPEG-nDOX conjugates. $P_{app} A \rightarrow B$ is a measure of ease with which substances are transported across epithelial layers. Our results (Figure 4.3) show $P_{app} A \rightarrow B$ of free DOX is 2.0×10^{-6} cm/s, which lies between G3NH₂-3DOX and G3NH₂-9PEG-3DOX. $P_{app} A \rightarrow B$ values of highly PEGylated dendrimer-DOX conjugate are significantly higher than that of free DOX. Both $P_{app} A \rightarrow B$ and cumulative mass of DOX at receiving side demonstrate PEGylation and

varying DOX payload could modulate the transepithelial transport of dendrimer-DOX conjugates across pulmonary epithelial layers.

It has been reported that the DOX translocates across polarized epithelial monolayer is through transcellular pathway (e.g. transcytosis) in which DOX molecules are taken up by epithelial cells on apical side and then dropped off on basolateral side.[259, 260] The transport of DOX through paracellular pathway hasn't been reported in literature. In contrast, dendrimer nanocarriers are able to cross epithelial barriers via paracellular route in conjunction with transcytosis.[42, 184, 218] and the rate of transport is affected by their size and surface chemistry. To understand the role of paracellular pathway in transepithelial transport of dendrimer-DOX conjugates, electrophysiological behavior of cell monolayer is evaluated by measuring the TEER value in the course of transport. The TEER values are summarized in Figure 4.4. Only a limited reduction (ca. 10%) is observed in the case of free DOX, demonstrating no obvious opening of intercellular tight junction proteins (e.g. actins and occludins) and good integrity of Calu-3 cell monolayer. It thus corroborates the fact that paracellular pathway plays little/no role in the transepithelial transport of DOX across pulmonary epithelial layer.[259] On the other hand, it is evident that dendrimer-DOX conjugates have pronounced impact on TEER of Calu-3 cell monolayer (ca. up to 40-60% decrease in the course of transport experiment), indicating the significant opening of intercellular tight junction, which is a robust evidence of paracellular transport.[261] Additionally, the TEER decreases as PEG density increases, demonstrating the highly PEGylated dendrimer can have stronger interaction with tight junctional proteins. The

opening of tight junction This is in accordance with the findings in Bharatwaj's work.[256] The TEER values of Calu-3 monolayer are reversible upon removal of dendrimer-DOX conjugates from apical side. As seen in Figure 4.4, all TEER values return to ca. 90% of their original values within 48 h. The reversibility of the TEER values revealed Calu-3 cells are not damaged

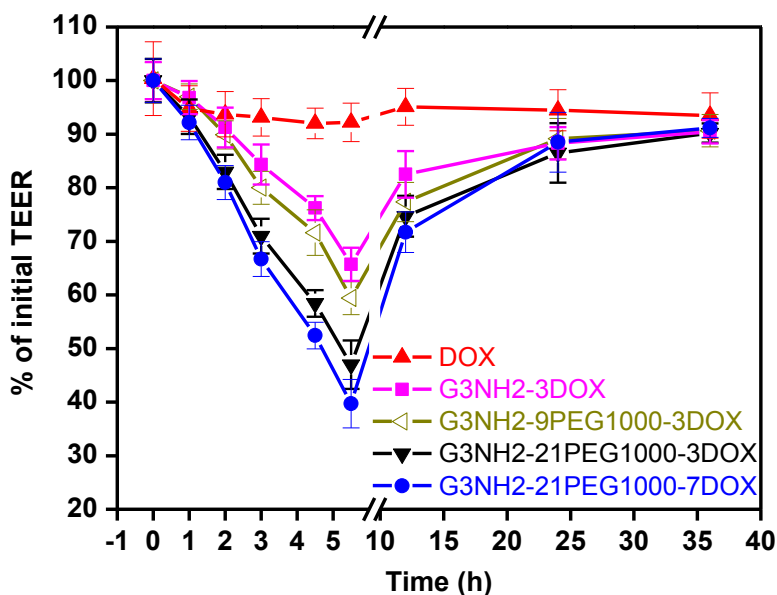


Figure 4.4 Variation in transepithelial electrical resistance (TEER) across polarized Calu-3 monolayer grown on Transwell® inserts during the 5 h *in vitro* transport experiments (n=6), and up to 36h after the completion of transport experiment (n=3) – after washing of the apical side of the monolayer where the conjugates had been pulsed.

significantly as the G3NH₂-mPEG-nDOX conjugates transport across.[41, 184]. Therefore, the combined results indicate PEG chains on dendrimer surface may promote the paracellular transport of dendrimer-DOX conjugate by interacting with intercellular tight junction and the interaction has no permanent damages on calu-3 monolayer.

On top of surface chemistry impact, the change on surface charge introduced by PEGylation should be considered. As discussed earlier, non-PEGylated dendrimer-DOX conjugate (G3NH₂-3DOX) were positively charged, whereas moderately (G3NH₂-9PEG1000-

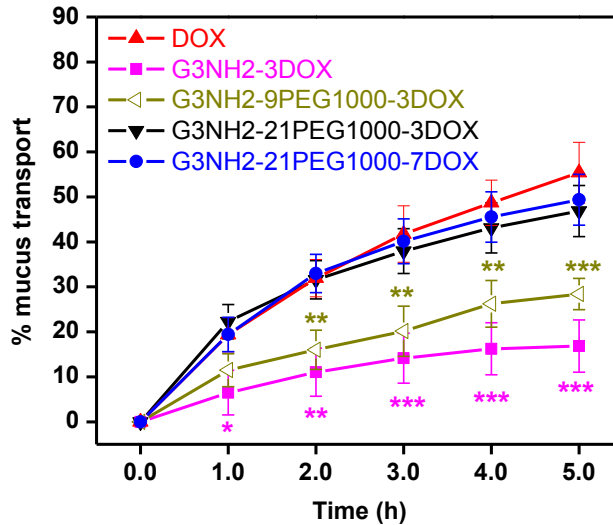


Figure 4.5 Transport of the acid-labile G3NH₂-mPEG1000-nDOX conjugates across the synthetic mucus layer as a function of time. Statistical significance was calculated with respect to free DOX by one-way ANOVA Dunnett's test (* $p < 0.05$).

3DOX) and highly (G3NH₂-21PEG1000-3DOX and G3NH₂-21PEG1000-7DOX) PEGylated dendrimer-DOX conjugates are near-neutral or slightly negative. The tight junctional opening by surface charge of dendrimers is ranked in the sequence: positive > negative > neutral.[41] The sequence is obtained based on the transport study on intestinal epithelial models (e.g. Caco-2 cell line). However, these intestinal cell monolayer models do not have mucus gel layer covered on apical side. The mucus layers on the top of respiratory epithelial monolayer (e.g. Calu-3 cell line) are able to trap invading nanocarriers, especially positively charged and hydrophobic particulates. Mucus is viscoelastic gel layer covering the organs and tissues that expose to external environment, such as lungs, stomach and vagina. Mucus gel is made up of crosslinked mucin fiber, lipids, salts,

proteins, nucleic acids and cellular debris.[72] The thickness of respiratory mucus layer ranges from 5 to 55 μm . [262, 263] The respiratory mucus can entrap inhaled particles and bacteria due to the presence of size-limiting pores, hydrophobic domains and polyvalent adhesion. The particulate-entrapped mucus gel is the rapidly cleared by mucociliary escalator and fast renewed mucus.[72, 264]

To study the retention of G3NH₂-mPEG-nDOX conjugates by mucus layer, we use synthetic human mucin gel to mimic mucus layer on cell monolayer. As shown in Figure 4.5, free DOX, G3NH₂-21PEG1000-3DOX and G3NH₂-21PEG1000-7DOX show similar capability to escape mucus trapping. Dendrimer-DOX conjugates with low PEG density transport across mucus gel at a much smaller rate. The similar trend is also reported our recent study and Schipper's work investigating the transport of deacetylated chitosan across mucus-covered intestinal epithelial cells.[265] G3NH₂-3DOX is positively charged, while G3NH₂-21PEG1000-3DOX and G3NH₂-21PEG1000-7DOX are negatively charged. A large amount of anionic charges (e.g. carboxyl and sulfate groups) in glycosylated domains of mucin fibers can significantly immobilize cationic dendrimers (G3NH₂-3DOX), while negatively charged dendrimers can relatively cross the mucus layer easily.[266-268]

At the end of transport experiment, we also calculate amount of dendrimer conjugates left in apical side of cell monolayer and internalized into Calu-3 cells. As seen in Figure 4.6, most of free DOX and dendrimer-DOX conjugates remain in apical side of cell monolayer (65-80% of added samples). Approximately, 6.4% G3NH₂-3DOX has been internalized by Calu-3 cells at terminal point (5.5 h), whereas PEGylated dendrimer-DOX conjugates have reduced internalization (4.4% for G3NH₂-9PEG1000-3DOX, 3.2% for G3NH₂-21PEG1000-3DOX, and 2.5% for G3NH₂-21PEG1000-7DOX). These results in combination with cumulative mass

transported across cell monolayer allow us to perform an overall mass balance study. Approximately, an average of 85% of added samples can be recovered. The 15% of the conjugates in loss may be attributed to a few factors including the presence of conjugates adhered to cell debris after lysis and the adsorption of conjugates to surfaces of the inserts.[256]

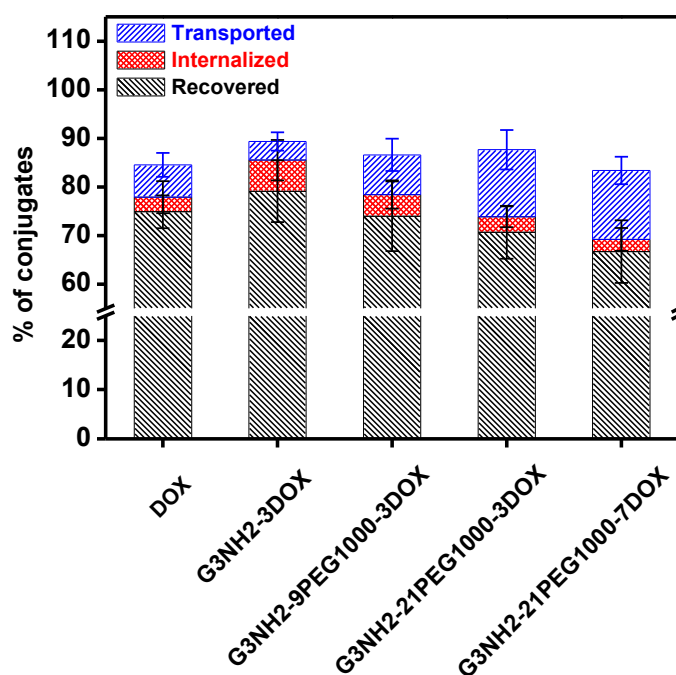


Figure 4.6 Mass balance of DOX conjugates during the *in vitro* transport experiments. The mass transported from apical to basolateral side ($A \rightarrow B$), the mass internalized into Calu-3 cells, and the mass retained on apical side were determined for the mass balance.

In summary, the transport of DOX across pulmonary epithelial epithelium can be significantly enhanced upon its conjugation to dendrimers and PEGylation. The significantly reduced TEER value and very limited internalization of dendrimer conjugates reveal that paracellular pathways play a vital role in the transport of PEGylated dendrimer-DOX across pulmonary epithelium.

4.4.4 Pseudo solution pMDI formulations of acid-labile G3NH₂-mPEG-nDOX conjugates

In Chapter 2, we have reported that the pseudo solution formulation of acid-labile G3NH₂-mPEG-nDOX conjugates in pMDIs can be readily prepared with a trace of cosolvent (ethanol). The physical stability and aerosol characteristics of the pMDI formulations improve significantly as the PEG density increases. In this work, a facile cosolvent-free preparation for the pMDI formulation was also developed (Method A). We selected the G3NH₂-21PEG1000-3DOX as model conjugate. A predetermined amount of conjugates (0.2 mg DOX per mL HFA227 propellant) was added to pressure proof glass vial and then slightly melted at ca. 60 °C for a few seconds. Propellant HFA227 was subsequently added to the conjugates. The molten PEGylated dendrimer conjugates are found well solvated by propellant even without sonication. The pMDI formulation of G3NH₂-21PEG1000-3DOX was also prepared with cosolvent method reported earlier (Method B). The solvation diameters (SDs) of the pMDI formulations prepared by both methods are determined using light scattering (LS). We use an HFA that is liquid at ambient conditions and a model liquid propellant — 2H, 3H perfluoropentane (HPFP).[81, 238] The measurement showed SDs of the formulation from Method A and Method B are similar: 27.3±8.5 nm vs. 26.1±7.8 nm, revealing that Method A can also prepare PEGylated dendrimer-DOX conjugates into pseudo solution pMDI formation. The size may represent aggregates of a few conjugates only, or even a single dendrimer conjugate whose SD in HPFP (26-28 nm for G3NH₂-21PEG1000-3DOX) turns out to be less than 3 times larger than their HD (SD in water – 10 nm G3NH₂-21PEG1000-3DOX).

To further understand thermal properties of G3NH₂-m21PEG1000-nDOX conjugate, differential scanning calorimetry (DSC) was used to monitor their molten behaviors and the results were plotted in Figure 4.7 (a). The melting point (mp) of G3NH₂-21PEG1000-3DOX is 45.72 °C,

which is similar to that of PEG (mp of pure PEG: 46.72 °C). Since G3NH₂ dendrimer is an amorphous polymer without melting point, PEG chains on surface are mainly responsible for melting behavior of the conjugate. It is believed that the molten PEG chains covering on dendrimer surface facilitate the solvation of the conjugates (acting as cosolvent).

4.4.5 Impact of heating process on aerosol performance of pseudo solution pMDI formulation

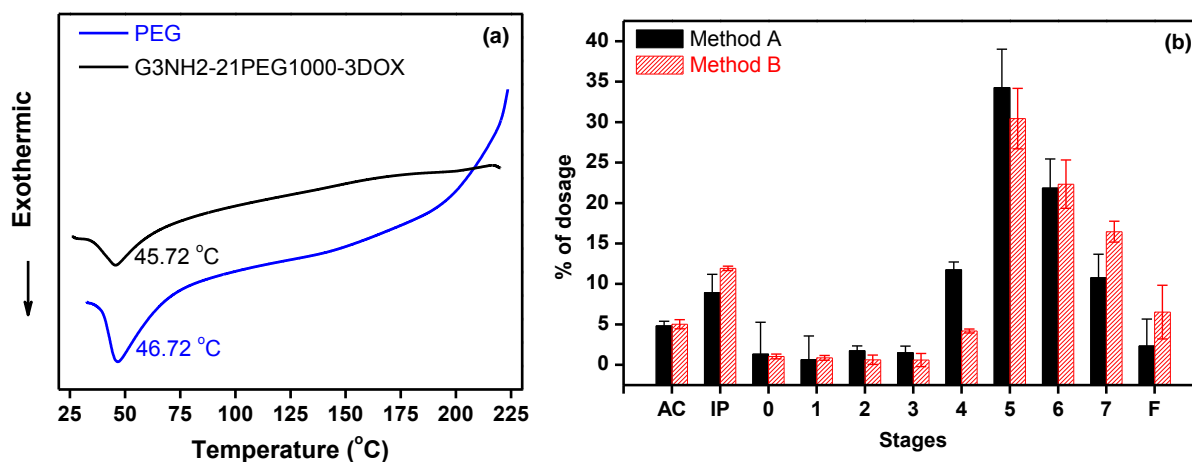


Figure 4.7 (a) Aerosol characteristics of the pMDI formulations containing the acid-labile G3NH₂-21PEG1000-3DOX conjugates. Method A = formulation prepared by heating the conjugate or conjugate and polymer mixture before addition of propellant; Method B = anhydrous ethanol (EtOH) at 0.37% v/v relative to HFA227 propellant was added to the formulation as cosolvent. (b) Differential scanning calorimetry (DSC) thermograms of PEG1000 and acid-labile G3NH₂-21PEG1000-3DOX conjugates.

The aerosol characteristics are key to a pMDI formulation. Andersen Cascade Impactor (ACI) is widely used as an *in vitro* model to determine drug deposition in the lungs. Lung deposition of the formulations by Method A and B are summarized in Figure 4.7 (b). The mass deposition on each stage is summarized in *Supplementary Information Table S1*. The formulations prepared by Method A and B showed similar the deposition fraction of the conjugates on ACI, mainly on from Stage 4 to 7 which corresponds to deep lung regions. Respirable fraction (RF), fine particle fraction (FPF), mass median aerodynamic diameter (MMAD), geometric standard deviation (GSD) and recovery are calculated according to the deposition data and listed

in Table 4.1. The RF and FPF are two major parameters to assess the efficiency of the pMDI formulation for pulmonary delivery.[82] RF (85.2±5.8%) and FPF (81.9±4.5%) of the formulation from Method A are slightly greater than those of Method B (RF: 82.0±4.8%; FPF: 78.1±4.3%), but no statistical significance is found. The FPFs obtained from both methods are much higher

Table 4.1 Median mass aerodynamic diameter (MMAD), geometric standard deviation (GSD), respirable fraction (RF) and fine particle fraction (FPF) of the pMDI formulations containing acid-labile G3NH₂-21PEG1000-3DOX conjugate and LA₄₆-EO₂₃-LA₄₆ triblock copolymer surfactants, as determined by Andersen Cascade Impactor (ACI). The formulations were prepared with Method A (no ethanol) and contained 0.2 mg DOX equivalent per mL HFA227 propellant and varying concentrations of LA₄₆-EO₂₃-LA₄₆ copolymer (0, 0.12 and 0.53 mM). Statistical significance was performed with respect to the pMDI formulation with 0 mM LA₄₆-EO₂₃-LA₄₆ prepared by Method A using one-way ANOVA Dunnett's test with **p*<0.05, ***p*<0.01, and ****p*<0.001. † denotes the formulation was prepared by the Method B, formulations containing anhydrous ethanol at 0.37% v/v relative to HFA227 propellant.

LA ₄₆ -EO ₂₃ -LA ₄₆	MMAD (µm)	GSD (µm)	RF (%)	FPF (%)	Recovery (%)
0 [†]	1.2±0.1	1.8±0.1	82.0±4.8	78.1±4.3	86.9±4.7
0	1.3±0.1	1.9±0.1	85.2±5.8	81.9 ±4.5	84.0±5.9
0.12	2.3±0.3**	1.9±0.1	82.4±6.6	68.7±5.8*	84.5±7.2
0.53	3.0±0.5***	2.2±0.1	79.2±8.9	58.4±6.1**	78.7±6.4

than those of commercial HFA-based suspension pMDIs (30-55% on average)[81, 269] and HFA-based solution formulations (60-80% on average).[239, 242] Additionally, the MMAD and GSD are similar for both methods, falling within the optimum range of aerodynamic diameters (5.0-0.5µm). The recovery for both formulations is similar. We believe that the loss of the delivered dose of the formulation containing G3NH₂-21PEG1000-3DOX is mainly from small particles with exhalable size range (aerodynamic diameter < 0.5 µm). It is noted that micronized particles are formed from pseudo solution pMDI formulation of nano-sized particles with propellant molecule

vaporizing. A phase separation mechanism for micronized particle formation is proposed in **Chapter 2**.

In summary, the pseudo solution of formulation of highly PEGylated dendrimer-DOX conjugates can be also prepared with a facile cosolvent-free method. The formulation prepared with this method shows superior aerosol properties and is conducive to deep lung deposition.

4.4.6 Deposition-tunable pMDI formulation of G3NH₂-mPEG-nDOX conjugates by the addition of triblock copolymer LA_n-EO_m-LA_n

It is observed in Figure 4.7 (b) that ca. 70% of the G3NH₂-21PEG1000-3DOX conjugate deposited on Stage 5 to 7 which corresponds to deep lung areas including terminal bronchioles and alveolar sacs. Therefore, the formulation tends to deliver chemotherapeutics to peripheral lung cancers.[270] However, some primary and secondary airway malignancies occur on upper (e.g. trachea) and lower respiratory (bronchi, primary and secondary bronchioles) tracts.[271, 272] As is well known, the addition of non-volatile excipients to pMDI formulations can increase their MMADs due to reduced vapor pressure of the propellant, thus leading to increased deposition of particles in central lung area.[78, 273] In this work, we selected triblock copolymer LA_n-EO_m-LA_n as nonvolatile excipients to adjust aerosol characteristics as experimental work and computational simulation has shown biocompatible polylactide homopolymers and copolymers are soluble excipients in HFA propellant,[58, 274, 275] which won't change the nature of pseudo solution of highly PEGylated dendrimer-DOX conjugates. Wu and da Rocha reported the copolymers with longer lactide (LA) repeat units are more capable of partitioning interaction between drug molecules.[58] Therefore, the LA_n-EO_m-LA_n copolymer with long PLA block was synthesized via ring opening polymerization of D, L-lactide (LA) with hydroxyl PEG (HO-PEG1000-OH) as macromolecular initiator.[258] The ¹HNMR and MALDI-TOF of resulting

LA_n-EO_m-LA_n copolymer (Figure 4.8) show the ratio of LA unit to PEG chain is 92:1 and the molecular weight is 7561.61Da. The triblock copolymer will be denoted as LA₄₆-EO₂₃-LA₄₆ from here. The G3NH₂-21PEG1000-3DOX conjugate was mixed with LA₄₆-EO₂₃-LA₄₆ copolymer and then heated slightly before HFA227 filling.

We studied the effect of PLA₄₆-PEG-PLA₄₆ concentration on the solvation diameters of the pMDI formulations by LS. The results show the SDs of the formulations range from ca. 26 to

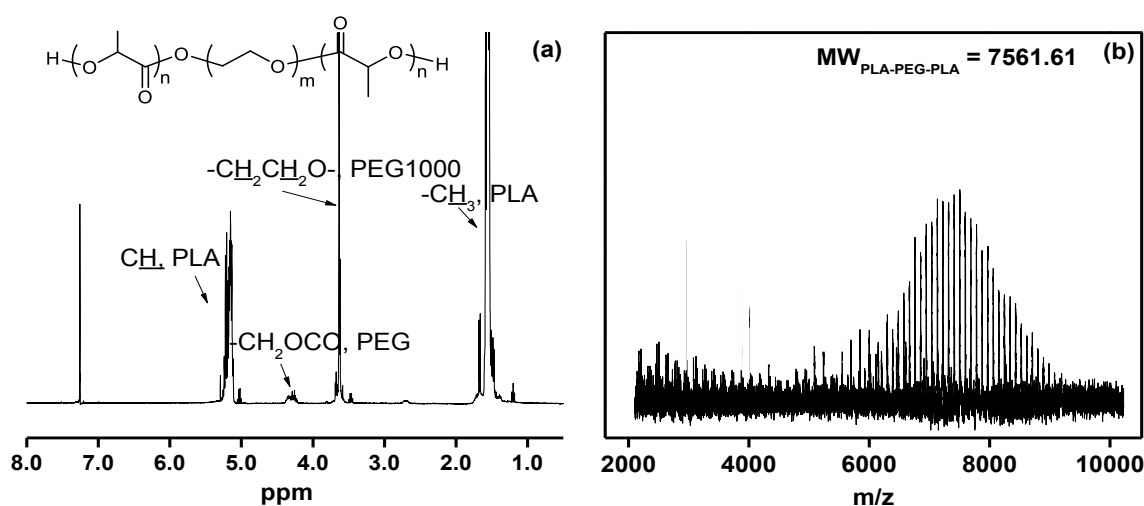


Figure 4.8 ¹H NMR and MALDI spectra of LA₄₆-EO₂₃-LA₄₆ triblock copolymer..

31 nm (PLA₄₆-PEG-PLA₄₆ concentration — 0 mM: 26.1±7.8 nm; 0.12 mM: 30.3±10.9 nm; 28.6±7.8 nm) and are not affected by the concentration of PLA₄₆-PEG-PLA₄₆ within 0 – 0.53 mM. This reflects the addition of LA_n-EO_m-LA_n copolymer does not affect the nature of solution formulation. The solvation diameter of LA₄₆-EO₂₃-LA₄₆ copolymer in HPFP is not detected with LS, possibly due to the random coiled conformation of linear polymer. It is thus believed that

LA_n-EO_m-LA_n copolymer is not able to form strong interaction with PEGylated dendrimer conjugate.

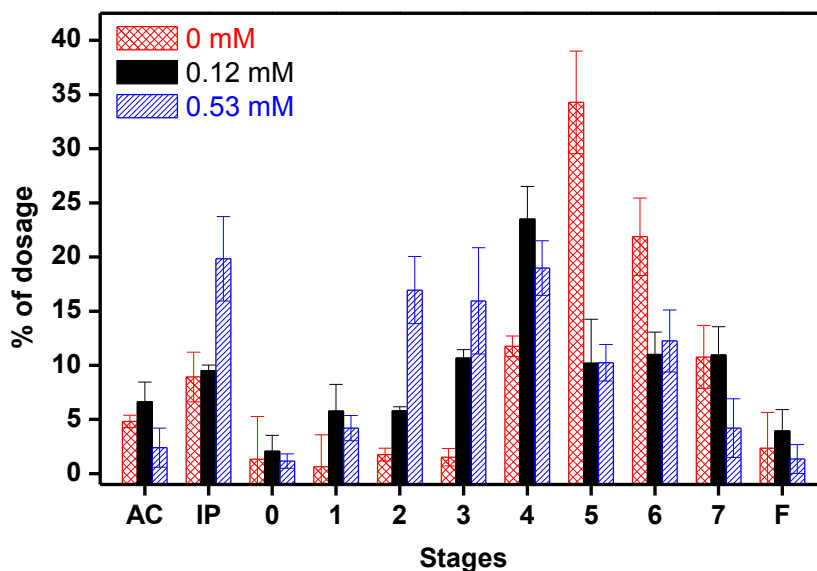


Figure 4.9 Effect of the concentration of LA₄₆-EO₂₃-LA₄₆ triblock copolymer on the aerosol characteristics of the pMDI formulations of G3NH₂-21PEG1000-3DOX in HFA227 (0.2 mg DOX equivalent per mL propellant). The formulation was prepared by Method A.

The effect of the concentration of LA₄₆-EO₂₃-LA₄₆ on the aerosol characteristics of the pMDI formulations is determined with ACI and the lung deposition is plotted in Figure 4.9. It is obviously observed that the deposition of G3NH₂-21PEG1000-3DOX on lower stages increases as the concentration of PLA₄₆-PEG-PLA₄₆ copolymer increases. The ratio of the deposition of conjugates on Stage 2-4 to Stage 5-7 ($F_{2-4/5-7}$) was 0.22 (15.0%:67.0%) for 0 mM, 1.24 (40.0%:32.1%) for 0.12 mM, and 1.94 (51.9%:26.7%) for 0.53 mM. According to the correlation of ACI stage to anatomical lungs, Stage 2 to 4 corresponds to lung anatomical regions such as trachea, primary and secondary bronchi, while Stage 5 to 7 corresponds to deep lung area including terminal bronchioles and alveoli. The shift of lung deposition to lower stages of ACI reveals the

formulation with LA₄₆-EO₂₃-LA₄₆ as excipient is capable of delivering PEGylated dendrimer conjugates to upper respiratory tract.

The aerosol parameters of these pMDI formulations are summarized in Table 1. As the concentration of PLA₄₆-PEG-PLA₄₆ increases, the RF of these pMDI formulations decreases slightly, while the FPF decreases with statistical significance. However, the lowest FPF is still greater than that of commercial HFA-based pMDI formulations (30-55% on average).[82] The MMAD of these formulations increases from 1.3 μm to 3.0 μm with the concentration of LA₄₆-EO₂₃-LA₄₆ increasing from 0 to 0.53 mM, which remain in the optimal range of particle size for oral inhalation (5-0.5 μm). The trend of change of FPF and MMAD with the addition of nonvolatile soluble excipient is in accordance with published results.[78]

In summary, the pseudo solution formulation of PEGylated dendrimer-DOX conjugate is tunable in terms of cancerous sites in the lungs by adjusting the concentration of PAL-PEG-PLA copolymer. For broad relevance, the PEGylated PAMAM dendrimers via oral inhalation can be used as a platform for delivering therapeutics of interest to treat other pulmonary disorders.

4.5 Conclusion

In this work, a series of PEGylated PAMAM dendrimers with acid-labile DOX conjugated have been synthesized. The conjugates were maintained stable at physiological condition (e.g. blood circulation), while were capable of releasing free DOX at acidic compartment (e.g. lysosome) causing comparable cytotoxicity to free DOX against lung cancer epithelial cell line (calu-3). *In vitro* transport of G₃NH₂-mPEG-nDOX conjugates across polarized lung epithelia model indicated the apparent transport of apical to basolateral side increased as PEG density increased, whereas cellular uptake rate declined due to attenuated interaction upon PEGylation. The significant reduction in TEER showed paracellular pathway played a vital role in sending the

conjugates across epithelial monolayer. Different from other epithelial cells (e.g. intestinal or colorectal epithelia), mucus gel layer secreted by airways epithelial cells withheld a large amount of conjugates. However, high degree of PEGylation can help the conjugates effectively escape from mucus entrapping—thus enhancing transcellular transport rate. The G3NH₂-mPEG-nDOX conjugates can be readily formulated into HFA-based pMDIs with two different methods: heating method and co-solvent aiding method, forming solution formulations. The pMDI solution formulations prepared by the two methods had very excellent physical stability and aerosol characteristics (high RF and FPF, and low MMAD and GSD). Considering cancerous lesions of the lungs and respiratory tract, the aerosol deposition was tunable by adjusting the concentrations of biodegradable LA_n-EO_m-LA_n triblock copolymers. Therefore, all combined results demonstrated that the acid-labile PEGylated PAMAM-DOX conjugates administered locally by oral inhalation are promising for treating lung adenocarcinoma. Broadly, the pMDI solution formulation containing PEGylated PAMAM dendrimers is also promising platform for treating other pulmonary disorders.

4.6 Acknowledgements

This work was supported in part by a National Science Foundation grant (NSF-CBET grant no. 0933144 and NSF-DMR grant no. 1508363) and the Nano@WSU. Professor Francine F. Padilha and Bruno V. Humia would like to thank Brazil's Science without Borders Program to support this research.

CHAPTER 5 — Conjugation to Poly(amidoamine) Dendrimers and Pulmonary Delivery Enhances the Antitumor Activity of Doxorubicin in Lung Metastasis

5.1 Introduction

Cancer is the second most common cause of death for both men and women in the United States, second only to heart diseases.[276] Amongst the many malignant tumors, lung cancers are the leading cause of death. More patients die from lung cancers than breast, pancreatic, and prostate cancers combined.[2] Although curative surgery is the first choice in the clinic for treating primary lung tumors, chemotherapy plays a vital role in inhibiting tumor growth after surgery, partly due to the high rates of recurrence.[277, 278] Additionally, the lungs are the most common site for metastasis for almost all other primary tumors.[279] Metastatic tumors are also associated with more than 90% of cancer-related deaths.[280] The development of new strategies that can help improve chemotherapeutic outcomes during the treatment of lung metastasis have, therefore, a significant potential societal impact.

One of the major challenges limiting the success of chemotherapeutic treatment in lung metastasis is the low concentration of anticancer agents in the lung tissue and lung tumor. Upon systemic administration, such as intravenous injection (i.v.), only a few percent of the total dose (TD) (< 4%) actually reaches the tumor site.[8] Because of typical systemic toxicity of anti-cancer therapeutics, increasing the overall administered dose so as to reach therapeutic local concentration of chemotherapeutics is usually not a viable strategy.[9] The study of the effectiveness of new chemotherapeutic strategies that consider local lung delivery are, therefore, also of great potential relevance as they promote local drug concentration while decreasing systemic exposure.

Doxorubicin (DOX) is one of the most effective anti-cancer therapeutics available in the clinic today [281] and has been widely used alone or in combination to treat a variety of malignant

cancers including lung tumors.[56, 57] DOX induces the apoptosis of cancer cells by intercalating itself to DNA double helix and thus inhibiting the progression of enzyme topoisomerase II. Other mechanisms include the production of high level reactive oxygen species (ROS) and cellular membrane disruption.[95] The applicability of DOX is to some extent limited, however, due to its damage to the cardiac tissue.[21] The accumulation of DOX in the heart results in increased oxidative stress, down-regulated protein function, decreased cardiac gene expression, and up-regulated apoptosis of cardiomyocytes, which eventually leads to lethal cardiomyopathy.[22]

There are, therefore, tremendous opportunities in the development of strategies that will enhance the local concentration of DOX in the lung tissue, while maximizing its intracellular delivery to lung tumor cells, and at the same time minimizing the systemic concentration of free DOX. Nanocarriers are uniquely suited in this aspect, as they can be used to modulate the pharmacokinetics (PK) and biodistribution of therapeutic agents.[282] Dendrimers are particularly interesting drug carrier systems as they are highly monodispersed (predictable PK/biodistribution) and can be easily functionalized with therapeutic agents through linkages that allow for temporal and spatial control of drug release. Dendrimer can also be modified with various ligands to control their interaction with the physiological environment and can also promote their cellular internalization.[31, 167, 212]

Based on the challenges and opportunities discussed earlier, the goal of this study was to investigate the effect of the conjugation of DOX to dendrimer and of the local administration of the carrier system to the lung tissue on the efficacy of DOX in reducing the metastatic lung tumor burden. We conjugate DOX to carboxyl-terminated, generation 4, poly(amidoamine) dendrimer (G4COOH) nanocarriers through an intracellularly-triggered (pH-responsive) drug release linker. We evaluated the impact of pH on the release kinetics of the conjugates – both at extracellular

physiological pH (7.4) and intracellular pH (lysosomal, 4.5). The ability of the conjugates gain access to and to kill B16F10 mouse melanoma cells was also investigated using flow cytometry and MTT assay. A mouse model of lung metastasis (from melanoma B16F10 cells) was established and the efficacy of the G4COOH-DOX conjugates in reducing the metastatic lung tumor burden and rate of survival was investigated. The effect of conjugation was assessed by comparing the results of the studies above to free DOX, while the impact of the local lung delivery was determined by comparing the effectiveness of the conjugates and free DOX delivered via pharyngeal aspiration (locally) and intra venous (i.v.). The potential of the conjugation of DOX to G4COOH and the pulmonary delivery route are also discussed in terms of the tissue distribution of the carriers, particularly to the lungs (target) and the cardiac tissue (to be avoided).

5.2 Materials

Generation 4, carboxyl-terminated, poly(amidoamine) dendrimer (G4COOH) was purchased from Dendritech, Inc (Miland, MI, USA). Doxorubicin hydrochloride (DOX) was purchased from LC Laboratories (Woburn, MA, USA). N-methylmorpholine (NMM) and isobutyl chloroformate (IBCF) were purchased from VWR Internationals (Radnor, PA, USA). Tert-butyl carbamate (TBC), trifluoroacetic acid (TFA), triethylamine (TEA), 2, 5-dihydroxybenzoic acid (2, 5-DHB), and 4% paraformaldehyde PBS solution were purchased from Sigma-Aldrich (St Louis, MO, USA). Phosphate buffer saline (PBS, 1X), Dulbecco's Modified Eagle's Medium (DMEM), penicillin (10,000 U/mL)-streptomycin (10,000 $\mu\text{g/mL}$), and trypsin-EDTA solution (0.25% trypsin and 0.53 mM EDTA) were purchased from Life Technologies (Grand Island, NY, USA). Fetal bovine serum (FBS) was purchased from Atlanta Biologicals (Flowery Branch, GA, USA). Deuterated dimethylsulfoxide (DMSO- d_6) was purchased from Cambridge Isotope Laboratories (Andover, MA, USA). Ultrapure deionized water (DI H₂O, $\Omega=18.0-18.2$) was sourced from a

Barnstead NANOpure DIamond System (D11911), equipment purchased from Thermo Fisher Scientific (Waltham, MA, USA). All anhydrous organic solvents including dimethylsulfoxide (DMSO), dimethylformamide (DMF), dichloromethane (DCM), and methanol (MeOH) were bought from VWR International (Radnor, PA, USA). Spectra[®]Por dialysis membrane (MWCO=3kDa) was purchased from Spectrum Laboratories, Inc (Rancho Dominguez, CA, USA). Amicon[®] Ultra 15 centrifugal filter device (MWCO=10kDa) was purchased from EMD Millipore (Billerica, MA, USA). Thin layer chromatography (TLC) Silica gel 60 F₂₅₄ plastic sheet was purchased from Merck KGaA (Darmstadt, Germany). All reagents were used as received unless otherwise noted.

5.3 Methods

5.3.1 Cell culture

Mouse melanoma cell line (B16F10), passage 5 to 10, was kindly gifted by Dr. Haipeng Liu, Department of Chemical Engineering and Materials Science at Wayne State University. B16F10 cells were seeded in a Corning[®] 75 cm² U-Shaped Canted Neck Cell Culture Flask (Corning Life Sciences. Tewksbury, MA, USA), and cultured with DMEM supplemented with 10% FBS and penicillin (100 U/mL)-streptomycin (100 µg/mL) (Pen-Strep). The cells were grown in a Thermo Scientific[™] CO₂ incubator (Thermo Fisher Scientific) at 37 °C and 5% CO₂. The medium was exchanged every two days and the cells were split as they reached ca. 70-80% confluence.

5.3.2 Animals for *in vivo* experiments

All animal experiments were performed in accordance with the guidelines of the Institutional Animal Care and Use Committee at Wayne State University. Male C57BL/6 mice (6-8 weeks, 20-22 g) were purchased from Charles River Laboratories (Wilmington, MA, USA).

The mice were housed under a 12 h light/dark cycle, allowed food and water *ad libitum*, and acclimatized for 1 week prior to any experiment.

5.3.3 Synthesis and characterization of dendrimer-DOX conjugates with an acid-labile bond (G4COOH-nDOX)

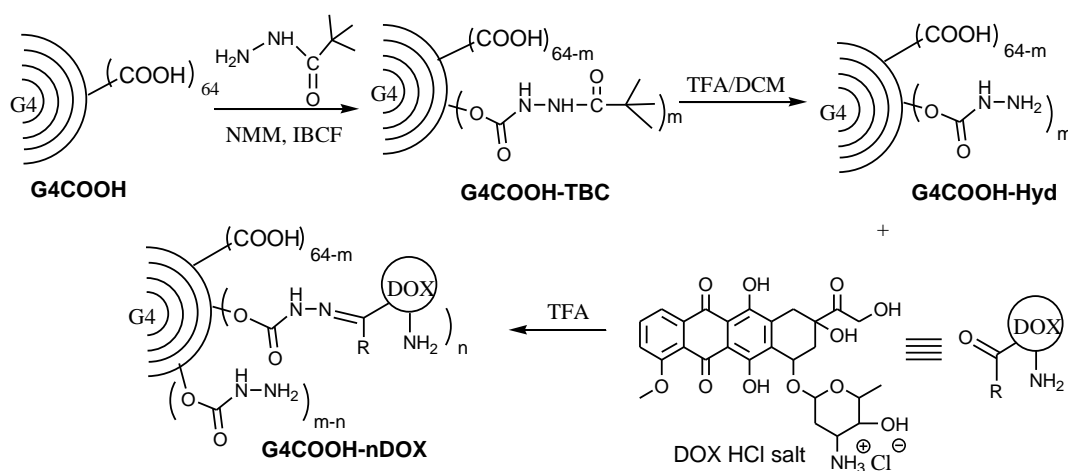


Figure 5.1 Synthesis of the generation 4, carboxyl-terminated PAMAM dendrimer (G4COOH) conjugated with acid-labile DOX (G4COOH-nDOX). NMM = N-methylmorpholine; IBCF = isobutyl chloroformate; TFA = trifluoroacetic acid; DCM = dichloromethane.

The synthetic route of the G4COOH-nDOX conjugate is shown in Figure 5.1. All the intermediates and final products were characterized with proton nuclear magnetic resonance (^1H NMR) for chemical composition and mass-assisted laser desorption/ionization-time of flight (MALDI-TOF) for molecular weight. The hydrodynamic diameter (HD) and zeta potential (ζ) of the intermediates and final products were measured with light scattering (LS). The methods for instrumentation can be found in *Supporting Information in Appendix 4*.

G4COOH (78.3 mg, 3.80 μmol) was mixed with NMM (117.98 μL , 1.07 mmol) and IBCF (133.64 μL , 1.02 mmol) in 8 mL DMSO/DMF (v/v, 10/90). The system was stirred at 0 $^\circ\text{C}$ for 5 min, and then TBC (32.1 mg, 0.243 mmol) was added to the above mixture.[113] The reaction was further stirred at 0 $^\circ\text{C}$ for 30 min and continued at room temperature for 48 h. The organic

solvent was completely removed under reduced pressure. The product was redissolved in 0.1 M phosphate buffer solution with pH value being adjusted to around 10. The product (G4COOH-mTBC) was purified with centrifugal filtration (MWCO=10kDa) and the product collected in filter was lyophilized for 24 h. $^1\text{H NMR}$ (ppm, DMSO- d_6): δ 9.52 (*s*, 32.30H, - NHBoc in TBC), 8.67 (*s*, 29.58H, - NHCO - in TBC), 7.89-7.70 (*m*, 156.84H, - NHCO - in G4COOH), 3.06 (*m*, 372.38H, - CONHCH_2 - (H_e) in G4COOH), 2.63-2.56 (*m*, 328.45H, - NCH_2 - (H_d) and - $\text{COCH}_2\text{CH}_2\text{CO}$ (H_{j3}) in G4COOH), 2.41 (*m*, 126.38H, - CH_2N - ($\text{H}_{b,c}$) in G4COOH), 2.29 (*m*, 150.53H, - $\text{CH}_2\text{CH}_2\text{CONHNH}$ - (succinic methylene, H_{j2}) in G4COOH), 2.18 (*m*, 248.00H, - CH_2CO - (H_a) in G4COOH), 1.36 (*m*, 305.54H, - $(\text{CH}_3)_3$ in TBC). **MALDI-TOF** m/z (Da): 20531.79.

The resulting G4COOH-mTBC (84.34 mg, 4.10 μmol) was dissolved in 5 mL TFA/DCM (80/20, v/v) and stirred at 0 °C for 30 min. The TFA was immediately removed under reduced pressure. The product was treated with 0.1 M phosphate buffer solution (pH 10). The product (G4COOH-mHyd) was purified with centrifugal filtration (MWCO=10kDa) and the conjugate collected in the filter was lyophilized for 24 h. $^1\text{H NMR}$ (DMSO- d_6 , ppm): δ 9.02 (*s*, 19.06H, NH_2NHCO - in hydrazide), 8.03 (*m*, 175.56H, - NHCO - in G4COOH), 3.05 (*m*, 258.24H, - CONHCH_2 - (H_e) in G4COOH), 2.620 (*m*, 188.96H, - NCH_2 - (H_d) and - $\text{COCH}_2\text{CH}_2\text{CO}$ - (H_{j3}) in G4COOH), 2.41 (*m*, 87.18H, CH_2N - ($\text{H}_{b,c}$) in G4COOH), 2.23 (*m*, 151.22H, - $\text{CH}_2\text{CONHNH}_2$ (succinic methylene (H_{j2}) in G4COOH), 2.18 (*m*, 248.00H, - CH_2CO - (H_a) in G4COOH). **MALDI-TOF** m/z (Da): 17780.33.

DOX (20 mg, 34.48 μmol) was dissolved in 40 mL anhydrous MeOH with a trace amount of TFA as catalyst (1.32 μL , 17.32 μmol). The G4COOH-mHyd (18.67 mg, 1.05 μmol) was added to the above organic mixture and the reaction was monitored with TLC until the reaction was completed. The MeOH was completely removed under reduced pressure. The product was

purified with centrifugal filtration (MWCO=10kDa) and the solution was monitored repeated for ending of centrifugal process. The product (G4COOH-nDOX) was lyophilized for 24 h. ¹H NMR (DMSO-d₆, ppm): δ 9.02 (s, 20.41H, NH₂NHCO- in hydrazide), 8.05 (m, 167.13H, -NHCO- and Ar-H in G4COOH and DOX), 5.26 (s, 11.99H, -CH- in DOX), 4.89 (d, 12.72H, -CH- in DOX), 4.570 (m, 24.72H, -CH₂OH in DOX), 4.17 (s, 11.02H, -CH- in DOX), 3.94 (s, 35.23H, -OCH₃ in DOX), 3.05 (m, 255.54H, -CONHCH₂- (H_e) in G4COOH), 2.620 (m, 217.26H, -NCH₂- (H_d) and -COCH₂CH₂CO- (H_{jr3}) in G4COOH), 2.41 (m, 109.82H, CH₂N- (H_{b,c}) in G4COOH), 2.29 (m, 152.93H, -CH₂CONHNH₂ (succinic methylene (H_{jr1, jr2}) in G4COOH), 2.18 (m, 248.00H, -CH₂CO- (H_a) in G4COOH), 1.86 and 1.65 (d, 23.96H, -CH₂- in DOX), 1.12 (s, 36.10H, -CH₃ in DOX). MALDI-TOF m/z (Da): 23860.59.

5.3.4 *In vitro* release of DOX from the G4COOH-nDOX conjugate

In vitro release of DOX was determined at both pH 7.4 and 4.5 that represent extracellular physiological pH and the lysosomal pH, respectively. A 2.0 mL of PBS (10 mM, pH 7.4) or citrate buffer (10 mM, pH 4.5) containing free DOX or G4COOH-12DOX conjugate (both with 1 μmol DOX or equivalent) was added to a dialysis bag (MWCO=3kDa), and the dialysis bag was immersed in 30 mL same medium as inside the bag. The *in vitro* release was performed by gently shaking the system at 37.0 ± 0.2 °C and in darkness. A 0.1 mL buffer solution from outside the dialysis bag was sampled at predetermined time points, and the absorption of DOX was determined using a Biotek Synergy 2 Multi-Mode Microplate Reader (Biotek Instruments, Inc. Winooski, VA, USA), at 490 nm and the amount of DOX was calculated with respect to an established calibration curve. These experiments were run in triplicate. The samples were returned after each measurement. The cumulative release of DOX from the conjugate was plotted as a function of time.

5.3.5 Cell kill (*in vitro*) of the G4COOH-nDOX conjugate

The ability of the G4COOH-12DOX conjugate to kill B16F10 melanoma cells was assessed using the MTT assay. The results benchmarked against free DOX as control. Briefly, sample-laden DMEM (no phenol red) was sterilized through 0.22 μm syringe filter (VWR International). 10,000 B16F10 cells were seeded in each well of tissue culture treated 96-well plate (VWR International) 24 h ahead of the experiment. The DMEM in each well was replaced with a 100 μL of the sample-laden DMEM (no phenol red). The medium was removed after 48h, and the cells were washed twice with 100 μL PBS (10 mM, pH 7.4). 100 μL of fresh DMEM (no phenol red) and 10 μL of MTT (5 mg/mL in PBS) were added to each well. After 4 h incubation at 37 $^{\circ}\text{C}$ and 5% CO_2 , 75 μL medium was removed and 60 μL DMSO was then added. The cells were allowed to sit in the incubator (37 $^{\circ}\text{C}$, 5% CO_2) for another 2 h. Finally, the absorbance of each well was recorded at 570 nm. The cell viability of B16F10 cells was plotted as a function of free- or dendrimer-conjugated DOX concentration (n=8 per concentration).

5.3.6 Cellular internalization of the G4COOH-nDOX conjugate by B16F10 cells

3×10^5 B16F10 cells/well were seeded in Costar[®] 24-well cell culture plate (Corning Life Science, Tewksbury, MA, USA) 24 h prior to the experiment. A 0.5 mL sterile Hanks Balanced Salt Solution (HBSS, 1X, pH 7.4) containing free DOX or G4COOH-12DOX (1 μM DOX or equivalent) was added to each well and then incubated with cells for different times (0.5, 1, 1.5, 2, 3, 4 and 5 h. n=3 per time point). The cellular internalization was terminated at each time point by washing the cells with cold HBSS (1X, pH 7.4). The cells were detached with 0.2 mL trypsin-EDTA and were then pelletized by centrifugation at 350 g. The collected cells were resuspended in 0.5 mL cold HBSS and immediately analyzed for DOX fluorescence with BD LSR II Analyzer with excitation/emission=488/590 (BD Bioscience, San Jose, CA, USA). At least 10,000 events

were counted for statistical significance. Median fluorescence intensity (MFI) was plotted as a function of time to evaluate the cellular internalization of free DOX and dendrimer conjugates.

5.3.7 Efficacy of free and dendrimer-conjugated DOX in treating lung metastasis

A 200 μL PBS containing 2×10^5 B16F10 cells were implanted to each mouse through tail vein to develop the lung metastasis model. At 5, 7 and 9 days post tumor implantation (DPI5, DPI7 and DPI9), 50 μL PBS containing free DOX or G4COOH-nDOX (20 μg of DOX equivalent per dose) was administered to each mouse via either pharyngeal aspiration (p.a. = lung delivery) or i.v. injection, which served as the control in terms of route of administration. The mice were deeply anesthetized with 2.5% v/v isoflurane/oxygen and then placed on a slant board in a supine position. The tongue was gently extended and a 50 μL sample-laden PBS was gradually dripped in the pharynx region with a Hamilton[®]900 series syringe (Hamilton Company. Reno, NV, USA). The tongue was not returned until after a few breaths. The mice were gently returned to the cage and monitored during a few minutes for recovery. The mice were observed daily for behaviour (e.g. diet, drinking, and motion) and body weight. The mice were euthanized at DPI17 or prior to terminal point if necessary. The terminal point criteria include weight loss of 20% or more, obvious signs of illness in addition to the tumor, inability to move freely or significant quivering, and inability to eat/drink properly. The nodule numbers in the lungs of each mouse were carefully counted (The lung metastases at late stages are characterized by large patches of nodules, so it's inappropriate/unlikely to count nodule number exactly at that phase). Kaplan-Meier survival curves were drawn by plotting survival rate as a function of DPI. The lungs of each mouse were also weighed out to evaluate tumor burden. These combined parameters are used to evaluate antitumor efficacy of free DOX and DOX-conjugated dendrimer conjugates. The cohort given with PBS was used as positive control group. We used 6 mice per cohort for statistical analysis.

5.3.8 Systemic distribution of the G4COOH-nDOX conjugate

As the mice were euthanized, the blood was collected by cardiac puncture and principle organs were excised for quantifying systemic distribution of DOX. The excised tissues are lungs, heart, liver, spleen, kidneys, stomach, brain, thymus, auxiliary lymph nodes (ALN), bronchial lymph nodes (BLN), cervical lymph nodes (CLN), mesenteric lymph nodes (MLN). The tissues were homogenized in 3 mL Triton X-100 (0.5% by weight) in PBS (0.5 M, pH 7.4) with D1000 Hand-held Homogenizer (Thermo Scientific) and DOX were extracted into the PBS at 37 °C for a period of 72 h in darkness. For liver, 5 mL solution was needed instead. The homogenate was pelletized by centrifugation (22,000 g, 4 °C, 10 min) and a 200 µL of the supernatant was taken to measure DOX fluorescence using Biotek Synergy 2 Multi-Mode Microplate Reader (excitation/emission=480±20/595±20 nm). The amount of DOX in each tissue was determined with respect to an established calibration curve, which was measured by spiking predetermined amount of DOX or dendrimer-DOX conjugate directly into corresponding tissue. The determination was performed in triplicate.

5.3.9 Statistical analysis

GraphPad Prism 5 software was used for data analysis. The statistical analysis between two systems was performed by *Student's t test*, while that among multiple systems by *one-way analysis of variance (ANOVA) with either Dunnett's test or Tukey post hoc test*. A P-value of 0.05 or less was considered to be statistically significant.

5.4 Results and discussion

5.4.1 Synthesis and characterization of the dendrimer-DOX conjugates (G4COOH-nDOX)

PAMAM dendrimers have been widely used as drug delivery nanocarriers in cancer chemotherapy due to highly controlled size, low toxicity, non-immunogenicity, and multiple functionalizable surface groups.[167] Hydrazone bonds have been recognized as one of the most promising acid-labile spacers in covalently bonding DOX to polymer due to its high sensitivity to mild acidity and relatively straightforward chemistry.[113, 283] In the study, DOX was conjugated G4COOH via hydrazone bonds. G4COOH was firstly modified on surface with Boc-protected hydrazide. The successful modification of -COOH groups was evidenced by two peak shifts -NHNH₂ in TBC: 7.83 ppm (-NH-) to 9.52 ppm (-NHBoc) and 3.89 ppm (-NH₂) to 8.67 ppm (-NHCO- adjacent to G4COOH). The protective Boc groups were subsequently removed to give rise to hydrazide groups (-NHNH₂), which was evidenced by the shift of -NHCO- (adjacent to G4COOH) peak from 8.67 to 9.02 ppm and disappearance of the peak at 9.52 ppm. The resulting -NH₂ groups of hydrazides were further reacted with carbonyl group of DOX, leading to formation of the hydrazone bonds, which are cleavable at mild acidic condition (pH≤5; e.g. intracellular lysosomal pH), but stable at near neutral condition (e.g. extracellular physiological pH). The detailed ¹H NMR and MALDI spectra of dendrimer-DOX conjugates and important intermediates are shown in Figure 5.2. DOX payload and molecular weight of dendrimer conjugate are quantified and summarized in Table 1. Approximately 12 DOX molecules are attached to each dendrimer according to ¹H NMR spectra, which was in agreement with MALDI results.

Table 5.1 Molecular weight (MW), number of conjugated doxorubicin (DOX) (n), hydrodynamic diameter (HD), and zeta potential (ζ) of generation 4, carboxyl-terminated PAMAM dendrimer (G4COOH) conjugate. DOX was conjugated through an acid-labile hydrazone linker. Results obtained by ^1H NMR, MALDI, and light scattering (LS) at 25°C. s.d. = standard deviation.

Conjugates	MW	DOX content (n)		HD \pm s.d. (nm)	$\zeta \pm$ s.d. (mV)
		$^1\text{HNMR}$	MALDI		
G4COOH	17104	0	0	4.7 ± 1.8	-6.6 ± 4.1
G4COOH-30Hyd	17780	0	0	3.6 ± 0.9	-0.5 ± 2.6
G4COOH-12DOX	23861	12.2	11.5	9.7 ± 3.5	$+13.8 \pm 7.0$

Size and surface charge and chemistry are some of primary parameters to be considered in the design of drug delivery systems as they strongly affect the interaction with the physiological environment, including the bioavailability, pharmacokinetics and pharmacodynamics of the conjugates. It can be seen that the hydrodynamic diameter (HD) of the dendrimer slightly decreased upon surface modification with hydrazides (4.7 to 3.6 nm), whereas it dramatically

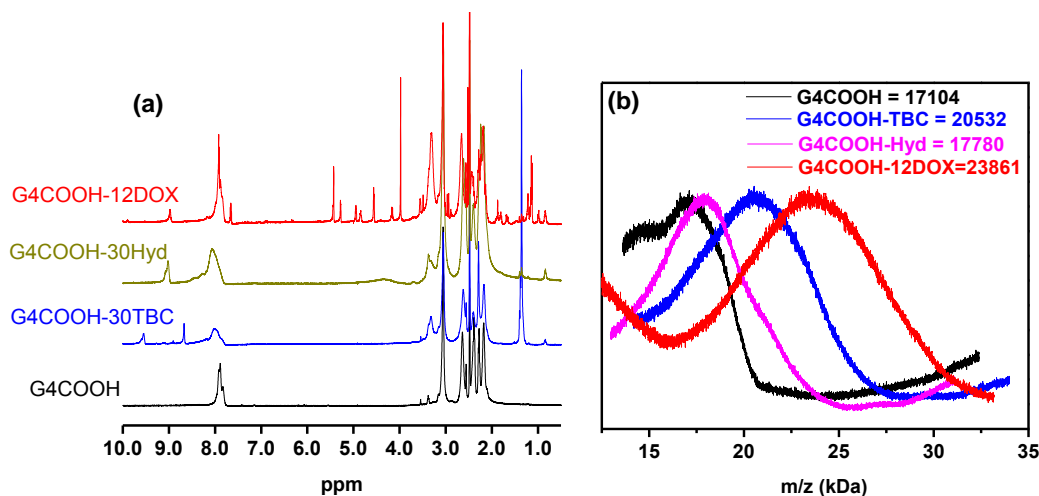


Figure 5.2 (a) ^1H NMR spectra of acid-labile G4COOH-12DOX conjugate. *Inset*: chemical structure of G4COOH-12DOX. Spectral shifts for all compounds are provided in Section 2.4 and (b) MALDI spectra of G4COOH-12DOX conjugate and intermediates.

increases upon conjugation of DOX (4.7 to 9.7 nm). The partial conversion of negatively charged

carboxylates to neutral tert-butyl groups (G4COOH-mTBC) attenuates the repulsion of peripheral carboxylates. Additionally, hydrophobic tert-butyl group will tend to be less solvated by the aqueous environment. Both effects lead to more collapsed architecture with respect to G4COOH. In contrast, the HD increase upon DOX attachment is mainly due to large number of bulky and rigid DOX molecules bonded onto the dendrimer surface. The dendrimer structure is expanded to some extent by the rigid DOX molecule through the interaction including hydrogen bonding and electrostatic force. It is also observed that the ζ increased from a negative value of -6.6 ± 4.0 mV for bare G4COOH, to a moderately high positive charge of $+13.8 \pm 7.0$ mV upon DOX conjugation. The remaining hydrazides (ca. 18) on surface and primary amines of DOX (ca. 12) are protonated at physiological pH (7.2-7.4), which cannot only offset negative charges from carboxylates, but provide extra positive charges. Therefore, the overall surface potential of dendrimer-DOX conjugate is positive, which may potentially enhance cellular internalization and promote interaction with the local epithelia.[49]

5.4.2 Sustained *in vitro* release of acid-labile G4COOH-12DOX conjugate

The ability of DOX release from dendrimer-DOX conjugate was determined at two pH values — mild acidic (e.g. lysosomal pH 5~4.5) and physiological (e.g. pH 7.4~7.2) conditions.[113, 115] The results are summarized in Figure 5.3.

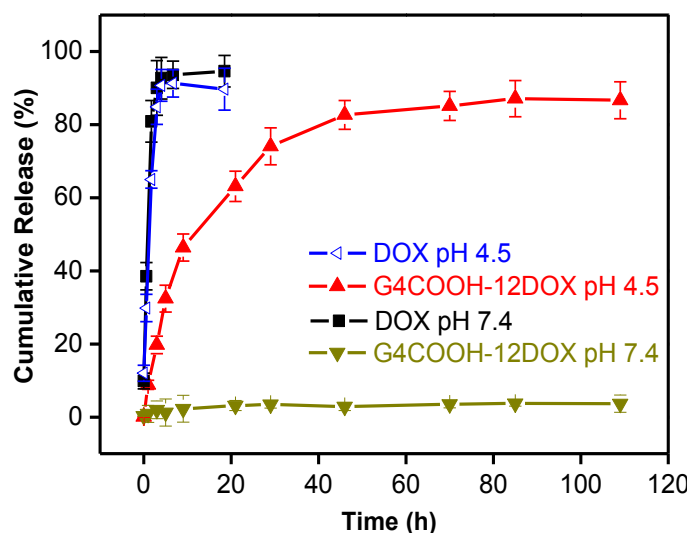


Figure 5.3 *In vitro* release profiles of DOX from acid-labile G4COOH-12DOX at (i) lysosomal pH = 4.5 and physiological pH = 7.4, both at 37 °C. Results represent mean \pm s.d. (n=3 per group). s.d. = standard deviation. The diffusion of free DOX out of dialysis membrane (MWCO=3000Da) is used as control.

As shown in Figure 3, the release of DOX from G4COOH was shown to be dependent on pH. A negligible (<4%) amount of DOX was released at pH 7.4, while in an acidic medium over 80% DOX was released from the conjugate at 48 h. In contrast, free DOX diffused out of dialysis membrane at a fairly rapid rate (over 90% release at approximately 7 h) for both pH values. Based on the release profile of free DOX, approximately 7% of DOX cannot be recovered likely due to interactions of DOX with the dialysis bag and photobleaching. Similar losses can be expected for the conjugates, indicating a recovery of over 86% from the “viable” DOX.

The acid-labile dendrimer-DOX conjugate demonstrates high stability at extracellular physiological pH, while a sustained DOX release at pH similar to that in acidic compartment. The high sensitivity of the dendrimer-DOX conjugates merely to acidic condition is of great relevance as it potentially decreases the concentration of free DOX in plasma by promoting intracellular release of DOX – spatial control. The decreased DOX concentration in plasma mitigates acute and chronic cardiac toxicity of DOX which limits long-term use as well as application in certain patient population.[284, 285] In lung tumor chemotherapy, only a few percent of dose of DOX can reach tumor lesion upon systemic administration.[8] The incidence of fatal myelosuppression (decreased bone marrow activity) and cardiomyopathy is significantly increased when cumulative dose is over a certain limit (e.g. 400-550 mg/m² of body surface area).[286] Therefore, spatially controlled DOX release — intracellularly — could potentially reduce the access of free DOX to systemic bloodstream and bone marrow.

5.4.3 Cell kill of B16F10 melanoma cells lines by the G4COOH-12DOX conjugates

The cytotoxicity of free DOX and G4COOH-12DOX against B16F10 cells was assessed by MTT assay. As shown in Figure 5.4, the G4COOH-12DOX (IC₅₀=6.01 μM) conjugate was slightly less toxic (2.3-fold less potent) than free DOX is against B16F10 melanoma cells at 48 h incubation. The difference in toxicity can be mainly ascribed to sustained release of conjugated DOX (see discussion in **Section 3.2**), differing cellular uptake extent and different subcellular trafficking pathways of free and conjugated DOX. Free DOX can directly diffuse through cellular membrane and reach the nucleus,[216] while the trafficking of conjugated DOX to nucleus is more complex. That is, dendrimer-bound DOX is internalized through endocytic pathways, followed by DOX release from dendrimers upon the cleavage of hydrazone in acidic compartments. The diffusion of released DOX out of lysosome is a time-consuming process as the internal membrane

of lysosomes is permeable to the base form of weak bases.[219] Mild acidity in lysosomes protonates a substantial majority of DOX ($[\text{DOX}+\text{H}]^+$) which need to be converted to free base for outflow. The forward conversion of cationic DOX to free base (both forms are at equilibrium) is driven by DOX efflux from lysosomes.[219]

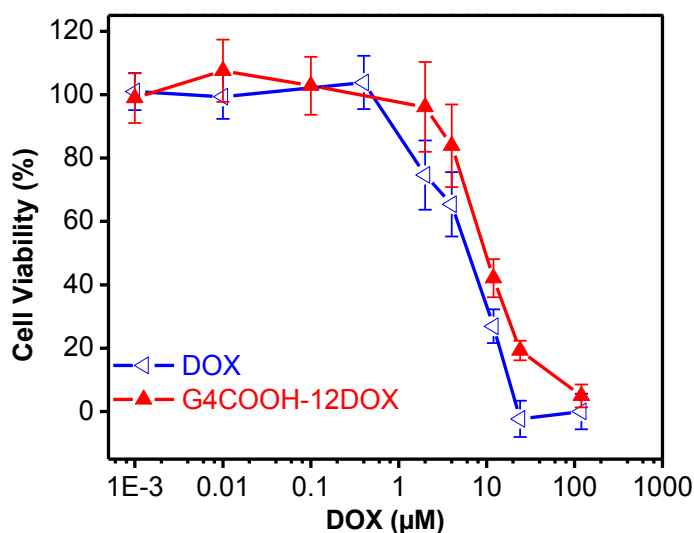


Figure 5.4 Cell kill of acid-labile G4COOH-12DOX as determined by MTT assay after 48 h incubation with B16-F10 melanoma cells. Free DOX is used as control. Results represent mean \pm s.d. (n=8 per group). s.d. = standard deviation. IC₅₀ was calculated based on non-linear regression Log(inhibitor) vs. Response (variable slope) with G4COOH-12DOX being 6.0 μM and free DOX being 2.6 μM .

It is also important to note that the therapeutic efficacy *in vivo* depends on the ability of the payload to reach the tumor site first and foremost (before it can be internalized), and nanocarrier systems are expected to perform better than the free therapeutic.[34, 287] Therefore, while less cytotoxic at a certain time point, the expectation is that the nanocarrier conjugates will outperform the free drug.

5.4.4 Enhanced cellular internalization of DOX by its conjugation to dendrimer conjugate

The cellular internalization of free DOX and G4COOH-12DOX conjugate by B16F10 cells was investigated as a function of time by flow cytometry (a period of 5 h at early stage of internalization). The early kinetics was evaluated by a plot of median fluorescence intensity (MFI) of DOX internalized within the cells as a function of time, as shown in Figure 5.5.

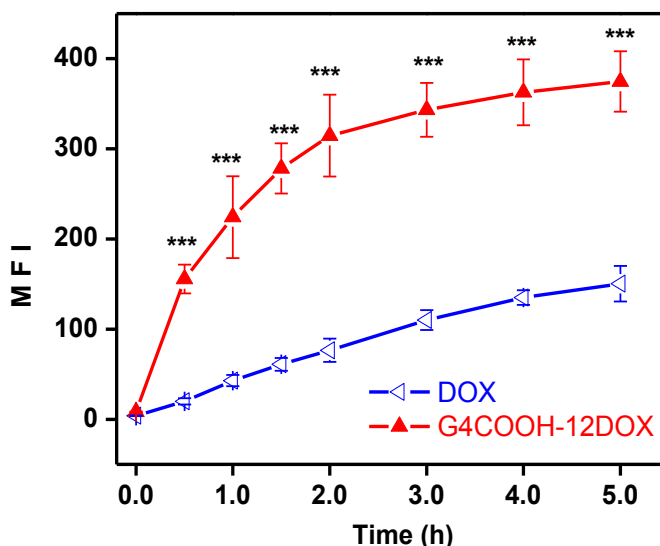


Figure 5.5 Cellular internalization of the acid-labile G4COOH-12DOX in B16-F10 melanoma cells as a function of time, as determined by flow cytometry. Results denote mean \pm s.d. ($n=3$ per group). Statistical significance is calculated with respect to free DOX by *Student's t test* ($*p<0.05$, $**p<0.01$, and $***p<0.001$). The rates of internalization of G4COOH-12DOX (conjugated DOX) and free DOX are 268.7 a.u.h^{-1} ($R^2 = 0.963$) and 35.7 a.u.h^{-1} ($R^2 = 0.981$), respectively. The rate is calculated by linear fitting of 3 initial time points.

It is observed that the rate and extent of internalization of DOX were enhanced upon the conjugation to dendrimer nanocarriers. The conjugated DOX had a rate of internalization of 268.7 a.u.h^{-1} within early times, which was approximately 7.5 fold greater than that of free DOX (35.7 a.u.h^{-1}). The overall extent of internalization of conjugated DOX was significantly different from that of free DOX, at least within the time frame of the experiment - 5h. However, the difference

narrowed down over time — the overall uptake of G4COOH-12DOX was 7.8, 4.1, and 2.5 times as high as free DOX at 0.5, 2, and 5 h incubation, respectively.

Earlier works show passive diffusion is responsible for cellular uptake of hydrophobic DOX, which is determined by concentration gradient and hydrophobicity of DOX,[216, 224] while dendrimers are internalized via various endocytosis including macropinocytosis,[226] receptor-mediated endocytosis,[217, 225, 226] and non-specific, adsorptive endocytosis.[225, 227, 228] The endocytosis is dictated by size, shape and surface chemistry. The significantly enhanced rate and extent of internalization of G4COOH-12DOX by B16F10 cells can be attributed to its positive charged surface upon DOX attachment. G4COOH-12DOX conjugate with a ζ of +13.8 mV is readily adsorbed on negative plasma membrane and quickly saturates the membrane,[227] which results in rapid internalization and uptake plateau (found at 1.5 - 2 h incubation). The non-specific, adsorptive endocytosis is faster and less energy-dependent than other endocytic pathways due to its electrostatic interaction.[217]

The apparent paradox between weaker *in vitro* potency and enhanced uptake of the conjugates, which has been also observed for other polymer-DOX systems conjugated through acid-labile bonds[34, 130] could be interpreted in the following way: (1) incubation time has a stronger effect on cell kill of acid-labile conjugates than free DOX due to sustained release from the conjugate. The ability of dendrimer-DOX conjugates to kill cancer cells *in vitro* is very close to that of free DOX as incubation is prolonged; (2) to a lesser extent, dendrimers are likely to disrupt endosomes and lysosomes due to the protonation of tertiary amines as their concentration in acidic compartments increases; The disruption of acidic compartment fails to release DOX from dendrimer conjugates, resulting in an underestimation of cell kill of the dendrimer-DOX conjugate by MTT assay when the concentration of conjugate is relatively high ; (3) dendrimer conjugates

are internalized through various endocytic pathways, including those whose vesicles do not evolve into acidic compartments.[166, 230] For instance, caveolae-mediated endocytosis ends up in neutral caveosomes, where DOX will have a lesser chance to be released from dendrimers.

In summary, the cellular uptake of DOX is significantly enhanced upon its conjugation to the dendrimer nanocarriers discussed here. This is relevant as greater intracellular concentration of DOX may be achieved while also minimizing also potentially decrease plasma concentration, which in turn is expected to mitigate systemic adverse effect, especially to the cardiac tissue.

5.4.5 Effect of the G4COOH-12DOX conjugates in treating lung metastasis

We investigated the impact of conjugation and route of delivery (p.a. and i.v.) on the efficacy of DOX in reducing the metastatic lung tumor burden. As shown in Figure 5.6, the development of numerous black nodules in the lungs showed that neither free nor conjugated DOX suppressed the proliferation of lung tumors when administered i.v. – note, however, that the intensity of tumor nodules appears to be slightly less in the case of G4COOH-12DOX compared to the free DOX group. Because the density of nodules is so high, it is hard to clearly count them and thus only a qualitative assessment can be achieved by visually inspecting the lung tissue.

In contrast, only a small number of lung nodules were observed in the treatment groups where DOX was administered via pulmonary route, revealing that either free or conjugated DOX delivered directly to the lungs significantly inhibits the growth of metastatic tumor in the lungs, and it is thus a superior route of administration when compared to i.v. . Additionally, the number of lung nodules in the G4COOH-12DOX p.a. group was also significantly fewer than that of DOX p.a. group (6.8 ± 0.5 : 10.3 ± 1.0 ; $p=0.0063$), demonstrating that conjugation further enhances treatment efficacy. While the counting of lung nodules can be employed to qualitatively evaluate tumor burden, it is somewhat limited as it is difficult to delineate single nodules, especially when

nodules are numerous and are of different sizes. Therefore, other methods should be also employed to further assess the effectiveness of therapeutics in reducing tumor burden. We selected the overall weight of lungs as a complementary parameter to the counting nodules protocol. The results are summarized in Figure 5.7 as a function of delivery route and conjugation.

The lung weights of two positive control groups — PBS i.v. (213 ± 24 mg, $p=0.0098$) and

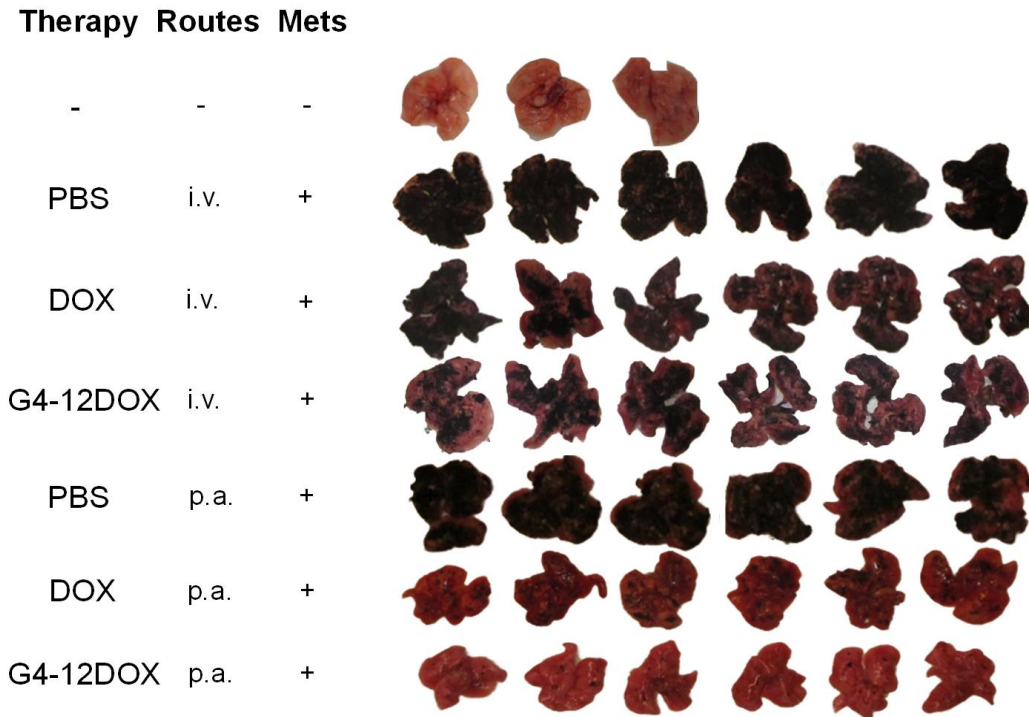


Figure 5.6 Images of lungs collected from C57BL/6 mice bearing lung metastases (n=6 per group). PBS, free DOX or G4COOH-12DOX is administered through i.v. or p.a. route. i.v.: intravenous injection; p.a.: pharyngeal aspiration (pulmonary route). The lungs excised from normal mice are used as negative control (top row). “+” in tumor column denotes mice bearing lung tumors from metastatic melanoma and “-” represents the lungs excised from negative control group.

PBS p.a. (201 ± 30 mg, $p=0.0177$) — were significantly greater than those of healthy mice (142 ± 11 mg). Among all treatment groups, neither DOX i.v. nor G4COOH-12DOX i.v. altered overall lung weights (DOX: 202 ± 22 mg and G4COOH-12DOX: 195 ± 26 mg; both were not significant) compared to their positive group (PBS i.v.). In contrast, the tumor-bearing mice treated with either

DOX p.a. (159 ± 18 mg, $p=0.0336$) or G4COOH-12DOX p.a. (152 ± 15 mg, $p=0.0259$) significantly reduced lung weights compared to PBS p.a. positive group. We also observed that the groups treated with same therapeutics but different routes showed significant difference in lung tumor burdens. That is, DOX group: i.v. : p.a. = 202 ± 22 mg : 159 ± 18 mg ($p=0.0415$); and G4COOH-12DOX group: i.v. : p.a. = 194 ± 26 mg : 152 ± 14 mg ($p=0.0489$).

The Kaplan–Meier survival curves (Figure 5.8) showed that 100% of mice were alive when

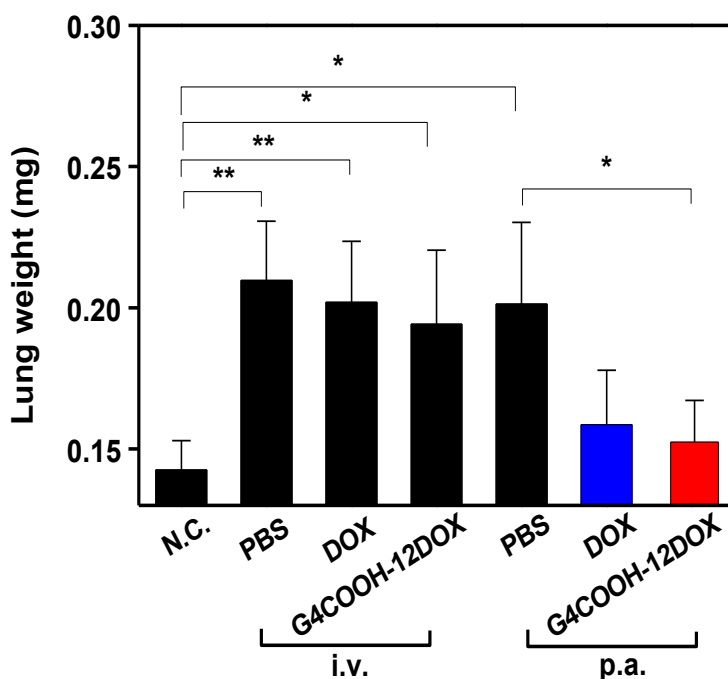


Figure 5.7 Weight of lungs excised from healthy C57BL/6 mice (negative control group; $n=3$ per group) and tumor-metastases bearing mice treated with different therapies ($n=6$ per group) at 17 days post implantation (DPI17). Results represent mean \pm s.d. Statistical analysis is performed with *one-way ANOVA Tukey's* test. $*p<0.05$, $**p<0.01$, and $***p<0.001$. p.a. = pharyngeal aspiration; i.v. = intravenous injection; s.d. = standard deviation.

treated with either DOX p.a. or G4COOH-12DOX p.a., which represents a significant improvement in treatment ($p=0.0185$ for both groups) compared to no treatment group (PBS p.a.), with only 1 mouse alive (16.7% survival rate) at terminal point. In contrast, the treatments via i.v.

route were ineffective — neither DOX i.v. (16.7% survival rate) nor G4COOH-12DOX i.v. group (33.3% survival rate) showed significant difference with respect to their positive control group (PBS i.v.=16.7% survival rate).

In summary, the results discussed above show that lung metastatic tumors can be

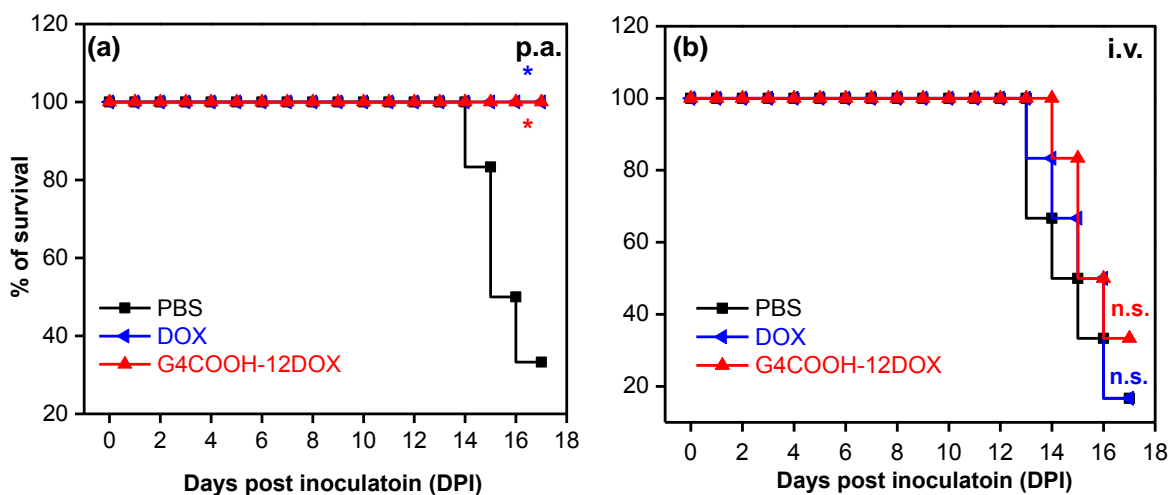


Figure 5.8 Survival rate of mice bearing lung metastases over 17 days, as plotted on a Kaplan-Meier survival curve. The survival rate of each group is analyzed using *Log-rank (Mantel-Cox) test* ($*p < 0.05$) with respect to the positive control of same administration route (PBS). n.s. = not significant.

significantly inhibited by pulmonary delivered DOX, thus leading to an improved survival rate.

The results also show that metastatic lung tumor burden is further relieved upon conjugation of DOX to dendrimer nanocarriers.

5.4.6 Impact of administration route and DOX conjugation on systemic biodistribution

Our *in vitro* results have showed that conjugation of DOX to dendrimer nanocarriers enhances the cellular uptake of DOX, while promoting intracellular release, demonstrating the potential to reduce systemic toxicity of DOX. However, the *in vivo* fate and distribution of DOX

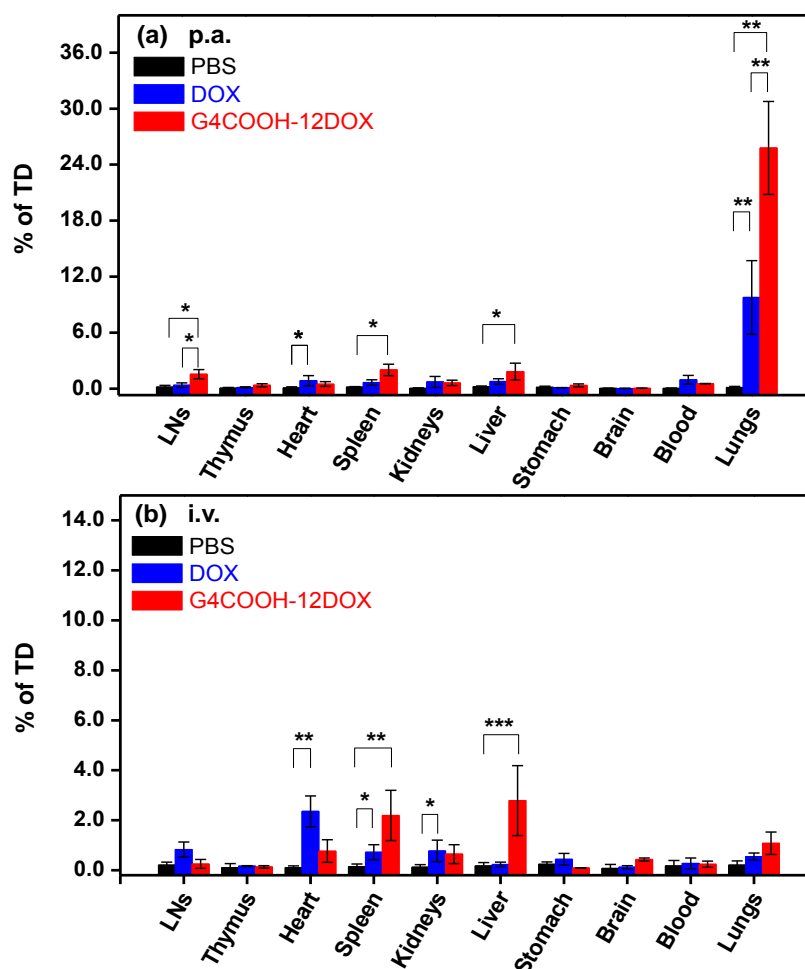


Figure 5.9 Systemic distribution of DOX and G4COOH-12DOX delivered via (a) p.a. and (b) i.v.. Mice bearing lung metastases were euthanized at 17 days post implantation (DPI17) or terminal point prior to DPI17. Results represent mean \pm s.d. (n=6 per group). The groups of same administration (p.a. or i.v.) are analyzed using *one-way analysis of variance (ANOVA)* with *Tukey's post hoc test*. * $p < 0.05$, ** $p < 0.01$ and *** $p < 0.001$. % of TD = % of total dosage. p.a. = pharyngeal aspiration; i.v. = intravenous injection; s.d. = standard deviation.

free or in conjugate form is much more complex as it is impacted by several factors, such as various *in vivo* barriers, which vary as a function of the delivery route. We investigate, therefore, the

distribution of systemically and locally (lung) delivered DOX (free or in conjugate form) in major organs. The systemic distribution results are summarized in Figure 5.9.

The results show that the DOX tissue distribution is strongly impacted by the route of administration and conjugation. The amount of DOX in the lungs at DPI17 (8 days after last dosing) followed the sequence: G4COOH-12DOX p.a. ($26.8 \pm 5.0\%$ of total dose - TD) > DOX p.a. ($9.8 \pm 4.3\%$ of TD) >> G4COOH-12DOX i.v. ($1.1 \pm 0.4\%$ of TD) \approx DOX i.v. ($0.5 \pm 0.1\%$ of TD). These results demonstrate that pulmonary delivery can potentially increase drug dose and prolong drug retention in lungs compared to systemic administration. This can be seen as an extra advantage compared to free DOX, which was not captured on the results presented while discussing number of tumor nodules or lung weight. It suggests that upon further optimization of dosages (concentration and number), there is the potential to either decrease total dosage or the number of dosages. For comparison, it is worth noticing that previous studies have shown that a large amount of DOX-loaded PLGA nanoparticles remained in the lungs one week after inhalation, and a detectable amount of DOX was still found up to 14 days post treatment.[142] Similarly, PEI-conjugated DOX could be still clearly seen 7 days after i.t. administration.[143]

We further analyzed the statistical difference of drug retention among all groups at DPI17. As shown in Figure 5.10 (a), *one-way ANOVA Tukey's* test showed the amount of DOX in the lungs of G4COOH-12DOX p.a. group was significantly greater with respect to that of all other groups — DOX p.a. group ($p=0.0194$), G4COOH-12DOX i.v. ($p<0.0001$), and DOX i.v. ($p<0.0001$). Additionally, the amount of DOX in the lungs of DOX p.a. group was also much greater than that of G4COOH-12DOX i.v. ($p=0.0038$) and DOX i.v. group ($p=0.0050$). However, no statistical difference was found between DOX i.v. and G4COOH-12DOX i.v. group.

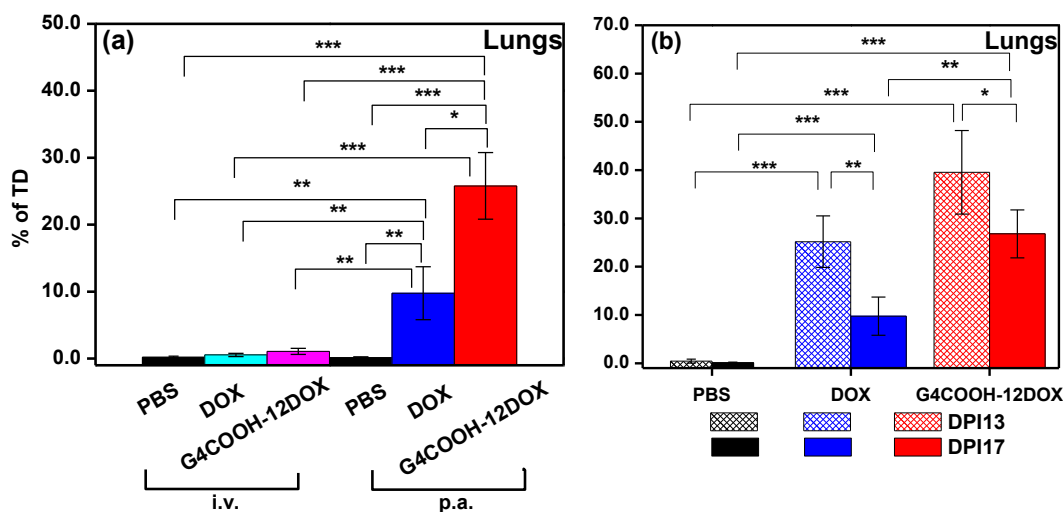


Figure 5.10 (a) Accumulation of DOX (free/conjugated form) in the lungs at terminal point (DPI17). Therapeutics were given through i.v. or p.a. route. Statistical analysis is performed with *one-way analysis of variance (ANOVA) with Tukey's post hoc test*. (b) Temporal effect on accumulation of DOX in the lungs. Therapeutics were given through p.a.. The mice were euthanized at DPI13 (n=3 per group) and DPI17 (n=6 per group). Statistical analysis is performed in 2 different ways: (i) all groups at DPI13 or DPI17 are analyzed with *one-way analysis of variance (ANOVA) with Tukey's post hoc test*; (ii) same therapy groups (e.g. DOX p.a.) at DPI13 and DPI17 are analyzed with *Student's t test*. * $p < 0.05$, ** $p < 0.01$ and *** $p < 0.001$. Results represent mean \pm s.d.. % of TD = % of total dosage. i.v. = intravenous injection; p.a. = pharyngeal aspiration; DPI = days post implantation; s.d. = standard deviation.

Our recent results demonstrated that the fate of PAMAM dendrimer nanocarriers administered to the lungs is greatly impacted by their surface charge — positively charged PAMAM dendrimers tend to reside locally (lungs) for longer, while neutral dendrimers tend to more effectively translocate into systemic circulation.[168] The HD of G4COOH-12DOX is ca. 10 nm, which is larger than the fenestration of the endothelial lining of vascular vessels (4-5 nm).[175] Compared to small molecule drugs, reverse diffusion of dendrimer conjugates into vascular vessels for clearance is thus reduced.[175] In the meantime, the reabsorption of interstitial dendrimer conjugates through lymphatics is also much attenuated in tumor tissues due to a lack of

effective lymphatic drainage.[287, 288] These conditions thus lead to a preferred retention of dendrimer-bound DOX in the lungs compared to free DOX.

Due to the enhanced local concentration of drug upon pulmonary administration, we investigated the temporal effect on pulmonary retention of locally delivered DOX and G4COOH-12DOX. We compared the content of DOX in the lungs at DPI13 (4 days after last dosing) and DPI17 (8 days after last dosing). The results are summarized in Figure 5.10 (b). At DPI13, the amount of DOX in the lungs was $39.1 \pm 8.5\%$ of total dose (TD) for G4COOH-12DOX p.a. and $25.2 \pm 5.3\%$ of TD for free DOX p.a. ($p=0.0765$). At DPI17, the % of TD decreased for both free and conjugated DOX. However, the elimination of free DOX from the lung tissue was much more substantial, decreasing at almost twice the rate when compared to conjugated DOX, being at $26.8 \pm 5.0\%$ of TD for G4COOH-12DOX p.a. and $9.8 \pm 4.0\%$ TD for free DOX p.a. ($p=0.0089$) at DPI17. Therefore, a higher DOX retention and a much greater p value between DPI13 and DPI17 demonstrates that conjugation to the dendrimer nanocarriers slow down the elimination of DOX from the lungs. The processes responsible for dendrimer-DOX and DOX clearance may include mucociliary escalator, pulmonary alveolar macrophage phagocytosis, translocation to systemic circulation and enzymatic degradation.[39, 72, 152, 201]

Interestingly, the groups treated with either DOX p.a. or G4COOH-12DOX p.a. showed lower cardiac accumulation of DOX compared to the distribution upon i.v. administration. No statistical difference was found between the two p.a. groups. Noticeably, intravenous injection of free DOX was the system that resulted in the greatest accumulation of DOX in the cardiac tissue compared to all other groups— Figure 5.11 (a). Considering the limited accumulation of DOX in heart upon pulmonary administration, the cardiac content of locally delivered DOX as a function of time (sampled at DPI13 and DPI17) was further investigated. As shown in Figure 5.11 (b), we

observed that at DPI13, the cardiac content of DOX in the groups treated with either DOX or G4COOH-12DOX were statistically greater than that of no treatment group, whereas they decreased slightly at DPI17 and only DOX p.a. group showed significant difference with respect to no treatment group at that terminal point. Comparing with i.v. injection route, however, the cardiac accumulation of DOX (even in DOX p.a. group) was still much less at DPI17.

The results show that the distribution of DOX to the heart tissue can be mitigated upon pulmonary delivery, and further upon conjugation to dendrimers. This is of great relevance as major adverse effects, including lethal cardiomyopathy, are known to limit the applicability of DOX in the treatment of a variety of cancers including lung metastasis.[289]

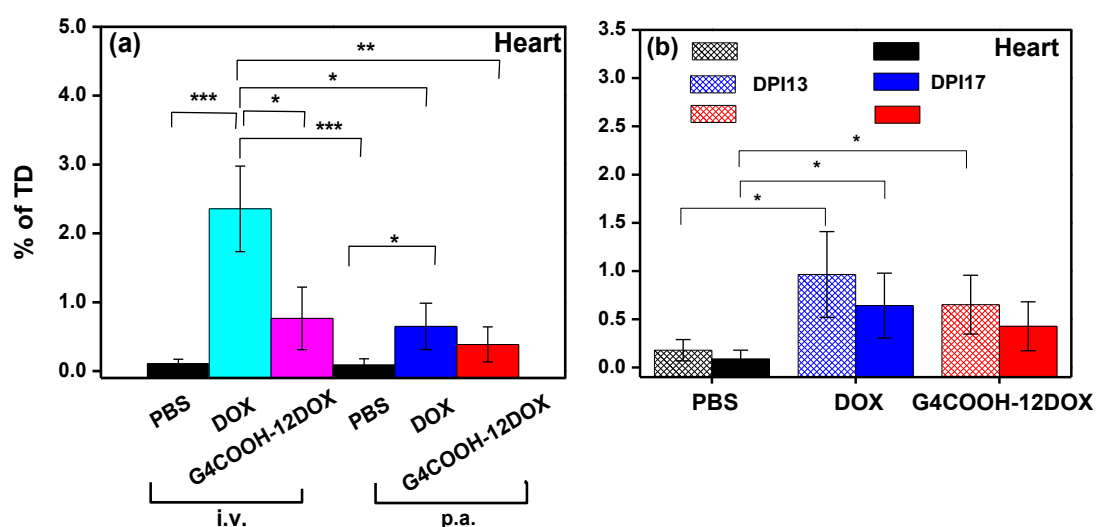


Figure 5.11 (a) Accumulation of DOX (free/conjugated form) in the heart at terminal point (DPI17). Therapeutics were given through i.v. or p.a.. Statistical analysis is performed with *one-way analysis of variance (ANOVA) with Tukey's post hoc test*. (b) Temporal effect on accumulation of DOX in the lungs. Therapeutics were given through p.a.. The mice were euthanized at DPI13 (n=3 per group) and DPI17 (n=6 per group). Statistical analysis is performed in 2 different ways: (i) all groups at DPI13 or DPI17 are analyzed with *one-way ANOVA Tukey's test*; (ii) same therapy groups (e.g. DOX p.a.) at DPI13 and DPI17 are analyzed with *Student's t test*. * $p < 0.05$, ** $p < 0.01$ and *** $p < 0.001$. Results represent mean \pm s.d.. % of TD = % of total dosage. i.v. = intravenous injection; p.a. = pharyngeal aspiration; DPI = days post implantation; s.d. = standard deviation.

Besides the ability to modulate the distribution of DOX in the lungs and heart, the results shown here demonstrate that the route of elimination of DOX is also impacted by the choice of delivery route and conjugation. As shown in Figure 5.9 (a) and (b), higher concentrations/percentage dosage of DOX was found in spleen and liver upon their conjugation to dendrimers independent of routes of administration. The clearance of polymeric delivery systems is dictated mainly by surface charge and particle size.[49] Positively charged nanocarriers (e.g. G4COOH-12DOX in our case) can be cleared and processed by mononuclear phagocytic system (MPS), whose targets are opsonized by plasma proteins and subsequently captured by phagocytes.[290, 291] Phagocytes, such as macrophages, mainly reside in or migrate to bone marrow, lymph nodes, liver and spleen.[292] It is also reported that dendrimer nanocarriers are cleared by glomerular filtration in kidneys.[193] In this work, small amounts of DOX in the case of G4COOH-12DOX conjugate (i.v.: $0.84 \pm 0.37\%$ of TD and p.a.: $0.60 \pm 0.29\%$ of TD) was found in kidneys at DPI17 (8 days after last dosing). This may be to some extent due to the fact that the time for observing renal accumulation of DOX is too long. Previous research has shown that PAMAM dendrimers can be detected in urine 2 h after i.v. injection.[199] On the other hand, it is also possible that renal pathway may not play a vital role in clearing these dendrimer-DOX conjugates. Renal glomeruli have round pores of approximately 6 nm in diameter. Therefore, the nanocarriers with diameter < 6 nm are rapidly to be cleared by glomerular filtration. The hydrodynamic diameter of G4COOH-12DOX (9.7 ± 3.5 nm) is greater than the size threshold for glomerular filtration.[49, 291] Additionally, nanocarrier-biomolecule coronas are instantaneously formed when nanocarriers are exposed to physiological fluids, since plasma proteins are readily adsorbed on positively charged nanocarriers with formed,[293, 294] leading to much greater physiological diameters than as light scattering measured.[291]

5.5 Conclusion

In this work, we demonstrated the potential of PAMAM-DOX conjugates upon pulmonary delivery for lung cancer treatment using an *in vivo* lung metastasis model. DOX was conjugated to G4COOH through an acid-sensitive bond, which has shown to provide a sustained intracellular release of DOX, but to be stable at extracellular physiological conditions. Upon conjugation to dendrimer, significant increase has been observed on the rate and extent of internalization of DOX by B16F10 cells at short times (up to 5 h). Nuclear colocalization study indicated that DOX can rapidly colocalize with nucleus, after being released from the conjugates. The dendrimer-DOX conjugates showed similar ability to kill cancer cells as free DOX did. The acid-labile dendrimer-DOX conjugates administered via pulmonary route remarkably reduced the mass and nodule number of lung tumors derived from metastatic B16F10 melanoma, thus significantly increasing survival rate of tumor-bearing mice. A high amount (ca. 30% of TD) of locally delivered dendrimer-DOX conjugates remained in the lungs 8 days after last dosing, significantly higher than that through i.v. injection. Interestingly, little DOX accumulated in heart tissues upon pulmonary delivery compared to systemic injection, which implicates greatly reduced risk of acute and chronic cardiac toxicity. Therefore, the dendrimer-based chemotherapeutic delivery system in combination with pulmonary administration technology (e.g. oral inhalation) is a potentially promising strategy for lung cancer treatment.

5.6 Acknowledgements

We would like to acknowledge financial support from National Science Foundation (NSF-CBET grant no.0933144 NSF-DMR grant no. 1508363) and the NanoIncubator at WSU. We would also like to thank Microscopy, Imaging and Cytometry Resources Core (MICR) for help with the confocal microscopy. The MICR is supported, in part, by NIH CenterGrant

P30CA022453 to the Karmanos Cancer Institute and the Perinatology Research Branch of the National Institutes of Child Health and Development, both at WSU.

5.7 Supplemental information

The procedures for ^1H NMR, MALDI-TOF and LS were provided in **Appendix C**

CHAPTER 6 — CONCLUSIONS AND FUTURE DIRECTIONS

6.1 Conclusions and future directions

Lung cancer is the leading cause of cancer death among both men and women in the United States. Adenocarcinoma accounts for more than 40% of all lung cancer cases. Doxorubicin (DOX) is an FDA-approved chemotherapeutic that has been widely used as primary anticancer drug in the treatment of a variety of cancers including lung cancers. However, rapid elimination, uncontrolled release, and life-threatening cardiotoxicity, has hindered the applicability of DOX and other potent anti-cancer agents. The treating efficacy for lung adenocarcinoma is also limited by low accumulation of DOX in the lungs which is generally administered through systemic route, and by severe cardiac toxicity. The development of polymeric carriers for the modulation of transport, targeting and controlled release of potent anti-cancer agents and their aerosol formulation for local lung delivery is of great relevance in the treatment of lung adenocarcinoma.

The main conclusions drawn from our studies and suggested future directions are discussed here:

(i). We have characterized the effect of PEGylation and route of administration on systemic and local distribution of PAMAM dendrimer. Our pharmacokinetic results show that dendrimers with high density of surface modification with PEG not only present long circulation times upon I.V. administration, but they also reach systemic circulation much faster and are found at much greater concentrations (ca. 13% of administered dose) than the non-PEGylated counter parts (2% of administered dose) upon pulmonary administration at t_{max} . PEGylation and route of administration also have profound effects on systemic and local (lung cell) distribution. While ca. 83% of G3NH₂ is found in the lungs upon pulmonary delivery at 6.5 hours post administration, only 2% reaches the lungs upon I.V. delivery. Interestingly, pulmonary delivery provide

dendrimers with ability to accumulate in lymph nodes, while no measurable concentration of neither bare dendrimers nor highly PEGylated dendrimers is found in the lymph nodes upon I.V. administration. Moreover, PEGylation also increased the transport of dendrimers to the lymph nodes upon lung delivery. The findings are valuable for the design of new dendrimer-based nanovaccines. No statistical difference was observed in terms of the overall percentage of cells found to take up the unmodified vs. PEGylated dendrimers in the lung. Myeloid and epithelial cells from the alveoli and airway internalized dendrimers effectively, independent of chemistry, with myeloid cells being responsible for most of the uptake. The biggest impact of the dendrimer chemistry was observed regarding uptake in endothelial cells, where PEGylated dendrimers were observed to be taken up by a large extent. This observation is in agreement with the idea of the fast transport across extracellular barriers and the lung epithelium leading to enhanced endothelial internalization en route to systemic circulation. The results shown here suggest that the pulmonary route of administration in combination with dendrimer chemistry can be used to passively target tissues of interest for treating a variety of medically relevant diseases of the lungs and other target tissues of tissues outside the lungs.

As the results show significantly higher local concentration of dendrimer nanocarriers in the lungs and potential to passively target various lymph nodes. The suggested further studies may focus on the following aspects: (1) the concentration of PAMAM dendrimers in lungs and lymph nodes as a function of time should be studied in details; (2) the mechanism for the accumulation of pulmonary delivered PAMAM dendrimers in various lymph nodes should be further elucidated — activation of antigen-presenting cells or passively leaking into draining lymph nodes; (3) One of major challenges that may limit the delivery of polymeric nanocarriers (e.g. PAMAM) to/through the lungs is the potential acute and chronic toxicological issues caused by delivered

particulates. To evaluate the acute toxicity PAMAM dendrimers caused in the lungs, inflammatory cytokines and immune response elicited in animal models should be studied with immunochemistry staining and flow cytometry. Tumor damage may be screened by histological staining; (4) in this work, PAMAM is used as model dendrimer to exploit the feasibility of dendrimers as anticancer drug carriers delivered to/through the lungs. Due to its non-degradable nature, potential chronic toxicity and biocompatibility may limit its clinical application. The transition from PAMAM to biodegradable dendrimers (e.g. hyperbranched polyester) are helpful to expand biomedical application of dendrimer.

(ii). We have developed PEGylated, acid-labile dendrimer-DOX conjugates which can achieve spatially and temporally sustained release of DOX. The conjugates upon pulmonary delivery can significantly inhibit tumor growth *in vivo* and improve survival rate. In detail, PEGylated poly(amidoamine) dendrimer nanocarriers with acid-labile DOX conjugates were synthesized. Due to hydrophobicity of DOX, dendrimer may crash out of aqueous solution when high payload DOX are attached. Aqueous solubility of dendrimer-DOX conjugates can be increased upon PEGylation of dendrimer nanocarriers. We developed direct PEGylation to synthesize dendrimer conjugates with low DOX payload and varying PEGylation degree, and two-step PEGylation especially for dendrimer conjugates with high drug payload and high PEGylation degree. The resulting PEGylated, acid-labile dendrimer-DOX conjugate released DOX only in acidic medium, and also intracellularly. The release can be modulated by PEG density on dendrimer surface. We also observed that the kinetics of cellular entry of the nanocarrier with DOX increased significantly compared to free DOX. At the highest PEGylation density, the rate of internalization of the nanocarrier containing DOX was even higher than that of free DOX. PEGylation density also affects cytotoxicity as seen by an increase in IC_{50} for DOX-conjugated

dendrimer compared to free DOX, due to the controlled release of the therapeutic. PEGylation significantly helped dendrimer nanocarriers escape mucus trapping compared to bare dendrimer, aiding their transport to the basolateral side. It is in accordance with in vivo pharmacokinetics. Reduced transepithelial electrical resistance (TEER) and limited cellular internalization demonstrated that paracellular transport plays a vital role in transporting dendrimer-DOX conjugates across airway epithelium. Upon pulmonary delivery of the acid-labile dendrimer-DOX conjugate, lung tumor burdens were significantly reduced and survival rate of mice were considerably improved, while i.v delivered therapeutics showed a very limited efficacy. The results can be correlated to significant greater concentration of therapeutics in the lungs — the observation extended to 8 days showed approximately 30% of total DOX remained in the lungs. On the other hand, less DOX were accumulated in heart tissues upon lung delivery, which can potentially mitigate cardiac toxicity.

The acid-labile dendrimer-DOX conjugates delivered to the lungs showed great promise in lung tumor treatment in this work, it thus deserves continuing studies in the following aspects: (1) combination therapy are believed to be an more effective way to fight cancers including lung tumors, it is potentially relevant to develop dendrimer conjugates for co-delivery of two or more therapeutics at the same time; (2) The acid-labile dendrimer-DOX conjugates are able to release DOX intracellularly. Although systemic toxicity of DOX can be significantly reduced by local delivery, the dendrimer conjugates are incapable of targeting to lung tumor cells. Therefore, next step may be focused on designing dendrimer conjugates with ability to selectively enter tumor cells. For example, the conjugation of MUC1 aptamer to dendrimer, whose receptors are overexpressed on lung cancer cells;[295] (3) gene therapy and immunotherapy are gaining more and more attention due to their significantly reduced side effects and high ability to kill cancer

cells. The conjugation of nucleic acid or antigens to dendrimers can significantly may prevent them from enzymatic degradation and increase their cellular uptake as well. Therefore, the combination of dendrimer-based immunotherapy/gene therapy in conjunction with dendrimer-based chemotherapy may be a potent therapy against lung cancers, while reduces systemic/local side effects; (4) we used pharyngeal aspiration to perform lung delivery, which may make difference in terms of aerosol deposition in the lungs compared to aerosolization. Therefore, further study may focus on the use of real aerosolizer such as Penn-Century Microsprayer.

(iii) Oral inhalation is well known for its high efficiency of lung deposition and non-invasive nature. The development of oral inhalation formulations for lung cancer treatment is potentially beneficial to millions of lung cancer patients. Our PEGylated, acid-labile dendrimer-DOX conjugates can be directly formulated in the propellant-based metered-dose inhalers (pMDIs) with a trace amount of ethanol (ca. 0.4% v/v), forming a solution aerosol formulation. The pMDI formulations containing high PEGylated dendrimer-DOX conjugates can also be readily formulated into propellant with a co-solvent free method. It is for the first time, to our best knowledge, that polymer nanocarrier drug delivery system is formulated into a solution aerosol formulation. The stability and aerosol characteristics increased significantly as PEG density increased and DOX payload decreased. The formulation of highly PEGylated dendrimer-DOX conjugates showed superior aerosol characteristics. The pMDI formulation is suitable for delivering drug to deep lung area such as alveolar region and terminal bronchi. Furthermore, the lung deposition position of dendrimer-DOX conjugates can be further modulated by adding biodegradable surfactants, in order to treat tumors in different pulmonary regions. Broadly, the PEGylated dendrimer conjugate in combination with metered dose inhalers showed great potentials to deliver therapeutics to/through the lungs.

Although the pMDI formulations containing PEGylated dendrimer-DOX conjugates showed superior aerosol properties, the drug dose in these formulations is still low (ca. 0.2 mg/mL). A few attempts can be made in future to address the low dose issue: (1) a simple method to increase DOX dose is to increase concentration of the conjugates in propellant. The aerosol properties could be compromised as the concentration is over a certain limit. Therefore, the guideline to improve drug dose is to maximize DOX payload in dendrimer nanocarriers, while minimize the fraction of other components (dendrimer+PEG). To achieve this goal, thorough studies on the effect of PEG density and DOX payload on aerosol performance should be performed to find the highest DOX payload and lowest PEG density, as well as optimal concentration without aerosol properties compromised. The smaller size of PEG (e.g. 750 Da or 550 Da) may be attempted for this purpose. However, the consequent alterations of *in vivo* pharmacokinetics and biodistribution are also needed to be taken into account and evaluated; (2) previous computational work showed ester and ether bonds have strong interaction with HFA propellant, enhancing the solubility/dispersibility of these bonds-containing molecules in HFA propellant. Hyperbranched polyester contains an abundance of ester bonds.[237] Much lower PEG density on surface are needed to solvate polyester dendrimer in HFA propellant. Therefore, a much higher concentration of PEGylated dendrimer-DOX can be reached; (3) a significant advantage DPI formulations hold over pMDI formulations is much higher dose of drug delivered to the lungs. Therefore, development of DPI formulations containing acid-labile dendrimer-DOX conjugates may also be considered.

APPENDIX A

SUPPLEMENTAL INFORMATION OF CHAPTER 2

S1. Proton magnetic nuclear resonance spectra (^1H NMR) and peak assignment

^1H NMR spectra were recorded with a 400 MHz Agilent Mercury spectrometer (Santa Clara, CA). Proton chemical shifts were reported in ppm (δ) and the peak of deuterated DMSO (DMSO- d_6) at 2.483 ppm was set as the reference peak. ^1H NMR (DMSO- d_6 , ppm) of **G3NH2-3Cy3**: δ 7.972-7.772 (m, 50.27H, NHCO of G3NH2), 7.614 (m, 3.28H, aromatic H of Cy3), 7.427 (m, 6.07H, aromatic H of Cy3), 7.163 (m, 17.94H, aromatic H of Cy3), 6.476 (d, 5.73H, $=\text{CH}$ of Cy3), 3.104 (m, 139.92H, CONHCH_2 of G3NH2), 2.599 (m, 86.75H, NCH_2 of G3NH2), 2.391 (m, 58.50H, CH_2N of G3NH2), 2.161 (m, 120H, CH_2CONH of G3NH2), 1.658 (s, 32.97H, CH_3 of Cy3), 1.509 (m, 5.88H, CH_2 of Cy3), 1.353 (m, 6.03H, CH_2 of Cy3). ^1H NMR (DMSO- d_6 , ppm) of **G3NH2-24PEG1000-3Cy3**: δ 7.907-7.784 (m, 40.82H, NHCO of G3NH2), 7.609 (m, 3.49H, aromatic H of Cy3), 7.431 (m, 6.34H, aromatic H of Cy3), 7.179 (m, 18.32H, aromatic H of Cy3), 6.481-6.444 (s, 5.51H, $=\text{CH}$ of Cy3), 4.014 (m, 47.64H, CH_2NHCO of G3NH2), 3.647-3.402 (m, 2043.61H, $\text{CH}_2\text{CH}_2\text{O}$ of PEG1000), 3.216 (69.95H, OCH_3 of PEG1000), 3.056 (m, 153.05H, CONHCH_2 of G3NH2), 2.622 (m, 87.78H, NCH_2 of G3NH2), 2.396 (m, 63.38H, CH_2N of G3NH2), 2.157 (m, 120H, CH_2CONH of G3NH2), 1.664 (s, 32.48H, CH_3 of Cy3), 1.537 (m, 6.02H, CH_2 of Cy3), 1.341 (m, 5.80H, CH_2 of Cy3).

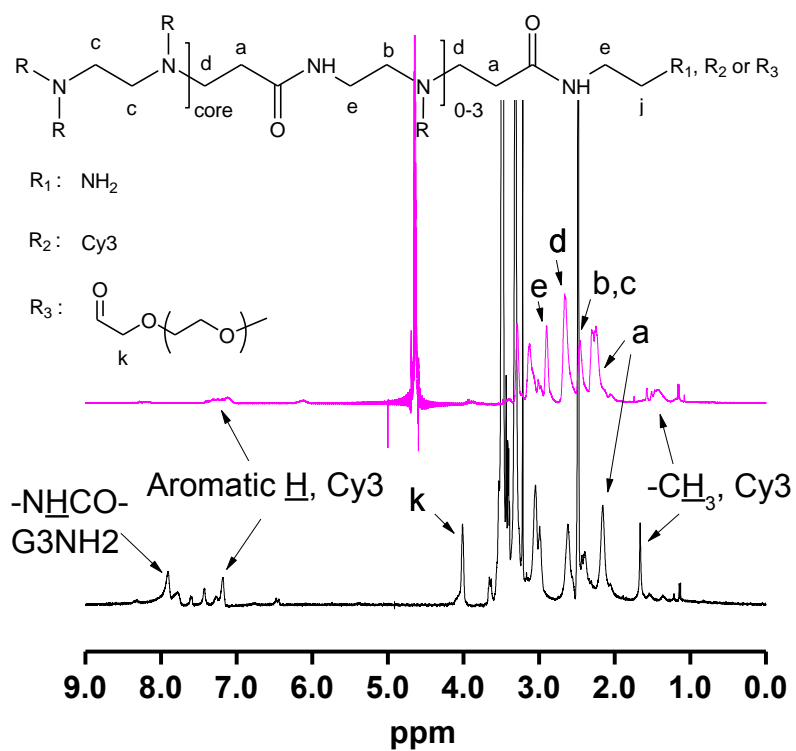


Figure S1. ^1H NMR spectra of G3NH2-Cy3 (pink line) in deuterated oxide (D_2O) and G3NH2-24PEG1000-3Cy3 (black line) in deuterated dimethylsulfoxide (DMSO_d6). Detailed chemical shifts discussed above. The inset is chemical structure of G3NH2-24PEG1000-3Cy3.

S2. Mass-assisted laser desorption/ionization-Time of Flight (MALDI-TOF)

MALDI-TOF mass spectra were performed on a Bruker Ultraflex spectrometer equipped with a pulsed nitrogen laser (337 nm) under positive ion reflector mode. 10 μl of sample (1.0 mg/ml) in DI H₂O was mixed with 10 μl of DHB (10 mg/ml) in methanol. 2 μl of the sample was spotted on a Bruker Daltonics MALDI plate. The spotted sample was dried gently by air flow. MALDI: G3NH₂-3Cy3 (m/z, 8285) and G3NH₂-24PEG1000-3Cy3 (m/z, 33312).

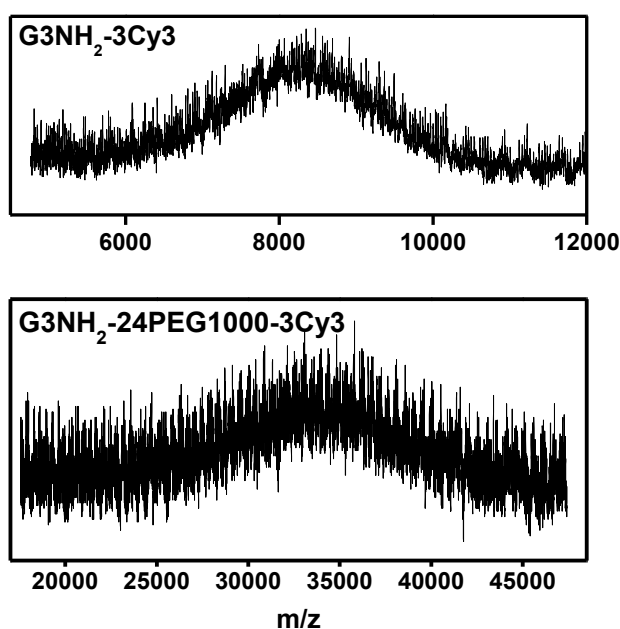


Figure S2. MALDI-TOF spectra of G3NH₂-3Cy3 and G3NH₂-24PEG1000-3Cy3.

S3. Single cell staining of pulmonary cellular populations

Lung cell populations tagged by fluorescent probe-labeled antibodies includes myeloid cells tagged by Percp-Cy5.5, endothelial cells tagged by PE-Cy7, surfactant protein C-secreted alveolar type II cells tagged by AF647 and ciliated airway epithelial cells tagged by pacific blue. These cells were prepared according to a preceding reported method [296] with slight modification as described below.

Primary Antibodies

Rat anti-mouse CD16/CD32 (Fc-Block; BD Biosciences. San Jose, CA, USA), 1:100 dilution in 0.15 or 0.3% saponin buffer. (Preparation: 1 μ l Fc-Block + 99 μ l 0.15 or 0.3% saponin buffer)

Rabbit polyclonal anti-mouse pro-surfactant protein-C (pro-SPC) antiserum, reactive with human and mouse proSPC (Abcam. Cambridge, MA, USA), 1:500 dilution in 0.15 or 0.3% saponin buffer. (Preparation: 1 μ l + 499 μ l 0.15% or 0.3% saponin buffer)

Rat anti-mouse β -tubulin (BD Biosciences. San Jose, CA, USA), 1:500 dilution in 0.15 or 0.3% saponin buffer. (Preparation: 1 μ l + 499 μ l saponin buffer)

Rat anti-mouse CD45-PerCP/Cy5.5, clone 30-F11 (BioLegend. San Diego, CA, USA), 1:50 dilution in 0.15 or 0.3 % saponin buffer. (Preparation: 2 μ l + 98 μ l saponin buffer)

Rat anti-mouse CD31-PE/Cy7, clone MEC13.3 (BioLegend. San Diego, CA, USA), 1:100 dilution in 0.15 or 0.3% saponin buffer. (Preparation: 1 μ l + 99 μ l saponin buffer)

Secondary antibodies

F(ab')₂-goat anti-rabbit IgG(H+L) secondary antibody, Alexa Fluor®647 conjugate (Life Technologies. Grand Island, NY, USA) 1:500 dilution in 0.15 or 0.3% saponin buffer. (Preparation: 1 μ l AF647 + 499 μ l saponin buffer)

F(ab')₂-goat anti-mouse IgG(H+L) secondary antibody, Pacific Blue conjugate (Life Technologies, Grand Island, NY, USA), 1:500 dilution in 0.15 or 0.3 saponin buffer solution.

(Preparation: 1 μ l + 499 μ l saponin buffer).

2. Incubated lungs connected with trachea in an additional 3 ml dispase per lung for 30 min at 37°C in a 6-well plate.

3. Placed the lungs into a 6 cm petridish filled with 6 ml DMEM containing 100 U/ml DNase and 25 mM HEPES. Removed the lung tissue from the trachea by gentle tapping with the back of a pair of tweezers.

4. Incubated for 10 min at room temperature with slight agitation.

5. Added 4 ml medium with a 10 ml serological pipet.

6. To further disarticulate the tissue, homogenize by pipetting up and down with a 1 ml pipet.

7. Pipetted the lung homogenate up and down again with a 10 ml serological pipet and transferred it to a 100 μ m nylon cell strainer placed on a 50 ml tube. Added 5 ml medium without DNase and processed the tissue through the cell strainer.

8. Passed the lung homogenate through the 40 μ m cell strainer into a fresh 50 ml tube.

9. Centrifuged the single cell suspension for 10 min at 350 g.

10. Discarded the supernatant and resuspended the pellet in 5 ml fresh medium.

11. To determine the amount of cells, dilute the suspension 1:2,000 in 10 ml CasyTon™ and count the cells using a Casy TT cell counter.

12. Centrifuged the single cell suspension for 10 min at 350 g.

13. Discarded the supernatant and resuspended the pellet in 4 ml fresh 1% paraformaldehyde solution and incubate for 15 min on ice.

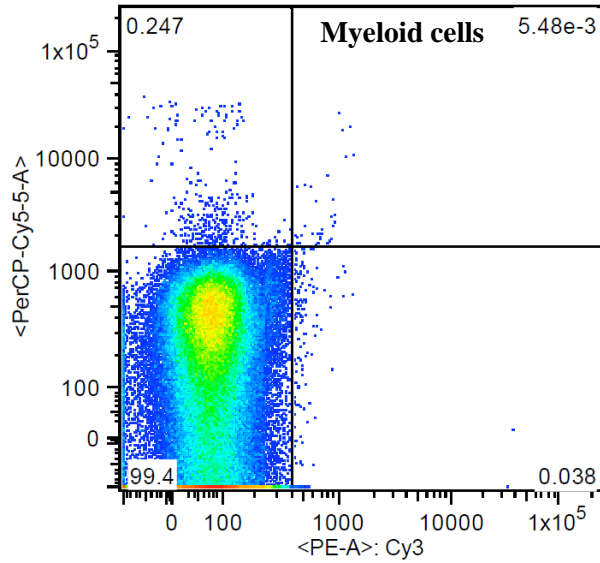
14. Centrifuged the fixed cells for 10 min at 350 g.

15. Discarded the supernatant and resuspended in 5 ml wash buffer.
16. Centrifuged cells for 10 min at 350 g.
17. Discarded the supernatant and resuspended the pellet in 4 ml wash buffer.
18. Transferred about 200,000 cells per lung sample into FACS tubes.
19. Prepared additional samples as blank controls.
20. Centrifuged the aliquots of 200,000 cells per FACS tube for 10 min at 350 g.
21. Discarded the supernatant, added 100 μ l 0.15% saponin buffer per sample for permeabilization, mix, and incubated for 20 min at 4 °C.
22. Centrifuged FACS tubes for 5 min at 350 g.
23. Discarded the supernatant, added 10 μ l diluted Fc-block, added 20 μ l of the appropriate dilutions of the antibodies against CD45, CD31, and pro-SPC and β -tubulin. Vortexed, and incubated for 25 min at 4°C in the dark.
24. Centrifuged the stained cells for 5 min at 350 g.
25. Discarded the supernatant, washed with 100 μ l 0.15% saponin once, and centrifuged the cells for 5 min at 350 g.
26. Discarded the supernatant, added 20 μ l of the appropriate dilution of the secondary antibody to pro-SPC and β -tubulin group. Mixed, and incubate for 25 min at 4°C in the dark.
27. Centrifuge the stained cells for 5 min at 350 g.
28. Discarded the supernatant, wash with 100 μ l 0.15% saponin buffer once and centrifuged the cells for 5 min at 350 g.
29. Discarded the supernatant, wash with 100 μ l once with wash buffer, centrifuged the cells again for 5 min at 350 g, and resuspended them in 200 μ l wash buffer.

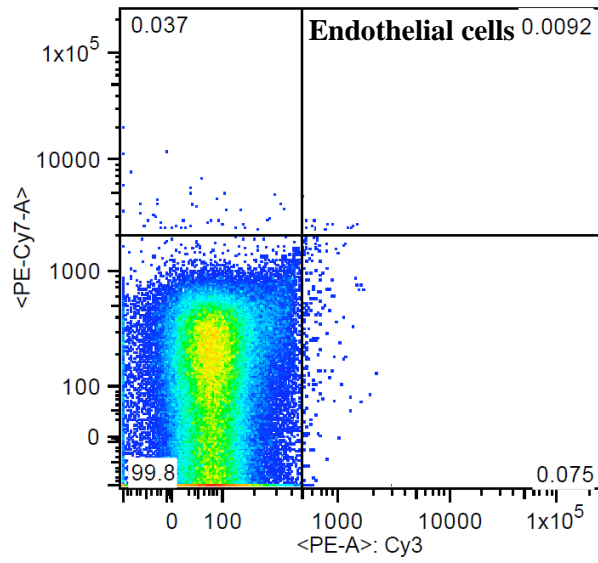
30. Gated the cells to exclude debris and cell clumps using flow cytometer. 160,000 events were at least counted.

Examples of FACS cellular biodistribution results for control groups, G3NH2-3Cy3 and G3NH2-24PEG1000-3Cy3

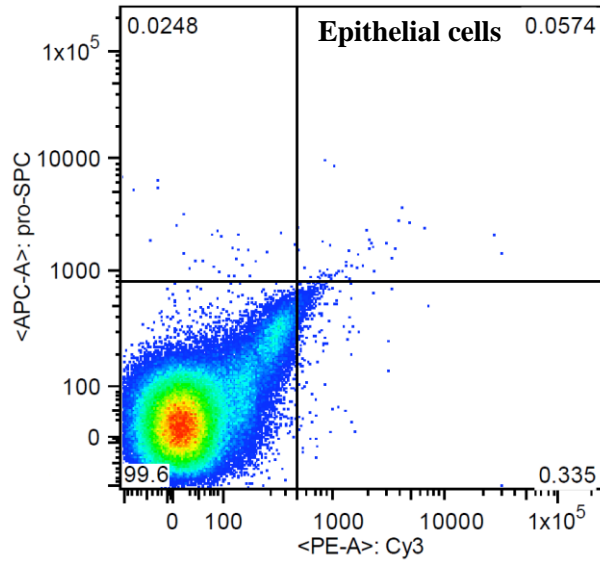
(a) Control



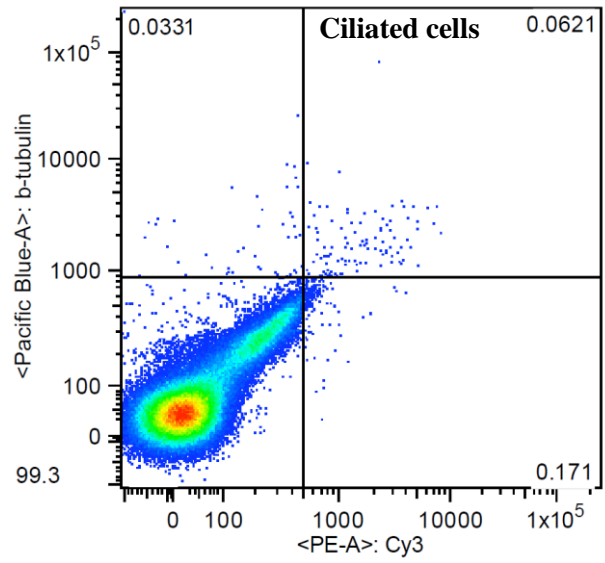
cells/singlets
blank
Event Count: 169120
sd101813__001.fcs



cells/singlets
blank
Event Count: 169120
sd101813__001.fcs

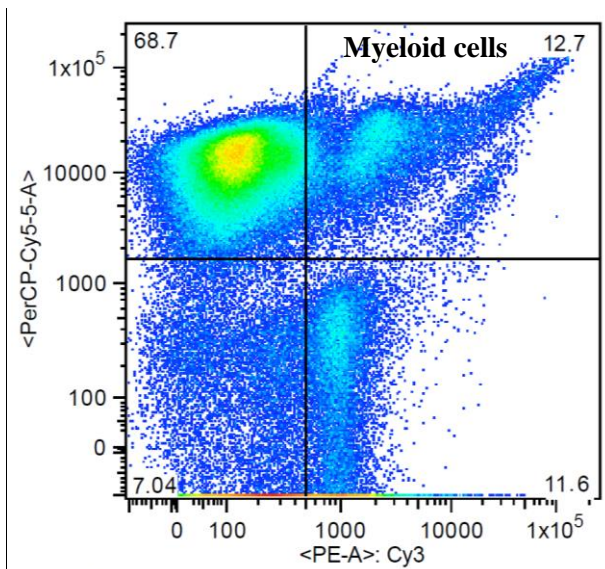


cells/singlets
blank
Event Count: 169120
sd101813__001.fcs

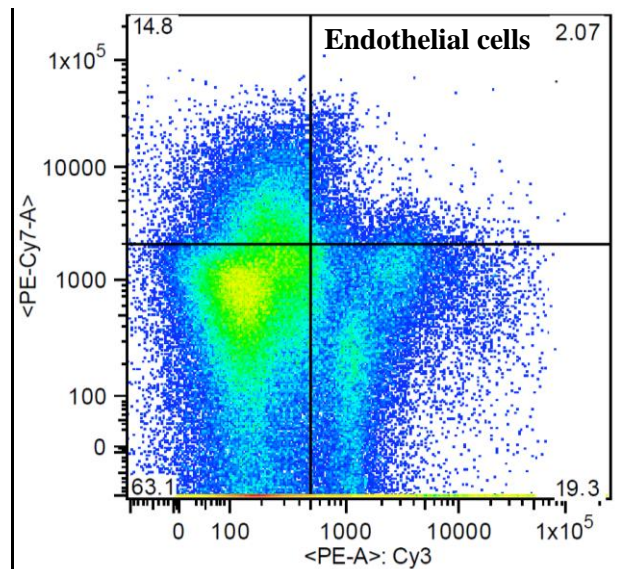


cells/singlets
blank
Event Count: 169120
sd101813__001.fcs

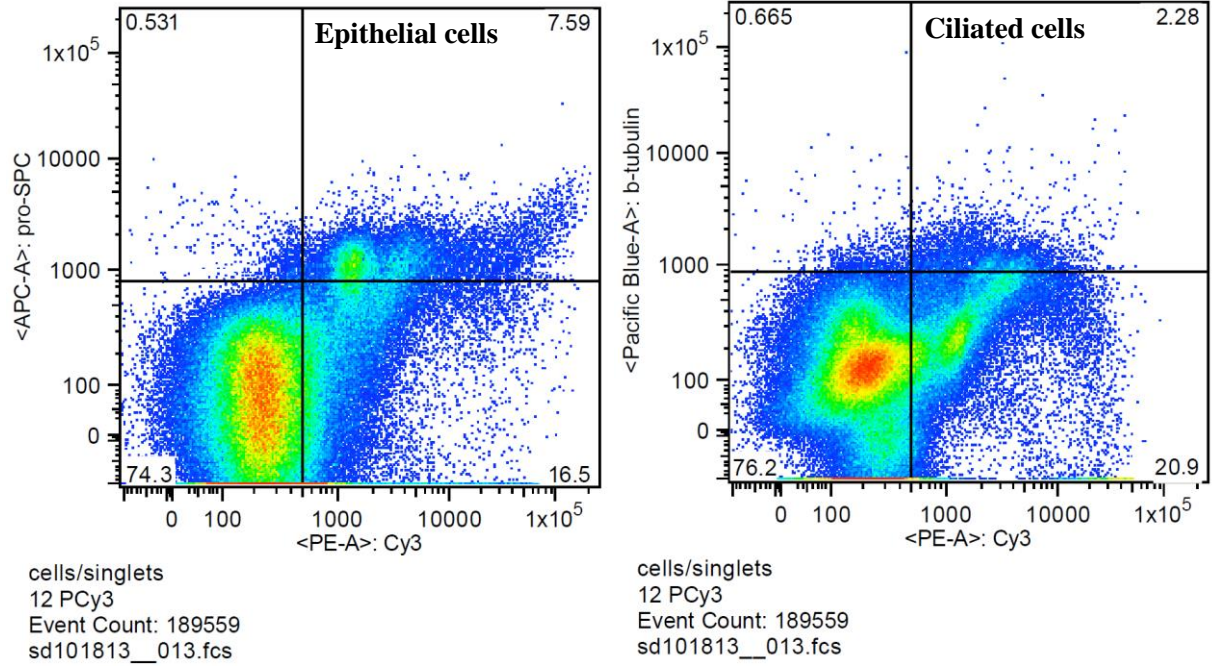
(b) G3NH2



cells/singlets
12 PCy3
Event Count: 189559
sd101813__013.fcs



cells/singlets
12 PCy3
Event Count: 189559
sd101813__013.fcs



(c) *G3NH2-24PEG1000K*

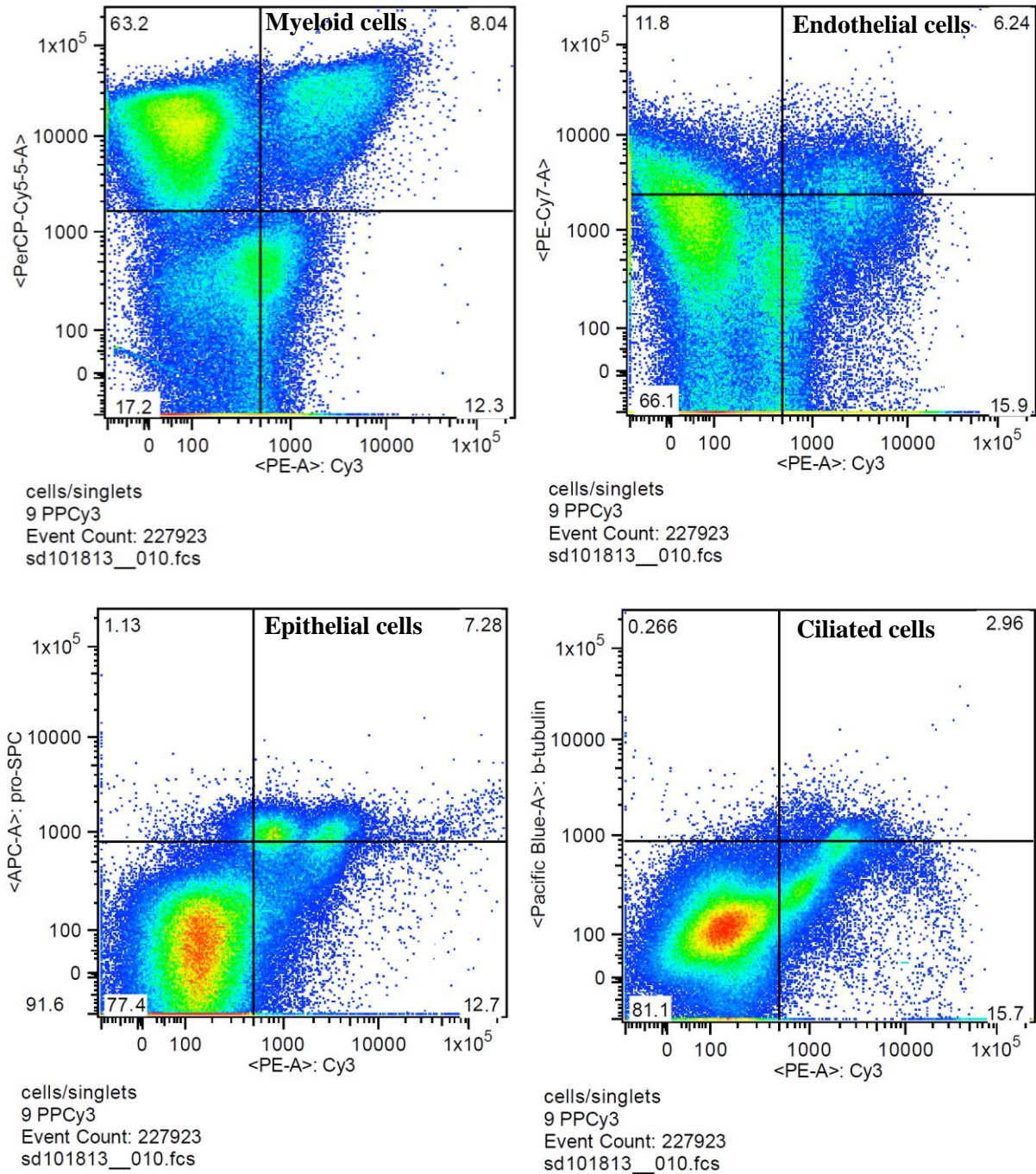


Figure S3. Dot plot of antibody-dye vs. Cy3-dendrimer, determined by flow cytometry.

Biodistribution of the conjugates in a per tissue mass basis.

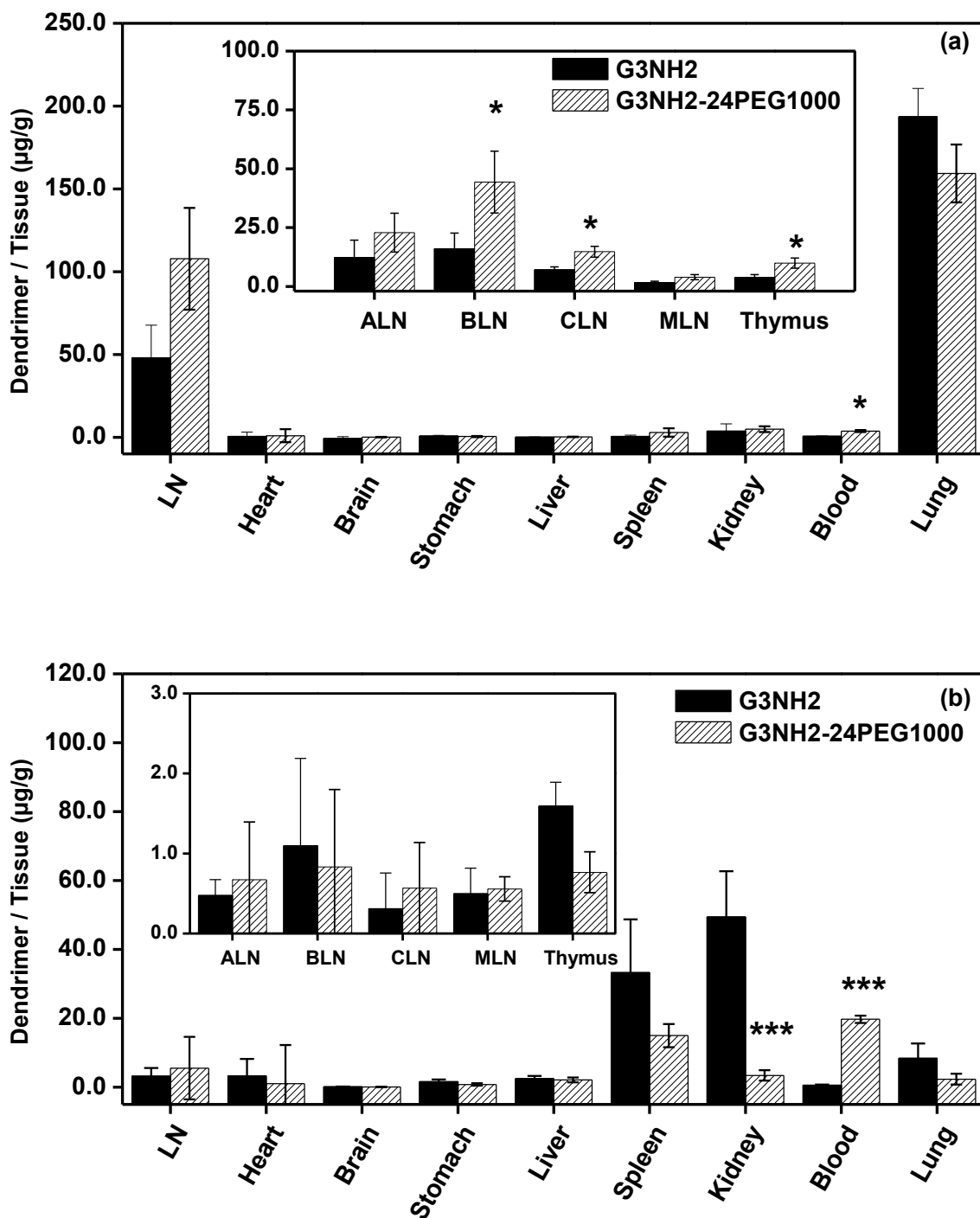


Figure S4. Effect of the PEGylation and route of administration on the whole body distribution of the conjugates. The statistical analysis was performed between G3NH2 and G3NH2-24PEG1000

with Student t-test (* $p < 0.05$, ** $p < 0.01$, and *** $p < 0.001$). Panel (a) pharyngeal aspiration and (b) intravenous administration, 6.5 h post administration. $n=3$ per group.

APPENDIX B

SUPPLEMENTAL INFORMATION OF CHAPTER 3

S1. Characterization

S1.1. Electrospray ionization (ESI)

A trace of sample (a few μg) was dissolved in methanol (mass spectrometry grade), and then diluted 50 times, also with methanol. The methanolic solution was injected into ZQ-Waters TERS/Micromass spectrometer (Waters) for determining the m/z value of the analyte.

S1.2. Mass-assisted laser desorption/ionization-time of flight mass spectrometry (MALDI-TOF)

MALDI-TOF was performed on a Bruker UltrafleXtreme mass spectrometer (Bruker) equipped with a pulsed nitrogen laser (337 nm) under positive ion reflector mode. The conjugates were dissolved in deionized water at a concentration of 1.0 mg/mL. 2, 5-dihydroxybenzoic acid (2, 5-DHB) in methanol (10 mg/mL) was used as matrix. 10 μL of conjugate solution was mixed with equal volume of 2, 5-DHB solution and 2 μL of the mixed solution was spotted on a Bruker Daltonics MALDI plate. The spotted sample was dried gently by air flow.

S1.3. Proton magnetic nuclear resonance (^1H NMR)

^1H NMR spectra were recorded on a Varian Mercury 400 (400 MHz) spectrometer (Agilent Technologies) using deuterated DMSO (DMSO_d_6). Proton chemical shifts were reported in ppm (δ) and DMSO_d_6 at 2.48 ppm was set as reference peak.

S1.4. Light scattering (LS)

Sample (1.0 mg/mL) was dissolved in phosphate buffer saline (PBS, pH 7.4). pH test indicated all sample solutions were neutral. Hydrodynamic diameters and zeta potentials were measured using Zetasizer Nano ZS (Malvern Instruments). The average and standard deviation

for hydrodynamic diameters and zeta potentials were calculated based on at least three measurements.

S2. Synthesis of PEGylated PAMAM dendrimer conjugates with acid-labile DOX (G3NH₂-mPEG-nDOX) and acid-nonlabile DOX (G3NH₂-mPEG-nDOXNL)

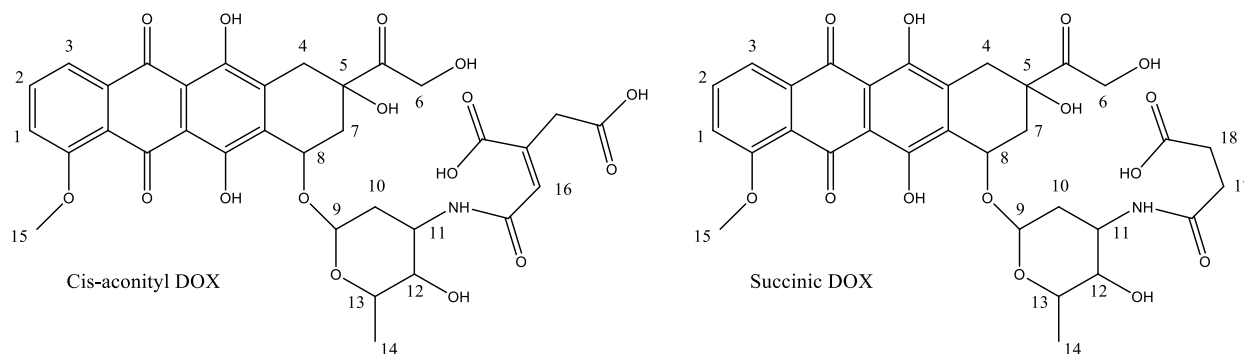


Figure S1. Protons in cis-aconityl DOX and succinic DOX.

S2.1. Synthesis of cis-aconityl DOX

The synthesis of cis-aconityl DOX was performed using a similar strategy to that reported in the literature,[297] with modifications. Briefly, 3 mL anhydrous p-dioxane solution of cis-aconityl anhydride (188.4 mg, 0.60 mmol) was added dropwise to a 6 mL DI H₂O DOX solution (86.7 mg, 0.15 mmol). The pH value of the aqueous solution was immediately adjusted to 9.0-9.2. The reaction was vigorously stirred for 20 min at 0-5 °C, and additionally 15 min at room temperature. The product was precipitated by acidifying the solution to pH 2.0 with 1 M hydrochloric acid (HCl aq) at 0 °C and then collected by centrifugation. The precipitate was redissolved in cold DI H₂O and the pH was adjusted to 9.0 with 1 M sodium hydroxide solution (NaOH aq). The precipitation-dissolution process was repeated twice. Finally, the red powder was lyophilized and stored at 4°C for future use. **Yield:** 61.7%. **TLC** (chloroform/methanol/acetic acid = 17/3/1 v/v, retention factor (R_f): 0.05 (DOX), 0.33 (cis-aconityl DOX)). **ESI** (m/z): 700.2016 ([cis-aconityl DOX + H]⁺), 722.1509 ([cis-aconityl DOX + Na]⁺), 738.1769 ([cis-

aconityl DOX + K⁺). ¹H NMR (DMSO-d₆, ppm) δ: 7.947 (s, 1.03H, Ar-H (H-2) in DOX), 7.771 (s, 0.97H, Ar-H (H-3) in DOX), 7.443 (s, 0.94H, Ar-H (H-1) in DOX), 6.397 (s, 0.96H, -CH=C- (H-16) in cis-aconitic acid), 5.263 (s, 0.99H, -CH- (H-9) in DOX), 4.890 (d, 1.02H, -CH- (H-5) in DOX), 4.570 (m, 1.95H, -CH₂OH (H-6) in DOX), 4.173 (s, 1.02H, -CH- (H-13) in DOX), 3.936 (s, 3.03H, -OCH₃ (H-15) in DOX), 3.575 (s, 1.03H, -CH- (H-12) in DOX), 2.986 and 2.807 (d, 1.95H, -CH₂- (H-4) in DOX), 2.161 and 2.054 (d, 2.05H, -CH₂- (H-7) in DOX), 1.859 and 1.647 (d, 1.96H, -CH₂- (H-10) in DOX), 1.122 (s, 3.10H, -CH₃ (H-14) in DOX). The sequence of all protons for cis-aconityl DOX was shown in Figure S1.

S2.2. Synthesis of succinic DOX

DOX (53.8 mg, 92.7 μmol) and TEA (32.6 μl, 0.23 mmol) were dissolved in 2.2 mL anhydrous DMSO. To the mixture a 1.0 mL anhydrous p-dioxane solution of succinic anhydride (13.9 mg, 0.14 mmol) was added dropwise. The reaction was stirred and monitored with TLC for completion. The purification for succinic DOX was same as that of cis-aconityl DOX described above. Finally, the precipitate was lyophilized until constant weight and stored at 4 °C for future use. **Yield:** 67.2%. **TLC** (chloroform/methanol/acetic acid = 17/3/1 v/v, Rf: 0.07 (DOX), 0.79 (succinic DOX)). **ESI** (m/z): 666.1815 ([succinic DOX + Na]⁺), 682.1591 ([succinic DOX + K]⁺). ¹H NMR (DMSO-d₆, ppm) δ: 7.942 (s, 0.99H, Ar-H (H-2) in DOX), 7.739 (m, 1.04H, Ar-H (H-3) in DOX), 7.441 (s, 0.97H, Ar-H (H-1) in DOX), 5.263 (s, 0.97H, -CH- (H-9) in DOX), 4.896 (d, 2.08H, -CH₂- (H-5) in DOX), 4.566 (m, 1.88H, -CH₂OH (H-6) in DOX), 4.195 (s, 0.95H, -CH- (H-13) in DOX), 3.922 (s, 3.06H, -OCH₃ (H-15) in DOX), 3.575 (s, 1.00H, -CH- (H-12) in DOX), 2.989 and 2.807 (d, 2.01H, -CH₂- in DOX), 2.732 (m, 4.14H, -CH₂- (H-17, 18) in succinic linker), 2.161 and 2.046 (d, 2.02H, -CH₂- (H-7) in DOX), 1.859 and 1.647 (d, 1.99H, -CH₂- (H-10) in

DOX), 1.125 (s, 3.09H, $-CH_3$ (H-14) in DOX). The sequence of all protons for succinic DOX was shown in Figure S1.

S2.3. Synthesis of acid-labile G3NH₂-mPEG-nDOX conjugates

Direct PEGylation

S2.3.1. Synthesis of acid-labile G3NH₂-nDOX conjugates (n=3)

Cis-aconityl DOX (23.6 mg, 33.6 μ mol), EDC (6.4 mg, 33.5 μ mol) and NHS (5.6 mg, 40.2 μ mol) were dissolved in 1 mL anhydrous DMSO and stirred for 1.5 h. To the mixture, a 2.2 mL solution of G3NH₂ (22.8 mg, 3.3 μ mol) and p-toluenesulfonic acid monohydrate (p-TSA) (5.6 mg, 29.7 μ mol) in anhydrous DMSO were added. The reaction was stirred for 48 h in darkness. The product was dialyzed against PBS (0.1 M pH 7.4) for 48 h, followed by DI H₂O for 24 h. The precipitate was removed by 0.45 μ m nylon syringe filter (VWR Internationals) and then lyophilized for 48 h. **MALDI-TOF** (m/z): 9133.32. **¹H NMR** (DMSO-d₆, ppm) δ : 8.053-7.689 (m, 57.61H, $-NHCO-$ in G3NH₂ and Ar-H (H-2, 3) in DOX), 7.429 (s, 2.95H, Ar-H (H-1) in DOX), 6.397 (s, 3.10H, $-CH=C-$ (H-16) in aconityl linker), 5.252 (s, 3.12H, $-CH-$ (H-9) in DOX), 4.896 (d, 3.19H, $-CH-$ (H-5) in DOX), 4.560 (m, 5.82H, $-CH_2OH$ (H-6) in DOX), 4.175 (s, 2.85H, $-CH-$ (H-13) in DOX), 3.938 (s, 9.88H, $-OCH_3$ (H-15) in DOX), 3.054 (m, 128.66H, $-CH_2-$ in G3NH₂), 2.620 (m, 119.14H, $-CH_2-$ in G3NH₂), 2.380 (m, 52.09H, $-CH_2-$ in G3NH₂), 2.181 (m, 120H, $-CH_2-$ in G3NH₂), 1.647 (d, 5.66H, $-CH_2-$ (H-10) in DOX), 1.126 (s, 9.69H, $-CH_3$ (H-14) in DOX).

S2.3.2. Synthesis of acid non-labile G3NH₂-nDOXNL conjugates (n=3)

The synthesis and purification of G3NH₂-3DOXNL was similar as to that for G3NH₂-3DOX. **MALDI-TOF** (m/z): 8914.62. **¹H NMR** (DMSO-d₆, ppm) δ : 8.119-7.653 (m, 60.34H, $-NHCO-$ in G3NH₂ and Ar-H (H-2, 3) in DOX), 7.437 (s, 2.91H, Ar-H (H-1) in DOX), 5.249 (s, 3.38H, $-CH-$ (H-9) in DOX), 4.902 (d, 3.10H, $-CH-$ (H-5) in DOX), 4.560 (m, 6.38H, $-CH_2OH$

(H-6) in DOX), 4.173 (s, 3.12H, -CH- (H-13) in DOX), 3.968 (s, 10.63H, -OCH_3 (H-15) in DOX), 3.078 (m, 114.72H, $\text{-CH}_2\text{-}$ in G3NH₂), 2.673 (m, 101.63H, $\text{-CH}_2\text{-}$ in succinic linker (H-17, 18) and $\text{-CH}_2\text{-}$ in G3NH₂), 2.430 (m, 57.37H, $\text{-CH}_2\text{-}$ in G3NH₂), 2.183 (m, 120H, $\text{-CH}_2\text{-}$ in G3NH₂), 1.653 (d, 6.16H, $\text{-CH}_2\text{-}$ (H-10) in DOX), 1.123 (s, 10.14H, -CH_3 in DOX).

S2.3.3. Synthesis of acid-labile G3NH₂-mPEG-3DOX and acid non-labile G3NH₂-mPEG-3DOXNL conjugates (m=9 or 21)

The G3NH₂-mPEG-3DOX and G3NH₂-mPEG-3DOXNL conjugates were synthesized in the same way. G3NH₂-21PEG-3DOX: a 0.3 mL anhydrous p-dioxane of PEG1K-SE (35.5 mg, 33.0 μmol) was added to G3NH₂-3DOX (5.2 mg, 0.58 μmol) which was in 2.0 mL PBS (0.1 M, pH 8.6). The reaction was stirred at 4 °C for 1 h and at room temperature for another 5 h. **MALDI-TOF** (m/z): 31219.72. **¹H NMR** (DMSO-d₆, ppm) δ : 8.053-7.689 (m, 57.61H, -NHCO- in G3NH₂ and Ar-H (H-2, 3) in DOX), 7.429 (s, 3.19H, Ar-H (H-1) in DOX), 6.393 (s, 2.93H, -CH=C- (H-16) in aconityl linker), 5.252 (s, 3.32H, -CH- (H-9) in DOX), 4.896 (d, 3.07H, -CH- (H-5) in DOX), 4.560 (m, 6.27H, $\text{-CH}_2\text{OH}$ (H-6) in DOX), 3.996 (m, 52.82H, $\text{-OCCH}_2\text{O-}$ in PEG and -OCH_3 (H-15) in DOX), 3.431 (m, 1587.3H, $\text{-OCH}_2\text{CH}_2\text{-}$ in PEG and -CH- (H-12) in DOX), 3.215 (s, 64.49H, -OCH_3 in PEG), 3.054 (m, 128.66H, $\text{-CH}_2\text{-}$ (H-4) in DOX and $\text{-CH}_2\text{-}$ in G3NH₂), 2.667 (m, 119.14H, $\text{-CH}_2\text{-}$ in G3NH₂), 2.410 (m, 52.09H, $\text{-CH}_2\text{-}$ in G3NH₂), 2.181 (m, 120H, $\text{-CH}_2\text{-}$ in G3NH₂), 1.659 (d, 4.95H, $\text{-CH}_2\text{-}$ (H-10) in DOX), 1.123 (s, 9.33H, -CH_3 (H-14) in DOX).

Two-step PEGylation

S2.3.4. PEGylation of G3NH₂ (G3NH₂-xPEG) (x = 7)

A 0.5 mL anhydrous p-dioxane of PEG1K-SE (65.7 mg, 56.7 μmol) was added dropwise to a 5 mL PBS (0.1 M, pH 8.6) of G3NH₂ (48.8 mg, 7.1 μmol). The reaction was stirred at 4 °C for 1 h and then at room temperature for another 5 h. The product was purified by dialysis against

DI H₂O for 48 h, and then lyophilized for 48 h. **MALDI-TOF** (m/z): 13979.13. **¹H NMR** (DMSO-d₆, ppm) δ: 8.047-7.769 (m, 52.86H, -NHCO- in G3NH₂), 4.025 (m, 14.29H, -OCCH₂O- in PEG), 3.461 (m, 714.9H, -OCH₂CH₂- in PEG), 3.215 (s, 21.09H, -OCH₃ in PEG), 3.057 (m, 112.43H, -CH₂- in G3NH₂), 2.676 (m, 100.17H, -CH₂- in G3NH₂), 2.419 (m, 47.23H, -CH₂- in G3NH₂), 2.181 (m, 120H, -CH₂- in G3NH₂).

S2.3.5. Synthesis of G3NH₂-xPEG-nDOX (x = 7, n = 7)

Cis-aconityl DOX (17.9 mg, 22.0 μmol), EDC (5.1 mg, 26.4 μmol) and NHS (3.1 mg, 26.4 μmol) were reacted in 1.0 mL anhydrous DMSO at room temperature for 1.5 h. To the cis-aconityl DOX solution was added a 5 mL solution of G3NH₂-7PEG (20.5 mg, 1.7 μmol) in anhydrous DMSO. The reaction was stirred for 48 h at room temperature. The product was dialyzed against DI H₂O for 48 h and then lyophilized for 48 h. **MALDI-TOF** (m/z): 18705.66.

S2.3.6. Synthesis of G3NH₂-mPEG-nDOX (m = 21, n = 7)

A 0.6 mL anhydrous p-dioxane solution of PEG1K-SE (57.4 mg, 49.6 μmol) was added dropwise to a 7.0 mL PBS (pH 8.6, 0.1 M) of G3NH₂-7PEG-7DOX (22.6 mg, 1.2 μmol). The reaction was stirred at 4 °C for 1 h and room temperature for another 5 h. The product was purified by dialysis against DI H₂O for 48 h and then lyophilized for 48 h. **MALDI-TOF** (m/z): 33844.20. **¹H NMR** (DMSO-d₆, ppm) δ: 8.130-7.811 (m, 67.26H, -NHCO- in G3NH₂ and Ar-H (H-2, 3) in DOX), 7.421 (s, 7.07H, Ar-H (H-1) in DOX), 6.399 (s, 6.4H, -CH=C- (H-16) in aconityl linker), 5.284 (m, 6.99H, -CH- (H-9) in DOX), 4.896 (d, 6.19H, -CH- (H-5) in DOX), 4.547 (m, 15.82H, -CH₂OH (H-6) in DOX), 4.033 (m, 68.92H, -OCCH₂O- in PEG and -OCH₃ (H-15) in DOX), 3.453 (m, 1928.8H, -OCH₂CH₂- in PEG and -CH- (H-12) in DOX), 3.214 (s, 65.37H, -OCH₃ in PEG), 3.068 (m, 135.78H, -CH₂- (H-4) in DOX and -CH₂- in G3NH₂), 2.658 (m, 76.09H, -CH₂- in

G3NH₂), 2.424 (m, 59.28H, -CH₂- in G3NH₂), 2.182 (m, 120H, -CH₂- in G3NH₂), 1.659 (d, 11.96H, -CH₂- (H-10) in DOX), 1.118 (m, 21.26H, -CH₃ (H-14) in DOX).

Table S1. IC₅₀ (μM) of free DOX and acid-labile G3NH₂-mPEG-nDOX conjugates calculated from Figure 3 (c) and (d). The cell viability profiles were fitted with a non-linear regression Log(Inhibitor) vs Response (variable slope).

Conjugates	72 h	144 h
DOX	0.52	0.45
G3NH ₂ -3DOX	21.80	1.41
G3NH ₂ -9PEG-3DOX	29.94	1.73
G3NH ₂ -21PEG-3DOX	48.53	2.38
G3NH ₂ -21PEG-7DOX	56.95	2.91

Table S2. Aerosol mass deposition (μg) of the pMDI formulation containing G3NH₂-mPEG-nDOX on stages of Andersen Cascade Impactor (ACI). The results was represented with mean \pm s.d. (n=3). AC, IP, 0-7, and F denote actuator, induction port, stage 0-7 and filter, respectively.

Stage	G3NH ₂ -3DOX	G3NH ₂ -9PEG-3DOX	G3NH ₂ -21PEG-3DOX	G3NH ₂ -21PEG-7DOX
AC	65.7 \pm 22.3	92.1 \pm 26.9	155.1 \pm 17.4	163.3 \pm 25.6
IP	389.1 \pm 45.6	909.9 \pm 58.0	368.4 \pm 28.7	185.6 \pm 7.9
0	61.6 \pm 29.2	26.8 \pm 9.9	31.9 \pm 9.0	11.3 \pm 6.6
1	23.6 \pm 14.7	26.2 \pm 17.4	27.1 \pm 9.0	20.6 \pm 1.2
2	19.3 \pm 8.2	26.4 \pm 4.6	19.6 \pm 18.1	34.3 \pm 5.2
3	16.5 \pm 6.5	20.4 \pm 13.5	18.1 \pm 25.1	10.3 \pm 10.8
4	14.9 \pm 14.7	76.6 \pm 37.5	129.3 \pm 7.6	76.3 \pm 6.9
5	16.7 \pm 8.2	120.0 \pm 25.1	939.8 \pm 115.3	494.8 \pm 57.5
6	16.3 \pm 13.2	96.3 \pm 12.9	689.8 \pm 91.9	317.4 \pm 28.8
7	19.5 \pm 14.0	84.8 \pm 10.6	508.2 \pm 39.9	100.3 \pm 12.1
F	24.1 \pm 22.9	41.1 \pm 4.8	201.3 \pm 72.4	13.7 \pm 8.2

APPENDIX C

SUPPLEMENTAL INFORMATION OF CHAPTER 5

S1. Characterization

S1.1 Mass-assisted laser desorption/ionization-time of flight mass spectrometry (MALDI-TOF)

MALDI-TOF mass spectra were performed on a Bruker UltrafleXtreme mass spectrometer equipped with a pulsed nitrogen laser (337 nm) under positive ion reflector mode. The conjugates were dissolved in deionized water at a concentration of 1.0 mg/mL. 2, 5-DHB in methanol (10 mg/mL) was used as matrix. 10 μ L of conjugate solution was mixed with equal volume of 2, 5-DHB solution and 2 μ L of the mixed solution was spotted on a Bruker Daltonics MALDI plate. The spotted sample was dried gently by air flow.

S1.2 Proton magnetic nuclear resonance (^1H NMR)

^1H NMR spectra were recorded on a Mercury 400 (400 MHz) spectrometer using deuterated DMSO (DMSO- d_6). Proton chemical shifts were reported in ppm (δ) and DMSO- d_6 at 2.48 ppm was set as reference peak.

S1.3 Light scattering (LS)

Sample (1.0 mg/mL) was dissolved in phosphate buffer saline (PBS, pH 7.4). pH test indicated all sample solutions were neutral. Hydrodynamic diameters and zeta potentials were measured using Zetasizer Nano ZS. The average and standard deviation for hydrodynamic diameters and zeta potentials were calculated based on at least three measurements.

APPENDIX D

PUBLICATION 1

Hindawi Publishing Corporation
Journal of Drug Delivery
Volume 2015, Article ID 535683, 10 pages
<http://dx.doi.org/10.1155/2015/535683>



Research Article

High-Resolution Imaging of Polyethylene Glycol Coated Dendrimers via Combined Atomic Force and Scanning Tunneling Microscopy

Shawn Riechers,¹ Qian Zhong,² Nai-Ning Yin,¹ Arpad Karsai,¹
Sandro R. P. da Rocha,² and Gang-yu Liu¹

¹Department of Chemistry, University of California, Davis, CA 95616, USA

²Department of Chemical Engineering & Materials Science, Wayne State University, Detroit, MI 48202, USA

Correspondence should be addressed to Gang-yu Liu; gylu@ucdavis.edu

Received 10 September 2014; Accepted 11 December 2014

Academic Editor: Kang Choon Lee

Copyright © 2015 Shawn Riechers et al. This is an open access article distributed under the Creative Commons Attribution License, which permits unrestricted use, distribution, and reproduction in any medium, provided the original work is properly cited.

Dendrimers have shown great promise as drug delivery vehicles in recent years because they can be synthesized with designed size and functionalities for optimal transportation, targeting, and biocompatibility. One of the most well-known termini used for biocompatibility is polyethylene glycol (PEG), whose performance is affected by its actual conformation. However, the conformation of individual PEG bound to soft materials such as dendrimers has not been directly observed. Using atomic force microscopy (AFM) and scanning tunneling microscopy (STM), this work characterizes the structure adopted by PEGylated dendrimers with the highest resolution reported to date. AFM imaging enables visualization of the individual dendrimers, as well as the differentiation and characterization of the dendrimer core and PEG shell. STM provides direct imaging of the PEG extensions with high-resolution. Collectively, this investigation provides important insight into the structure of coated dendrimers, which is crucial for the design and development of better drug delivery vehicles.

1. Introduction

Dendrimers provide an alternative and potent means for drug delivery due to their nanometer size and the ability to incorporate various functionalities on their interior and exterior. Modern chemical synthesis capabilities allow various functionalities to be incorporated on the dendrimer exterior in order to optimize performance in terms of drug binding, transport, targeting, delivery, and biocompatibility [1–3]. Polyamidoamine (PAMAM) dendrimers, for example, have been tailored for enhanced drug solubility, retention time, targeting, and efficacy [1–3]. In addition to optimizing delivery, another issue is the reduction or elimination of cytotoxicity, which has been addressed by masking the terminal functional groups and charge [4]. This can be accomplished by adding biologically compatible terminal groups such as carboxylate, hydroxyl, acetamide, lipid, or

polyethylene glycol (PEG) [2]. Among these, PEG is the most widely used due to its minimal or nontoxicity, nonimmunogenicity, and nonantigenicity and has been approved by the FDA in oral intravenous and pulmonary pharmaceutical formulations [5–8]. It is known that PEG chains adopt a variety of conformations, lengths, and packing density and that these structural presentations directly affect biocompatibility [9–11]. In some cases, PEG alters dendrimer's drug loading capacity, retention time, and thus their delivery performance [8, 12, 13]. Therefore, the characterization of PEG coating prior to animal testing is of great importance. While computational studies have been carried out to probe PEG conformation on dendrimers surfaces, experimental studies are lacking due to the difficulties in obtaining high-resolution structural characterization of PEG when bound to soft materials, such as dendrimers [11, 14]. Our prior work shows that high-resolution structural characterization

APPENDIX E

PUBLICATION 2

Effect of the Conjugation Density of Triphenylphosphonium Cation on the Mitochondrial Targeting of Poly(amidoamine) Dendrimers

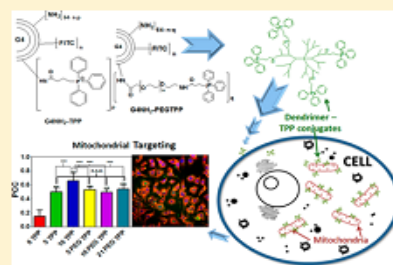
Elizabeth R. Bielski, Qian Zhong, Matthew Brown, and Sandro R. P. da Rocha*

Department of Chemical Engineering and Materials Science, Wayne State University, Detroit, Michigan 48202, United States

Supporting Information

ABSTRACT: Many clinically relevant diseases with known poor therapeutic outcomes, including cancer and neurodegenerative disorders, have been directly linked to mitochondrial dysfunction. The ability to efficiently target therapeutics to intracellular organelles such as mitochondria may represent new opportunities for the effective treatment of such ailments. The present study reports the synthesis, cellular uptake, cytotoxicity, and mitochondrial colocalization of conjugates of triphenylphosphonium cation (TPP) to amine-terminated, generation 4, poly(amidoamine) (PAMAM) dendrimer (G4NH₂) nanocarriers. The mitochondrial-targeting moiety TPP was either directly conjugated to G4NH₂ (G4NH₂-TPP) or to the dendrimer through a flexible polyethylene glycol (PEG) linker (G4NH₂-PEGTPP). Conjugation was done at various TPP densities to assess their biological activity and potential for mitochondrial-targeted drug delivery. Tests in an *in vitro* model of the human alveolar carcinoma (A549 cells) showed that even at a low TPP density (~5 TPP) both the cellular internalization and mitochondrial targeting increase significantly, as determined by fluorescence activated cell sorting (FACS) and confocal microscopy (CM), respectively. At a density of ~10 TPP per G4NH₂, further increase in cellular internalization and mitochondrial targeting was achieved. However, at this higher density, the nanocarriers also showed pronounced cytotoxicity. It was observed that the toxicity of the conjugates is decreased upon the addition of a PEG linker between the dendrimer and TPP (G4NH₂-PEGTPP), while the mitochondrial targeting ability of the nanocarriers is not affected as the PEG density increases. The proposed strategies indicate that TPP-conjugated G4NH₂ dendrimers represent a potentially viable strategy for the targeting of therapeutic molecules to mitochondria, which may help improve therapeutic outcomes of diseases related to mitochondrial dysfunction.

KEYWORDS: mitochondrial targeting, PAMAM dendrimers, polyethylene glycol, PEG, triphenylphosphonium cation, TPP, drug delivery



1. INTRODUCTION

Mitochondria are responsible for maintaining cellular homeostasis and producing cellular energy (adenosine triphosphate, ATP) via oxidative phosphorylation.^{1,2} They are also key players in the production of reactive oxygen species as well as regulating calcium homeostasis and the intrinsic apoptotic pathway.^{1,3,4} Mitochondria are organelles of great relevance in a variety of important highly energy-dependent tissues, including brain, heart, and muscle.^{1,5} As a consequence, mitochondrial dysfunction has been linked to a range of diseases in these tissues (and others) including neurodegenerative and neuromuscular disorders, cancer, ischemia-reperfusion injury, metabolic diseases such as diabetes and obesity, chronic autoimmune inflammatory diseases, kidney and liver diseases, and aging.^{1,3,6–10} In spite of the clinical relevance of these mitochondrial-related diseases many still lack effective therapeutic options.^{1,11} The ability to design mitochondrial-targeting systems may therefore provide valuable alternative strategies to enhance therapeutic outcomes of mitochondrial-

related diseases while at the same time minimizing side effects associated with the therapeutic molecules.¹²

One major class of mitochondrial-targeting molecules is delocalized lipophilic cations (DLCs). Triphenylphosphonium cation (TPP),^{1,3} one of the most common DLCs, has been shown to accumulate preferentially at the inner mitochondrial membrane,³ at concentrations approximately 5–10-fold greater in the cytoplasm compared to the extracellular environment, with a further accumulation of hundreds of times within the mitochondria when compared to the cytoplasm.⁵ The colocalization efficiency of TPP with the mitochondria is related to its lipophilic nature and delocalized positive charge, which allows TPP to permeate through membrane bilayers (hydrophobic) that have large negative potentials such as that of the mitochondria: 150–180 mV.^{13,14} The unique properties

Received: April 23, 2015

Revised: June 19, 2015

Accepted: July 9, 2015

Published: July 9, 2015

REFERENCES

- [1] R. Siegel, D. Naishadham, A. Jemal, Cancer statistics, 2012, CA: a cancer journal for clinicians, 62 (2012) 10-29.
- [2] R. Siegel, D. Naishadham, A. Jemal, Cancer statistics, 2013, CA: a cancer journal for clinicians, 63 (2013) 11-30.
- [3] W.D. Travis, Pathology & Genetics: Tumours of the Lung, Pleura, Thymus, and Heart, Iarc, 2004.
- [4] S.A. Kenfield, E.K. Wei, M.J. Stampfer, B.A. Rosner, G.A. Colditz, Comparison of aspects of smoking among the four histological types of lung cancer, Tobacco control, 17 (2008) 198-204.
- [5] A.C. Society, Breast cancer facts & figures 2007-2008, in, American Cancer Society Atlanta, 2007.
- [6] G.A. Otterson, M.A. Villalona-Calero, S. Sharma, M.G. Kris, A. Imondi, M. Gerber, D.A. White, M.J. Ratain, J.H. Schiller, A. Sandler, Phase I study of inhaled Doxorubicin for patients with metastatic tumors to the lungs, Clinical cancer research, 13 (2007) 1246-1252.
- [7] S. Sharma, D. White, A.R. Imondi, M.E. Placke, D.M. Vail, M.G. Kris, Development of inhalational agents for oncologic use, Journal of Clinical Oncology, 19 (2001) 1839-1847.
- [8] C. Cheng, A. Haouala, T. Krueger, F. Mithieux, J.Y. Perentes, S. Peters, L.A. Decosterd, H.-B. Ris, Drug uptake in a rodent sarcoma model after intravenous injection or isolated lung perfusion of free/liposomal doxorubicin, Interactive cardiovascular and thoracic surgery, 8 (2009) 635-638.
- [9] H.J. Broxterman, C.H. Versantvoort, S.C. Linn, Multidrug resistance in lung cancer, in: Lung Cancer, Springer, 1995, pp. 193-222.

- [10] L.C. Kennedy, L.R. Bickford, N.A. Lewinski, A.J. Coughlin, Y. Hu, E.S. Day, J.L. West, R.A. Drezek, A New Era for Cancer Treatment: Gold-Nanoparticle-Mediated Thermal Therapies, *Small*, 7 (2011) 169-183.
- [11] E.C. Dreaden, S.C. Mwakwari, Q.H. Sodji, A.K. Oyelere, M.A. El-Sayed, Tamoxifen– Poly (ethylene glycol)– Thiol Gold Nanoparticle Conjugates: Enhanced Potency and Selective Delivery for Breast Cancer Treatment, *Bioconjugate chemistry*, 20 (2009) 2247-2253.
- [12] S. Taetz, N. Nafee, J. Beisner, K. Piotrowska, C. Baldes, T. Mürdter, H. Huwer, M. Schneider, U. Schaefer, U. Klotz, The influence of chitosan content in cationic chitosan/PLGA nanoparticles on the delivery efficiency of antisense 2'-O-methyl-RNA directed against telomerase in lung cancer cells, *European journal of pharmaceutics and biopharmaceutics*, 72 (2009) 358-369.
- [13] L. Brannon-Peppas, J.O. Blanchette, Nanoparticle and targeted systems for cancer therapy, *Advanced drug delivery reviews*, (2012).
- [14] A. Papagiannaros, K. Dimas, G.T. Papaioannou, C. Demetzos, Doxorubicin–PAMAM dendrimer complex attached to liposomes: cytotoxic studies against human cancer cell lines, *International journal of pharmaceutics*, 302 (2005) 29-38.
- [15] W. Sun, N. Fang, B.G. Trewyn, M. Tsunoda, I.I. Slowing, V.S. Lin, E.S. Yeung, Endocytosis of a single mesoporous silica nanoparticle into a human lung cancer cell observed by differential interference contrast microscopy, *Analytical and bioanalytical chemistry*, 391 (2008) 2119-2125.
- [16] W. Lin, Y.-w. Huang, X.-D. Zhou, Y. Ma, In vitro toxicity of silica nanoparticles in human lung cancer cells, *Toxicology and applied pharmacology*, 217 (2006) 252-259.
- [17] I. Ahmad, M. Longenecker, J. Samuel, T.M. Allen, Antibody-targeted delivery of doxorubicin entrapped in sterically stabilized liposomes can eradicate lung cancer in mice, *Cancer research*, 53 (1993) 1484-1488.

- [18] S. Santra, C. Kaittanis, J. Grimm, J.M. Perez, Drug/Dye-Loaded, Multifunctional Iron Oxide Nanoparticles for Combined Targeted Cancer Therapy and Dual Optical/Magnetic Resonance Imaging, *Small*, 5 (2009) 1862-1868.
- [19] I.J. Lerner, B. Kennedy, The prevalence of questionable methods of cancer treatment in the United States, *CA: a cancer journal for clinicians*, 42 (1992) 181-191.
- [20] A. Coates, S. Abraham, S.B. Kaye, T. Sowerbutts, C. Frewin, R. Fox, M. Tattersall, On the receiving end—patient perception of the side-effects of cancer chemotherapy, *European Journal of Cancer and Clinical Oncology*, 19 (1983) 203-208.
- [21] K. Hagane, T. Akera, J. Berlin, Doxorubicin: mechanism of cardiodepressant actions in guinea pigs, *Journal of Pharmacology and Experimental Therapeutics*, 246 (1988) 655-661.
- [22] K. Chatterjee, J. Zhang, N. Honbo, J.S. Karliner, Doxorubicin Cardiomyopathy, *Cardiology*, 115 (2010) 155-162.
- [23] J. Kopeček, P. Kopečková, T. Minko, Z.-R. Lu, HEMA copolymer–anticancer drug conjugates: design, activity, and mechanism of action, *European journal of pharmaceutics and biopharmaceutics*, 50 (2000) 61-81.
- [24] R. Duncan, Polymer conjugates as anticancer nanomedicines, *Nature Reviews Cancer*, 6 (2006) 688-701.
- [25] M. Yokoyama, T. Okano, Y. Sakurai, H. Ekimoto, C. Shibasaki, K. Kataoka, Toxicity and antitumor activity against solid tumors of micelle-forming polymeric anticancer drug and its extremely long circulation in blood, *Cancer research*, 51 (1991) 3229-3236.
- [26] S. Acharya, S.K. Sahoo, PLGA nanoparticles containing various anticancer agents and tumour delivery by EPR effect, *Advanced drug delivery reviews*, 63 (2011) 170-183.

- [27] Y. Cheng, J. Wang, T. Rao, X. He, T. Xu, Pharmaceutical applications of dendrimers: promising nanocarriers for drug delivery, *Frontiers in bioscience: a journal and virtual library*, 13 (2007) 1447-1471.
- [28] B. Twaites, C. de las Heras Alarcón, C. Alexander, Synthetic polymers as drugs and therapeutics, *Journal of Materials Chemistry*, 15 (2005) 441-455.
- [29] J.-O. Henck, S.R. Byrn, Designing a molecular delivery system within a preclinical timeframe, *Drug discovery today*, 12 (2007) 189-199.
- [30] Y. Cheng, T. Xu, The effect of dendrimers on the pharmacodynamic and pharmacokinetic behaviors of non-covalently or covalently attached drugs, *European journal of medicinal chemistry*, 43 (2008) 2291-2297.
- [31] D.A. Tomalia, A.M. Naylor, W.A. Goddard, Starburst dendrimers: molecular-level control of size, shape, surface chemistry, topology, and flexibility from atoms to macroscopic matter, *Angewandte Chemie International Edition in English*, 29 (1990) 138-175.
- [32] D.A. Tomalia, H. Baker, J. Dewald, M. Hall, G. Kallos, S. Martin, J. Roeck, J. Ryder, P. Smith, Dendritic macromolecules: synthesis of starburst dendrimers, *Macromolecules*, 19 (1986) 2466-2468.
- [33] I.J. Majoros, A. Myc, T. Thomas, C.B. Mehta, J.R. Baker, PAMAM dendrimer-based multifunctional conjugate for cancer therapy: synthesis, characterization, and functionality, *Biomacromolecules*, 7 (2006) 572-579.
- [34] S. Zhu, M. Hong, G. Tang, L. Qian, J. Lin, Y. Jiang, Y. Pei, Partly PEGylated polyamidoamine dendrimer for tumor-selective targeting of doxorubicin: the effects of PEGylation degree and drug conjugation style, *Biomaterials*, 31 (2010) 1360-1371.

- [35] N.K. Kunda, S. Somavarapu, S.B. Gordon, G.A. Hutcheon, I.Y. Saleem, Nanocarriers targeting dendritic cells for pulmonary vaccine delivery, *Pharmaceutical research*, 30 (2013) 325-341.
- [36] L. Gram, J. Christiansen, First-pass metabolism of imipramine in man, *Clinical pharmacology and therapeutics*, 17 (1975) 555.
- [37] B. Vogelgesang, H. Echizen, E. Schmidt, M. Eichelbaum, Stereoselective first-pass metabolism of highly cleared drugs: studies of the bioavailability of L-and D-verapamil examined with a stable isotope technique, *British journal of clinical pharmacology*, 58 (2004) S796-S803.
- [38] M.F. Paine, D.D. Shen, K.L. Kunze, J.D. Perkins, C.L. Marsh, J.P. McVicar, D.M. Barr, B.S. Gillies, K.E. Thummel, First-pass metabolism of midazolam by the human intestine, *Clinical Pharmacology & Therapeutics*, 60 (1996) 14-24.
- [39] H.S. Choi, Y. Ashitate, J.H. Lee, S.H. Kim, A. Matsui, N. Insin, M.G. Bawendi, M. Semmler-Behnke, J.V. Frangioni, A. Tsuda, Rapid translocation of nanoparticles from the lung airspaces to the body, *Nature biotechnology*, 28 (2010) 1300-1303.
- [40] M. Semmler-Behnke, S. Takenaka, S. Fertsch, A. Wenk, J. Seitz, P. Mayer, G. Oberdörster, W.G. Kreyling, Efficient elimination of inhaled nanoparticles from the alveolar region: evidence for interstitial uptake and subsequent reentrainment onto airways epithelium, *Environmental health perspectives*, 115 (2007) 728.
- [41] K.M. Kitchens, R.B. Kolhatkar, P.W. Swaan, N.D. Eddington, H. Ghandehari, Transport of poly (amidoamine) dendrimers across Caco-2 cell monolayers: influence of size, charge and fluorescent labeling, *Pharmaceutical research*, 23 (2006) 2818-2826.

- [42] M. El-Sayed, M. Ginski, C. Rhodes, H. Ghandehari, Transepithelial transport of poly (amidoamine) dendrimers across Caco-2 cell monolayers, *Journal of controlled release*, 81 (2002) 355-365.
- [43] D. Lu, A.J. Hickey, Pulmonary vaccine delivery, *Expert review of vaccines*, 6 (2007) 213-226.
- [44] R. Chojniak, L. Yu, R. Younes, Response to chemotherapy in patients with lung metastases: how many nodules should be measured?, *Cancer Imaging*, 6 (2006) 107.
- [45] G. Pilkington, A. Boland, T. Brown, J. Oyee, A. Bagust, R. Dickson, A systematic review of the clinical effectiveness of first-line chemotherapy for adult patients with locally advanced or metastatic non-small cell lung cancer, *Thorax*, (2015) thoraxjnl-2014-205914.
- [46] W.-H. Lee, C.-Y. Loo, H.-X. Ong, D. Traini, P.M. Young, R. Rohanizadeh, Synthesis and Characterization of Inhalable Flavonoid Nanoparticle for Lung Cancer Cell Targeting, (2015).
- [47] X. Wang, S. Li, Y. Shi, X. Chuan, J. Li, T. Zhong, H. Zhang, W. Dai, B. He, Q. Zhang, The development of site-specific drug delivery nanocarriers based on receptor mediation, *Journal of Controlled Release*, 193 (2014) 139-153.
- [48] J. Gautier, E. Allard-Vannier, E. Munnier, M. Soucé, I. Chourpa, Recent advances in theranostic nanocarriers of doxorubicin based on iron oxide and gold nanoparticles, *Journal of Controlled Release*, 169 (2013) 48-61.
- [49] A. Albanese, P.S. Tang, W.C. Chan, The effect of nanoparticle size, shape, and surface chemistry on biological systems, *Annual review of biomedical engineering*, 14 (2012) 1-16.
- [50] S. Bosselmann, R.O. Williams III, Has nanotechnology led to improved therapeutic outcomes?, *Drug development and industrial pharmacy*, 38 (2012) 158-170.

- [51] M. Semmler-Behnke, W.G. Kreyling, J. Lipka, S. Fertsch, A. Wenk, S. Takenaka, G. Schmid, W. Brandau, Biodistribution of 1.4- and 18-nm Gold Particles in Rats, *Small*, 4 (2008) 2108-2111.
- [52] G.M. Ryan, L.M. Kaminskas, B.D. Kelly, D.J. Owen, M.P. McIntosh, C.J. Porter, Pulmonary administration of PEGylated polylysine dendrimers: Absorption from the lung versus retention within the lung is highly size dependent, *Molecular Pharmaceutics*, (2013).
- [53] O.M. Merkel, A. Beyerle, D. Librizzi, A. Pfestroff, T.M. Behr, B. Sproat, P.J. Barth, T. Kissel, Nonviral siRNA delivery to the lung: Investigation of PEG- PEI polyplexes and their in vivo performance, *Molecular pharmaceutics*, 6 (2009) 1246-1260.
- [54] O.M. Merkel, T. Kissel, Nonviral pulmonary delivery of siRNA, *Accounts of chemical research*, 45 (2011) 961-970.
- [55] A.K. Mohammad, L.K. Amayreh, J.M. Mazzara, J.J. Reineke, Rapid lymph accumulation of polystyrene nanoparticles following pulmonary administration, *Pharmaceutical research*, 30 (2013) 424-434.
- [56] M. Koukourakis, S. Koukouraki, A. Giatromanolaki, S. Archimandritis, J. Skarlatos, K. Beroukas, J. Bizakis, G. Retalis, N. Karkavitsas, E. Helidonis, Liposomal doxorubicin and conventionally fractionated radiotherapy in the treatment of locally advanced non-small-cell lung cancer and head and neck cancer, *Journal of clinical oncology*, 17 (1999) 3512-3521.
- [57] G.A. Otterson, M.A. Villalona-Calero, W. Hicks, X. Pan, J.A. Ellerton, S.N. Gettinger, J.R. Murren, Phase I/II Study of inhaled doxorubicin combined with platinum-based therapy for advanced non-small cell lung cancer, *Clinical Cancer Research*, 16 (2010) 2466-2473.
- [58] L. Wu, S.R. da Rocha, Biocompatible and biodegradable copolymer stabilizers for hydrofluoroalkane dispersions: a colloidal probe microscopy investigation, *Langmuir*, 23 (2007) 12104-12110.

- [59] V. Pinzani, F. Bressolle, I.J. Haug, M. Galtier, J.P. Blayac, P. Balmès, Cisplatin-induced renal toxicity and toxicity-modulating strategies: a review, *Cancer chemotherapy and pharmacology*, 35 (1994) 1-9.
- [60] S.M. Swain, F.S. Whaley, M.S. Ewer, Congestive heart failure in patients treated with doxorubicin, *Cancer*, 97 (2003) 2869-2879.
- [61] J.A. Endicott, V. Ling, The biochemistry of P-glycoprotein-mediated multidrug resistance, *Annual review of biochemistry*, 58 (1989) 137-171.
- [62] F. Gagnadoux, J. Hureauux, L. Vecellio, T. Urban, A. Le Pape, I. Valo, J. Montharu, V. Leblond, M. Boisdron-Celle, S. Lerondel, Aerosolized chemotherapy, *Journal of aerosol medicine and pulmonary drug delivery*, 21 (2008) 61-70.
- [63] T. Tatsumura, S. Koyama, M. Tsujimoto, M. Kitagawa, S. Kagamimori, Further study of nebulisation chemotherapy, a new chemotherapeutic method in the treatment of lung carcinomas: fundamental and clinical, *British journal of cancer*, 68 (1993) 1146.
- [64] N.V. Koshkina, J.C. Waldrep, L.E. Roberts, E. Golunski, S. Melton, V. Knight, Paclitaxel liposome aerosol treatment induces inhibition of pulmonary metastases in murine renal carcinoma model, *Clinical cancer research*, 7 (2001) 3258-3262.
- [65] B.P. Wittgen, P.W. Kunst, K. van der Born, A.W. van Wijk, W. Perkins, F.G. Pilkiewicz, R. Perez-Soler, S. Nicholson, G.J. Peters, P.E. Postmus, Phase I study of aerosolized SLIT cisplatin in the treatment of patients with carcinoma of the lung, *Clinical cancer research*, 13 (2007) 2414-2421.
- [66] National Institutes of Health Clinical Center (CC). Inhaled Doxorubicin in Treating Patients With Advanced Solid Tumors Affecting the Lungs In: ClinicalTrials.gov [Internet]. Bethesda

(MD): National Library of Medicine (US). 2000- [2014 Nov 04]. Available from: <http://clinicaltrials.gov/ct2/show/NCT00020124> NLM Identifier: NCT00020124

[67] J.S. Patton, P.R. Byron, Inhaling medicines: delivering drugs to the body through the lungs, *Nature Reviews Drug Discovery*, 6 (2007) 67-74.

[68] J.C. Sung, B.L. Pulliam, D.A. Edwards, Nanoparticles for drug delivery to the lungs, *Trends in biotechnology*, 25 (2007) 563-570.

[69] M.M. Bailey, C.J. Berkland, Nanoparticle formulations in pulmonary drug delivery, *Medicinal research reviews*, 29 (2009) 196-212.

[70] R.A. Cone, Barrier properties of mucus, *Advanced drug delivery reviews*, 61 (2009) 75-85.

[71] I. Ahmad, T.M. Allen, Antibody-mediated specific binding and cytotoxicity of liposome-entrapped doxorubicin to lung cancer cells in vitro, *Cancer research*, 52 (1992) 4817-4820.

[72] S.K. Lai, Y.-Y. Wang, J. Hanes, Mucus-penetrating nanoparticles for drug and gene delivery to mucosal tissues, *Advanced drug delivery reviews*, 61 (2009) 158-171.

[73] B. Amsden, Solute diffusion within hydrogels. Mechanisms and models, *Macromolecules*, 31 (1998) 8382-8395.

[74] B. Amsden, An obstruction-scaling model for diffusion in homogeneous hydrogels, *Macromolecules*, 32 (1999) 874-879.

[75] S.S. Olmsted, J.L. Padgett, A.I. Yudin, K.J. Whaley, T.R. Moench, R.A. Cone, Diffusion of macromolecules and virus-like particles in human cervical mucus, *Biophysical journal*, 81 (2001) 1930-1937.

[76] M.S. Ali, J.P. Pearson, Upper airway mucin gene expression: a review, *The Laryngoscope*, 117 (2007) 932-938.

- [77] A. Voss, W.H. Finlay, Deagglomeration of dry powder pharmaceutical aerosols, *International journal of pharmaceutics*, 248 (2002) 39-50.
- [78] P.B. Myrdal, P. Sheth, S.W. Stein, Advances in metered dose inhaler technology: formulation development, *AAPS PharmSciTech*, 15 (2014) 434-455.
- [79] M.W. Nagel, K.J. Wiersema, S.L. Bates, J.P. Mitchell, Size analysis of a pressurized metered dose inhaler-delivered solution formulation by an Aerosizer®-LD time-of-flight aerosol particle size spectrometer, *Journal of aerosol medicine*, 15 (2002) 75-85.
- [80] L. Wu, M. Al-Haydari, S.R. da Rocha, Novel propellant-driven inhalation formulations: engineering polar drug particles with surface-trapped hydrofluoroalkane-philes, *European journal of pharmaceutical sciences*, 33 (2008) 146-158.
- [81] L. Wu, B. Bharatwaj, J. Panyam, S.R. da Rocha, Core-shell particles for the dispersion of small polar drugs and biomolecules in hydrofluoroalkane propellants, *Pharmaceutical research*, 25 (2008) 289-301.
- [82] D.S. Conti, D. Brewer, J. Grashik, S. Avasarala, S.R. da Rocha, Poly (amidoamine) Dendrimer Nanocarriers and their Aerosol Formulations for siRNA Delivery to the Lung Epithelium, *Molecular Pharmaceutics*, (2014).
- [83] R.N. Dalby, P.R. Byron, Comparison of output particle size distributions from pressurized aerosols formulated as solutions or suspensions, *Pharmaceutical research*, 5 (1988) 36-39.
- [84] S. Newman, P. Anderson, *Respiratory drug delivery: Essential theory and practice*, 2009.
- [85] S.P. Newman, Principles of metered-dose inhaler design, *Respiratory care*, 50 (2005) 1177-1190.
- [86] H.D. Smyth, The influence of formulation variables on the performance of alternative propellant-driven metered dose inhalers, *Advanced drug delivery reviews*, 55 (2003) 807-828.

- [87] W.-J. Pigram, W. Fuller, L. Hamilton, Stereochemistry of intercalation: interaction of daunomycin with DNA, *Nature*, 235 (1972) 17-19.
- [88] L. Kelland, The resurgence of platinum-based cancer chemotherapy, *Nature Reviews Cancer*, 7 (2007) 573-584.
- [89] National Cancer Institute, Cancer Drug Information: Doxorubicin Hydrochloride, in, 2007.
- [90] J. Pritchard, J. Brown, E. Shafford, G. Perilongo, P. Brock, C. Dicks-Mireaux, J. Keeling, A. Phillips, A. Vos, J. Plaschkes, Cisplatin, doxorubicin, and delayed surgery for childhood hepatoblastoma: a successful approach—results of the first prospective study of the International Society of Pediatric Oncology, *Journal of clinical oncology*, 18 (2000) 3819-3828.
- [91] J.A. Ortega, E.C. Douglass, J.H. Feusner, M. Reynolds, J.J. Quinn, M.J. Finegold, J.E. Haas, D.R. King, W. Liu-Mares, M.G. Sensel, Randomized comparison of cisplatin/vincristine/fluorouracil and cisplatin/continuous infusion doxorubicin for treatment of pediatric hepatoblastoma: a report from the Children's Cancer Group and the Pediatric Oncology Group, *Journal of clinical oncology*, 18 (2000) 2665-2675.
- [92] G. Minotti, P. Menna, E. Salvatorelli, G. Cairo, L. Gianni, Anthracyclines: molecular advances and pharmacologic developments in antitumor activity and cardiotoxicity, *Pharmacological reviews*, 56 (2004) 185-229.
- [93] Clinicaltrials.gov: Natnial Institutes of Health, Keywords "doxorubicin and cancer", in.
- [94] R.D. Olson, P.S. Mushlin, Doxorubicin cardiotoxicity: analysis of prevailing hypotheses, *The FASEB journal*, 4 (1990) 3076-3086.
- [95] C.F. Thorn, C. Oshiro, S. Marsh, T. Hernandez-Boussard, H. McLeod, T.E. Klein, R.B. Altman, Doxorubicin pathways: pharmacodynamics and adverse effects, *Pharmacogenetics and genomics*, 21 (2011) 440.

- [96] P. Mohan, N. Rapoport, Doxorubicin as a molecular nanotheranostic agent: effect of doxorubicin encapsulation in micelles or nanoemulsions on the ultrasound-mediated intracellular delivery and nuclear trafficking, *Molecular Pharmaceutics*, 7 (2010) 1959-1973.
- [97] C.A. Frederick, L.D. Williams, G. Ughetto, G.A. Van der Marel, J.H. Van Boom, A. Rich, A.H. Wang, Structural comparison of anticancer drug-DNA complexes: adriamycin and daunomycin, *Biochemistry*, 29 (1990) 2538-2549.
- [98] X.B. Xiong, Z.S. Ma, R. Lai, A. Lavasanifar, The therapeutic response to multifunctional polymeric nano-conjugates in the targeted cellular and subcellular delivery of doxorubicin, *Biomaterials*, 31 (2010) 757-768.
- [99] X.H. Zeng, R. Morgenstern, A.M. Nystrom, Nanoparticle-directed sub-cellular localization of doxorubicin and the sensitization breast cancer cells by circumventing GST-Mediated drug resistance, *Biomaterials*, 35 (2014) 1227-1239.
- [100] M. Han, Mitochondrial Delivery of Doxorubicin via Triphenylphosphine Modification for Overcoming Drug Resistance in MDA-MB-435/DOX Cells, *Molecular pharmaceutics*, (2014) 140519153522008.
- [101] G. Takemura, H. Fujiwara, Doxorubicin-induced cardiomyopathy: from the cardiotoxic mechanisms to management, *Progress in cardiovascular diseases*, 49 (2007) 330-352.
- [102] K.C. Nitiss, J.L. Nitiss, Twisting and ironing: Doxorubicin cardiotoxicity by mitochondrial DNA damage, *Clinical Cancer Research*, 20 (2014) 4737-4739.
- [103] A.V. Kuznetsov, R. Margreiter, A. Amberger, V. Saks, M. Grimm, Changes in mitochondrial redox state, membrane potential and calcium precede mitochondrial dysfunction in doxorubicin-induced cell death, *Biochim. Biophys. Acta-Mol. Cell Res.*, 1813 (2011) 1144-1152.

- [104] F.A. de Wolf, R.W. Staffhorst, H.P. Smits, M.F. Onwezen, B. de Kruijff, Role of anionic phospholipids in the interaction of doxorubicin and plasma membrane vesicles: drug binding and structural consequences in bacterial systems, *Biochemistry*, 32 (1993) 6688-6695.
- [105] S. Mitra, U. Gaur, P. Ghosh, A. Maitra, Tumour targeted delivery of encapsulated dextran–doxorubicin conjugate using chitosan nanoparticles as carrier, *Journal of controlled release*, 74 (2001) 317-323.
- [106] K.A. Janes, M.P. Fresneau, A. Marazuela, A. Fabra, M.a.J. Alonso, Chitosan nanoparticles as delivery systems for doxorubicin, *Journal of controlled release*, 73 (2001) 255-267.
- [107] S.C. Steiniger, J. Kreuter, A.S. Khalansky, I.N. Skidan, A.I. Bobruskin, Z.S. Smirnova, S.E. Severin, R. Uhl, M. Kock, K.D. Geiger, Chemotherapy of glioblastoma in rats using doxorubicin-loaded nanoparticles, *International Journal of Cancer*, 109 (2004) 759-767.
- [108] A.E. Gulyaev, S.E. Gelperina, I.N. Skidan, A.S. Antropov, G.Y. Kivman, J. Kreuter, Significant transport of doxorubicin into the brain with polysorbate 80-coated nanoparticles, *Pharmaceutical research*, 16 (1999) 1564-1569.
- [109] G.H. Mickisch, A. Rahman, I. Pastan, M.M. Gottesman, Increased effectiveness of liposome-encapsulated doxorubicin in multidrug-resistant-transgenic mice compared with free doxorubicin, *Journal of the National Cancer Institute*, 84 (1992) 804-805.
- [110] A. Gabizon, R. Catane, B. Uziely, B. Kaufman, T. Safra, R. Cohen, F. Martin, A. Huang, Y. Barenholz, Prolonged circulation time and enhanced accumulation in malignant exudates of doxorubicin encapsulated in polyethylene-glycol coated liposomes, *Cancer research*, 54 (1994) 987-992.

- [111] F. Hudecz, H. Ross, M.R. Price, R.W. Baldwin, Immunoconjugate design: a predictive approach for coupling of daunomycin to monoclonal antibodies, *Bioconjugate chemistry*, 1 (1990) 197-204.
- [112] C.C. Lee, E.R. Gillies, M.E. Fox, S.J. Guillaudeu, J.M. Fréchet, E.E. Dy, F.C. Szoka, A single dose of doxorubicin-functionalized bow-tie dendrimer cures mice bearing C-26 colon carcinomas, *Proceedings of the National Academy of Sciences*, 103 (2006) 16649-16654.
- [113] P.-S. Lai, P.-J. Lou, C.-L. Peng, C.-L. Pai, W.-N. Yen, M.-Y. Huang, T.-H. Young, M.-J. Shieh, Doxorubicin delivery by polyamidoamine dendrimer conjugation and photochemical internalization for cancer therapy, *Journal of Controlled Release*, 122 (2007) 39-46.
- [114] L. Han, R. Huang, S. Liu, S. Huang, C. Jiang, Peptide-conjugated PAMAM for targeted doxorubicin delivery to transferrin receptor overexpressed tumors, *Molecular Pharmaceutics*, 7 (2010) 2156-2165.
- [115] B. Řihová, T. Etrych, M. Pechar, M. Jelinková, M. Štastný, O. Hovorka, M. Kovář, K. Ulbrich, Doxorubicin bound to a HPMA copolymer carrier through hydrazone bond is effective also in a cancer cell line with a limited content of lysosomes, *Journal of controlled release*, 74 (2001) 225-232.
- [116] P.A. Vasey, S.B. Kaye, R. Morrison, C. Twelves, P. Wilson, R. Duncan, A.H. Thomson, L.S. Murray, T.E. Hilditch, T. Murray, Phase I clinical and pharmacokinetic study of PK1 [N-(2-hydroxypropyl) methacrylamide copolymer doxorubicin]: first member of a new class of chemotherapeutic agents—drug-polymer conjugates, *Clinical cancer research*, 5 (1999) 83-94.
- [117] H.S. Yoo, E.A. Lee, T.G. Park, Doxorubicin-conjugated biodegradable polymeric micelles having acid-cleavable linkages, *Journal of controlled release*, 82 (2002) 17-27.

- [118] H. Maeda, J. Wu, T. Sawa, Y. Matsumura, K. Hori, Tumor vascular permeability and the EPR effect in macromolecular therapeutics: a review, *Journal of controlled release*, 65 (2000) 271-284.
- [119] J.M. de la Fuente, C.C. Berry, M.O. Riehle, A.S. Curtis, Nanoparticle targeting at cells, *Langmuir*, 22 (2006) 3286-3293.
- [120] A. Michihara, K. Toda, T. Kubo, Y. Fujiwara, K. Akasaki, H. Tsuji, Disruptive effect of chloroquine on lysosomes in cultured rat hepatocytes, *Biological and Pharmaceutical Bulletin*, 28 (2005) 947-951.
- [121] B. Poole, S. Ohkuma, Effect of weak bases on the intralysosomal pH in mouse peritoneal macrophages, *The Journal of cell biology*, 90 (1981) 665-669.
- [122] A. Kakinoki, Y. Kaneo, Y. Ikeda, T. Tanaka, K. Fujita, Synthesis of poly (vinyl alcohol)-doxorubicin conjugates containing cis-aconityl acid-cleavable bond and its isomer dependent doxorubicin release, *Biological and Pharmaceutical Bulletin*, 31 (2008) 103-110.
- [123] G.M. Dubowchik, R.A. Firestone, L. Padilla, D. Willner, S.J. Hofstead, K. Mosure, J.O. Knipe, S.J. Lasch, P.A. Trail, Cathepsin B-labile dipeptide linkers for lysosomal release of doxorubicin from internalizing immunoconjugates: model studies of enzymatic drug release and antigen-specific in vitro anticancer activity, *Bioconjugate chemistry*, 13 (2002) 855-869.
- [124] P.A. Trail, D. Willner, J. Knipe, A.J. Henderson, S.J. Lasch, M.E. Zoeckler, M.D. TrailSmith, T.W. Doyle, H.D. King, A.M. Casazza, Effect of linker variation on the stability, potency, and efficacy of carcinoma-reactive BR64-doxorubicin immunoconjugates, *Cancer research*, 57 (1997) 100-105.

- [125] S. Zhu, M. Hong, L. Zhang, G. Tang, Y. Jiang, Y. Pei, PEGylated PAMAM dendrimer-doxorubicin conjugates: in vitro evaluation and in vivo tumor accumulation, *Pharmaceutical research*, 27 (2010) 161-174.
- [126] Y. Nie, M. Günther, Z. Gu, E. Wagner, Pyridylhydrazone-based PEGylation for pH-reversible lipopolyplex shielding, *Biomaterials*, 32 (2011) 858-869.
- [127] A. Malugin, P. Kopečková, J. Kopeček, Liberation of doxorubicin from HPMA copolymer conjugate is essential for the induction of cell cycle arrest and nuclear fragmentation in ovarian carcinoma cells, *Journal of controlled release*, 124 (2007) 6-10.
- [128] S. Nicoletti, K. Seifert, I.H. Gilbert, Water-soluble polymer–drug conjugates for combination chemotherapy against visceral leishmaniasis, *Bioorganic & medicinal chemistry*, 18 (2010) 2559-2565.
- [129] K. Ulbrich, V.r. Šubr, Polymeric anticancer drugs with pH-controlled activation, *Advanced drug delivery reviews*, 56 (2004) 1023-1050.
- [130] T. Minko, P. Kopečková, V. Pozharov, J. Kopeček, HPMA copolymer bound adriamycin overcomes MDR1 gene encoded resistance in a human ovarian carcinoma cell line, *Journal of controlled release*, 54 (1998) 223-233.
- [131] V. Omelyanenko, P. Kopečková, C. Gentry, J. Kopeček, Targetable HPMA copolymer-adriamycin conjugates. Recognition, internalization, and subcellular fate, *Journal of controlled release*, 53 (1998) 25-37.
- [132] C. Delgado, G.E. Francis, D. Fisher, The uses and properties of PEG-linked proteins, *Critical reviews in therapeutic drug carrier systems*, 9 (1991) 249-304.
- [133] S. Zalipsky, Chemistry of polyethylene glycol conjugates with biologically active molecules, *Advanced drug delivery reviews*, 16 (1995) 157-182.

- [134] M. Tobio, R. Gref, A. Sanchez, R. Langer, M. Alonso, Stealth PLA-PEG nanoparticles as protein carriers for nasal administration, *Pharmaceutical research*, 15 (1998) 270-275.
- [135] L. Kaminskas, Z. Wu, N. Barlow, G. Krippner, B. Boyd, C. Porter, Partly-PEGylated Poly-L-lysine dendrimers have reduced plasma stability and circulation times compared with fully PEGylated dendrimers, *Journal of pharmaceutical sciences*, 98 (2009) 3871-3875.
- [136] R. Webster, E. Didier, P. Harris, N. Siegel, J. Stadler, L. Tilbury, D. Smith, PEGylated proteins: evaluation of their safety in the absence of definitive metabolism studies, *Drug Metabolism and Disposition*, 35 (2007) 9-16.
- [137] M.S. Peach, S.G. Kumbar, J.L. Brown, C.T. Laurencin, Recent developments in nanoparticle based targeted delivery of chemotherapeutics, *Current Bioactive Compounds*, 5 (2009) 170-184.
- [138] A. Kellar, C. Egan, D. Morris, Preclinical Murine Models for Lung Cancer: Clinical Trial Applications, *BioMed Research International*, 2015 (2015).
- [139] T.L. McLemore, M.C. Liu, P.C. Blacker, M. Gregg, M.C. Alley, B.J. Abbott, R.H. Shoemaker, M.E. Bohlman, C.C. Litterst, W.C. Hubbard, Novel intrapulmonary model for orthotopic propagation of human lung cancers in athymic nude mice, *Cancer research*, 47 (1987) 5132-5140.
- [140] W.W. Overwijk, N.P. Restifo, B16 as a mouse model for human melanoma, *Current Protocols in Immunology*, (2001) 20.21. 21-20.21. 29.
- [141] R. Giavazzi, A. Decio, Syngeneic murine metastasis models: B16 melanoma, in: *Metastasis research protocols*, Springer, 2014, pp. 131-140.
- [142] I. Kim, H.J. Byeon, T.H. Kim, E.S. Lee, K.T. Oh, B.S. Shin, K.C. Lee, Y.S. Youn, Doxorubicin-loaded highly porous large PLGA microparticles as a sustained-release inhalation system for the treatment of metastatic lung cancer, *Biomaterials*, 33 (2012) 5574-5583.

- [143] C. Xu, P. Wang, J. Zhang, H. Tian, K. Park, X. Chen, Pulmonary Codelivery of Doxorubicin and siRNA by pH-Sensitive Nanoparticles for Therapy of Metastatic Lung Cancer, *Small*, 11 (2015) 4321-4333.
- [144] D.S. Conti, B. Bharatwaj, D. Brewer, S.R. da Rocha, Propellant-based inhalers for the non-invasive delivery of genes via oral inhalation, *Journal of controlled release*, 157 (2012) 406-417.
- [145] D. Lu, L. Garcia-Contreras, P. Muttill, D. Padilla, D. Xu, J. Liu, M. Braunstein, D.N. McMurray, A.J. Hickey, Pulmonary immunization using antigen 85-B polymeric microparticles to boost tuberculosis immunity, *The AAPS journal*, 12 (2010) 338-347.
- [146] B. Bharatwaj, L. Wu, J.A. Whittum-Hudson, S.R. da Rocha, The potential for the noninvasive delivery of polymeric nanocarriers using propellant-based inhalers in the treatment of Chlamydial respiratory infections, *Biomaterials*, 31 (2010) 7376-7385.
- [147] C. Jacobs, R.H. Müller, Production and characterization of a budesonide nanosuspension for pulmonary administration, *Pharmaceutical research*, 19 (2002) 189-194.
- [148] M. Horiguchi, H. Kojima, H. Sakai, H. Kubo, C. Yamashita, Pulmonary administration of integrin-nanoparticles regenerates collapsed alveoli, *Journal of controlled release*, (2014).
- [149] Q. Zhang, Z. Shen, T. Nagai, Prolonged hypoglycemic effect of insulin-loaded polybutylcyanoacrylate nanoparticles after pulmonary administration to normal rats, *International journal of pharmaceutics*, 218 (2001) 75-80.
- [150] C.-W. Park, X. Li, F.G. Vogt, D. Hayes, J.B. Zwischenberger, E.-S. Park, H.M. Mansour, Advanced spray-dried design, physicochemical characterization, and aerosol dispersion performance of vancomycin and clarithromycin multifunctional controlled release particles for targeted respiratory delivery as dry powder inhalation aerosols, *International journal of pharmaceutics*, 455 (2013) 374-392.

- [151] Food and Drug Administration., FDA approves Afrezza to treat diabetes in: FDA News Release, 2014.
- [152] M. Semmler-Behnke, S. Takenaka, S. Fertsch, A. Wenk, J. Seitz, P. Mayer, G. Oberdörster, W.G. Kreyling, Efficient elimination of inhaled nanoparticles from the alveolar region: evidence for interstitial uptake and subsequent reentrainment onto airways epithelium, *Environmental health perspectives*, (2007) 728-733.
- [153] J. Zhang, L. Wu, H.-K. Chan, W. Watanabe, Formation, characterization, and fate of inhaled drug nanoparticles, *Advanced drug delivery reviews*, 63 (2011) 441-455.
- [154] Y.-B. Wang, A.B. Watts, J.I. Peters, R.O. Williams Iii, The impact of pulmonary diseases on the fate of inhaled medicines—A review, *International journal of pharmaceutics*, 461 (2014) 112-128.
- [155] S. Sawatdee, P. Hiranphan, K. Laphanayos, T. Srichana, Evaluation of sildenafil pressurized metered dose inhalers as a vasodilator in umbilical blood vessels of chicken egg embryos, *European Journal of Pharmaceutics and Biopharmaceutics*, 86 (2014) 90-97.
- [156] K. Berkenfeld, A. Lamprecht, J.T. McConville, Devices for Dry Powder Drug Delivery to the Lung, *AAPS PharmSciTech*, 16 (2015) 479-490.
- [157] R.B. Lipton, S.D. Silberstein, Episodic and Chronic Migraine Headache: Breaking Down Barriers to Optimal Treatment and Prevention, *Headache: The Journal of Head and Face Pain*, 55 (2015) 103-122.
- [158] A.S. Dharmadhikari, M. Kabadi, B. Gerety, A.J. Hickey, P.B. Fourie, E. Nardell, Phase I, single-dose, dose-escalating study of inhaled dry powder capreomycin: a new approach to therapy of drug-resistant tuberculosis, *Antimicrobial agents and chemotherapy*, 57 (2013) 2613-2619.

- [159] D.S. Pearlman, J. Kottakis, D. Till, G.D. Cioppa, Formoterol Delivered via a Dry Powder Inhaler (Aerolizer*): Results from Long-term Clinical Trials in Children, *Current Medical Research and Opinion*®, 18 (2002) 445-455.
- [160] E.N. Cline, M.-H. Li, S.K. Choi, J.F. Herbstman, N. Kaul, E. Meyhöfer, G. Skiniotis, J.R. Baker, R.G. Larson, N.G. Walter, Paclitaxel-conjugated PAMAM dendrimers adversely affect microtubule structure through two independent modes of action, *Biomacromolecules*, 14 (2013) 654-664.
- [161] P. Daftarian, A.E. Kaifer, W. Li, B.B. Blomberg, D. Frasca, F. Roth, R. Chowdhury, E.A. Berg, J.B. Fishman, H.A. Al Sayegh, Peptide-conjugated PAMAM dendrimer as a universal DNA vaccine platform to target antigen-presenting cells, *Cancer research*, 71 (2011) 7452-7462.
- [162] P.M. Heegaard, U. Boas, N.S. Sorensen, Dendrimers for vaccine and immunostimulatory uses. A review, *Bioconjugate chemistry*, 21 (2009) 405-418.
- [163] D.S. Conti, D. Brewer, J. Grashik, S. Avasarala, S.R. da Rocha, Poly (amidoamine) dendrimer nanocarriers and their aerosol formulations for siRNA delivery to the lung epithelium, *Molecular pharmaceutics*, 11 (2014) 1808-1822.
- [164] M.J. Cloninger, Biological applications of dendrimers, *Current opinion in chemical biology*, 6 (2002) 742-748.
- [165] R. Esfand, D.A. Tomalia, Poly (amidoamine)(PAMAM) dendrimers: from biomimicry to drug delivery and biomedical applications, *Drug discovery today*, 6 (2001) 427-436.
- [166] O.P. Perumal, R. Inapagolla, S. Kannan, R.M. Kannan, The effect of surface functionality on cellular trafficking of dendrimers, *Biomaterials*, 29 (2008) 3469-3476.
- [167] R. Duncan, L. Izzo, Dendrimer biocompatibility and toxicity, *Advanced drug delivery reviews*, 57 (2005) 2215-2237.

- [168] B. Bharatwaj, A.K. Mohammad, R. Dimovski, F.L. Cassio, R.C. Bazito, D. Conti, Q. Fu, J. Reineke, S.R. da Rocha, Dendrimer Nanocarriers for Transport Modulation Across Models of the Pulmonary Epithelium, *Molecular pharmaceutics*, 12 (2015) 826-838.
- [169] L.M. Kaminskas, B.J. Boyd, C.J. Porter, Dendrimer pharmacokinetics: the effect of size, structure and surface characteristics on ADME properties, *Nanomedicine*, 6 (2011) 1063-1084.
- [170] L.E. van Vlerken, T.K. Vyas, M.M. Amiji, Poly (ethylene glycol)-modified nanocarriers for tumor-targeted and intracellular delivery, *Pharmaceutical research*, 24 (2007) 1405-1414.
- [171] D.E. Owens III, N.A. Peppas, Opsonization, biodistribution, and pharmacokinetics of polymeric nanoparticles, *International journal of pharmaceutics*, 307 (2006) 93-102.
- [172] L.M. Kaminskas, B.J. Boyd, P. Karellas, G.Y. Krippner, R. Lessene, B. Kelly, C.J. Porter, The impact of molecular weight and PEG chain length on the systemic pharmacokinetics of PEGylated poly l-lysine dendrimers, *Molecular pharmaceutics*, 5 (2008) 449-463.
- [173] C. Kojima, C. Regino, Y. Umeda, H. Kobayashi, K. Kono, Influence of dendrimer generation and polyethylene glycol length on the biodistribution of PEGylated dendrimers, *International journal of pharmaceutics*, 383 (2010) 293-296.
- [174] H. He, Y. Li, X.-R. Jia, J. Du, X. Ying, W.-L. Lu, J.-N. Lou, Y. Wei, PEGylated Poly (amidoamine) dendrimer-based dual-targeting carrier for treating brain tumors, *Biomaterials*, 32 (2011) 478-487.
- [175] H. Liu, D.J. Irvine, Guiding Principles in the Design of Molecular Bioconjugates for Vaccine Applications, *Bioconjugate chemistry*, (2015).
- [176] J.C. Leemans, N.P. Juffermans, S. Florquin, N. van Rooijen, M.J. Vervoordeldonk, A. Verbon, S.J. van Deventer, T. van der Poll, Depletion of alveolar macrophages exerts protective effects in pulmonary tuberculosis in mice, *The journal of immunology*, 166 (2001) 4604-4611.

- [177] J.L. Flynn, Immunology of tuberculosis and implications in vaccine development, *Tuberculosis*, 84 (2004) 93-101.
- [178] K. Sarlo, K.L. Blackburn, E.D. Clark, J. Grothaus, J. Chaney, S. Neu, J. Flood, D. Abbott, C. Bohne, K. Casey, Tissue distribution of 20nm, 100nm and 1000nm fluorescent polystyrene latex nanospheres following acute systemic or acute and repeat airway exposure in the rat, *Toxicology*, 263 (2009) 117-126.
- [179] B. Bharatwaj, Polymeric nanocarriers for the regional and systemic delivery of therapeutics to and through the lungs, in, Wayne State University, digitalcommons.wayne.edu, 2012.
- [180] O.M. Merkel, L.M. Marsh, H. Garn, T. Kissel, Flow Cytometry-Based Cell Type-Specific Assessment of Target Regulation by Pulmonary siRNA Delivery, in: *Nanotechnology for Nucleic Acid Delivery*, Springer, 2013, pp. 263-273.
- [181] T.J. Berg JM, Stryer L. , *Biochemistry: Section 3.2: Primary Structure: Amino Acids Are Linked by Peptide Bonds to Form Polypeptide Chains.*, 5th ed., New York: W H Freeman, 2002.
- [182] L. Yang, S.R.P. da Rocha, PEGylated, NH₂-Terminated PAMAM Dendrimers: A Microscopic View from Atomistic Computer Simulations, *Molecular Pharmaceutics*, 11 (2014) 1459-1470.
- [183] E.R. Bielski, Q. Zhong, M. Brown, S.R. da Rocha, Effect of the Conjugation Density of Triphenylphosphonium Cation on the Mitochondrial Targeting of Poly (amidoamine) Dendrimers, *Molecular pharmaceutics*, (2015).
- [184] B. Bharatwaj, R. Dimovski, D.S. Conti, S.R. da Rocha, Polymeric Nanocarriers for Transport Modulation across the Pulmonary Epithelium: Dendrimers, Polymeric Nanoparticles, and their Nanoblends, *The AAPS journal*, 16 (2014) 522-538.

- [185] M. Kondoh, K. Yagi, Tight junction modulators: promising candidates for drug delivery, *Current medicinal chemistry*, 14 (2007) 2482-2488.
- [186] E.E. Schneeberger, R.D. Lynch, The tight junction: a multifunctional complex, *American Journal of Physiology-Cell Physiology*, 286 (2004) C1213-C1228.
- [187] B.J. Boyd, L.M. Kaminskas, P. Karellas, G. Krippner, R. Lessene, C.J. Porter, Cationic poly-L-lysine dendrimers: pharmacokinetics, biodistribution, and evidence for metabolism and bioresorption after intravenous administration to rats, *Molecular pharmaceutics*, 3 (2006) 614-627.
- [188] M. Peracchia, S. Harnisch, H. Pinto-Alphandary, A. Gulik, J. Dedieu, D. Desmaele, J. d'Angelo, R. Müller, P. Couvreur, Visualization of in vitro protein-rejecting properties of PEGylated stealth[®] polycyanoacrylate nanoparticles, *Biomaterials*, 20 (1999) 1269-1275.
- [189] M. Ogris, S. Brunner, S. Schüller, R. Kircheis, E. Wagner, PEGylated DNA/transferrin-PEI complexes: reduced interaction with blood components, extended circulation in blood and potential for systemic gene delivery, *Gene therapy*, 6 (1999) 595-605.
- [190] J.L. Perry, K.G. Reuter, M.P. Kai, K.P. Herlihy, S.W. Jones, J.C. Luft, M. Napier, J.E. Bear, J.M. DeSimone, PEGylated PRINT nanoparticles: the impact of PEG density on protein binding, macrophage association, biodistribution, and pharmacokinetics, *Nano letters*, 12 (2012) 5304-5310.
- [191] U. Wattendorf, H.P. Merkle, PEGylation as a tool for the biomedical engineering of surface modified microparticles, *Journal of pharmaceutical sciences*, 97 (2008) 4655-4669.
- [192] D.M. Sweet, R.B. Kolhatkar, A. Ray, P. Swaan, H. Ghandehari, Transepithelial transport of PEGylated anionic poly (amidoamine) dendrimers: implications for oral drug delivery, *Journal of controlled release*, 138 (2009) 78-85.

- [193] V.J. Venditto, C.A.S. Regino, M.W. Brechbiel, PAMAM dendrimer based macromolecules as improved contrast agents, *Molecular Pharmaceutics*, 2 (2005) 302-311.
- [194] H.S. Choi, W. Liu, P. Misra, E. Tanaka, J.P. Zimmer, B.I. Ipe, M.G. Bawendi, J.V. Frangioni, Renal clearance of quantum dots, *Nature biotechnology*, 25 (2007) 1165-1170.
- [195] A. Koide, S. Kobayashi, Modification of amino groups in porcine pancreatic elastase with polyethylene glycol in relation to binding ability towards anti-serum and to enzymic activity, *Biochemical and biophysical research communications*, 111 (1983) 659-667.
- [196] J.-P. Amorij, V. Saluja, A.H. Petersen, W.L. Hinrichs, A. Huckriede, H.W. Frijlink, Pulmonary delivery of an inulin-stabilized influenza subunit vaccine prepared by spray-freeze drying induces systemic, mucosal humoral as well as cell-mediated immune responses in BALB/c mice, *Vaccine*, 25 (2007) 8707-8717.
- [197] D. Nardelli-Haefliger, F. Lurati, D. Wirthner, F. Spertini, J.T. Schiller, D.R. Lowy, F. Ponci, P. De Grandi, Immune responses induced by lower airway mucosal immunisation with a human papillomavirus type 16 virus-like particle vaccine, *Vaccine*, 23 (2005) 3634-3641.
- [198] R. Shayan, M.G. Achen, S.A. Stacker, Lymphatic vessels in cancer metastasis: bridging the gaps, *Carcinogenesis*, 27 (2006) 1729-1738.
- [199] S.S. Nigavekar, L.Y. Sung, M. Llanes, A. El-Jawahri, T.S. Lawrence, C.W. Becker, L. Balogh, M.K. Khan, 3H dendrimer nanoparticle organ/tumor distribution, *Pharmaceutical research*, 21 (2004) 476-483.
- [200] F. Blank, P. Stumbles, C. von Garnier, Opportunities and challenges of the pulmonary route for vaccination, *Expert opinion on drug delivery*, 8 (2011) 547-563.
- [201] A.G. Harmsen, B.A. Muggenburg, M.B. Snipes, D.E. Bice, The role of macrophages in particle translocation from lungs to lymph nodes, *Science*, 230 (1985) 1277-1280.

- [202] A.C. Kirby, M.C. Coles, P.M. Kaye, Alveolar macrophages transport pathogens to lung draining lymph nodes, *The Journal of Immunology*, 183 (2009) 1983-1989.
- [203] S.L. Murphy, J. Xu, K.D. Kochanek, Deaths: final data for 2010, *National vital statistics reports*, 61 (2013) 1-118.
- [204] American Cancer Society, *Cancer Facts & Figures 2014*, in, 2014.
- [205] Lung Cancer, in: *Basic Information About Lung Cancer*, Centers for Disease Control and Prevention, Atlanta, GA, 2013.
- [206] S. Wieland, A. Mita, S. Piantadosi, R. Natale, D. Levitt, Phase 2 Study of Aldoxorubicin Versus Topotecan for Relapsed/Refractory Small Cell Lung Cancer, in: *Annals of Oncology*, OXFORD UNIV PRESS GREAT CLARENDON ST, OXFORD OX2 6DP, ENGLAND, 2014.
- [207] F.S. Carvalho, A. Burgeiro, R. Garcia, A.J. Moreno, R.A. Carvalho, P.J. Oliveira, Doxorubicin-Induced Cardiotoxicity: From Bioenergetic Failure and Cell Death to Cardiomyopathy, *Medicinal research reviews*, 34 (2014) 106-135.
- [208] M. Bristow, M. Billingham, J. Mason, J. Daniels, Clinical spectrum of anthracycline antibiotic cardiotoxicity, *Cancer treatment reports*, 62 (1978) 873-879.
- [209] F. Villani, G. Beretta, A. Guindani, Evaluation of early doxorubicin-induced cardiotoxicity by means of systolic time intervals, *Cancer chemotherapy and pharmacology*, 3 (1979) 249-251.
- [210] K. Chatterjee, J. Zhang, N. Honbo, J.S. Karliner, Doxorubicin cardiomyopathy, *Cardiology*, 115 (2009) 155-162.
- [211] F.S. Carvalho, A. Burgeiro, R. Garcia, A.J. Moreno, R.A. Carvalho, P.J. Oliveira, Doxorubicin-Induced Cardiotoxicity: From Bioenergetic Failure and Cell Death to Cardiomyopathy, *Medicinal Research Reviews*, 34 (2014) 106-135.

- [212] A.R. Menjoge, R.M. Kannan, D.A. Tomalia, Dendrimer-based drug and imaging conjugates: design considerations for nanomedical applications, *Drug discovery today*, 15 (2010) 171-185.
- [213] M.L. Bender, General Acid-Base Catalysis in the Intramolecular Hydrolysis of Phthalamic Acid, *Journal of the American Chemical Society*, 79 (1957) 1258-1259.
- [214] S. Riechers, Q. Zhong, N.-N. Yin, A. Karsai, S.R. da Rocha, G.-y. Liu, High-Resolution Imaging of Polyethylene Glycol Coated Dendrimers via Combined Atomic Force and Scanning Tunneling Microscopy, *Journal of drug delivery*, 2015 (2015).
- [215] E.R. Bielski, Q. Zhong, M. Brown, S.R. da Rocha, Effect of the Conjugation Density of Triphenylphosphonium Cation on the Mitochondrial Targeting of Poly (amidoamine) Dendrimers, *Molecular pharmaceutics*, 12 (2015) 3043-3053.
- [216] G. Speelmans, R.W. Staffhorst, B. de Kruijff, F.A. de Wolf, Transport Studies of Doxorubicin in Model Membranes Indicate a Difference in Passive Diffusion across and Binding at the Outer and Inner Leaflet of the Plasma Membrane, *Biochemistry*, 33 (1994) 13761-13768.
- [217] K.M. Kitchens, A.B. Foraker, R.B. Kolhatkar, P.W. Swaan, H. Ghandehari, Endocytosis and interaction of poly (amidoamine) dendrimers with Caco-2 cells, *Pharmaceutical research*, 24 (2007) 2138-2145.
- [218] R. Jevprasesphant, J. Penny, D. Attwood, A. D'Emanuele, Transport of dendrimer nanocarriers through epithelial cells via the transcellular route, *Journal of controlled release*, 97 (2004) 259-267.
- [219] C. De Duve, T. De Barsey, B. Poole, A. Trouet, P. Tulkens, F. Van Hoof, Lysosomotropic agents, *Biochemical pharmacology*, 23 (1974) 2495-2531.

- [220] A. Kakinoki, Y. Kaneo, Y. Ikeda, T. Tanaka, K. Fujita, Synthesis of poly (vinyl alcohol)-doxorubicin conjugates containing cis-aconityl acid-cleavable bond and its isomer dependent doxorubicin release, *Biological and Pharmaceutical Bulletin*, 31 (2008) 103-110.
- [221] T. Minko, P. Kopečková, V. Pozharov, J. Kopeček, HPMA copolymer bound adriamycin overcomes MDR1 gene encoded resistance in a human ovarian carcinoma cell line, *Journal of controlled release*, 54 (1998) 223-233.
- [222] E.A. Nance, G.F. Woodworth, K.A. Sailor, T.-Y. Shih, Q. Xu, G. Swaminathan, D. Xiang, C. Eberhart, J. Hanes, A dense poly (ethylene glycol) coating improves penetration of large polymeric nanoparticles within brain tissue, *Science translational medicine*, 4 (2012) 149ra119-149ra119.
- [223] H.L. Kutscher, P. Chao, M. Deshmukh, S.S. Rajan, Y. Singh, P. Hu, L.B. Joseph, S. Stein, D.L. Laskin, P.J. Sinko, Enhanced passive pulmonary targeting and retention of PEGylated rigid microparticles in rats, *International journal of pharmaceutics*, 402 (2010) 64-71.
- [224] F. Frezard, A. Garnier-Suillerot, DNA-containing liposomes as a model for the study of cell membrane permeation by anthracycline derivatives, *Biochemistry*, 30 (1991) 5038-5043.
- [225] K.M. Kitchens, R.B. Kolhatkar, P.W. Swaan, H. Ghandehari, Endocytosis inhibitors prevent poly (amidoamine) dendrimer internalization and permeability across Caco-2 cells, *Molecular Pharmaceutics*, 5 (2008) 364-369.
- [226] L. Albertazzi, M. Serresi, A. Albanese, F. Beltram, Dendrimer internalization and intracellular trafficking in living cells, *Molecular Pharmaceutics*, 7 (2010) 680-688.
- [227] F.P. Seib, A.T. Jones, R. Duncan, Comparison of the endocytic properties of linear and branched PEIs, and cationic PAMAM dendrimers in B16f10 melanoma cells, *Journal of controlled release*, 117 (2007) 291-300.

- [228] G. Sahay, D.Y. Alakhova, A.V. Kabanov, Endocytosis of nanomedicines, *Journal of controlled release*, 145 (2010) 182-195.
- [229] A. Khakpoor, M. Panyasrivanit, N. Wikan, D.R. Smith, A role for autophagolysosomes in dengue virus 3 production in HepG2 cells, *Journal of General Virology*, 90 (2009) 1093-1103.
- [230] H. Hillaireau, P. Couvreur, Nanocarriers' entry into the cell: relevance to drug delivery, *Cellular and Molecular Life Sciences*, 66 (2009) 2873-2896.
- [231] D. Lu, A.J. Hickey, Pulmonary vaccine delivery, (2007).
- [232] S.W. Stein, P. Sheth, P.D. Hodson, P.B. Myrdal, Advances in metered dose inhaler technology: hardware development, *AAPS PharmSciTech*, 15 (2014) 326-338.
- [233] S. Jones, Suspension versus solution metered dose inhalers: different products, different particles?, *Journal of Drug Delivery Science and Technology*, 21 (2011) 319-322.
- [234] U. Chokshi, P. Selvam, L. Porcar, S.R. da Rocha, Reverse aqueous emulsions and microemulsions in HFA227 propellant stabilized by non-ionic ethoxylated amphiphiles, *International journal of pharmaceutics*, 369 (2009) 176-184.
- [235] D.S. Conti, J. Grashik, L. Yang, L. Wu, S.R. da Rocha, Solvation in hydrofluoroalkanes: how can ethanol help?, *Journal of Pharmacy and Pharmacology*, 64 (2012) 1236-1244.
- [236] M.L. Reid, F. Benaouda, R. Khengar, S.A. Jones, M.B. Brown, Topical corticosteroid delivery into human skin using hydrofluoroalkane metered dose aerosol sprays, *International journal of pharmaceutics*, 452 (2013) 157-165.
- [237] R.P. Peguin, S.R. da Rocha, Solvent– solute interactions in hydrofluoroalkane propellants, *The Journal of Physical Chemistry B*, 112 (2008) 8084-8094.
- [238] P.G. Rogueda, HPFP, a model propellant for pMDIs, *Drug development and industrial pharmacy*, 29 (2003) 39-49.

- [239] S. Stein, J. Stefely, Reinventing metered dose inhalers: from poorly efficient CFC MDIs to highly efficient HFA MDIs, *Drug Deliv. Technol*, 3 (2003) 46-51.
- [240] K.D. Ostrander, H.W. Bosch, D.M. Bondanza, An in-vitro assessment of a NanoCrystal™ beclomethasone dipropionate colloidal dispersion via ultrasonic nebulization, *European journal of pharmaceuticals and biopharmaceutics*, 48 (1999) 207-215.
- [241] C. Leach, P. Davidson, R. Boudreau, Improved airway targeting with the CFC-free HFA-beclomethasone metered-dose inhaler compared with CFC-beclomethasone, *European Respiratory Journal*, 12 (1998) 1346-1353.
- [242] J.S. Stefely, Novel excipients for inhalation drug delivery: expanding the capability of the MDI, *Drug Delivery Technol*, 2 (2002) 62-64.
- [243] T.C. Carvalho, J.I. Peters, R.O. Williams, Influence of particle size on regional lung deposition—what evidence is there?, *International Journal of Pharmaceutics*, 406 (2011) 1-10.
- [244] P. Zarogoulidis, E. Chatzaki, K. Porpodis, K. Domvri, W. Hohenforst-Schmidt, E.P. Goldberg, N. Karamanos, K. Zarogoulidis, Inhaled chemotherapy in lung cancer: future concept of nanomedicine, *International journal of nanomedicine*, 7 (2012) 1551.
- [245] K. Koushik, D.S. Dhand, N.P. Cheruvu, U.B. Kompella, Pulmonary delivery of deslorelin: large-porous PLGA particles and HP β CD complexes, *Pharmaceutical research*, 21 (2004) 1119-1126.
- [246] K.R. Murphy, R. Dhand, F. Trudo, T. Uryniak, A. Aggarwal, G. Eckerwall, Therapeutic equivalence of budesonide/formoterol delivered via breath-actuated inhaler vs pMDI, *Respiratory medicine*, (2015).

- [247] L.E. Mather, A. Woodhouse, M.E. Ward, S.J. Farr, R.A. Rubsamen, L.G. Eltherington, Pulmonary administration of aerosolised fentanyl: pharmacokinetic analysis of systemic delivery, *British journal of clinical pharmacology*, 46 (1998) 37-43.
- [248] S.D. Tarver, T.H. Stanley, Absorption and Bioavailability of Oral transmucosal Fentanyl Citrate, *Anesthesiology*, 75 (1991) 223-229.
- [249] J.S. Patton, Mechanisms of macromolecule absorption by the lungs, *Advanced Drug Delivery Reviews*, 19 (1996) 3-36.
- [250] J.S. Patton, C.S. Fishburn, J.G. Weers, The lungs as a portal of entry for systemic drug delivery, *Proceedings of the American Thoracic Society*, 1 (2004) 338-344.
- [251] O.M. Merkel, I. Rubinstein, T. Kissel, siRNA Delivery to the lung: What's new?, *Advanced drug delivery reviews*, 75 (2014) 112-128.
- [252] A. Misra, A.J. Hickey, C. Rossi, G. Borchard, H. Terada, K. Makino, P.B. Fourie, P. Colombo, Inhaled drug therapy for treatment of tuberculosis, *Tuberculosis*, 91 (2011) 71-81.
- [253] X. Li, M. Takashima, E. Yuba, A. Harada, K. Kono, PEGylated PAMAM dendrimer-doxorubicin conjugate-hybridized gold nanorod for combined photothermal-chemotherapy, *Biomaterials*, 35 (2014) 6576-6584.
- [254] A. Saovapakhiran, A. D'Emanuele, D. Attwood, J. Penny, Surface modification of PAMAM dendrimers modulates the mechanism of cellular internalization, *Bioconjugate chemistry*, 20 (2009) 693-701.
- [255] H.-T. Chen, M.F. Neerman, A.R. Parrish, E.E. Simanek, Cytotoxicity, hemolysis, and acute in vivo toxicity of dendrimers based on melamine, candidate vehicles for drug delivery, *Journal of the American Chemical Society*, 126 (2004) 10044-10048.

- [256] B. Bharatwaj, A.K. Mohammad, R. Dimovski, F.L. Cássio, R.C. Bazito, D. Conti, Q. Fu, J.J. Reineke, S.R. da Rocha, Dendrimer Nanocarriers for Transport Modulation across Models of the Pulmonary Epithelium, *Molecular pharmaceutics*, 12 (2015) 826-838.
- [257] W. Wang, W. Xiong, Y. Zhu, H. Xu, X. Yang, Protective effect of PEGylation against poly (amidoamine) dendrimer-induced hemolysis of human red blood cells, *Journal of Biomedical Materials Research Part B: Applied Biomaterials*, 93 (2010) 59-64.
- [258] Q. Zhong, J. Ren, Q. Wang, Preparation and characterization of polylactide-block-poly (butylene adipate) polyurethane thermoplastic elastomer, *Polymer Engineering & Science*, 51 (2011) 908-916.
- [259] L. Bromberg, V. Alakhov, Effects of polyether-modified poly (acrylic acid) microgels on doxorubicin transport in human intestinal epithelial Caco-2 cell layers, *Journal of controlled release*, 88 (2003) 11-22.
- [260] K.O. Hamilton, E. Topp, I. Makagiansar, T. Siahaan, M. Yazdanian, K.L. Audus, Multidrug Resistance-Associated Protein-1 Functional Activity in Calu-3 Cells, *Journal of Pharmacology and Experimental Therapeutics*, 298 (2001) 1199-1205.
- [261] S. Sadekar, H. Ghandehari, Transepithelial transport and toxicity of PAMAM dendrimers: implications for oral drug delivery, *Advanced drug delivery reviews*, 64 (2012) 571-588.
- [262] M.T. Clunes, R.C. Boucher, Cystic fibrosis: the mechanisms of pathogenesis of an inherited lung disorder, *Drug Discovery Today: Disease Mechanisms*, 4 (2007) 63-72.
- [263] A. Verkman, Y. Song, J.R. Thiagarajah, Role of airway surface liquid and submucosal glands in cystic fibrosis lung disease, *American Journal of Physiology-Cell Physiology*, 284 (2003) C2-C15.

- [264] M.R. Knowles, R.C. Boucher, Mucus clearance as a primary innate defense mechanism for mammalian airways, *Journal of clinical investigation*, 109 (2002) 571-577.
- [265] N.G. Schipper, K.M. Vårum, P. Stenberg, G. Ocklind, H. Lennernäs, P. Artursson, Chitosans as absorption enhancers of poorly absorbable drugs: 3: Influence of mucus on absorption enhancement, *European journal of pharmaceutical sciences*, 8 (1999) 335-343.
- [266] C. Valenta, The use of mucoadhesive polymers in vaginal delivery, *Advanced drug delivery reviews*, 57 (2005) 1692-1712.
- [267] D.A. Norris, P.J. Sinko, Effect of size, surface charge, and hydrophobicity on the translocation of polystyrene microspheres through gastrointestinal mucin, *Journal of applied polymer science*, 63 (1997) 1481-1492.
- [268] R. Kircheis, L. Wightman, E. Wagner, Design and gene delivery activity of modified polyethylenimines, *Advanced drug delivery reviews*, 53 (2001) 341-358.
- [269] J.C. McCabe, F. Koppenhagen, J. Blair, X.-M. Zeng, ProAir® HFA delivers warmer, lower-impact, longer-duration plumes containing higher fine particle dose than Ventolin® HFA, *Journal of aerosol medicine and pulmonary drug delivery*, 25 (2012) 104-109.
- [270] A.F. Gazdar, R.I. Linnoila, Y. Kurita, H.K. Oie, J.L. Mulshine, J.C. Clark, J.A. Whitsett, Peripheral airway cell differentiation in human lung cancer cell lines, *Cancer Research*, 50 (1990) 5481-5487.
- [271] P. Macchiarini, Primary tracheal tumours, *The lancet oncology*, 7 (2006) 83-91.
- [272] P. Muto, V. Ravo, G. Panelli, G. Liguori, G. Fraioli, High-dose rate brachytherapy of bronchial cancer: treatment optimization using three schemes of therapy, *The Oncologist*, 5 (2000) 209-214.

- [273] I.Y. Saleem, H.D. Smyth, Tuning aerosol particle size distribution of metered dose inhalers using cosolvents and surfactants, *BioMed research international*, 2013 (2013).
- [274] J. Stefely, D. Duan, P. Myrdal, D. Ross, D. Schultz, C. Leach, Design and utility of a novel class of biocompatible excipients for HFA-based MDIs, *RDD VII*, (2000).
- [275] R.P. Peguin, L. Wu, S.R. da Rocha, The ester group: How hydrofluoroalkane-philic is it?, *Langmuir*, 23 (2007) 8291-8294.
- [276] S.L.M. Kenneth D. Kochanek, Jiaquan Xu, Elizabeth Arias., Mortality in the United States, 2013, in, *Centers for Disease Control and Prevention*, 2014, pp. 8.
- [277] H. Wada, S. Hitomi, T. Teramatsu, Adjuvant chemotherapy after complete resection in non-small-cell lung cancer. West Japan Study Group for Lung Cancer Surgery, *Journal of clinical oncology*, 14 (1996) 1048-1054.
- [278] K.S. Albain, R.S. Swann, V.W. Rusch, A.T. Turrisi, F.A. Shepherd, C. Smith, Y. Chen, R.B. Livingston, R.H. Feins, D.R. Gandara, Radiotherapy plus chemotherapy with or without surgical resection for stage III non-small-cell lung cancer: a phase III randomised controlled trial, *The Lancet*, 374 (2009) 379-386.
- [279] G.P. Gupta, J. Massagué, Cancer metastasis: building a framework, *Cell*, 127 (2006) 679-695.
- [280] D.X. Nguyen, P.D. Bos, J. Massagué, Metastasis: from dissemination to organ-specific colonization, *Nature Reviews Cancer*, 9 (2009) 274-284.
- [281] R.H. Blum, S.K. Carter, Adriamycin: a new anticancer drug with significant clinical activity, *Annals of Internal Medicine*, 80 (1974) 249-259.
- [282] S. Mura, J. Nicolas, P. Couvreur, Stimuli-responsive nanocarriers for drug delivery, *Nature materials*, 12 (2013) 991-1003.

- [283] T. Etrych, M. Jelínková, B. Říhová, K. Ulbrich, New HPMA copolymers containing doxorubicin bound via pH-sensitive linkage: synthesis and preliminary in vitro and in vivo biological properties, *Journal of Controlled Release*, 73 (2001) 89-102.
- [284] T. Tokudome, K. Mizushige, T. Noma, K. Manabe, K. Murakami, T. Tsuji, S. Nozaki, A. Tomohiro, H. Matsuo, Prevention of doxorubicin (adriamycin)-induced cardiomyopathy by simultaneous administration of angiotensin-converting enzyme inhibitor assessed by acoustic densitometry, *Journal of cardiovascular pharmacology*, 36 (2000) 361-368.
- [285] D. Cardinale, A. Colombo, M.T. Sandri, G. Lamantia, N. Colombo, M. Civelli, G. Martinelli, F. Veglia, C. Fiorentini, C.M. Cipolla, Prevention of high-dose chemotherapy-induced cardiotoxicity in high-risk patients by angiotensin-converting enzyme inhibition, *Circulation*, 114 (2006) 2474-2481.
- [286] A.M. Rahman, S.W. Yusuf, M.S. Ewer, Anthracycline-induced cardiotoxicity and the cardiac-sparing effect of liposomal formulation, *International journal of nanomedicine*, 2 (2007) 567.
- [287] N. Malik, E.G. Evagorou, R. Duncan, Dendrimer-platinate: a novel approach to cancer chemotherapy, *Anti-cancer drugs*, 10 (1999) 767-776.
- [288] U. Prabhakar, H. Maeda, R.K. Jain, E.M. Sevick-Muraca, W. Zamboni, O.C. Farokhzad, S.T. Barry, A. Gabizon, P. Grodzinski, D.C. Blakey, Challenges and key considerations of the enhanced permeability and retention effect for nanomedicine drug delivery in oncology, *Cancer research*, 73 (2013) 2412-2417.
- [289] P.K. Singal, N. Iliskovic, Doxorubicin-induced cardiomyopathy, *New England Journal of Medicine*, 339 (1998) 900-905.

- [290] K. Xiao, Y. Li, J. Luo, J.S. Lee, W. Xiao, A.M. Gonik, R. Agarwal, K.S. Lam, The effect of surface charge on in vivo biodistribution of PEG-oligocholeic acid based micellar nanoparticles, *Biomaterials*, 32 (2011) 3435-3446.
- [291] H. Kobayashi, R. Watanabe, P.L. Choyke, Improving Conventional Enhanced Permeability and Retention (EPR) Effects; What Is the Appropriate Target?, *Theranostics*, 4 (2014) 81-89.
- [292] D.E. Owens, N.A. Peppas, Opsonization, biodistribution, and pharmacokinetics of polymeric nanoparticles, *International journal of pharmaceutics*, 307 (2006) 93-102.
- [293] R.M. Pearson, V.V. Juettner, S. Hong, Biomolecular corona on nanoparticles: a survey of recent literature and its implications in targeted drug delivery, *Frontiers in chemistry*, 2 (2014).
- [294] A. Åkesson, M. Cárdenas, G. Elia, M.P. Monopoli, K.A. Dawson, The protein corona of dendrimers: PAMAM binds and activates complement proteins in human plasma in a generation dependent manner, *RSC Advances*, 2 (2012) 11245-11248.
- [295] R. Savla, O. Taratula, O. Garbuzenko, T. Minko, Tumor targeted quantum dot-mucin 1 aptamer-doxorubicin conjugate for imaging and treatment of cancer, *Journal of Controlled Release*, 153 (2011) 16-22.
- [296] O. Merkel, L. Marsh, H. Garn, T. Kissel, Flow Cytometry-Based Cell Type-Specific Assessment of Target Regulation by Pulmonary siRNA Delivery, in: M. Ogris, D. Oupicky (Eds.) *Nanotechnology for Nucleic Acid Delivery*, Humana Press, 2013, pp. 263-273.
- [297] W.-C. Shen, H.J.-P. Ryser, cis-Aconityl spacer between daunomycin and macromolecular carriers: a model of pH-sensitive linkage releasing drug from a lysosomotropic conjugate, *Biochemical and Biophysical Research Communications*, 102 (1981) 1048-1054.

ABSTRACT**DENDRIMER NANOCONJUGATES AND THEIR ORAL INHALATION FORMULATIONS FOR LUNG CANCER THERAPY**

by

QIAN ZHONG**May 2016****Advisor:** Dr. Sandro da Rocha**Major:** Materials Science**Degree:** Doctor of Philosophy

Lung cancers are leading cause of cancer death for both men and women in the world. Lungs are also one of the primary organs to which almost all cancer can spread. Chemotherapy plays a crucial role in the fight against both primary lung cancers and lung metastases. Doxorubicin (DOX) is a potent anticancer drug that has been approved for treating many cancers including lung cancers. However, only a few percent of systemically administered DOX can be found in the lungs. The issue is further complicated by dose-limiting toxicity of DOX. Another major challenge in the use of DOX is its cardiac toxicity. Free DOX in bloodstream can accumulate in cardiac tissues, thus leading to fatal heart damages. On the other hand, the lungs are considered as a portal to external environment and suitable for local delivery. Additionally, oral inhalation (OI) has long been accepted as the preferred mode of administration of therapeutics to the lungs. To address these discussed challenges, we used a strategy — polymeric nanocarriers (PNCs) to achieve the spatial and temporal drug release and local delivery of drug to the lungs. In this work, we designed polyamidoamine dendrimer (PAMAM) conjugates which can only release DOX intracellularly, while being stable in physiological environment. We observed the PAMAM-DOX conjugates upon local delivery to the lungs can significantly inhibit tumor growth both *in vitro* and *in vivo*.

We also successfully prepared the PAMAP-DOX conjugates into propellant-based aerosol formulations which is conducive to deep lung areas. To our knowledge, it is for the first time that polymeric nanocarrier-based drug delivery system has been formulated into propellant-based aerosol formulations.

AUTOBIOGRAPHICAL STATEMENT

Qian Zhong received his B.E degree (Bachelor of Engineering) in Materials Science and Engineering from Tongji University, China in 2006 and M.S degree (Master of Science) in Materials Science and Engineering from Tongji University, China in 2009. He joined department of Chemical Enigneering and Materials Science at Wayne State University, MI, US in winter of 2011 to pursue a degree of Doctor of Phylosophy in Materials Science. His research, under the guidance of Dr. Sandro da Rocha is focused on strategies to develop dendrimer-based nanomedicines for lung cancer chemotherapy and immunotherapy, as well as oral inhalation formulation of nanomedicnes for lung delivery. He has authored or coauthored 6 peer reviewed publications and 3 patents/patent disclosure. He will be submitting 4 more publications with contributions as a first author and 5 more publications with contributions as second author.